DEVELOPMENT AND APPLICATION OF MAGNETOENCEPHALOGRAPHIC METHODS IN THE INVESTIGATION OF THE HUMAN VISUAL SYSTEM

STEPHEN DAVID HALL

Doctor of Philosophy

ASTON UNIVERSITY

March 2004

Development and Application of Magnetoencephalographic Methods in the Investigation of the Human Visual System.

Stephen David Hall

Doctor of Philosophy

2004

This thesis is an exploration of the organisation and functioning of the human visual system using the non-invasive functional imaging modality magnetoencephalography (MEG). Chapters one and two provide an introduction to the human visual system and magnetoencephalographic methodologies. These chapters subsequently describe the methods by which MEG can be used to measure neuronal activity from the visual cortex. Chapter three describes the development and implementation of novel analytical tools; including beamforming based analyses, spectrographic movies and an optimisation of group imaging methods. Chapter four focuses on the use of established and contemporary analytical tools in the investigation of visual function. This is initiated with an investigation of visually evoked and induced responses; covering visual evoked potentials (VEPs) and event related synchronisation/desynchronisation (ERS/ERD). Chapter five describes the employment of novel analysis methods in the investigation of cortical contrast response and demonstrates distinct contrast response functions in striate and extra-striate regions of visual cortex. Chapter six uses synthetic aperture magnetometry (SAM) to investigate the phenomena of visual cortical gamma oscillations in response to various visual stimuli; concluding that pattern is central to its generation and that it increases in amplitude linearly as a function of stimulus contrast, consistent with results from invasive electrode studies in the macaque monkey. Chapter seven describes the use of driven visual stimuli and tuned SAM methods in a pilot study of retinotopic mapping using MEG; finding that activity in the primary visual cortex can be distinguished in four quadrants and two eccentricities of the visual field. Chapter eight is a novel implementation of the SAM beamforming method in the investigation of a subject with migraine visual aura; the method reveals desynchronisation of the alpha and gamma frequency bands in occipital and temporal regions contralateral to observed visual abnormalities. The final chapter is a summary of main conclusions and suggested further work.

For Karlina

3

Acknowledgments.

Table of Contents

Table of Figures

Chapter 1

Function and Organisation of the Human Visual System

1   Function and Organisation of the Human Visual System.

1.1   Overview

Chapter one is a basic introduction to the human visual system, providing an overview of how information from the visual world is transferred to the visual cortex and the organisation of processing units within the brain. It begins with a description of the anatomy and physiology of the visual structures and continues by explaining how the light received by the eye is converted to electrical signals conducted to the brain. Following this an explanation of the intermediary brain structures, the lateral geniculate nuclei (LGN) and superior collicular nuclei (SCN) and their role in our understanding of visual-cortical organisation is provided. Subsequently the arrangement of the visual cortex is described, including the organisation of the retino-cortical projections and briefly the topic of retinotopy is introduced. The visual cortex is then discussed more comprehensively, including the known details of cellular arrangement in primary visual cortex (V1) and the projections to other areas. The functional specialisation of cell populations, enabling the representation of such stimulus features as orientation and direction are succinctly discussed, as are distinctions between simple and complex cells.

The magnocellular and parvocellular pathways, ventral and dorsal streams and the dual stream hypothesis are discussed, followed by anatomical and functional description of the extra-striate visual cortical areas; V2, V3, V3a, V4 and V5.

The aim of this chapter is to provide a simplistic overview of the human visual systems structure and sufficiently introduce the reader to the matters further discussed in the experimental chapters.

1.2   Visual Input

1.2.1   Introduction

The visual system receives and processes electromagnetic energy in the 400 to 700 nanometre range, comprising 'the visible spectrum'. This energy is transformed into electrical energy/impulses by the photo receptors of the retina which are then transmitted to the visual cortex of the brain.

1.2.2   The Eye

Light enters the eye through a system of refractive lenses and is projected onto the retina at the rear of the eye. The retina converts the light into a neuronal signal which is conducted to the brain via the optic nerve (fig. 1-1).
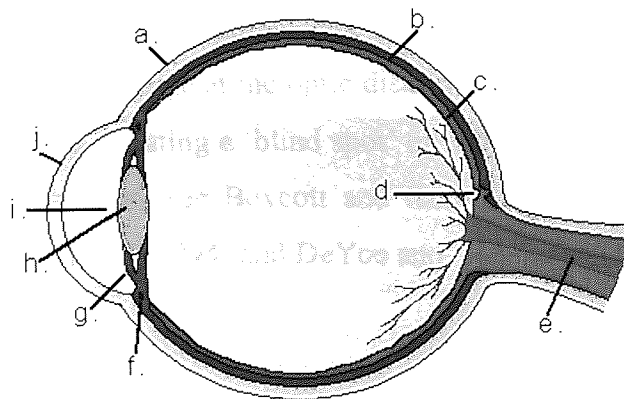
Figure 1-1. The Eye. (a.) The Sclera. (b.) The Choroid. (c.) The Retina. (d.) The Fovea. (e.) The Optic Nerve. (f.) The Cilliary Body. (g.) The Iris. (h.) The Crystalline Lens. (i.) The Pupil. (j.) The Cornea.

Light entering the eye is focused onto the central point of the retina (also known as the 'fovea') by a dual lens system. The cornea performs initial light refraction, whilst the crystalline lens performs 'fine focusing' adjustments. Ciliary muscles relax, increasing lens diameter for far vision and contract decreasing lens diameter to focus on near objects, enabling the eye to remain focused on objects as their position and distance change. The iris adjusts the pupil (the aperture) to accommodate the amount of light in the environment, making the pupil larger in low light and smaller in bright light. The lens system projects an inverted image onto the retina at the rear of the eye, which then conveys the information to the optic nerve.

1.2.3   The Retina and Fovea

The retina is a ten-layered sheet of receptor and nerve cells lining the inside of the eye directly opposite the lens. The retina of each eye has approximately 126 million receptor cells containing photosensitive pigments that convert the electromagnetic energy projected via the lens into specific neural impulses. The receptors comprise approximately 120 million rods and 6 million cones.

The *macula lutea*; a small, circular area of the retina with yellow pigment is responsible for high acuity vision. The image is focused on the macula, which contains the fovea; where visual acuity is highest. The fovea contains densely packed red and green cones, is absent of rods or blue cones and is where we experience our sharpest, most acute vision and colour discrimination. The yellow pigment of the macula absorbs short-wavelength (blue) light, as does the lens. The foveal pit contains no blue cones and so we are effectively colour blind for blue at the point of sharpest focus on the retina, resulting in better blue perception in the periphery and reduction of foveal resolution of detail.

The converted electromagnetic energy from the photoreceptors selectively activates the ganglion nerve cells in subsequent retinal layers, which collect and aggregate nerve impulses and have axons that converge at the optic disk to form the optic nerve. The optic disk has no photoreceptor cells, creating a 'blind spot' on the retina. For reviews of retinal neuron composition and properties see Boycott and Kolb (1973); Schiller and Malpeli (1978); Schiller *et al.,*(1986); Kolb (1994) and DeYoe and Van Essen (1988).

1.2.4   Rod and Cone Receptors

The photoreceptor population of the retina are composed of rod and cone receptors, which encode the extreme range of light conditions that humans can perceive. Rods are responsible for low light or 'scotopic' vision and cones for moderate to bright light or 'photopic' vision.

Rods have exceptional light sensitivity and can respond to a single photon. They are a thousand times more sensitive, but slower to respond to light than cones. They are primarily distributed in peripheral visual field, are unable to detect colour and are the reason for our perception in shades of grey under dim light conditions.

Cones are responsible for colour vision; encoded by three types of cone receptor: long wavelength or 'L' cones are red sensitive, medium wavelength or 'M' cones are green sensitive and short wavelength or 'S' cones are blue sensitive. Cones are responsible for high resolution images and also encode information about image luminance.

Rods and cones differ in their retinal distribution; in the fovea only cones are present, the cone density decreases rapidly outside the fovea and becomes fairly equal in the peripheral retina.

1.2.5   Retinal Coding

The outputs from the three types of cone are able to encode enough information to determine luminance level at supra-scotopic levels and decipher 12 million colours (Wandell, 1995). This is explained by the 'opponent process theory', by which addition or subtraction of outputs creates three distinct chromatic pathways. L+M cones provide an achromatic luminance channel, L-M cones provide a red/green channel and S-(L+M) cones provide a blue/yellow channel. The luminance channel dominates when resolving detail and plays a key role in spatial vision through form perception and high acuity and in temporal vision through discrete motion perception.

The retinal representation of the visual scene is conveyed in a largely parallel manner that begins with receptor specialisation in the retina, where processing of colour content is one specialisation. Other cells respond to pattern, with spatial frequency specificity determined by receptive field size. Some cells are edge detectors and differentially respond to precisely oriented edges, whilst others respond to motion speed or motion direction. Firing patterns of the cell population are equally complex, as some fire when stimulated, whilst others fire continuously until stimulated (Levitan and Kaczmarek, 1997). This complexity of encoding at the retina is merely the input encoding device, which provides sufficient permutations of differential signals for the brain to decipher the perceived visual world.

1.2.6   The Retinal Projection

The retinal ganglia project from various regions of the retina and consequently encode information concerning specific regions of visual field. These project to the lateral geniculate nuclei (LGN) in the thalamic region and superior colliculus (SCN) in the brainstem region of the brain. The parvocellular (P) ganglion cells (primarily from the fovea) project to the LGN, whilst the magnocellular (M) ganglion cells (primarily from the periphery (see p20)) project to both the LGN and the SCN.

The arrangement of features in the visual scene is projected onto the retina, which in turn is projected to the LGN in a manner which preserves the retinal location and segregates the neural arrangement into functionally distinct layers (Hubel and Weisel, 1977; Perry *et a.l*, 1984; Rodieck and Watanabe, 1993). The way in which the visual

features and retinal location are then projected to specific cortical locations in a mapped manner is referred to as 'retinotopy' (section 1.4.5).

The retinal ganglion cells from each location in the retina project to the contralateral LGN (fig. 1-2). The visual input from the right side of the visual scene is projected onto the left side of the retina, which in turn is projected to the left hemisphere of the brain. This visual signal preservation is the same in the opposite side of the visual field. The ganglion cells cross over at the optic chiasm and terminate in the LGN, before being projected to the visual cortex. For information on the connections of the LGN see Schiller and Logothetis (1990) and Schiller *et al.* (1990a, 1990b).
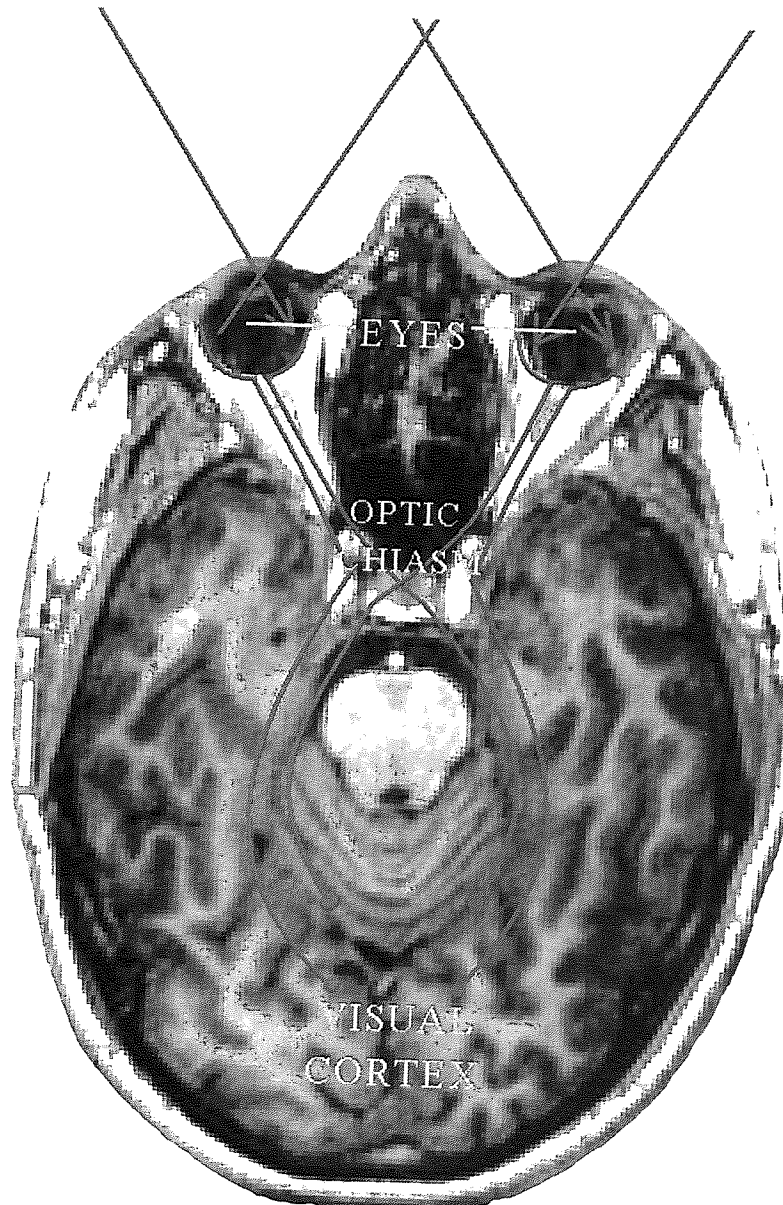
Figure 1-2. The visual projections from the eye to the visual cortex. Schematic demonstrating the flow of information from the left of the visual scene (green) and the right of the visual scene (red) from the retina to the visual cortex in the contralateral hemisphere.

1.2.7 The Lateral Geniculate Nuclei (LGN) and Superior Colliculus Nuclei (SCN).

The primate LGN has been widely investigated; there are two LGN, one in each hemisphere of the brain, located in the thalamus. Staining of the LGN with Golgi materials reveals six distinct layers. Perry *et al.* (1984) used the tracer 'horseradish peroxidase' to identify the locations to which different cell types send their projections. They discovered that approximately 90% of retinal gangion cells project to the LGN; most of which were classified as magnocellular or parvocellular cells. The four superficial layers of the LGN are the parvocellular layers, whereas the two deeper layers are the magnocellular layers. There are also cell bodies between these layers called intercalated zones (Fitzpatrick *et al.*, 1983). Accordingly, the parvocellular and magnocellular axons of the retina terminate in the associated areas in the LGN; the intercalated zones may receive signals from a further distinct class of neurons of the retina.

Each layer contains a complete map of half of the visual field arranged in register (Wandell, 1995) and therefore adjacent areas correspond to the same point in the visual field (Hubel and Weisel, 1977) (fig. 1-3). Further tracer experiments by Perry *et al.*,(1980) revealed that approximately 10% of the retinal ganglion cell projections terminate in the SCN. For a review of experiments revealing the anatomical and physiological basis of the early visual streams see Rodieck and Watanabe (1993). The LGN receives the majority of the retinal output; however of the connections in the LGN only approximately 10 percent of the synapses are efferent. The majority of the synapses (60%) are efferent and afferent connections with the visual cortex and the remainder are connections with other regions of the brain (Sherman and Koch, 1990).

The separate nature of the magnocellular and parvocellular layers extending from the discrete neuronal populations in the retina to their terminations in the LGN; at which point they are in distinct layers is largely accepted; however the extent of their segregation in the visual system is the substance of much debate.
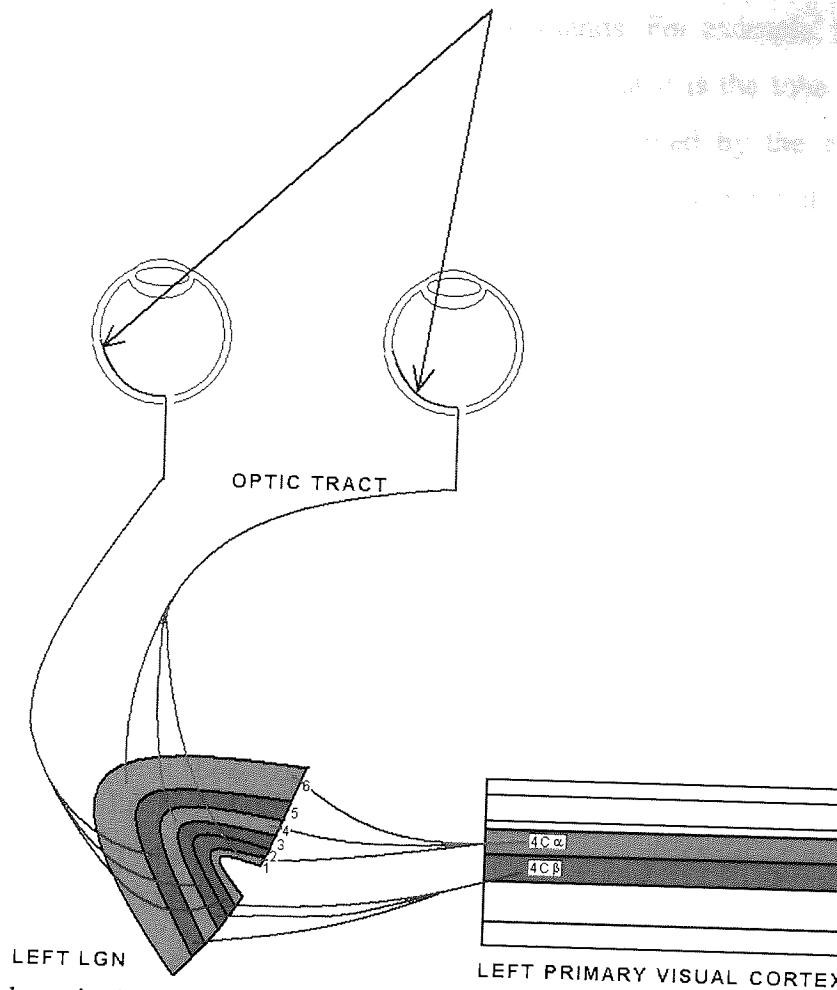
Figure 1-3. Visual cortical Projections via the lateral geniculate nuclei (LGN). Schematic demonstrates the projections from the retina of each eye and how it projects to the magnocellular (red) and parvocellular (blue) layers of the LGN and how these then project to layers 4Cα and 4Cβ of the primary visual cortex (V1).

1.3   The Visual Cortex

1.3.1   Introduction

The human cortex is a 2mm thick sheet of neurons with a surface area of 1,400 cm^2 (Hämäläinen, 1993). It is a folded structure and therefore structured into ridges called 'gyri' and troughs called 'sulci'. Important to the discipline of functional neuroimaging is the inter-subject diversity of the sulcal patterning in the human brain (further discussed in chapter 8). Although the major structures are present in the majority of individuals; such as the central sulcus, rolandic fissure and calcarine fissure (fig 1-4). However, the location of these structures has a degree of variation and smaller sulci even more so. The human brain is partitioned into four lobes by the common structural landmarks (fig. 1-4) previously mentioned. These are called frontal, parietal, temporal and occipital lobes, all of which have two hemispheres (left and right). The lobes are segregated to a large degree by the functions which they perform and the cell populations within a particular lobe are often

active in response to particular stimuli or functional demands. For example, the occipital lobe is also referred to as the visual cortex due to the fact that it is the lobe of the brain mainly engaged in the processing of visual information received by the eye. A large number of connections from the LGN project to the primary visual cortex; also referred to as V1, the striate cortex and Brodmann area 17.
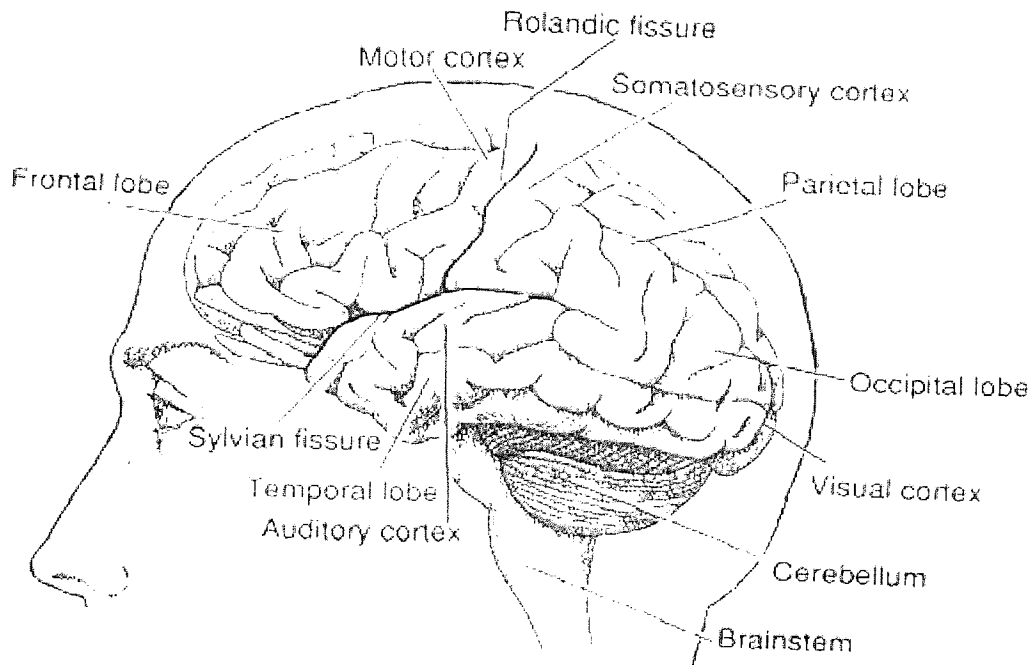
Figure 1-4. Location of the four lobes of the brain. Demonstrates the frontal, temporal, parietal and occipital lobes and the features by which they are demarcated (redrawn from Haines *et al.,* 2000).

1.3.2   Primary Visual Cortex (V1).

The primary visual cortex (V1) is a large cortical area, containing approximately 10^8 neurons, in comparison to the 10^6 neurons in the LGN (Wandell, 1995). V1 is the best defined area of the visual cortex, with anatomical boundaries agreed on by numerous studies throughout history (For example: Gennari, 1782; Brodmann, 1909 and Stensaas *et al.,* 1974. V1 extends over the depth of the calcarine fissure in the occipital cortex, but varies in size and precise location, producing a degree of difficulty in generalisation between subjects (tootell, 1998). There is much emphasis within the visual system on central vision. Around 80 % of cells in the visual cortex are dedicated to processing the central 10 degrees of vision. This is referred to as cortical magnification. The architecture of the visual cortex is arranged in a consistent manner to that of the retina and LGN and as discussed previously is retinotopically arranged in terms of visual field location (fig. 1-5). These features are relevant in chapters 3-7, as visual field stumilation dictates the region of expected cortical activation.
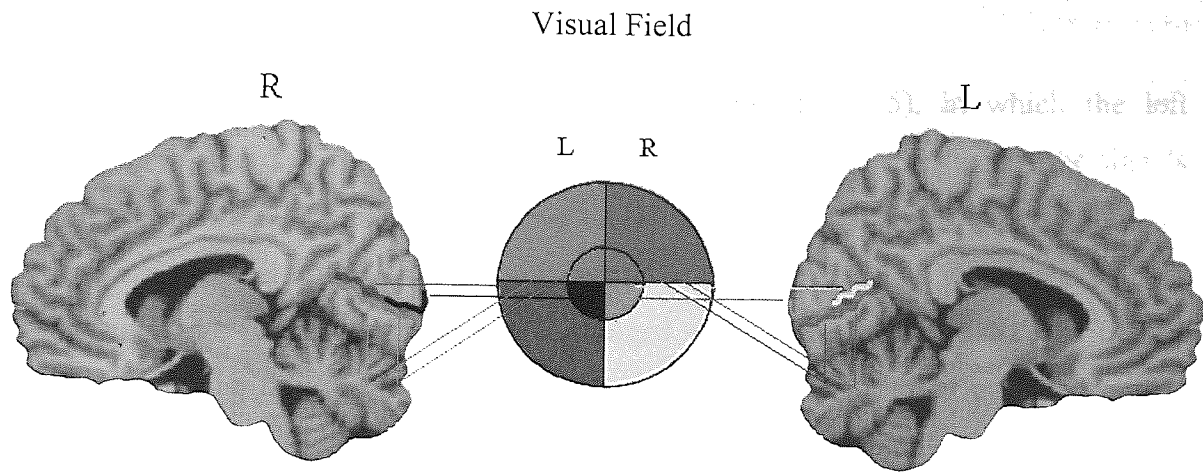
Visual Field

Figure 1-5. Retinotopic arrangement of the primary visual cortex in the human. 3D schematic of the representation of the visual field in the primary visual cortex. Quadrants of visual field project to the contralateral hemisphere and inverted bank of the calcarine sulcus (i.e. top to bottom). Central visual field projects to the posterior region of the visual cortex, whereas the peripheral visual field projects to the anterior.

V1 is segregated into six distinct cellular layers, based on relative density of neurons, axons, synapses and interconnections to the rest of the brain (Wandell, 1995). Superficial layer 1 has few neurons but many axons, dendrites and synapses, collectively called the 'neuropil'. Layers 2 and 3 consist of a dense array of cell bodies and local dendritic interconnections. This layer appears to have direct connections with the intercalated layers of the LGN (Fitzpatrick *et al.*, 1983; Hendry and Yoshioka, 1994). The outputs of layers 2 and 3 send their projections to other visual cortical areas and are difficult to distinguish based on simple histology stains. Layer 4 is subdivided into 4A, 4B and 4C, which in turn are subdivided by connective taxonomy. Layer 4B receives input from 4Cα and contains mainly cortical projections and axons. Layer 4C receives parvocellular and magnocellular projections from the LGN, with magnocellular projecting to the upper layer (4Cα) and parvocellular projecting to the lower level (4Cβ). Layers 5 and 6 contain relatively few cell bodies and send projections back to the SCN and LGN respectively (Lund *et al.*, 1975). The signals to and from area V1 are highly complex; the exact function of which is the subject of much speculation and investigation (Gray and McKormick, 1996; Engel *et al.*, 1997; Kreiter and Singer, 1996; Friedman-Hill *et al.*, 2000). Approximately 25% of all neurons in V1 are inhibitory (Wandell, 1995). The structure of the neurons leading from the retinas to the cortex defines many of the fundamental properties of V1, these are discussed in section 1.3.3.

1.3.3 LGN projections to V1

Each hemisphere has a restricted field of view (fig. 1-5), in which the left hemisphere receives only right visual field input and vice versa. Further to this the signals reaching the cortex interconnect respecting three other basic principles: firstly, they are organised with respect to the eye of origin; secondly, they are arranged with respect to the type of ganglion cell and thirdly, they are arranged with respect to the spatial position of the ganglion cell within the retina. Within the LGN information about eye of origin is preserved by the layered structure. The connections from the ipsilateral eye are in layers 2, 3 and 5, whilst the input from the contralateral eye connect to layers 1, 4 and 6 (fig. 1-3). The projections from the LGN to the primary visual cortex remain segregated in layers $4C\alpha$ and $4C\beta$.

1.3.4 Functional Specialisation of Visual Cortical Cell Physiology.

Information from the input to the retina is preserved at the cortical level and is arranged in a manner that affords optimal efficiency and maximal yield at the information processing stage (Fries *et al.*, 2001). Anatomical differentiation methods can visualise the ocular dominance columns (Hubel and Weisel, 1977; Bishop, 1984). Tritiated amino acids injected into the eye are transported from the retina to the cortex across synaptic junctions. Tangential sectioning and exposure of visual cortex to photographic emulsion reveals light and dark stripes corresponding with the presence of tritiated praline, revealing patterned arrangement of ocular-cortical connections, which are arranged in bands of approximately $800\mu m$ in the human (Hubel *et al.*, 1978; Horton and Hoyt, 1991). In superficial layers of V1 many neurons respond to signals from both eyes, approximately 80% of which are binocularly driven.

1.3.5 Retinotopy

The majority of information entering visual cortex first passes through V1, although there is also a sub-cortical route going via the midbrain that projects to the prestriate cortex, it is after this stage that incoming information from the retina is amalgamated. The collection of cells in each hemisphere of V1 forms a topographic map of the contralateral hemifield of visual space. The organisation of the projecting neurons directly relates to the region of the retina from which they originate; hence the term 'retinotopy'. Implanted electrode experiments by Brindley and Lewin (1968), Dobelle *et al.*,(1978) and Bak *et al.*,(1990) identified that the eccentricity of the stimulus with regard

to the central point of vision can be mapped onto the surface of the Calcarine Sulcus, with the central 10 degrees of vision (the fovea) having proportionally the largest anatomical representation (fig. 1-6). Additionally, the receptive fields (RFs) in V1 increase in size the further out into the periphery they get; consequently the RFs projecting from regions close to the fovea are small and highly specific, whereas the RFs of peripheral cells are larger and less specific. The boundaries of the visual areas can be demarcated and regional stimulus specificity defined using specific sequences of visual stimuli with functional magnetic resonance imaging (fMRI) (Sereno *et al.,* 1995; Tootell *et al.,* 1997, 1998 a,b). The interested reader may find details of the methods in DeYoe *et al.,* (1996); Sereno *et al.,* (1995); Engel *et al* ., (1997); Goebel *et al.,* (1998); Wandell, (1999) and Press, (2001), this subject is further discussed in chapter 7, where it forms the basis for the work described.
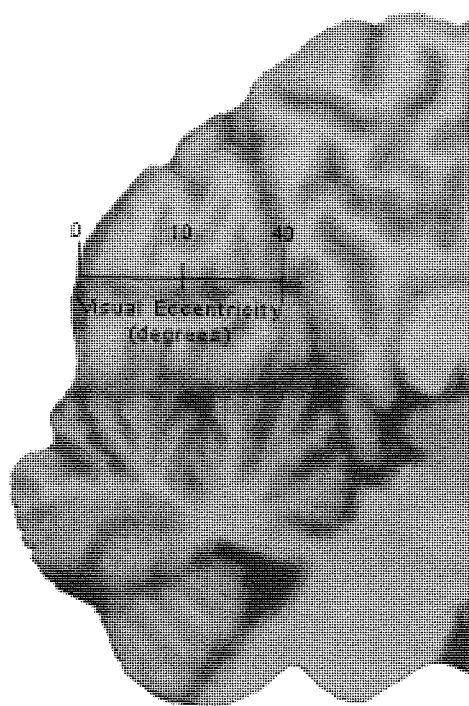
Figure 1-6. Cortical representation of visual eccentricity. Superimposed scale indicates the approximate region devoted to the processing of foveal (0-10°) and peripheral (>10°), this demonstrates that foveal processing occupies anatomically the majority of the visual cortex.

Visual cortical neurons display further degrees of specificity (Hubel and Weisel, 1959, 1962, 1968, 1977; Hubel, 1982). Some are direction sensitive, responding to stimuli moving in one direction but not the opposite direction. Some are binocular, responding to stimuli from both eyes and others are orientation selective. The receptive field properties are the result of neural computations that occur at the visual cortical level, affording analysis and classification of form, texture, motion and the estimation of depth. The

majority of cells in V1 are termed 'simple cells', for which the exact position of the stimulus with regard to the receptive field is critical, as even a small displacement results in a profound decrease in the response (Hubel and Weisel, 1965). This can be determined by an informal test of linearity (Skottun *et al.*, 1991), where the response of simple cells to complicated shapes can be directly derived from the response to small spot stimuli (Hubel, 1988). However, complex cells do not satisfy superposition; therefore the response of complex cells to sweeping a line across the cells receptive field cannot be obtained from individual flashes of the line.

1.3.6   Orientation Selectivity

Simple cell receptive fields differ from those of retinal ganglion cells or cells in the LGN. The receptive fields of simple cells consist of adjacent excitatory and inhibitory regions, as illustrated in fig. 1-7. Simple cells display orientation selectivity, in that they respond to stimuli in some orientations better than others; the orientation that evokes the maximal response is defined as the cell's preferred orientation (Wandell, 1995). Orientation preference is arranged in columns of similarity (Hubel and Weisel, 1977; Hubel and Livingston, 1987; Obermayer and Blasdel, 1993; Blasdel, 1992 and Tootell *et al.*, 1983). These orientation columns converge at particular points, shown to be high in cytochrome oxidase (Hubel and Livingston, 1987; Blasdel, 1992). These regions are of high metabolic activity as all orientations activate cells at these points, giving rise to a negative correlation between cytochrome oxidase and orientation selectivity; although the visual-functional significance of the enzyme itself is unknown (Wong-Riley, 1979; Humphrey and Hendrickson, 1980; Livingston and Hubel, 1982; Hendrickson, 1985). The interested reader may find reviews of these experiments in Hubel and Livingston (1987) and Wandell (1995).

In V1 orientation selective neurons are found in layers 2 and 3, but are quite rare in layer 4. Simple cell receptive fields consist of adjacent excitatory and inhibitory regions that are longer in one direction than the other (fig. 1-7), where the main axis of the receptive field defines the preferred orientation. Stimuli oriented along the main axis of this field are more effective at exciting or inhibiting the cell than stimuli in the other direction. The arrangement of the contributing cell population determines the type of response i.e. excitatory or inhibitory and the overall length of the cell arrangement determines the spatial specificity of the receptive field.
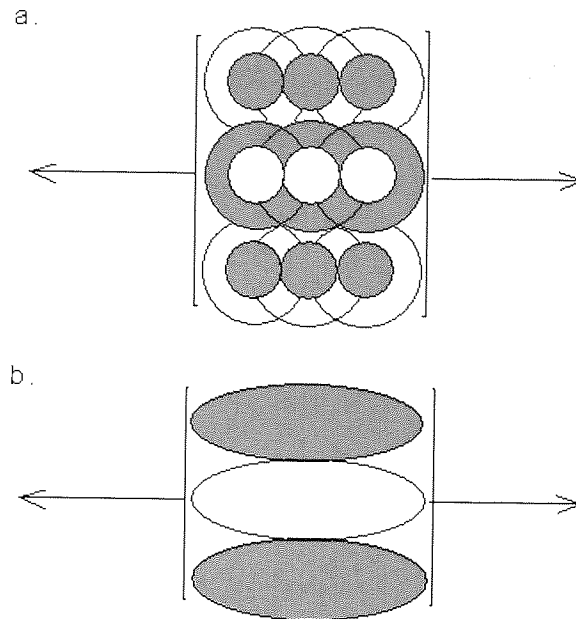
Figure 1-7. Receptive fields of simple cells. (a) The underlying layout of the cell population, with differential 'excitatory' or 'inhibitory' centre and surround determines the overall receptive field layout (b). The longer the arrangement of cells in the population, the longer the receptive field of the cell.

1.3.7   Direction Selectivity

Hubel and Weisel (1968) found that certain cortical neurons in the monkey respond well when a stimulus moves in one direction and poorly or not at all when in the opposite direction; a feature called 'direction selectivity'. This was shown using moving bar stimuli, to which the cells demonstrated orientation selectivity that favoured a specific motion direction. The direction selective neurons in the cortex are found in certain layers of the cortex and are relatively rare or absent in other layers. The main layers in which activity occurs are 4A, B, Cα and 6 (Hawken, 1988). These layers receive input mainly from the magnocellular pathway and send projections to selected brain areas such as area V5 (human homologue of MT) (Dubner and Zeki, 1971; Zeki, 1983a,b, 1990a,b, 1993). The specific mechanism underlying the direction selectivity process is unclear, but it is suggested that it might be the result of orientation selective neurons activated with temporal displacement that afford a cumulative response in a particular direction (Wandell, 1995).

1.3.8 Contrast Sensitivity

Simple and complex cells can be discerned by their response to contrast-reversing sinusoidal gratings. The simple cell response appears as a half wave rectified sinusoid, whereas a complex cell demonstrates a full wave rectified sinusoid (fig. 1-8). This demonstrates that simple cells display a frequency which matches that of the stimulus, whereas the full wave rectification of complex cells means that they demonstrate a 'frequency doubling' effect (harmonic), which is a typical property of cells in visual area V1 (De Valois *et al.*, 1982).
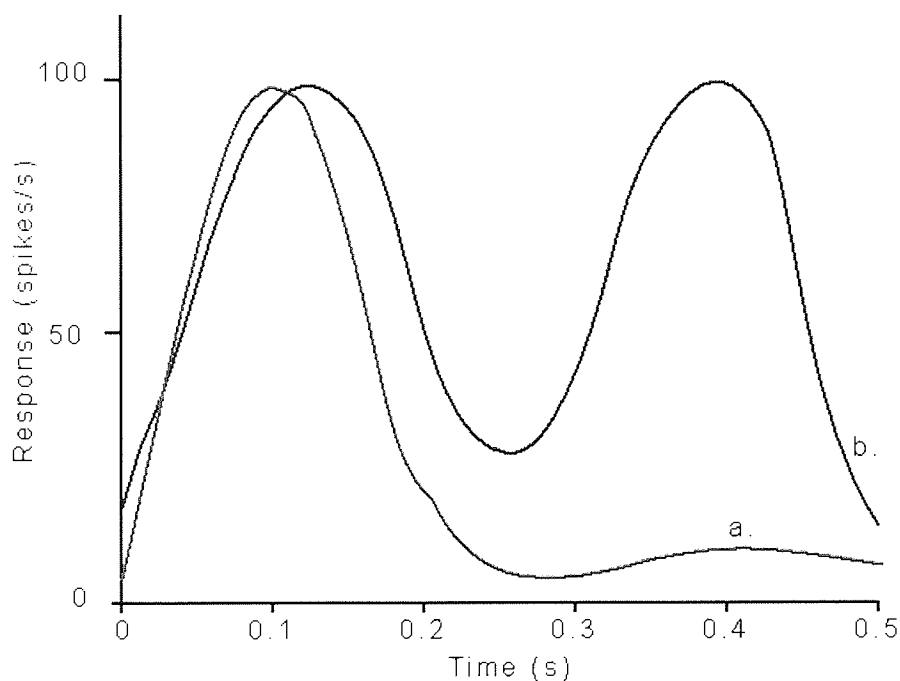
Figure 1-8. Contrast Reversal response. (a) Simple cells response with a half wave rectified sinusoid (red). (b) Complex cells respond with a full wave rectified sinusoid (blue) (redrawn from De Valois *et al* (1982)).

1.3.9 Contrast Response

Movshon *et al.* (1978a,b) and Tolhurst and Dean (1987) tested the linearity of cat simple cells and found that they could predict quantitatively a range of simple cell responses from the measurements of the simple cell contrast sensitivity function. The contrast response function at the cellular level is thought to be a non-linear process, due to the differential response to spatial frequency (section 1.3.10). A number of models have been suggested to describe and explain how this process occurs, for example Heeger (1992) suggested that the process is the result of the neurons initial linear response, determined by the contrast of the stimulus divided by a second signal, determined by the

pooled activity of the population of cortical neurons. The result is that the response is dependent upon individual neuronal specificity and neuronal population sensitivity. This non-linearity serves the purpose of adjusting the saturation level so that it depends on the neurons sensitivity enabling the neuronal response to remain constant across a wide range of contrast levels. The interested reader may find further recent work in this area in (Watson and Solomon, 1997; Kontsevich and Tyler, 1999; Boynton *et al.*, 1999; Graham and Sutter, 2000; Yu and Lee, 2003 and Hammett *et al.*, 2003). The cortical response to varied contrast is a widely debated topic and is discussed in greater detail in the introduction to chapter 5, where cortical contrast response is investigated as the basis for investigating photosensitive epilepsy.

1.3.10 Spatial frequency

The contrast sensitivity function of both classes of cortical cells is narrower than those of the retinal ganglion cells and within small distances of the visual cortex there is considerable variation in the most effective spatial frequency of the stimulus (Shapley, 1990). This suggests either a further processing step or a further cellular distinction that remains unidentified in the visual cortex. However, the question of how a discrete patch of retinal neurons recombine to produce the varied spatial receptive field properties of the visual cortex remains unanswered. Throughout this thesis grating stimuli are commonly used that have spatial frequency of 3 cycles per degree (cpd). This is based upon the finding that 3cpd is the most effective spatial frequenct in eliciting cortical responses.

1.4 The Visual Streams

1.4.1 Introduction

The previous sections discussed the flow of information from the retina to the cortex. It is clear that there are visual streams that begin at the retina and continue along separate neural pathways to the brain. The receptive field properties of the neurons become progressively more sophisticated, with cortical neurons showing greater specificity than those of the retina. The specialisation continues throughout the cortex along with a degree of separation in the visual streams. The complexity of the computations involved in visual encoding are reliant upon the properties of the cortical neurons.

1.4.2 The Magnocellular and Parvocellular Pathways

Although the segregation of the visual streams continues to be the source of much speculation and debate due to the numerous interconnections at all stages of the visual streams, there is much evidence to suggest that, although not necessarily isolated, the

magnocellular and parvocellular pathways play distinctly different roles in visual processing. The magnocellular pathway is the portion of the visual system concerned with perception of form, motion, depth and subtle luminance differences. M cells produce transient, rapid responses to stimulation; their speed is due to heavy myelination of the LGN projections to the primary visual, secondary visual and parietal cortex (McGuire *et al.*, 1989). This structural difference means that nerve impulses in the magnocellular projections reach visual cortex 7-10 ms faster than those in the parvocellular pathway and are thought to facilitate fast localisation and identification of visual features (Steinman and Steinman, 1998), however the M-pathway has lower acuity and poorer resolution with regard to the P-pathway.

The parvocellular pathway is concerned with the perception of detailed spatial vision, colour, reading and discrete information analysis. P-cells have a sustained response, with constant response for the duration that the stimulus is in the receptive field (RF). The magnocellular pathway is generally categorized as the transient attention or 'where' pathway, whilst the parvocellular pathway is the sustained attention or 'what' pathway (Ungerleider and Mishkin, 1982; Merigan and Maunsell, 1993, Steinman and Steinman, 1998). The centre of the visual field is devoted to a very small area of the retina (the fovea), yet requires the most detailed processing and so is given the largest share of the available cortex (Sekular and Blake, 1984). Classification of the M and P pathway functions has been extensively studied with lesioning studies in the macaque monkey (e.g. Merigan, 1989; Merigan and Maunsell, 1990 and Schiller *et al.*, 1990a). These studies used ibotenic acid to create lesions specific to the magnocellular or parvocellular regions of the LGN and recorded responses to specific visual stimuli. It was discovered that parvocellular lesions resulted in loss of colour distinction, whereas magnocellular lesions dramatically affected response to flicker and motion.

1.4.3   Cortical Termination of LGN Projections

Physiological measurements reveal the convergence of magnocellular and parvocellular streams on individual neurons in the visual cortex (Malpeli *et al.*, 1981; Nealey and Maunsell, 1994). These experiments demonstrated the ability of lidocaine and g-aminobutyric acid (GABA) to block the activity of these pathways by administration at discrete regions of the LGN, important in defining the projections as excitatory or inhibitory. Support of the overlapping neuronal inputs is provided by retrograde tracer studies identifying the separate pathways (Lachica, 1992). As previously discussed; cytochrome oxidase experiments demonstrate the connectivity between visual area V1 and

the adjacent area V2, particularly the projections from layer 4B (Livingston and Hubel, 1982, 1987a); these studies reveal a striped appearance in primary visual cortical areas.

1.4.4   The Ventral and Dorsal Pathways

Although the magnocellular and parvocellular pathways essentially terminate in the visual cortex, the projections to further visual cortical areas remain segregated in the majority of their projections. At progressively later stages of the pathways there are increasing numbers of cross connections between the visual areas and therefore the visual streams. However, for the purpose of simplicity in functional neuroimaging it is often necessary to refer to the separate processing pathways; this is particularly true of investigation of higher visual cortical processing and behavioural studies.

The divided cortical streams send their projections to the inferior temporal lobe and the posterior parietal lobe (Baizer *et al.*, 1991) and are referred to as the ventral and dorsal streams respectively. Baizer *et al.*, (1991) report that the input to parietal areas comes primarily from the peripheral visual field, whilst the neurons in the temporal lobe receive most of their input from locations near the fovea, supporting the concept that the separate visual streams perform separate tasks (Ungerleider and Mishkin, 1982). The functional specialization of the two pathways is generally regarded as consistent with the magnocellular and parvocellular specialisations in primary visual cortex, which then project in a serial manner through higher visual cortical areas that undertake more sophisticated processing of the projected signals. Clinical support for the two stream hypothesis is observed in patients with damage in the parietal stream of one hemisphere; a condition known as 'hemineglect', whereby they have difficulty orienting or reaching for objects in the visual periphery (Ungerleider and Mishkin, 1982, Merrigan and Maunsell, 1993). Conversely, clinical symptoms of damage to the temporal stream are an impaired form discrimination or recognition and impaired visual memory. However, the full extent of segregation in the visual streams is unclear as there are a number of known connections between the two areas as indeed each visual area exhibit numerous projections to several other visual cortical areas (Rockland and Pandya, 1979; Felleman and Van Essen, 1991).
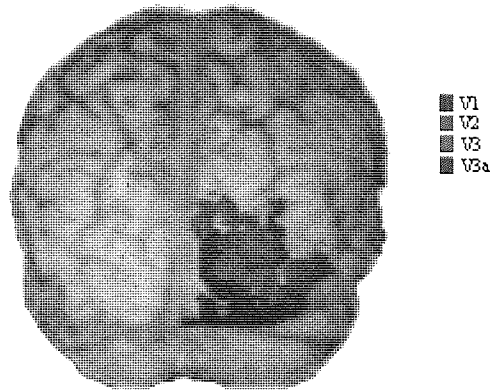
Figure 1-9. Visual areas. 3-dimensional image of visual areas V1 (blue), V2 (green), V3 (red) and V3a (purple) as defined using retinotopic stimuli in fMRI BOLD experiment.

1.4.5   Extra-Striate Visual Areas

The past two decades have seen numerous experiments in various modalities explore the functional significance of discrete regions of the visual cortex. Experiments by Zeki (1980, 1983, 1993) found colour contrast to be particularly effective in activation of area V4, forming the basis for the theory that it is the area responsible for colour perception. Similarly, movement related activation of neurons in area MT determined this as the motion area (Dubner and Zeki, 1971). Livingston and Hubel (1984a,b, 1987a,b, 1988) formed theories of the perceptual streams, anatomy and the perceptual significance of the spatially progressing visual signal, which supported Zeki's views and hypothesised spatially defined regions for the processing of colour, form, stereo and motion (for a review see Livingston and Hubel, 1988).

1.4.6   Area V2

Cortical area V2 is difficult to distinguish from the adjacent extra-striate areas based upon cytoarchitecture identified by cytochrome oxidase dispersion. The majority of projections in V2 originate in V1 and project on to other extra-striate areas (Zeki and Shipp, 1988; Van Essen et al., 1992). The retinotopic organisation of V1 that reflect the visual scene is also present in area V2, dictating that all points correspond to adjacent points of the visual image (Zeki, 1969; Cragg, 1969). V2 is located on the medial surface surrounding V1 and borders the lingual gyrus (Van Essen and Zeki, 1979). The function of V2 is not directly determined, but lends more toward being visually multi-modal rather than functionally discrete. It contains projections to most other defined visual areas (V1, V3, V4, V4A and V5) and as such has been suggested to play a role in the processes specialised at those areas. Roe and Ts'o (1995) suggest that V2 has three functional maps;

thin stripes containing a colour map, thick stripes containing a directional map and interstripes containing an orientation map.

1.4.7 Area V3

Visual area V3 lies along the medial side of the brain along the cuneus and lingual gyrus (Van Essen and Zeki, 1979). Early studies by Zeki (1978c) suggest that regardless of colour content of the visual scene, cells in V3 respond to precisely oriented lines. From this V3 was suggested to be a region involved in the processing of form. fMRI is able to delineate V3 based on polar angle; and as such it is classified in terms of Talairach coordinates (Crognale *et al.*, 2002).

1.4.8 Area V3a (accessory)

Visual V3a does not receive an input from V1, instead receiving projections mainly from V3. There are functional similarities between the two areas and although known to be distinct, the exact roles and full segregation is as yet unclear and as such is still generally referred to with V3 as the V3 complex (Zeki, 1993). However, a recent functional imaging study by Tootell *et al.* (1997) provided Talairach coordinates based upon functional investigation. An fMRI study by Kastner *et al.* (2000) recently found V3a to play a role in texture segregation. The study by Tootell *et al.* (1997) found V3a to be highly contrast and motion sensitive in their fMRI investigations. A discrepancy in the activation with the classical retinotopic stimuli however, suggests that this region may be reclassified as V3A and V3B (Press *et al.*, 2001), although it has been suggested that errors in the method requires complete re-evaluation of the dorsal occipital cortex (tootell and Hadjikhani, 2001).

1.4.9 Area V4

Visual area V4 is situated on the lateral side of the brain bordering V3A. It's primary input arrives from V2, however it also receives input from foveal regions of V1. It also has a further subdivision called V4A that receives input from V4, V2 and a small amount from V1, yet due to lack of functional distinction is usually only referred in conjunction with V4 as V4 complex (Zeki, 1977). Originally functionally determined by macaque studies (Zeki, 1973, 1977), it has been supported by more recent studies (Desimone and Schein, 1987) including human functional imaging (Zeki, 1993) to be

responsible for colour processing. It is seen to be wavelength selective indicating preservation of retinal encoding of the cone photoreceptors (section 1.2.4). Furthermore it plays a part in the detection of motion and has recently been found to play a part in texture segregation (Kastner *et al.*, 2000). Schiller (1993) found only mild deficits in colour detection and discrimination in monkeys with selective lesions of V4. Schoppig *et al.* (1999) found that V4 plays an important role in colour constancy (Clarke *et al.*, 1998) and colour short-term memory, but not in simple colour discrimination. Suggesting a role in colour processing but not wavelength specificity; indeed, recent subdivision of this region suggests a separate segment responsible for much of the colour processing; referred to as V8 (Hadjikhani *et al.*, 1998).

1.4.10   Area V5

Visual area V5 (Zeki, 1983a, 1983b) lies along the superior temporal sulcus and extends laterally bordering V4 (Dubner and Zeki, 1971). It is often referred to as area MT (middle temporal) from the original identification in the owl monkey (Dubner and Zeki, 1971). It receives direct projections from area V1 and is generally found to be responsible for various aspects of motion processing (Zeki, 1983a, 1983b, 1993). The response in implanted electrodes was seen in the rhesus monkey to respond to stimuli on one direction but not in the opposite direction and was unresponsive to other attributes.

Chapter 2

Magnetoencephalography (MEG): Neuronal Basis, Hardware and Signal Analysis Techniques

2 Magnetoencephalography (MEG): Neuronal Basis, Hardware and Signal Analysis Techniques

2.1 Overview

Chapter two is an introduction to the emerging functional imaging modality 'magnetoencephalography' (MEG). It begins with a description of the components included in the MEG system, using the Aston Neuromagnetometer as a specific example and discusses the use of the super conduction quantum interface device (SQUID) which requires a dewar (vacuum) to maintain cryogenic temperatures to facilitate superconduction. It continues by discussing the issue of noise reduction and the methods of attenuation and cancellation, including the use of a magnetically shielded room (MSR) and design of the flux transformer; in particular magnetometers and gradiometers and the sensor array used in the Aston MEG system.

Following this is a section that focuses on the neuronal basis of the magnetic signal measured with MEG. This section details the action potential, post synaptic potential and the generation of electrical current and therefore magnetic field generation; briefly discussing the issues of open and closed morphology of cells and corresponding net magnetic field generation. The subsequent section introduces the technical details of MEG source localisation; including the computation of the relationship between measured field and cortical activity (the forward problem) and the estimation of the primary current given the non-uniqueness of the measurement (the inverse problem).

Finally the chapter discusses the approaches to solving the inverse problem using various signal analysis methods. It describes in brief detail some of the available methods, such as: multiple signal classification (MUSIC), minimum norm estimate (MNE) and low resolution electromagnetic tomography (LORETA). In addition those methods employed in the experimental chapters: dipole fitting with Monte-Carlo statistical analysis, synthetic aperture magnetometry (SAM) and 'group SAM', virtual electrodes (VEs) and time-frequency analysis are described in more detail.

The aim of this chapter is to introduce the reader to the methods used throughout the thesis and provide an understanding of the physiological significance of the recorded MEG signal.

2.2 Background

Magnetoencephalography is an emerging functional imaging modality used to investigate neuronal activity in the human brain (Hämäläinen, 1993). Since its inception as a crude single channel system in 1968 when David Cohen and colleagues (Francis Bitter Magnetic Laboratory, MIT) first detected alpha activity from the human brain (Cohen, 1968); it has progressed to a state of the art whole head system incorporating up to ~300 channels with detection thresholds several orders of magnitude higher than the original systems. MEG is a technique closely related to electroencephalography (EEG), which measures electrical potentials arising as a result of underlying neuronal activity in the various cortical layers of the brain. An obstacle associated with analysis of the EEG signal is current conduction through biological media. The variability of such factors as skull thickness and the conductivity values of the different tissues, even at the individual level, makes it very difficult to accurately distinguish the sources generators of an EEG signal (Barkley, 2004) (further discussed in section 2.8.3). Conversely, MEG is based on magnetic fields associated with underlying electrical currents. Magnetic fields are less restricted by biological tissue and can therefore be measured in a manner that is able to provide more accurate estimates of source location based upon relative field strength (see Barkley, 2004 for a review). There are difficulties associated with the measurement of magnetic signals due to the many strong environmental magnetic fields, which act as noise sources in the recording of brain activity. In addition, there are further difficulties associated with source localisation within an unknown volume such as the head and in confidently determining the number of active sources underlying a signal. These problems are the 'forward' and 'inverse' problems and are described along with their solutions in this chapter.

2.3 MEG Instrumentation

An MEG system is composed of a series of components designed to detect magnetic fields with optimal sensitivity in an environment which maximises the signal to noise ratio (SNR). SNR is maximised at the acquisition level by use of a flux transformer such as the gradiometer (used in the MEG system at Aston) to reduce noise conduction to the Super Conducting Quantum Interface Device or SQUID (Zimmerman, 1970). Further to this a magnetically shielded room (MSR) is used to shield external environmental noise. SNR is further optimised by filtering and rejection methods included in the signal

computation and finally at the analysis level using specifically designed computing algorithms to reject noise and artefact to an optimal level.

2.3.1   The Super Conducting Quantum Interference Device (SQUID)

The neuromagnetic field created by the activity of the cortical neurons is in the femtoTesla (fT) range (1 fT = 10^{-15}T). A typical MEG signal is 50-500fT (Hämäläinen, 1993). This is comparatively weak alongside environmental magnetic fields such as the Earth's magnetic field (10^{-4} Tesla). The SQUID is the only device with sufficient sensitivity for high quality biomagnetic measurements (Zimmerman *et al.*, 1970; Ryhanen, 1989). The SQUID comprises a loop of superconducting metal, formerly composed of Lead (Pb) alloys and Niobium (Nb), but now constructed from refractory metals. Superconductivity refers to a material having an electrical resistance of zero. The SQUID construction is completed by interruption by two Josephson (1962) junctions, a non-superconducting material that interferes with the flow of current allowing quantifiable measurements of electron flow. The materials used in SQUIDS are superconducting at cryogenic temperatures of 4K (-269°C), which requires the use of a vacuum insulated vessel called a Dewar containing liquid helium (LHe).

2.3.2   The Dewar

The cryogenic submersion of the superconducting components requires a constant supply of liquid helium (LHe) in the system. Because of the difference in temperature between LHe and the environment (~280°C) there is a constant state change in the helium which is lost as a gas at a rate of approximately 11 litres per day for a whole head MEG system (151 channel Omega, CTF systems Inc.). In order to maintain the low temperature of the LHe, it is contained within a vacuum container called a 'Dewar'. This component is constructed of fibreglass reinforced epoxy (non-metallic), normally constructed as a one piece head section for structural integrity and optimal cooling of the integrated SQUID circuitry.

2.3.3   Noise Reduction

2.3.3.1   Flux Transformers

Because of the SQUIDs sensitivity to magnetic field variations it is necessary to use a flux transforming device, known as a 'Gradiometer' as an initial receiver prior to flux transfer to the SQUID. The gradiometer is a type of magnetometer composed of a series of coils that are differentially affected by a magnetic field as a function of its decay (proportional to the square of the distance). Consequently, a gradiometer measures the gradient of the magnetic field rather then the magnetic field itself (Vrba, 1997) and is able to reject distal magnetic interference (noise). The purpose of using gradiometers is to cancel unwanted sources of interference. Various gradiometer configurations are shown in figure 2-1. The lower coil is called a pickup coil, where the coil wound in the opposite direction is called compensation coil with the distance between the two coils referred to as the baseline; an arrangement also known as a first-order gradiometer. This type of coil is optimal for use under realistic environmental noise conditions and in the construction of multi-channel systems; hence it is used in the Aston MEG system.
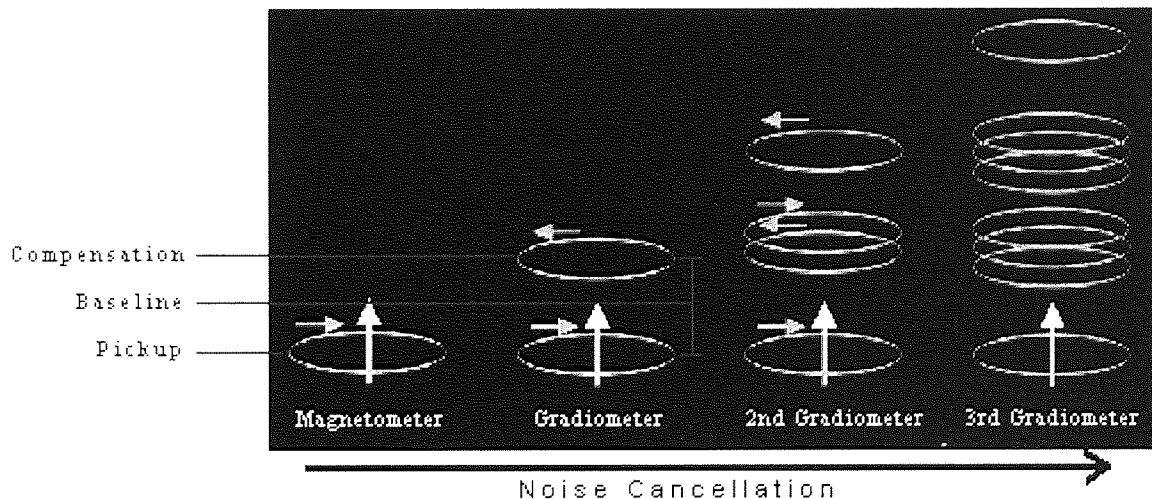
Figure 2-1. Schematic diagram of flux transformer type and noise cancellation. Demonstrates some of the various flux transformers including the first order gradiometer used in the Aston MEG system (Redrawn from CTF Systems Inc., Port Coquitlam, Canada (http://www.vsmmedtech.com/ctf/techlib/MEG_theory.asp)).

2.3.3.2   The Magnetically Shielded Room (MSR)

Environmental magnetic noise is produced by numerous factors including vehicles, electrical devices, mains power supplies and geomagnetic sources (Hämäläinen, 1993). All of these sources produce magnetic fields several orders of magnitude larger than the

biomagnetic signals generated by the human brain (fig. 2-2). It is for this reason that the MEG system is typically housed in a magnetically shielded room (MSR) (fig. 2-3b). The cancellation of noise by the use of gradiometers and adaptive cancellation is in the order of 10^4, whereas the added shielding provided by the MSR further increases noise reduction to approximately 10^6. The magnetic shielding is generated by the use of layered μ metal, which provides adequate ferromagnetic shielding by generation of eddy currents, which cancel the magnetic noise from the environment (Cuffin and Cohen, 1977).

Magnetic Fields

B (Teslas)
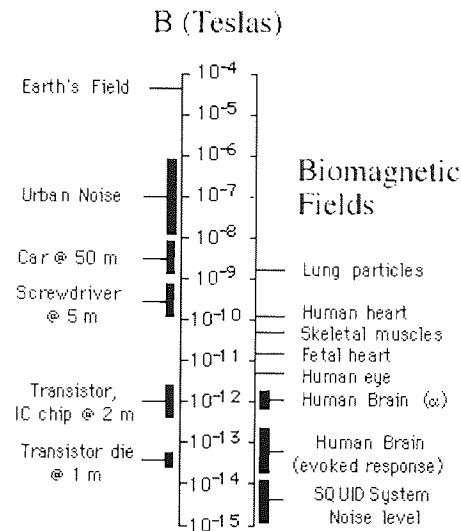
Figure 2-2. Magnetic field strengths of the human brain compared to noise sources, Reproduced from CTF Systems Inc., Port Coquitlam, Canada (http://www.vsmmedtech.com/ctf/techlib/MEG_theory.asp).

2.3.4   The Sensor Array

The array of sensors in a modern MEG system comprises between 150 and 300 sensors. These sensors are arranged in a manner which places them as close to the head as possible (~2-3cm), with an average sensor spacing of 3.1cm (CTF Systems 151 Channel System) spanning the entirety of the head. Provisions are made in the shape of the helmet for access to the ears and eyes for auditory and visual presentations (fig. 2-3a).

2.3.5 Head Localisation

During the course of an MEG experiment it is essential that the subjects head does not move significantly with respect to the sensors; thus it is often secured using an inflatable cuff. However, the head movement must be verified with respect to the sensors in order to accurately reconstruct the source location. This is done by recording the position of a set of three digital coils before and after the scan and using a bite bar system (fig. 2-3c) and a spatial digitisation system (Polhemus Isotrak, Kaiser Aerospace Inc.) (fig. 2-3d) to reconstruct the surface of the scalp. The scalp surface is then coregistered with the individual subjects MRI volume scan using the software 'Align' (www.ece.drexel.edu/ICVA/Align/align11.html). The interested reader can read further details on: bite-bar creation, digitisation and coregistration in appendix C.
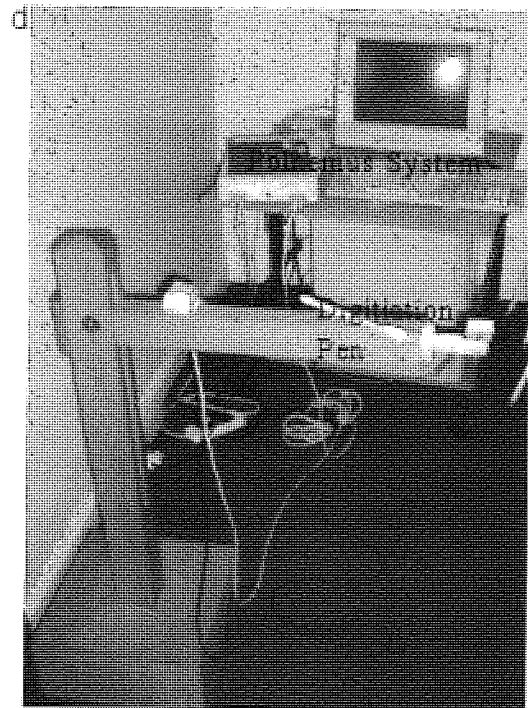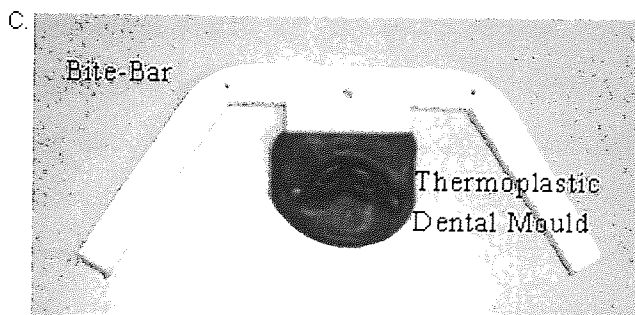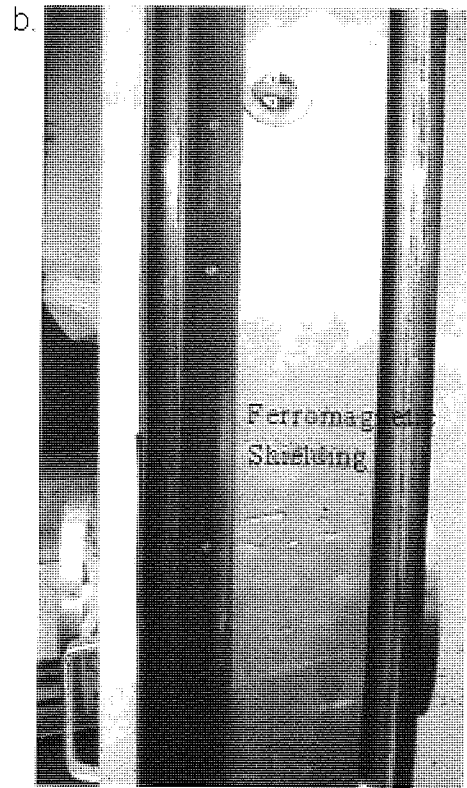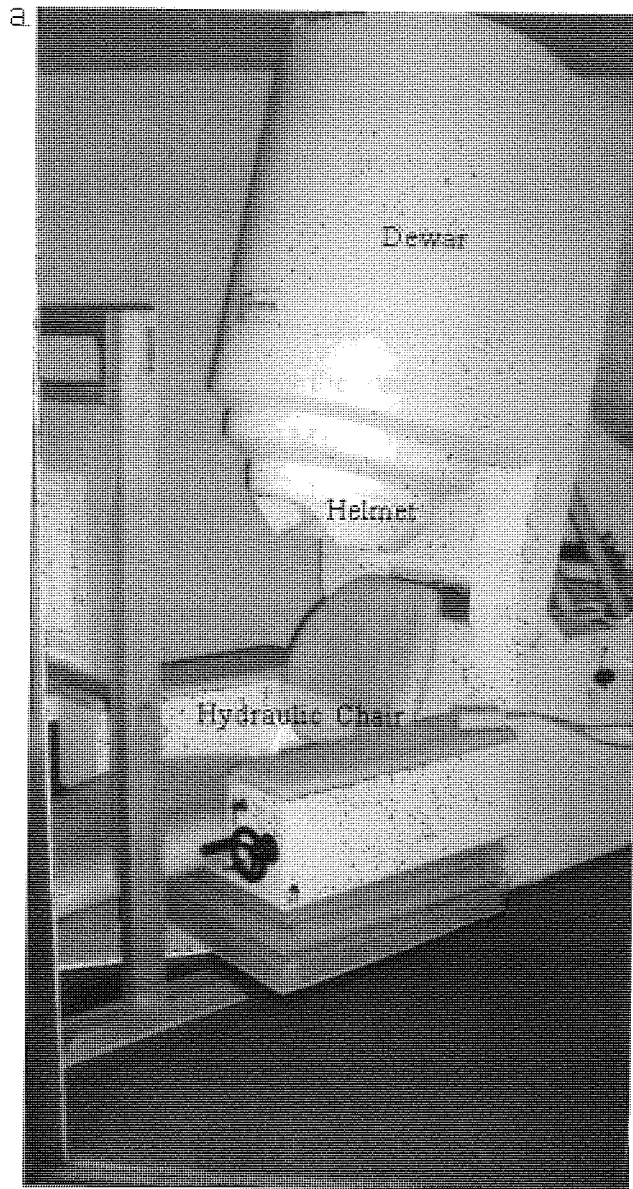
Figure 2-3. Meg system and recording environment. (a.) MEG system. (b.) Magnetically shielded room (MSR). (c.) Bite-Bar. (d.) Polhemus head digitisation system.

2.4 The Neuronal Basis of the MEG signal

The magnetic signal measured by the MEG sensors outside the head is induced by electrical activity occurring inside the head. Using MEG, the minimum magnetic field measurable from within the human head is approximately 10^{-13} Tesla (Hämäläinen, 1993), which reflects the simultaneous activity of $>10^4$ cortical neurons. The neuron is the cellular unit of current generation associated with the magnetic field reflected in the MEG signal, with current generated by the ionic flux occurring in and around the various compartments of the cell. The primary MEG signal is thought to be the result of the intracellular current and post synaptic potentials (PSP) occurring at the receptive terminal of the synaptic cleft (Okada, 1982; Wikswo, 1989). Recent results indicate that the intracellular current from dendrites also contributes significantly to the measured magnetic field of MEG (Okada, 2000).

2.4.1 The Neuron

The neuron is the excitable cell responsible for the generation of the neuromagnetic signal measured by MEG. The neuron shares the properties of most other cells, containing the necessary organelles for metabolic processes. It has a soma (cell body) containing the nucleus and other organelles, but also has structures specialised for cellular communication called 'dendrites' and an 'axon'. Ionic conduction across these structures results in the excitation of neighbouring cells dependent upon the electrical properties associated with the activation status of the extra-cellular environment. There are several phases of excitable behaviour which result in electrical current generation by the neuron, all of which depend upon the alteration of endogenous ion concentrations. The first stage of activity is the action potential, which is initiated by depolarisation of the axon. This is then followed by repolarisation of the axon and synaptic activation at the terminal end of the axon. The plasma membrane of the neuron is essentially a capacitor and resistor in parallel. It provides resistance to the flow of ions between intra and extra cellular compartments and accordingly it can be thought of as a resistor with membrane resistance (Rm) measured in Ohms (θ). In addition, the lipid bi-layer provides an extremely thin insulating layer between two conducting solutions, allowing the membrane to act as a capacitor (a device capable of separating and storing electrical charge), with membrane capacitance (Cm) measured in Farads (F). The charge across the cell is determined by the ionic balance of the intra and extra cellular solutions determined by sodium (Na+), Potassium (K+), Chlorine (Cl-) and various organic (A-) ion fluxes across the cell membrane. In the cortical

layers of the brain there are the specialised neurons that give rise to the MEG signal, which are mainly generated by the pyramidal cells (fig. 2-4).
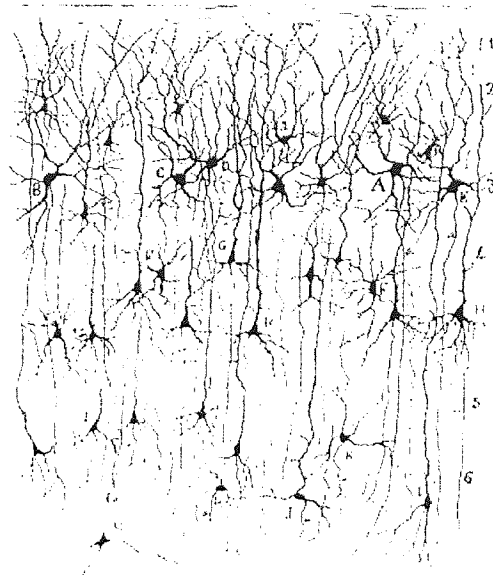
Figure 2-4. Image drawn by histologist Ramon y Cajal in 1888. Showing a Golgi stained transverse section of rat cortex (3mm thickness). 1% of neurons are stained enabling observation of: (H) Pyramidal Cells and (F) Stellate cells.

2.4.2 The Action Potential

The action potential is an 'all or nothing' event which is dependent upon the electrical state of the cell, determined by the potential difference across the cell membrane (expressed as internal relative to external) or membrane potential (Vm). The resting potential (Vr) of the cell is typically around -70mV. The action potential event is a depolarisation which occurs if an influx of cations reduces the membrane potential beyond a threshold value (typically Vr + 10-20 mV). Above the membrane threshold, voltage gated sodium channels (VGSC) allow rapid ionic influx, which cascades along the axon resulting in depolarisation of the neuron, at which point Vm becomes approximately 50mV. An ensuing efflux of K+ ions (hyperpolarisation) returns the Vm to a negative value (typically Vr – 10-15mV), termed 'after-hyperpolarisation' and is a period of inactivity for the cell. The internal compartment of the axon incurs an 'intracellular current', whereas the surrounding extracellular compartment has ionic flux which give rise to an 'extracellular (volume) current' (fig. 2-6b). For a review of the ionic transfer involved in action potential propagation see Wikswo (1989).
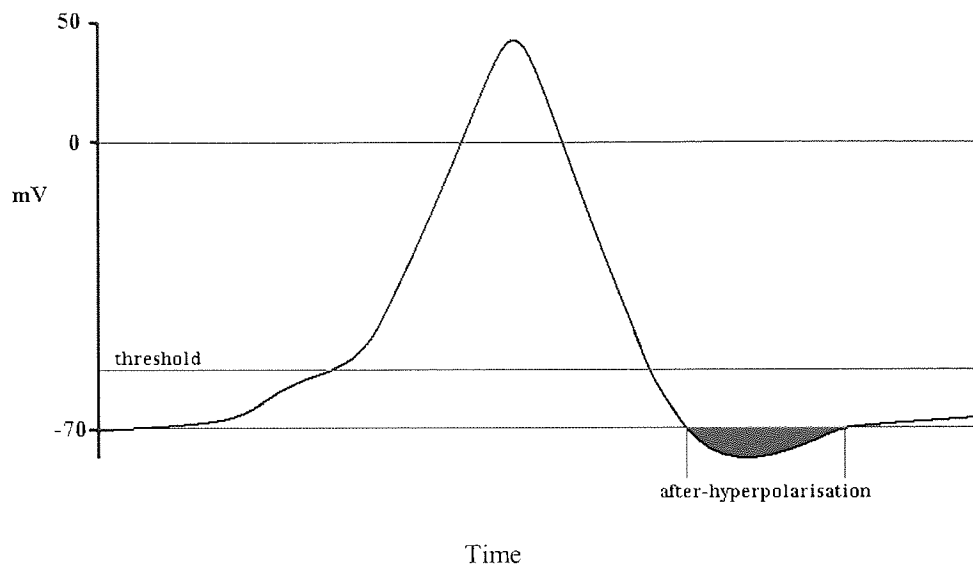
Figure 2-5. Schematic representation of an action potential. Showing typical threshold voltage (~-50mV), resting potential (~-70mV) amplitude (~50mV) and after-hyperpolarisation (shaded green).
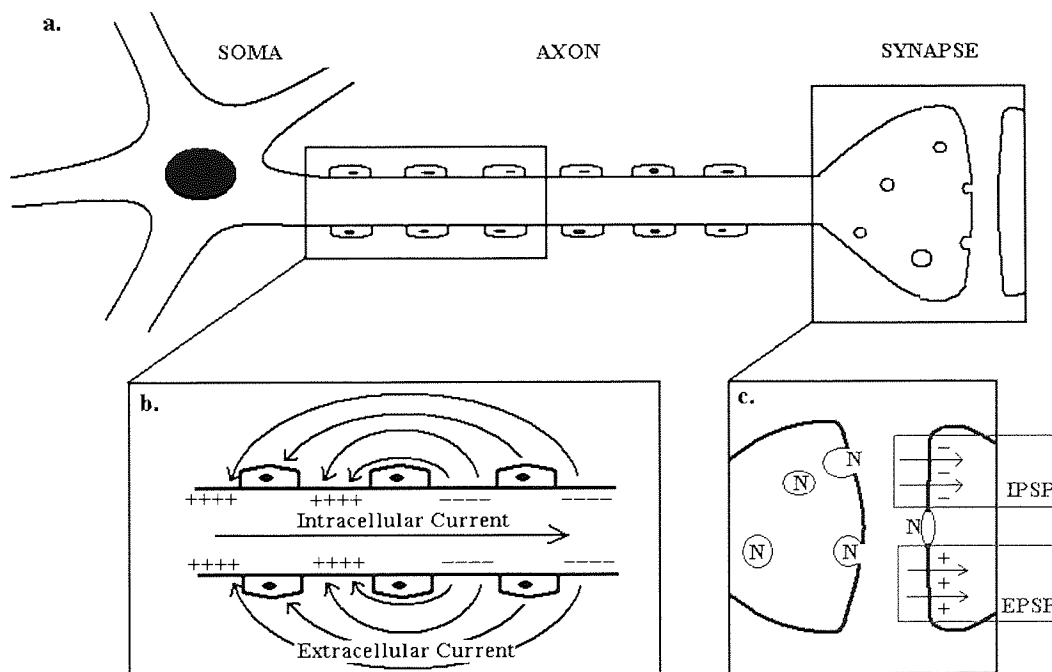
Figure 2-6. The electrical properties of the neuron. (a.) the structure of the neuron showing the cell body (Soma), axon and synapse. (b.) the intracellular and extracellular (volume) currents generated by the propagation of an action potential. (c.) synaptic activity showing neurotransmitter (N) release bringing about an excitatory or inhibitory post synaptic potential (EPSP and IPSP respectively), dependent upon the neurotransmitter.

2.4.3   The Post Synaptic Potential (PSP)

Following propagation of the action potential down the extent of the axon the elevated cation level activates voltage gated calcium channels in the synaptic terminal. An influx of calcium ($Ca{++}$) brings about neurotransmitter release into the synaptic cleft (fig. 2-6c). The specific neurotransmitter type determines the activity at the post synaptic membrane and is specifically determined by receptor interaction. An excitatory neurotransmitter such as Glutamate (glu) causes increased membrane permeability to sodium ions ($Na+$) whereas an inhibitory neurotransmitter such as gamma-amino butyric acid (GABA) elevates permeability to chlorine ions ($Cl-$). The response of an inhibitory post synaptic potential (IPSP) is the opposite of an excitatory post synaptic potential (EPSP). An EPSP results in an elevated cation concentration, which induces an action potential, whereas an IPSP increases the anion concentration, resulting in a hyperpolarized neuronal state which effectively alters the activation threshold of that neuron.

2.4.4   The Magnetic Field

As discussed previously, the ionic movements at various locations of the neuron result in current generation in and around the cell (figs 2-6 and 2-7), which give rise to fields. As a result of specific physical attributes at the cellular, tissue and organ levels, only certain currents give rise to measurable magnetic fields outside the intact human head (Okada, 1982). The movement of ions across the axon membrane generates a transmembrane current (J^i) (fig. 2-7). However, the cylindrical nature of the axon and therefore radial symmetry of ionic flow (fig. 2-7) results in cancellation of opposing fields and therefore no measurable contribution to the MEG signal (Swinney and Wikswo, 1980; Plassey, 1981).

The intracellular current (J_i) and extracellular current (J_e), collectively known as the primary current (Jp) are the main source of the magnetic field (B) measured in MEG (Okada, 1982; Tripp, 1983). Experimental evidence in various *in vitro* preparations (Okada, 1982, 1989) demonstrates that the intracellular current is directly related to the evoked magnetic field and is therefore likely to be the main contributor to the MEG measurement.
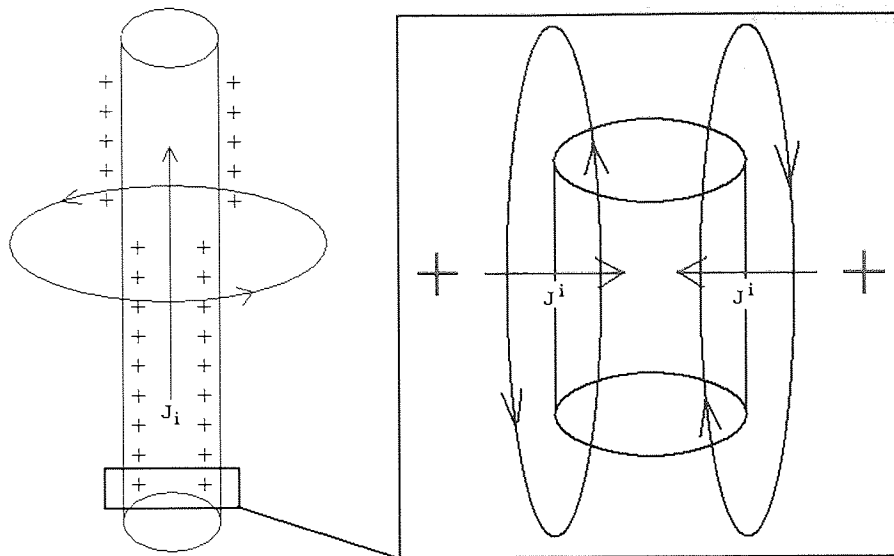
Figure 2-7. Magnetic field generated by the neuron. Left schematic demonstrates the intracellular current produced along the axon as a result of ionic displacement (primary current). Right schematic demonstrates the transmembrane current flow and demonsrates how symmetrical opposition of current flow causes cancellation.

The physical attributes of the cell are equally important in determining its contribution to the measured magnetic field; As discussed by Okada in Williamson et al., (1981). The overall magnetic field depends upon 'open' or 'closed' field morphology of the cell and its detection outside the head is related to its tangential or radial orientation. Stellate cells (fig. 2-8a) typically have 'closed field' morphology, with dendrites extending radially from a central soma, which generates self cancelling magnetic fields. Pyramidal cells (fig. 28b) typically have 'open field' morphology consisting of dendrite, soma and axon in a linear arrangement, effectively generating a net magnetic field.
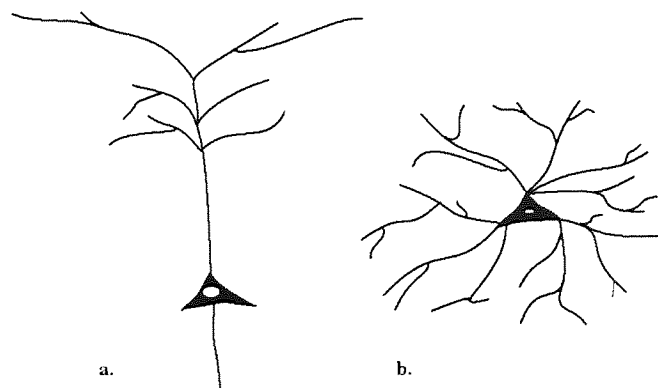
Figure 2-8. Cell type and field generation. (a) Pyramidal cell generates an open field and (b) stellate cell generates a closed field.

As described by Geselowitz theory (Geselowitz, 1970), the measured magnetic field is due to the tangential components of the primary current. The radial sources are not detected outside the head. This dictates that the signal detected in MEG are primarily

generated by the sulcal wall. As explained by Hillebrand and Barnes (2003) this poses relatively little problem due to the fact that only orientations less than 15 degrees perpendicular to the surface are truly silent and because of the nature of cortical activation (typically activates extended cortical regions), the majority of activations will incur some tangential component, suggesting that distance from the sensors is the greatest restriction due to detectability (Hillebrand and Barnes, 2003).

2.5   Source Localisation

2.5.1   Introduction

Each of the MEG sensor channels records magnetic field fluctuations over time. In their simplest form these data are typically displayed as traces which represent cortical activity on a millisecond by millisecond basis. This can be displayed as a field map, which is a 2-dimensional representation of the magnetic field fluctuations over the entire channel space. The topographical arrangement of signal measurements can be used to compute location of active brain areas by solving the inverse problem (section 2.7.3). However, before this can be done it is first necessary to solve the forward problem (section 2.7.2).

2.5.2   The Forward Problem

The forward problem is the one of computing what the output of the gradiometers would be if a certain region of cortex were active; thus, although data from individual sensors can be recorded it is of no use in source localisation until its neuronal significance is determined. In order to do this it is necessary to make some assumptions about the source itself and the head within which it is generated. The source itself is typically modelled as a current dipole (Okada, 1982) and a patch of active cortex may be considered as a layer of current dipoles (Meijs *et al.*, 1988). This single dipole model (for a review see Snyder, 1991) is largely successful in MEG, because at the sensors measurement distance (2-3cm) many sources appear dipolar (Hämäläinen and Sarvas, 1989; Hari, 1991). The dipole model forms the basis for all signal analysis methods, including minimum norm and beamforming methods. However, the discrete variability of cortical activity now detectable using contemporary methods encourages the search for more appropriate models (chapter 9).

In a similar approach to the modelling of the source as a dipole; the head is most simply modelled as a volume conductor. Unlike EEG, where the different conductivity profiles of the tissues require detailed models such as the boundary element model (BEM)

or finite element models (FEM) (Gezelowitz, 1970; Hämäläinen and Sarvas, 1989), the effects of tissue on magnetic fields are effectively constant. As a result of this in MEG it is usually sufficient to use a spherical model to represent the inner part of the skull (Mondt, 1989). Similarly a multiple spheres model (Huang, 1990) can be applied to model the structure of the brain more closely.

With these assumptions it is possible to use Maxwell's equations, determine the relationship between total current density, magnetic field and potential distribution, making the following assumptions:

- The medium is homogeneous and isotropic, turning all tensors into constant scalars.
- The magnetic permeability is that of free space.
- The medium is linear.
- Time dependencies of signals with frequencies far below 1 kHz, can be neglected for most values of the tissue parameters. Thereby neglecting the effect of capacitance and reducing the problem to a stationary one (Broek, 1997).

By applying the law of Biot and Savart to act as a spatial low pass filter, it is possible to compute solutions to the forward problem for different volume conductor models (Mosher *et al.*, 1997; Mosher *et al.*, 1999).

2.5.3 The Inverse Problem

The inverse problem is one of estimating the primary currents from the measurements of potentials (EEG) or magnetic fields (MEG) at the surface of the head. However, the solution to this problem is non-unique in that there are an infinite number of source configurations that could produce the same measured field or potential. This problem is further complicated by the existence of magnetically or electrically silent sources. In MEG it is found that radially oriented sources fail to produce a magnetic field outside a spherically symmetrical volume conductor (Baule and McFee, 1965; Cuffin and Cohen, 1977, 1983; Wood *et al.*, 1985). Furthermore, cells with closed field morphology (fig. 2-8) (Okada, 1982) and tissues of spiral-like conductivity (Roth and Wikswo, 1986) consequently produce no measurable magnetic field. However, recent findings suggest it is the entirely radial sources which prove silent rather than only entirely tangential sources that are detectable (Hillebrand and Barnes, 2002).

The non-uniqueness problem has no direct solution (Helmholtz, 1853) and therefore in order to reduce the non-uniqueness it is necessary to add *a priori* information. These constraints are typically assumptions made about the temporal or spatial extent of the activity. A common spatial constraint is the use of the subject's anatomical MRI to reconstruct the cortical surface. Similarly the orientation of the sources can be constrained, making the assumption that most sources are perpendicular to the cortical surface, as

majority pyramidal cells are (Okada, 1982; Snyder, 1991). Temporal constraints typically relate to the time course of the neuronal activity with respect to a known factor, such as the onset of a stimulus. These constraints are widely used in many approaches to the inverse problem (Scherg and Von Cramon, 1985a,b). The following section on analysis methods describes MEG analysis methods which introduce various distinct *a priori* assumptions to localise cortical activity. For a detailed description of the approaches to the inverse problem see Hämäläinen *et al.* (1993), Press *et al.* (1992) and Silvey (1978).

2.6   Analysis Methods

2.6.1   Overview

The signal acquisition process of MEG is the initial stage of the experimental procedure. The signal processing aspect of MEG is the major aspect of the process and is highly time consuming. In addition, due to the relative novelty of MEG at a hardware level, the signal analysis approach is in perpetual development. There are a wide range of approaches to investigating the spatial, temporal and spectral aspects of MEG data; discussed in this section. The various signal analyses methods available for solving the inverse problem are briefly discussed, together with a more detailed description of the analysis methods which are further developed and employed in the following experimental chapters.

2.6.2   Dipole Fitting

Dipole fitting is an approach to the inverse problem that approximates the current flow underlying field generation over a small area by minimising the measured and predicted field patterns in terms of the 'least squares'(fig. 2-9) (Scherg, 1985a). A typical approach is to determine the optimal fit at a given time interval time using either a variable or restrained orientation profile. A time window approach may be adopted to determine the size, orientation and strength of a specific dipole by the least squares estimate using a predetermined analysis time window. The dipole fit approach to source localisation enables the identification of time locked responses and requires the collection of multiple trials, averaged across trials effectively cancelling all non-time-locked amplitude fluctuations; considered in this approach to be noise. The signal to noise ratio (SNR) of time locked activity such as evoked potentials is therefore greatly increased. Dipole modelling is currently the most commonly adopted approach to solving the inverse problem. The sensor number and distribution of the current (150-300 channels) systems are optimal for use in

dipole fitting; i.e. an increased number would not improve resolution (Vrba, personal communication). However, although dipole fitting provides a good estimate of cortical activity, it is only useful in the analysis of time-locked events arising from focal sources and becomes increasingly unstable as the number of active sources increases.
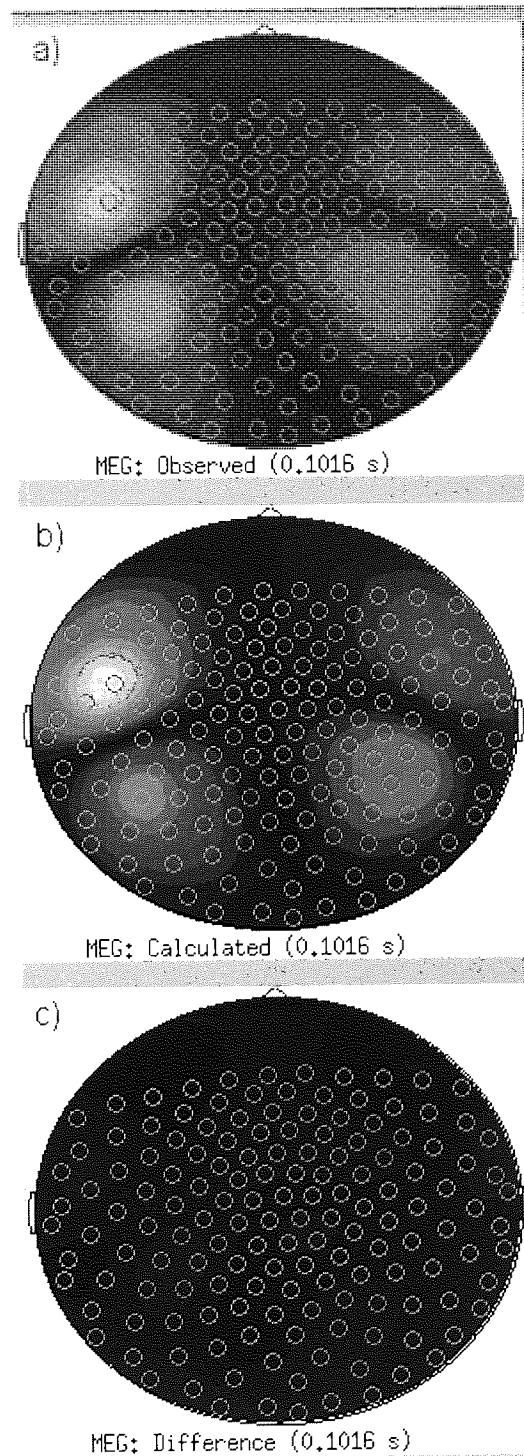
Figure 2-9. Field map demonstrating dipole fit calculation following auditory stimulation. The minimisation process using: (a) observed magnetic field. (b) calculated magnetic field and (c) difference or residual between the plots. Confident dipole placement (between red and blue) is represented by low residual difference.

Where dipole fitting is shown in this thesis a spatio-temporal fit algorithm was employed. This assumes that during the time interval of observation (evoked potential peaks) the activation(s) are stationary (i.e. variations in the field are due only to variations in the strengths of sources). The sources are positioned iteratively until they account for the maximum proportion of the temporal variance (Koles, 1998). In the present studies reduced chi-square error values are considered (Supek and Aine, 1997), in which error values equal to one indicate that differences between modelled and measured fields are equivalent to the noise (agreement between model and measurement). Error values substantially above one indicate that the source is over modelled (i.e. the modelling error is larger than measurement noise); whilst values substantially below one suggest that the source is under- modelled (i.e. the measured noise can be further explained by additional sources).

2.6.3   Monte-Carlo Analysis

Monte-Carlo statistical analysis is a method which analyses the stability of a source localisation, such as a dipole. Although theoretically it can be applied to most analysis methods, here it is described in conjunction with the dipole fitting method. In this method, following identification of an optimal dipolar configuration, a dipole fit to different iterations of noisy data is repeated many times (>100) resulting in a cluster of fit solutions, the volume from which a specific confidence boundary can be visualised (typically $p<0.05$) within which 95% of the solutions are located (fig. 2-10).

Figure 2-10. Example of Dipole and Monte-Carlo statistical volume located on a subject coregistered anatomical MRI. The orange represents the dipole localisation for time (t), whilst the green ellipsoid represents the 95 % confidence interval volume of the Monte-Carlo analysis.

6.4   Multiple Signal Classification (MUSIC)

The MUSIC algorithm (Schmidt, 1981; Schmidt, 198
entifies cortical activity based upon the assumption that the lea
urce locations are orthogonal to specific features of the noise
'81). Partitioning of signal and noise subspace requires an ad
creasing the probability of error. MUSIC can be used to an
tivity by 'prewhitening' the data using background MEG activi
is is often impractical, as it is not always possible to identify l
ily background brain activity. The technique has limitations bas
gnal-noise segregation and the prewhitening of the data, of
entified peak localisation. Further related techniques have
cursively applied and projected (RAP) MUSIC (Mosher and Le

6.5   Spatial Filtering

There are two general approaches to spatial filtering tec
ethod in which the filter weight is independent of the mea
ethod', in which the filter weight depends on the measureme
laptive spatial filter is the minimum-norm estimate or '
noniemi, 1984; Hämäläinen and Ilmoniemi, 1994; Wang *et al.*
amformer approaches, such as synthetic aperture magnetome
id Vrba, 1997) are examples of the adaptive approach.

6.6   Minimum Norm Estimate (MNE)

The minimum-norm spatial filter technique is based up
lage reconstruction in CT systems. This approach defines sc
easured and predicted fields and searching for the global minim
owever, as the number of solutions increases so too do the
creasing the likelihood of error, as the solution finds local r
inima. The impaired performance of the MNE is due to a misn
strumentation, rather than the method itself.

2.6.7 Low Resolution Electromagnetic Tomography (LORETA)

LORETA (Pascual-Marqui *et al.*, 1994; Wagner *et al.*, 1996) is another popular application of the non-adaptive spatial filter approach. Developed for use with EEG, it has subsequently been applied to MEG. This approach seeks to identify the 'smoothest' of all possible current distribution solutions, using a variation of the minimum norm formulation. It provides a low resolution, 'blurred' image of cortical electrical activity, which preferentially identifies superficial sources. It is frequently used in the analysis of visual and auditory evoked potentials.

2.6.8 Beamformers

'Beamforming' is an adaptive spatial filtering technique, of which there are two main approaches: the 'Eigen-vector' beamformer and the 'Scalar minimum variance' beamformer. The spatial filter weights are obtained by solving the constrained optimization problem. In the minimum variance algorithms, the filter weights are adjusted to minimize the total output signal power from sources outside the region of interest, whilst maintaining the signal from the source location. When using the scalar-type beamformer it is necessary to estimate the orientation to estimate the source activity at a specific location. As this is generally unknown, several techniques have been developed to identify an optimal estimate (Sekihara and Scholz, 1995; Mosher *et al.*, 1992). The application of a spatial filter weight vector focuses the sensitivity of a sensor array on a specific region of interest affording post-processing reconstruction of source distribution.

A problem with most adaptive beamformer techniques is a high sensitivity to errors in the forward modelling of the data covariance matrix, which often provides noisy spatio-temporal reconstruction. A technique called 'diagonal loading' was developed to overcome this performance problem (Cox *et al.*, 1987; Carlson, 1988). Diagonal loading uses the regularized inverse of the measurement covariance matrix, instead of its direct matrix inverse. This technique was then applied to the MEG source localization problem (Robinson and Vrba, 1999; Gross and Ioannides, 1999; Gross *et al.*, 2001); it is known that the regularization leads to a trade-off between the spatial resolution and the SNR of the beamformer output.

2.6.9 Synthetic Aperture Magnetometry (SAM)

Synthetic Aperture Magnetometry or 'SAM' was introduced as a method of signal processing for whole head MEG by Vrba and Robinson (1999). It is a non-linear minimum variance beamformer which provides tomographic images of cortical activity within a specified spectral frequency band. In contrast to the dipole method it does not provide a solution to the inverse problem. Rather, it reconstructs cortical activity in a manner that avoids the inverse problem (Robinson and Vrba, 1998). The basis for the technique lies in the beamformer detection method developed for fixed array radar (e.g. Van Veen *et al.*, 1988). It is a method by which the data from all sensors is weighted to provide information about neuronal activity at a particular location in the brain, which is then repeated to define the activity at all possible locations within the brain. In both radar systems and MEG this emphasizes changes which occur at every given location. In the case of the radar this might be a plane in the sky and in MEG an electrical source in the brain (fig. 2-11).
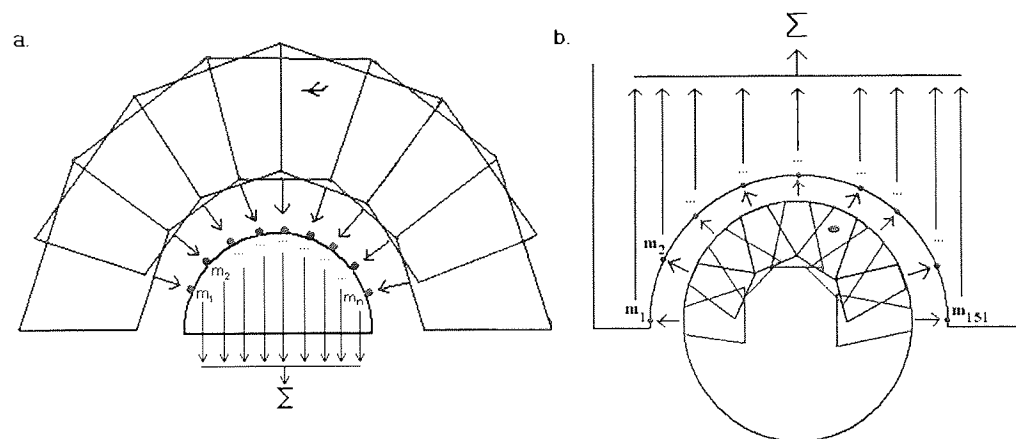
Figure 2-11. Schematic representation of SAM. Demonstrating the use of the beamforming method used in (a) radar and (b) SAM. Red and blue lines used only to clarify the non independent contribution of all sensors to the signal analysis.

SAM uses the distance sensitivity of the gradiometer (Vrba, 2001a,b) to optimally reconstruct the activity for voxels within the brain, by minimising the signal power for all other points within the three dimensional sensor space. At each voxel within the brain, the result is a fixed configuration of values or 'weights', which is independently defined for each sensor. SAM analysis is conducted by predefining a frequency range of interest and comparing the activity between two time intervals. The outcome of SAM is therefore an estimation of band-limited power change between conditions and therefore brain states. Its application as a subtractive method is a highly attractive advantage of the method and is particularly useful in identifying event related synchronisation/desynchronisation (ERS/ERD) (Pfurtscheller and Lopes da Silva, 1999a). For the interested reader details of

the method and review of its application are found in (Barnes *et al.*, 2000; Hillebrand *et al.*, 2004 and 'SAM in a nutshell' (appendix C)).

2.6.10   Group Analysis

2.6.10.1 Group SAM

In the analysis of groups of individuals using SAM, it is possible to observe activity that is common accross the subjects within that group. This is done using a method called 'group SAM', which uses spatial normalisation and averaging of SAM images. The method normalises the individuals brain and subsequent cortical activity to a common 'template' brain, creaed from an average of several hundred brains. This method uses a piece of software called *mri3DX* (Singh *et al.*, 2002) to effectively average activity from all brains and recreate this on the template brain.

2.6.10.2 Statistical non-Parametric Modelling (SnPM)

This approach is a statistically oriented approach based upon the statistical parametric modelling (SPM) software used for fMRI (http://www.fil.ion.ucl.ac.uk/spm). This approach is similar to that of group SAM in that it generates an image of activity of common location between subjecs in a frequency band of interest. SnPM uses the General Linear Model to construct pseudo *t*-statistic images, which are then assessed for significance using a standard non-parametric multiple comparisons procedure based on randomisation/permutation testing.It provides a thresholded statistical image on a glass brain template, utilising the data from a range of participants under the same experimental conditions and comparing the active and passive periods.

2.6.11   Virtual Electrode Analysis (VE)

As described previously, SAM analysis involves the description of each point in the brain by calculating the weighted sum of all sensors. This weights calculation can be used independently of the SAM algorithm to recreate the temporal activity at a given location. Subsequent to source localisation, if there is a specific region of interest (ROI), the peak SAM location can be defined (using CTF coordinates) and the neuronal activity at that

point in the brain reconstructed (Singh *et al.*, 2002; Barnes and Hillebrand, 2003; Fawcett *et al.*, 2004; Hillebrand *et al.*, 2004, Submitted; Hall *et al.*, 2004c).

2.6.12   Time-Frequency Analysis

In addition to reconstructing the neuronal activity at a given location, it is also possible to generate various time-frequency analyses of the activity occurring at a specific locus of activity using the virtual electrode method. This is done using the same SAM weights file created for a VE with the use of one of several methods. Most simply an averaged time-frequency spectrogram can be constructed using a Fourier-transform window, which is passed over sequential time segments to create an image of spectral change; alternatively, a Morlett-wavelet approach can be used which does not incur the same degree of time-frequency trade off that Fourier analysis does. Additionally, methods have been developed to facilitate statistical testing of spectral power change, of which Mann-Whitney, Bootstrap and permutation testing are available. Where time-frequency analysis has been used in this thesis, Morlet-wavelet, analysed with Mann-Whitney statistical testing has been applied.

Chapter 3

Development and Optimisation of MEG Analysis Methods

3 Development and Optimisation of MEG Analysis Methods

3.1 Overview

Chapter three is a collection of methods based discussions that detail the development of novel applications for existing analytical tools for application in various modes of investigation. The chapter is divided into four sections; the first three of which are developmental sections. The final section is a description of commonly used methods throughout the thesis as a direct point of reference. The first section describes the development of an analysis mode that allows observation of the cortical activity in an extended topographical region over time; using (1) a static 'virtual electrode cortical matrix' method and (2) a dynamic 'spectrographic movie' method. This latter method allows the observation of spectral activity in 3-dimensional space as it evolves temporally, the only restriction being the nedd for a predetermined frequency window.

The second section is a description of manipulations made of the recently developed SAM beamforming method, which describes three variation of its implementation for different types of analysis. This includes a short window method for evoked potential analysis, and a sustained 'tuning' approach used for steady state observation of driven cortical activity. Finally, a passive method is described for the investigation of temporally evoked activity, used in the investigation of such thing as cortical spreading depression (CSD) and with possible application in the investigation of neuronal substrate interaction. The third section is a description of an investigation into the effect of SAM image smoothness on the outcome and significance of subsequent group SAM and statistical non parametric modelling SnPM. In brief, this investigation finds that the typical SAM analysis approach finds a detailed solution in each of the individual subjects, which proves to be too spatially discrete in the computationally discrete in the computation of the group image. The results suggest that a method with greater smoothness (2-3cm) is the optimal method in the analysis of groups of subjects; based upon the visual cortex.

The final section is a collection of analytical details that are common to many of the thesis chapters; such as coregistration, visual presentation and calculation of Michelson Contrast, placed here for reference purposes. The aim of this chapter is to discuss methodological developments and considerations in order

that the reader may have a comprehensive awareness of them prior to their employment in subsequent chapters.

3.2 Virtual Electrode Cortical Matrices and Spectrographic Movies

3.2.1 Introduction

Recent developments in MEG analysis tools such as SAM, spectrograms and virtual electrodes provide interchangeable methods of investigating cortical activity in terms of spatial and temporal detail. However, these methods are essentially restricted to a single domain; SAM analysis generates a spatial map of cortical activity over a predefined time window, whilst virtual electrodes and spectrograms both generate representations of the time course of cortical activity at a predefined spatial location. Although able to identify activity with spatial and temporal accuracy, these methods require recurrent processing of the temporal information at each of the selected loci, which must subsequently be compared using the original spatial map. This section describes a pilot method used to visualise the cortical activity occurring over a specific time window; enabling spatial visualisation of spectrally defined activity with millisecond temporal resolution. This approach allows a basic visualisation of the movement of activity across the cortex by presenting a static array of virtual electrodes or more intricately by generating a spectrographic movie of the activity.

3.2.2 Methods and Results

The initial step of this procedure is to determine the spatial extent of the cortical surface that is intended to be visualised. In the explanation and description of the methods in this section the visual cortex is used as the model. However, as discussed later, recent information suggests that the method would be more informative using a finer spatial mesh. The software *mri3DX* (http://www.aston.ac.uk/lhs/staff/singhkd/mri3dX/index.html) produces a three dimensional image of a subject's brain by reconstructing the individual slices of the MRI volume scan. This allows three-dimensional interaction with the anatomical features of the brain such as specific gyri and sulci and therefore allows a more accessible approach to feature definition. The initial step is to select a region of interest (ROI) and produce an array of coordinates on the cortical surface (fig. 3-1). This is done using a roughly triangular matrix system in order that the coordinates can be more easily linked.
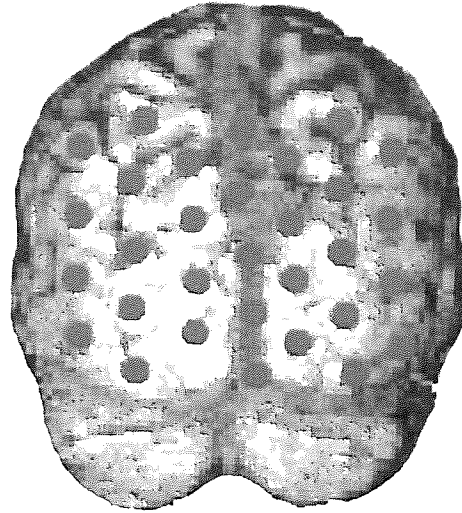
Figure 3-1. Anatomical definitions for virtual electrode array defined by the individual cortical surface, using mri3DX. Pink dots are an example of the array employed in definition of the visual cortex; 3D view of occipital lobe.

Following on from this an output of the coordinates in Talairach space (talairach and Tournoux, 1988) are converted into CTF coordinates that are compatible with the *SAMMenu* software (CTF Systems Inc., Port Coquitlam, Canada). This then generates a set of weighted values for each of the coordinates that are specified, this is known as a virtual electrode (VE). This can then be used to generate a simple static array of virtual electrodes which represent the matrix of cortical locations (fig. 3-2), using the normal sensor data reader *DataEditor* (CTF Systems Inc., Port Coquitlam, Canada).
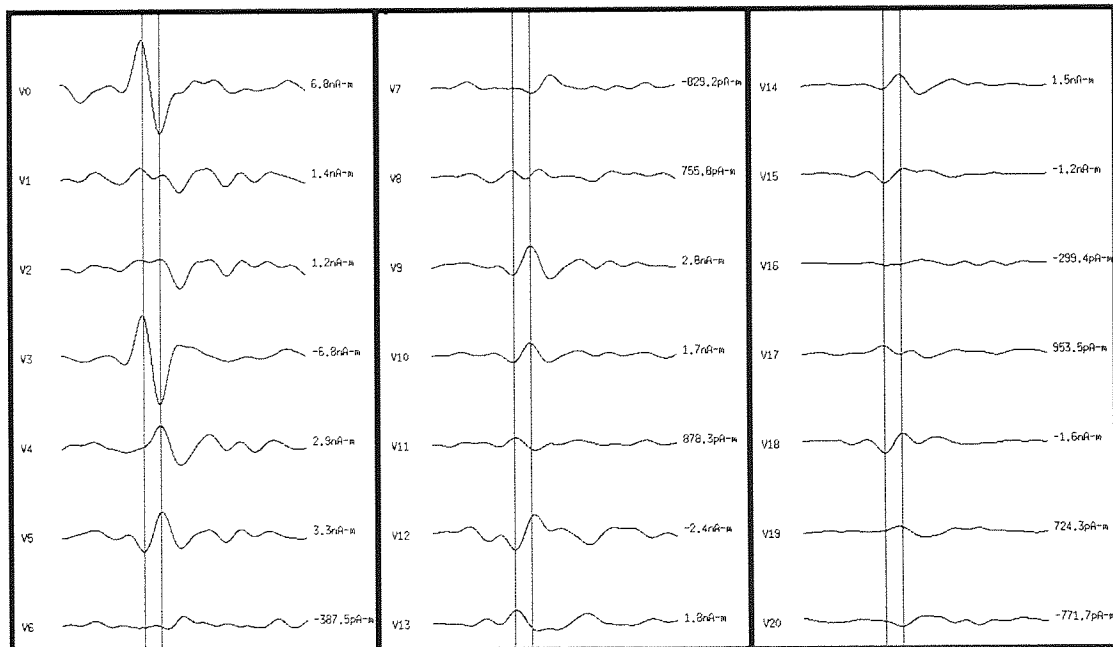
Figure 3-2. Virtual electrode array demonstrating the evoked activity across the right visual cortex in a pattern onset paradigm, demonstrating the two discrete waveforms in striate (V0) and extrastriate (V9) locations.

Alternatively, it is then possible to use the weights information to generate a time frequency plot at each of the VE locations specified using the software *'Spectrogram'* (the Wellcome Trust Lab for MEG Studies, Aston University, Birmingham, UK). The specified coordinates are then joined by triangulation of their coordinates in order that they are recreated in three-dimensional space and connected by a triangular mesh to those points adjacent on the cortical surface, thereby creating a 'virtual cortex', which can then be rotated in space in order to observe the desired location (fig. 3-3). This is of particular use if large regions of the cortex are investigated, as discussed later.

-160° Rotation

-80° Rotation

-40° Rotation

-20° Rotation
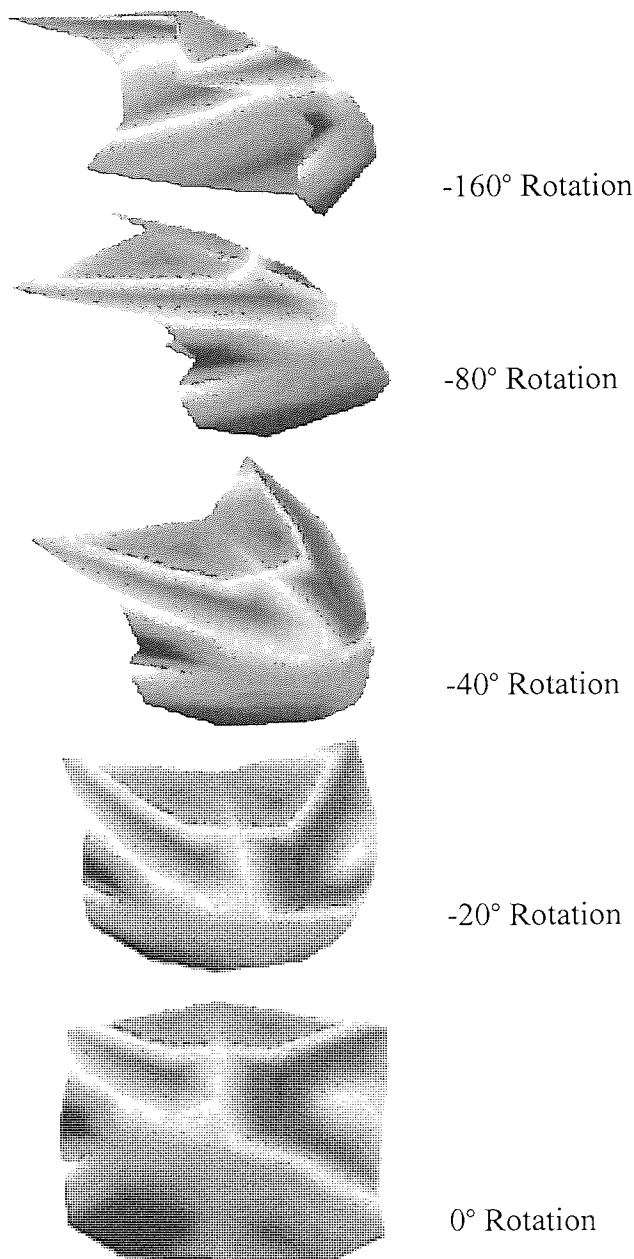
0° Rotation

Figure 3-3. Example of the spectrographic movie implemented over the occipital cortex in an evoked potential paradigm. Demonstrates facility for 3-Dimentional rotation of the virtual electrode cortical matrix in the post processing stage; 31 virtual electrodes (see fig. 3-1).

The spectral data are then reconstructed at the correct location with respect to adjacent virtual electrodes. A specific frequency window is then selected and the activity in that window is then computed as a function of spatial location. This activity is normalised to a common baseline and the activity within each of the triangular sections is computed as the averaged sum of activity at the three points comprising its borders (fig. 3-4). The outcome of this approach is the creation of a movie (MPEG), which visualises the cortical activity in a given frequency band at millisecond resolution over a specified time window. An example of one of these movies can be observed in the attached CDROM.
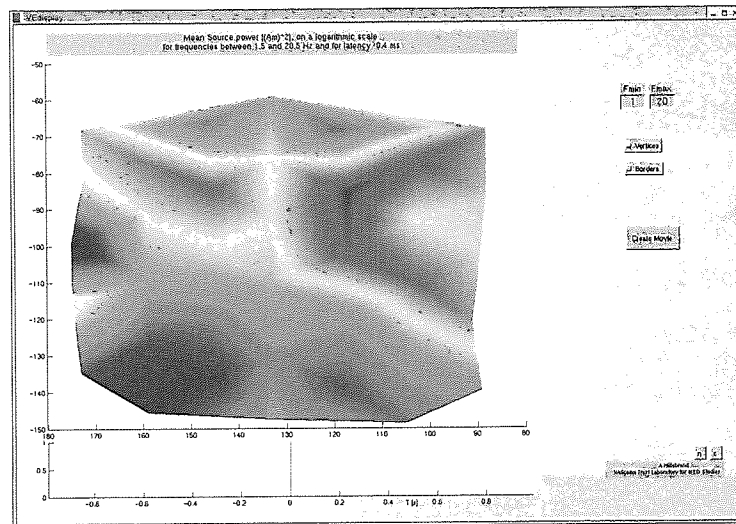
Figure 3-4. Spectrogram matrix console for defining spectral and spatial parameters. Showing time scale and frequency of interest.

3.2.3 Discussion and Further Work

The methods described here are the initial step in creating a simplistic method of visualising the data acquired in an MEG experiment in much the same way as a field map gives an illustration of the unfiltered magnetic fields detected in each of the sensors. This method has an unlimited number of sensors as they are recreated virtually. Additionally, where the field map is a representation of the activity measured ~2-3cm above the surface of the head, this is a reconstruction of the neuronal activity which occurs at the cortical surface, which is suggested to be comparable to the invasive measurements made using local field potential (LFP) measurements (Hall *et al,* 2004c). The restriction of this technique at the time of development was the computational intensity required to generate the movie. However, the current computing abilities are better equipped to cope with such demands and are able to complete the task in less than a quarter of the time. Furthermore, the scope for improvements in the software and an informed approach to factors such as sampling rate suggest that this could be developed as a tool for use in convenient interpretation of results and has particular scope for development as a clinical tool. The full

extent of the spatially specific nature of the virtual electrode has become recently apparent and suggests that even small deviations from a single point can result in large changes in the activity which occurs (Barnes *et al.*, 2004). This implies that the method would currently be of particular use in the investigation of spatially specific and evolving cortical activity, for example: investigation of epilepsy would allow visualisation of the evolving activity. Developments in computing power and methodological improvements lead toward an ultimate goal of a densely represented cortical surface, enabling immediate identification of the activity over the entire cortex; needing only to determine the spectral band of interest.

3.3   Synthetic Aperture Magnetometry Manipulation for Task Dependent Analysis

3.3.1   Introduction

This section is a brief overview and reference section discussing the use of the SAM beamformer in the investigation and analysis of various cortical activities. This describes the investigation of evoked potentials, driven stimuli and spontaneously occurring activity.

3.3.2   Evoked potential analysis

This implementation of the SAM beamformer is aimed at identifying the evoked potential activity. Although a primary benefit of beamforming approaches is the ability to identify non time-locked activity, factors such as an absence of *a priori* assumptions regarding the number of active sources provide benefits over dipole modelling (Barnes and Hillebrand, 2003). In the identification of evoked potentials SAM is beneficial in that is an unambiguous measure that is not subject to user bias, as is the case with dipole fitting.

This approach was made on a trial and error basis in the knowledge that SAM (as with all beamformers) is subject to the limitation that spatially separate yet covariant sources will be suppressed (Mosher *et al.*, 1992; Mosher and Leahy., 1998; Van Veen *et al.*, 1997). This posed a particular risk as the smaller the temporal window, the greater the likelihood of sources having a high enough temporal correlation (>0.7) for cancellation to occur. The chance of this occurrence was immediately reduced by the use of only a single quadrant visual stimulus. In addition to reducing magnetic field cancellation from opposing sources of the cruciform arrangement, this also reduces the likelihood of a simultaneous evoked potential arising from another location in the visual cortex.

The frequency window was defined by observing the typical peak to peak latencies of the evoked potentials measured, the majority of which were in the 80-160ms range, which generate frequency components in the 6.25-12.5Hz range. An illustration of this concept is shown in figure 3-5 using typical VEPs from the VEP standard 2003 (Odom *et al.*, 2003). However, these average latencies are shorter than the typical obtained in our lab or indeed in this thesis. In order that no longer components would be missed the frequency window was extended from 3-12Hz. With a typical time window of 0-300ms post stimulus onset (active) versus -300-0ms (passive) this method was useful in examining pattern-onset (Hall *et al.*, 2004a, pattern-reversal, luminance onset, contrast increment and contrast decrement responses(chapters 3 and 4) .
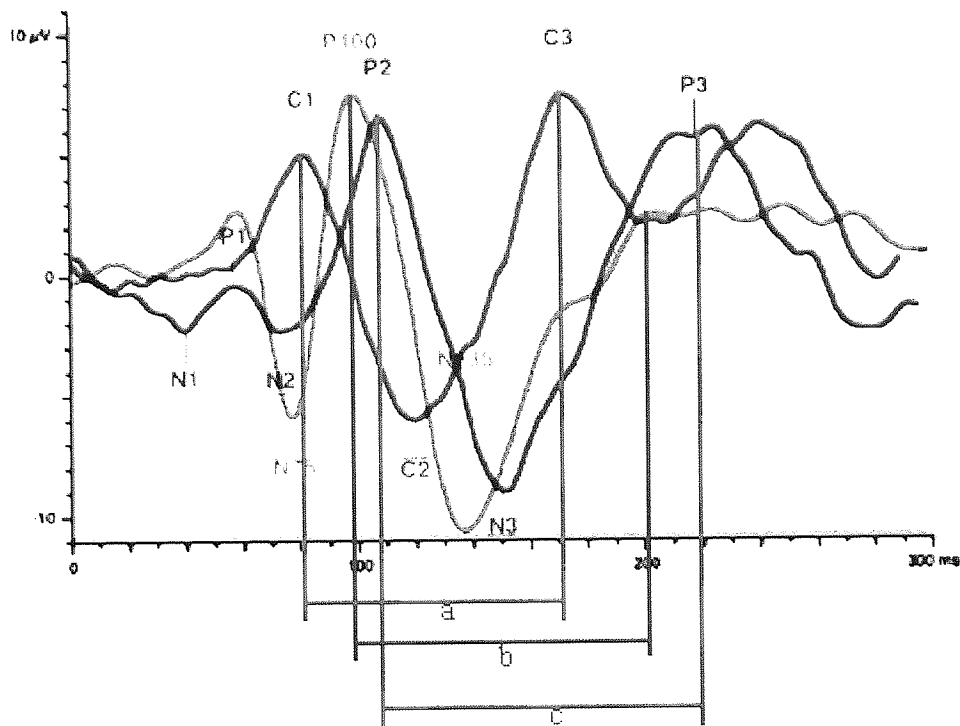
Figure 3-5. Evoked potential frequency schematic. Overlay of pattern-onset, pattern-reversal and flash VEPs, showing peak to peak latencies of (a) 80ms, (b) 100ms and (c) 120ms, producing frequency spikes at 12.5Hz, 10Hz and 8.3Hz respectively. Trace taken from the VEP standard 2003 (Odom *et al.*, 2003).

3.3.3 Sustained/driven stimulus analysis

Using the same principle discussed above, which was shown to be able to distinguish transient magnetic field variation in a specific frequency range, it was hypothesised that at higher frequencies where the transient evoked potential becomes a steady state evoked potential (typically >10Hz (Harding, 2003, personal communication) and more sinusoidal in nature, it would be possible to measure the location based upon the driving frequency. In order to investigate this, a stimulus (pattern-onset-offset) was presented at 16Hz and a SAM analysis window of 14-18Hz was used to localise this activity. Chapter 6 discusses the success of this methodology and how it was subsequently applied to retinotopic mapping study.

3.3.4   Non-driven baseline comparison

The typical approach to MEG investigation using many methods, including SAM and Spectrogram analysis, is to define trials as active and passive in a sequential order. This method provides a passive phase, which consistently precedes the active phase, whereby one segment contains an imposed difference with respect to the other (i.e. pattern-onset vs. blank). In this thesis a novel form of SAM analysis was developed in order to observe changes which occur over longer periods of time and are independent of a driving stimulus. In this method a period of baseline is taken either at the beginning or the end of the experimental period dependent upon the type of experiment. In the application demonstrated in this thesis (Chapter 7) it was used to investigate the development of an episode of migraine visual aura (Hall *et al.*, 2004) in which the visual abnormalities had already begun in the patient. Because of this it was necessary to acquire the period of baseline at the end of the experimental run rather than at the beginning. This procedure, as described in chapter 7 involves the division of the observed activity into temporal windows of interest; in this case 2 minute segments of a 20 minute run were taken. Within the two minutes the window was broken down into 2 second blocks (n=120), essentially providing an averaged spectral profile for that two minute period, which is then compared to the baseline segment. This approach allows elucidation of the temporal evolution of cortical activity with has high signal to noise ratio (SNR). This method is useful in the analysis of spontaneous cortical activity as seen in migraine/cortical spreading depression or indeed epilepsy. However, a principal application of this procedure is in the assessment of neural substrate interaction, whereby the effect of a drug over a particular time period can be determined, sub-therapeutic levels.

3.4 Optimal beamformer resolution for MEG group imaging

3.4.1 Introduction

It is well accepted that in neuroimaging modalities (PET, fMRI, MEG) it is necessary to determine the optimal spatial smoothing for a group imaging study (Friston, 1996). Recent studies (Gross, 2003; Barnes et al., 2004; Barnes and Hillebrand, 2003) highlighted the highly homogenous smoothness of MEG beamforming images.

The full width at half maximum (FWHM) is the variable used to describe the smoothness of the image; an increase in FWHM value represents an increase in the smoothness of the image. The FWHM across the beamformer image varies with system sensitivity and source signal to noise ratio (SNR) (Van Veen and Vrba, 1999; Gross, 2003; Barnes et al., 2004; Vrba, 2003 personal communication), with lower SNR resulting in smoother beamformer images. This is possibly the reason why it has been neglected in previous MEG imaging studies (Singh et al., 2002, 2003).

The interested reader is directed to Barnes et al., 2004, for a description of FWHM investigations previous to this investigation. In SAM, computation at the individual level, attempts to optimise source identification and localisation by refining smoothing parameters to account for changes in the order of 2-5mm. Although this is ideal for analysis at the individual level, in translation to the group level it is likely to result in cancellation or misrepresentation of the actual activity due to the intrinsic variability of the cortex and errors in coregistration.

In SAM analysis the smoothness of the image and the noise sensitivity are intrinsically related, i.e. as smoothness increases the noise sensitivity decreases, this decreases spatial resolution. In the SAM algorithm, this trade-off is governed by the 'Backus-Gilbert' parameter (μ).

In this investigation SAM analysis of a data set produced by driven visual stimuli (10Hz) are investigated using varied values of the Backus-Gilbert parameter in subjects and subsequently SnPM (Singh et al., 2003) to investigate the effects on the p-value of the peak in the group image. The advantage being that it forms an inherent part of the SAM analysis, rather than post-processing stage.

3.4.2   Methods

The construction of a beamformer image consists of: (1) the construction of the beamformer weights and (2) the application of the beamformer weights to the measured MEG data. The beamformer weights form an optimal spatial filter that relates the signal at a target location in the brain to the measured MEG signals. This is governed by:

$$y(t) = \mathbf{W}_\theta^T \, \mathbf{m}(t),$$

(Equation 3.1)

where $\mathbf{m}(t)$ is a column vector of N MEG channels at a single latency t, $\mathbf{W}_\theta$ a column vector containing the beamformer weights for target location θ and $y(t)$ is the beamformer output for this target location.

The weights are computed as (Robinson and Vrba, 1999):

$$\mathbf{W}_\theta = \left(\mathbf{H}_\theta^T [\mathbf{C} + \mu\Sigma]^{-1} \mathbf{H}_\theta \right)^{-1} \mathbf{H}_\theta^T [\mathbf{C} + \mu\Sigma]^{-1},$$

(Equation 3.2)

where $\mathbf{H}_\theta$ is the lead field of a source at target location θ and $\mathbf{C}$ is the data covariance matrix. We consider only a single (optimum) orientation for the source element and therefore $\mathbf{H}_\theta$ is a column vectors with N rows. The lead field vector contains the sensitivity of a given sensor geometry to a current source at a given location (in this work an equivalent current dipole to model the current flow). $\mathbf{C}$ is the $N*N$ data covariance matrix and Σ the noise covariance matrix of the same dimensions. The Backus-Gilbert regularisation parameter, μ, specifies the trade-off between spatial selectivity and noise sensitivity. A large value for μ means a low spatial resolution (smooth beamformer images), whereas a small value means a high spatial resolution but images that are sensitive to noise. The Backus-Gilbert parameter will be varied to alter the smoothness of the beamformer images computed in this study.

Various parameters can be computed based on the beamformer output, for example one can statistically compare the beamformer output for the active (subject performs a task) and passive phase (subject is at rest or performs a control task) of an experiment (Robinson and Vrba, 1999). A volumetric image of neuronal activity (called a Statistical Parametric Map or SPM) can subsequently be obtained by sequentially constructing an optimum set of weights for each target location in a pre-defined grid within the brain and

computing the statistical metric of interest. Recently Singh *et al.*, (2002, 2003) has shown that these SPMs can be group-averaged in order to highlight the brain regions that are most consistently activated across a group of subjects. These studies showed a remarkable spatial correspondence between the results obtained with group-fMRI and group-MEG in a biological motion and a language task, demonstrating the feasibility of this approach. In this work group-averaged beamformer images are computed following the procedure described in Singh *et al.* (2002, 2003).

3.4.3 MEG experiment

The stimulus consisted of horizontally oriented sinusoidal gratings of 3 cycles per degree (cpd) at a Michelson contrast of 100%. The subject fixated a central point whilst the stimulus was displayed in the lower right quadrant of the visual field. The gratings were presented with abrupt onset for 50 ms followed by 50 ms of a 'blank' screen of equal mean luminance to the stimulus, thus producing a flicker rate of 16Hz. The subjects (n=8) passively viewed 150 trials of the stimulus from a distance of 2 metres. The Backus-Gilbert (μ) parameter was varied from 0 to 90 and group-averaged SAM images were computed.

3.4.4 Results

Initial analysis of the results was performed using the SAM beamformer method restricted to 14-18 Hz. In all subjects there was event related synchronisation (ERS) in the visual cortex with peaks of activity in and around primary visual cortex. This activation was further investigated at the group level using the statistical non-parametric modelling (SnPM) method (Singh *et al.*, 2002a). This produced an image of group activity which showed little activity in the visual cortex (fig. 3-6 μ0) and a peak statistical value of p=0.2. Following this, SAM analysis was repeated with a range of Backus Gilbert 'smoothing' (μ) values from normal (0) to 90 and group analysis using SnPM was repeated for μ values of 0 to 90 (fig. 3-6).
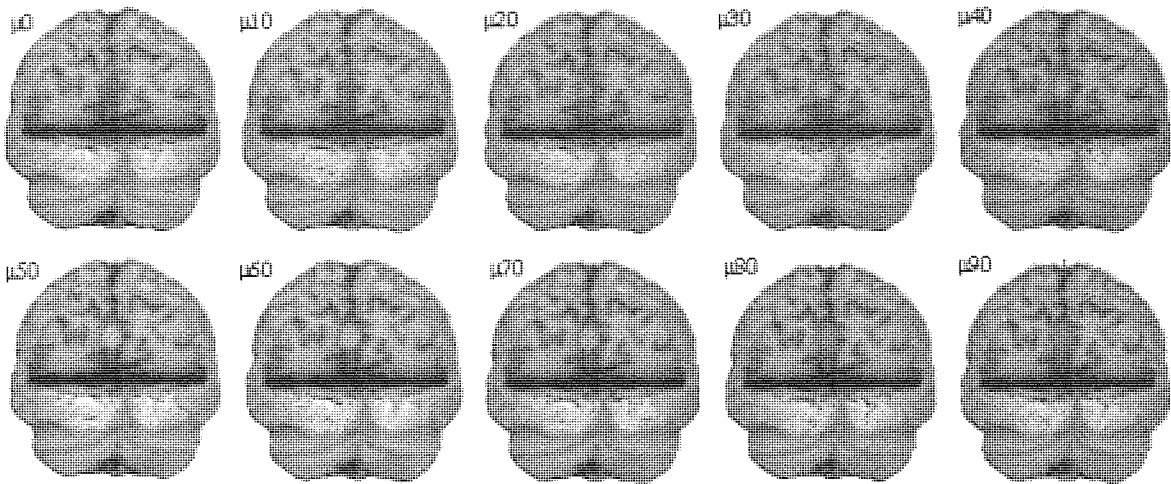
Figure 3-6. SnPM images produced from SAM data with Backus Gilbert (μ) ranging from 0-90. Shows increased strength of the V1 activation in the group image.

μ	0	10	20	30	40	50	60	70	80	90
p	0.12	0.2	0.34	0.69	0.7	0.75	0.69	0.68	0.67	0.51

Table 3-1. Data table of the significance values (p) at each of the Backus Gilbert (μ) values, p-values denote significance level of the SnPM group image activation in the primary visual cortical activation.

The anatomical coordinates of the maximal p-value at $\mu 0$ were used to obtain p-values for selected values of μ (fig. 3-7). This shows that increasing the smoothing variable has a direct effect on the significance level of the group image.
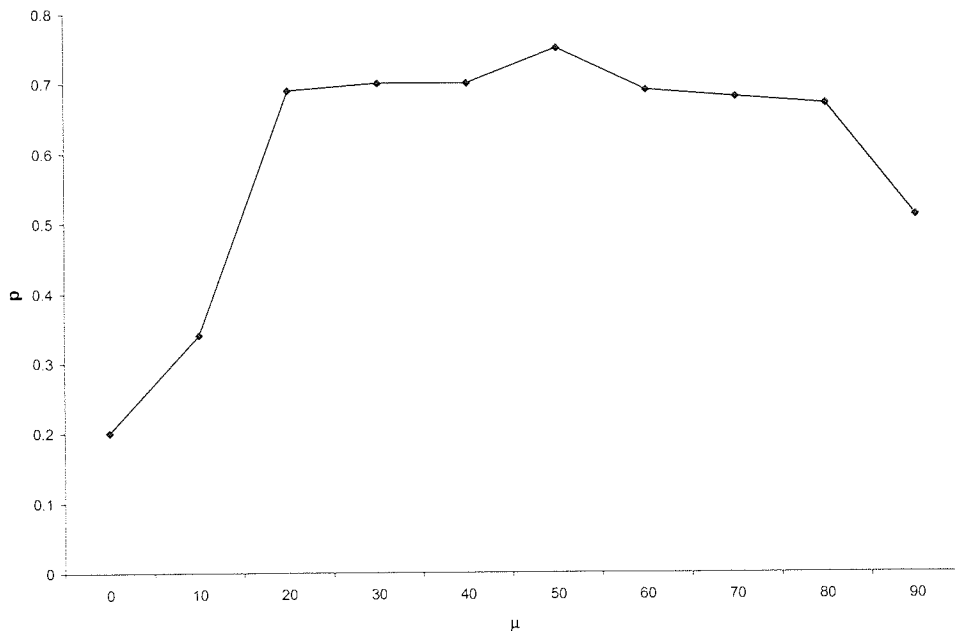
Figure 3-7. Graph showing the effect of varying the Backus Gilbert parameter on the group image significance. Demonstrates a peak at μ 50.
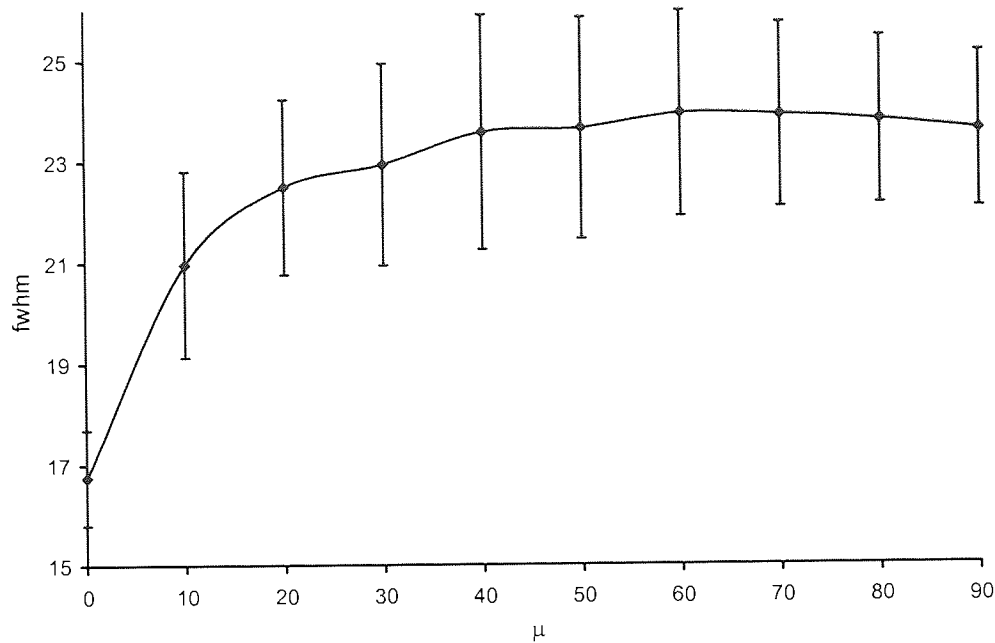
Figure 3-8. Graph showing the relationship between the Backus Gilbert parameter (μ) and the FWHM value ±1.96SEM. Demonstrates a saturation of FWHM above μ50 (fwhm values are expressed as mm).
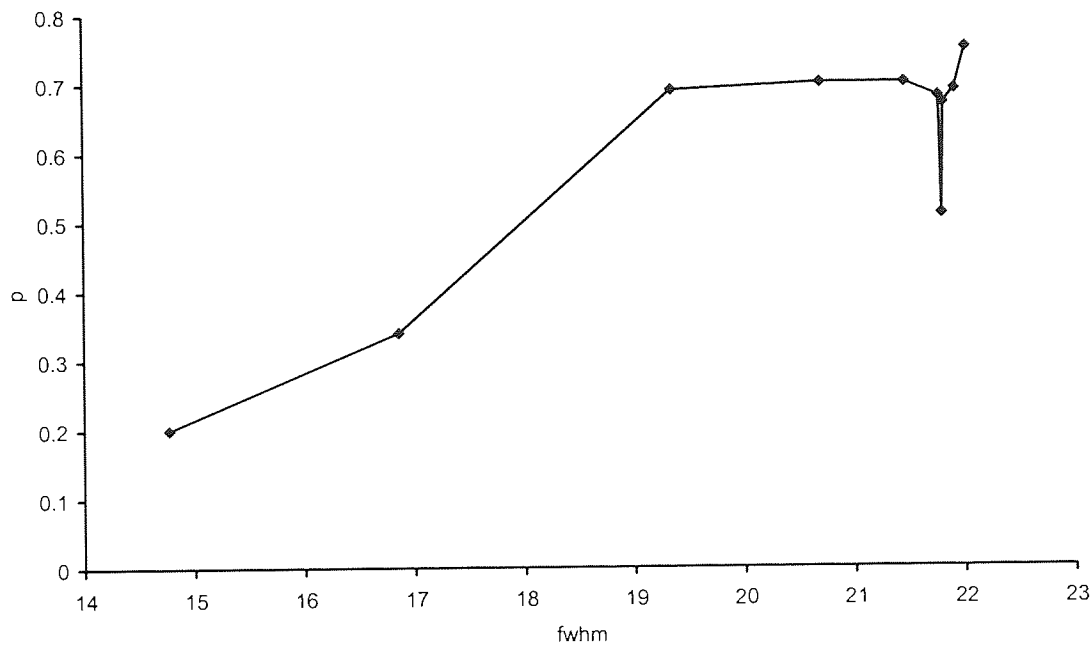
Figure 3-9. Plot of the computed significance significance of the group image for values of FWHM distance (mm). The fluctuation above FWHM 21 reflects reduction in the p-value for μ values above 50.

3.4.5 Discussion

These results demonstrate that the FWHM and μ are directly related to local image smoothness and applied this to recorded MEG data to show how using a low resolution beamformer gives images of optimal smoothness. This optimal smoothness has a direct effect on the group statistical image, revealing significant activation not seen with unsmoothed images. We have shown how the beamformer can be directly and computationally effectively optimised to produce low spatial resolution images appropriate for group imaging and conclude that a FWHM of ~20mm is optimal for group imaging based on the visual cortex.

This work has important implications in group MEG analysis as it suggests that the smoothness of the individual image has a direct effect on the group result. By smoothing the image at the individual level, this method takes account of the spatial inhomogeneity between subjects prior to the group level. The example shown is specific to the visual cortex and therefore is likely to vary across the rest of the cortex. Furthermore, the individual optimum is likely to vary somewhat across subjects and therefore introduces some concerns regarding group imaging as a reliably informative approach.

The results suggest that based upon the visual cortex, the same stimulus induces activity that varies by up to 3cm between subjects, drawing some concerns about the approach as an informative measure.

3.5 Standard Applied Methods

3.5.1 Description

There are commonly applied methods which are consistent throughout a large proportion of this thesis. Although the specifics vary from one chapter to the next, in order to avoid repetition and provide succinct exploration of the various topics, those factors which are constant throughout are described here. Thus where reference is made to 'section 3.5' in the text, it is intended to assuage superfluous explanation.

3.5.2 SAM and Virtual Electrodes

Throughout the course of this thesis SAM and virtual electrodes (VEs) are referred to extensively as the primary mode of analysis. The relative novelty of these methods dictates that an explanation of the methods and/or reference to publications that have used/ described the methods is necessary in publication. The methods themselves and their varied implementations are discussed in chapters 2 and 3; here are details pertaining to chapters within:

- We analysed the responses using the recently developed synthetic aperture magnetometry (SAM) beamforming method (Robinson and Vrba, 1999; Vrba and Robinson, 2001); which has high spatial and temporal resolution and a demonstrable spatial coincidence with the fMRI BOLD response (Singh *et al.*, 2002, 2003). A number of groups have recently used SAM as a method of MEG signal analysis (Ishii *et al.*, 1999, 2003; Taniguchi *et al.*, 2000; Xiang *et al.*, 2001; Vrba and Robinson, 2001a,b; Hirata *et al.*, 2002; Ukai *et al.*, 2002; Singh *et al.*, 2002, 2003; Gaetz and Cheyne, 2003; Ihara *et al.*, 2003; Fawcett *et al.*, 2004; Furlong *et al.*, 2004; Hall *et al.*, 2004a,b,c,e).

- Additionally, we used a spatially selective reconstruction of neuronal activity derived from the SAM beamformer implementation, called a 'Virtual Electrode' (VE) (Singh *et al.*, 2002; Barnes and Hillebrand, 2003; Fawcett *et al.*, 2004; Hall *et al.*, 2004a,b,c,e; Hillebrand *et al.*, 2004).

3.6   Presentation, Recording and Analysis

The majority of experimental chapters in this thesis make use of visually presented stimuli, which are generated in the same manner throughout. Similarly the same MEG system, peripheral hardware and noise rejection configurations remain standard. Finally the coregistration methods, hardware and software remain constant throughout; these are the details relevant to subsequent chapters:

The research described in this thesis was conducted with the approval of the Aston University Human Sciences Ethical Committee and written informed consent was obtained from all participants prior to commencement of the study. Data were recorded using a 151 channel whole head MEG system (CTF Systems Inc., Port Coquitlam, Canada) at a sampling rate of 625 Hz, using a 3rd order gradiometer configuration with a 50Hz comb filter and 200 Hz anti-aliasing filter. Ten subjects passively viewed stimuli, reflected through a window in the scanner room by a front silvered mirror at a distance of two metres.

The stimuli were generated on a VSG 3/2 graphics card, presented on a gamma corrected Eizo Flexscan T562-T monitor with a refresh rate of 85Hz. Details of stimulus cycle, duration and presentation were chosen in order to avoid adaptation, masking and attentional effects. A single quadrant was used in order to avoid cancellation effects from sources on opposing banks of the calcarine sulcus (Taguchi *et al.*, 2002).

Following data collection, a 3-D digitiser (Polhemus Isotrak, Kaiser Aerospace Inc.) was used to digitise the subjects scalp surface, which was then coregistered with the individual subject anatomical MRI scan using the software 'Align' (www.ece.drexel.edu/ICVA/Align/align11.html).

Where stimulus contrast is referred to it is calculated as Michelson Contrast also denoted in this thesis as C_m; it is defined by the equation:

$$C_m = [L_{max} - L_{min} / L_{max} + L_{min}] \times 100$$

(Equation 3.3)

where L_{max} and L_{min} represent the maximum and minimum luminance, respectively.

Chapter 4

Investigation of the Visually Evoked and Induced Responses using magnetoencephalography (MEG)

4 Investigation of the Visually Evoked and Induced Responses using magnetoencephalography (MEG)

4.1 Overview

Chapter four describes a series of experiments and analyses designed to investigate the evoked and induced activity in the visual cortex following visual stimulation. The approaches used in this chapter are based upon the methods that are well characterised using electroencephalography (EEG) for use in clinical assessment and is intended to investigate and characterise and further dissect the magnetic correlates of these responses.

The chapter begins with an introduction to the basic clinical visual evoked potential (VEP) types, describing pattern onset, pattern reversal and flash VEPs, describing latency and morphology observed electrophysiologically and discusses clinical relevance. Subsequently the oscillatory activities that are intrinsic features of the cortex are discussed in terms of frequency range and variations as a function of stimulation.

The rationale of this study is then presented and discusses the implications of a wider understanding of the evoked and induced activity following visual stimulation in terms of clinical and experimental application.

The experimental investigation analyses the response to pattern-onset, pattern-offset, pattern-reversal, luminance-onset, luminance-offset, contrast-increment and contrast-decrement and analyses them using progressively more sophisticated methods. Raw sensor data is used to characterise latency where possible, followed by localisation using dipole analysis with Monte-Carlo and ultimately SAM and virtual electrode analysis to comprehensively classify evoked activity and event related synchronisation /desynchronisation (ERS/ERD).

The aim of this chapter is to investigate the evoked and induced activity comparative to current understanding from EEG; in doing so enabling comparison of the magnetic signal with the electrical signal. Furthermore, it intends to provide comparative analysis using two of the available methods and demonstrate the benefits of SAM. Finally it seeks to classify consistent cortical activity in a manner which provides a basis for normalisation in normal and clinical investigation.

4.2   Introduction

The visual evoked response (VER) is the term given to the cortically measured activity generated following visual stimulation. The activity which occurs can be loosely divided into evoked or induced and transient or sustained*. The most commonly measured and well documented VER is the visual evoked potential (VEP) or visual evoked cortical potential (VECP), measured using electroencephalography (EEG). VEPs are transient evoked activities, typically of low amplitude in comparison to spontaneous cortical activity and are therefore best visualised using time locked averaging. This method amplifies time locked changes in signal amplitude, cancelling non time-locked activity, which is typically eliminated by averaging over large numbers of trials. The exact neuronal activity underlying the VEP phenomena is not fully understood, however it is generally assumed that the response is the result of the initial volley of activity arriving at the visual cortex. At this point large numbers of similar neurons are activated at the same point in time, giving rise to stimulus specific visual evoked potentials. Induced activities can be either transient or sustained and consist of amplitude fluctuations in spectral frequencies, which demonstrate no phase locking to the stimulus and are therefore effectively cancelled by averaging (tallon-Baudry and Bertrand, 1999). There is typically a degree of temporal connection to the visual stimulus; whereby fluctuations occur with approximate lag time and either rapidly subside (transient) or remain for the duration of the stimulation (sustained).

In all of the observed activities, whether short or long lived, there is a change in synchronous activity or power. An increase in synchrony is sometimes referred to as event-related synchronisation (ERS); whereas a decrease in synchronous power is referred to as event-related desynchronisation (ERD) (Pfurtscheller and Lopes da Silva, 1999a,b). In this chapter ERS and ERD are used in reference to induced activity, which is investigated in specific frequency bands (section 3.3). Alternatively, although the evoked activity is identified based upon elevated synchrony of its frequency components (section 3.4.3.3), it is referred to as evoked activity for the purpose of distinguishing these neuronal mechanisms.

---

*Evoked activity is time-locked and often spatially phase-locked to the stimulus, whereas induced activity has no specific temporal relationship with the event. Transient activity is short lived and independent of the static nature of the stimulus, whereas sustained activity remains for the duration of the stimulus. A third activity is the result of the driving stimulus, which produces a 'steady-state' form of the transient activity, which is sinusoidal and contains the temporal signature of the stimulus (tallon-Baudry and Bertrand, 1999)

4.2.1 The Visual Evoked Potential (VEP)

There are a number of types of VEP: flash or luminance onset VEP, pattern onset VEP, pattern reversal VEP and pattern offset VEP (typically discussed as a feature of the pattern onset VEP). The waveform of the VEP depends upon the temporal frequency of the stimulus. At rapid rates of stimulation (>10Hz), the waveform becomes approximately sinusoidal and is termed steady-state. At low temporal frequencies, the waveform consists of a number of discrete deflections and is referred to as a transient VEP. Each of the different VEPs have been categorised in terms of the latency and morphology of their positive and negative elements (measured using EEG) using separate classifications. VEPs may also be elicited by other stimuli, such as motion or colour (Harding et al., 1996; Odom *et al.,* 2004) and, as discussed in this thesis, contrast increments (increments in stimulus contrast).

These VEPs may be used to stimulate and measure neural subsystems or to assist in localizing visual field defects. The characteristics of the typical flash, pattern onset and pattern reversal VEPs have been characterised in terms of their observed EEG activity and are of specific interest for clinical applications as discussed in the following sections.

4.2.2 The Flash VEP

The flash VEP is a widely used clinical tool in the investigation of visual affective disorders. Particularly useful in the investigation of photosensitive epilepsy (PSE) using a faster rate or 'strobe' effect to induce steady state evoked potentials, which in the photosensitive patient often results in abnormal photo-paroxysmal response (PPR) or occipital spikes (A comprehensive review of PSE can be found in Harding and Jeavons (1995). Flash VEP is of particular use when optical factors (e.g. fixation) or poor cooperation make the use of pattern stimulation inappropriate. The components of the flash VEP are divided into positive (P) and negative (N) and categorised by the order in which they appear in the EEG trace (fig. 4-1). Flash VEPs are much more variable across subjects than pattern responses but show little inter-ocular asymmetry. The visual evoked potential to flash stimulation consists of a series of negative and positive waves. The earliest detectable response has a peak latency of approximately 30 ms post-stimulus and components are recordable with peak latencies of up to 300 ms. The nomenclature described henceforth, is recommended to automatically differentiate the flash VEP from the pattern reversal VEP. The most robust components are the N2 and P2 peaks.

Measurement of P2 amplitude is determined as the difference between the positive P2 peak at around 120 ms and the preceding N2 negative peak at around 90 ms.
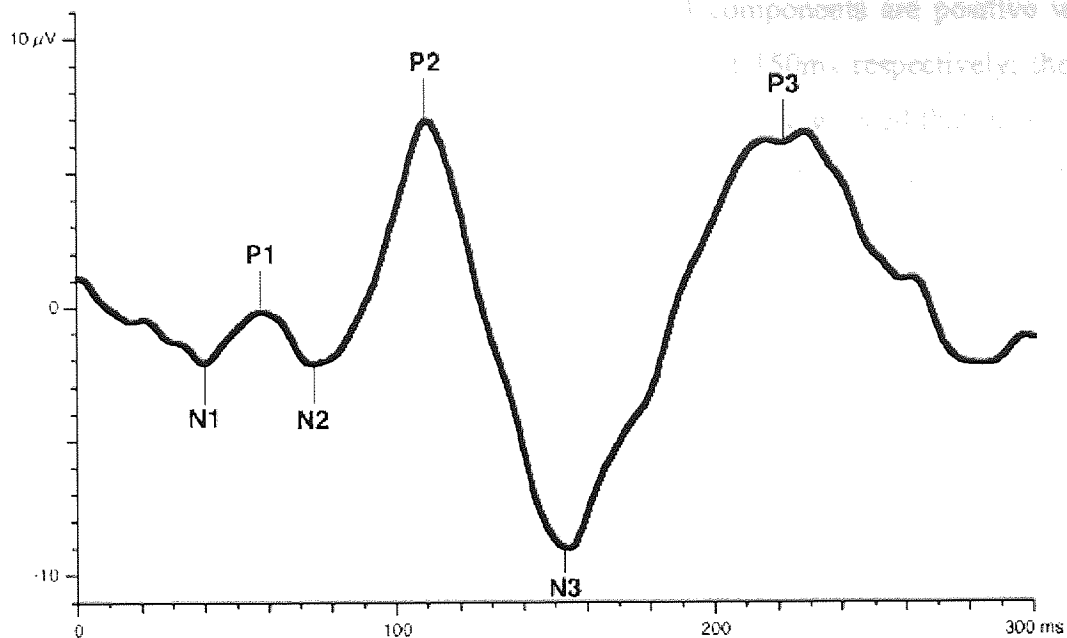
Figure 4-1. Typical flash VEP. The nomenclature indicates the positive (P) and negative (N) peaks of the EEG following stimulation with a single luminance flash. Successive positive and negative peaks are numbered sequentially. Image redrawn from Harding *et al.,* (1996).

As with many VEP components there is a large amount of variability between subjects concerning which feature is observed and the latency of those features. In the flash VEP the N1 and P1 components show considerable variation and have been shown to vary as a function of age (Wright and Furlong, 1988; Crognale *et al.*, 2002). However, the P2 component seen at around 120ms is more stable and is found at around this time in the majority of subjects. The later components N3, P3 and N4 are very variable and are often considered to be components of higher cognitive processes. Some research suggests that components occurring before 100ms occur in the primary visual cortex, while components following 100ms occur at increasingly higher areas of visual cortical processing. The latency of the flash VEP P2 component is suggested to be a robust pre-determinant of Alzheimer's (Orwin *et al* ., 1986; Bajalan *et al.,* 1986; Wright *et al.*, 1986).

4.2.3   Pattern Onset VEP

Pattern onset VEP is intended to specifically stimulate pattern detectors in the human visual system and as such it is necessary to generate a stimulus of equal mean luminance to its background to minimally activate luminance detectors. The pattern-onset is the presentation of a patterned stimulus (typically bars or a checkerboard) onto a blank background for a determined length of time. The removal of the patterned stimulus is the 'pattern offset' phase and, although a symmetrical component of the stimulus cycle, has a

completely different VEP response (Odom *et al.*, 2003). Amplitudes are measured from the preceding negative peak. The pattern onset response is generally defined as having three components: C1, C2 and C3 (fig. 4-2). The C1 and C3 components are positive when measured with the EEG and occur at approximately 75 and 150ms respectively; the C2 component is negative and occurs at approximately 100ms. It is suggested that the C2 and C3 components represent the visual cortical response to specific pattern detail of the stimulus, such as edges and contours. The C1 component is thought to be the transient response to the stimulus contrast (Odom *et al.*, 2004).
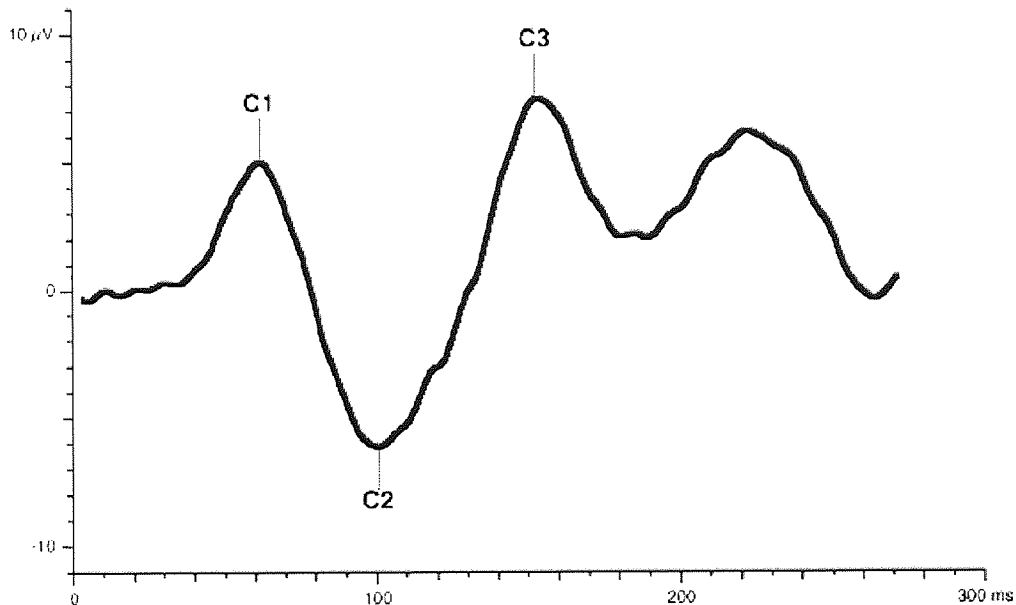
Figure 4-2. Pattern Onset and Offset VEP. The nomenclature indicates the latency and relative amplitude of the C1, C2 and C3 pattern onset response and unclassified pattern offset response at approximately 250ms, as measured using EEG. Image redrawn from Harding *et al.*, (1996).

Due to the underlying variation in visual cortical structure and neuronal populations, the pattern-onset VEP is known to be quite variable across subjects (reviewed in Chapter 5). Features such as spatial and temporal frequency of the pattern are known to produce variability in the VEP (Crognale *et al.*, 1997) as are factors such as colour (Leonards and Singer, 1997; McKeefry, 2001) and motion (Bach and Ullrich, 1997) with latency and amplitude of the response modulated by spatial frequency and contrast (Chapter 1).

The pattern-offset VEP has a single component at approximately 250ms (fig. 4-2) following the offset of the stimulus, as it is typically not studied separately there is no reported 'standard'. The activity which occurs is variable in latency, as is often the case with components of longer latencies. The pattern onset/offset technique can be useful in the detection of malingering and in patients with nystagmus and is employed in the clinical

investigation of epilepsy (Harding and Jeavons, 1995) and migraine (Evans *et al.*, 2002; Patel *et al* 2003).

4.2.4   Pattern Reversal

The pattern reversal VEP occurs in response to a patterned stimulus which does not either appear or re-appear, but instead reverses in phase at a particular time interval. The stimulus is typically either a grating or a checkerboard pattern and so a reversal is the immediate exchange of black and white components. The stimulus is commonly used and so is well characterised in terms of its component latencies. The peak of activity found in response to pattern reversal experiments is a positive inflection at around 100 ms and so is referred to as the P100 (fig.4-3). For pattern reversal, the VEP consists of N75, P100 and N135 peaks. The nomenclature designates peaks as negative (N) and positive (P) followed by the typical mean peak latency. It is recommended to measure the amplitude of P100 from the preceding N75 peak. The peak latency of P100 shows relatively little variation between subjects and also shows minimal inter-ocular differences. P100 amplitude also shows low inter-ocular difference but much greater variability across subjects. P100 latency is affected by non-pathophysiologic parameters such as pattern size, pattern contrast, pattern mean luminance, refractive error, poor fixation and miosis (Odom *et al.*, 2004)..
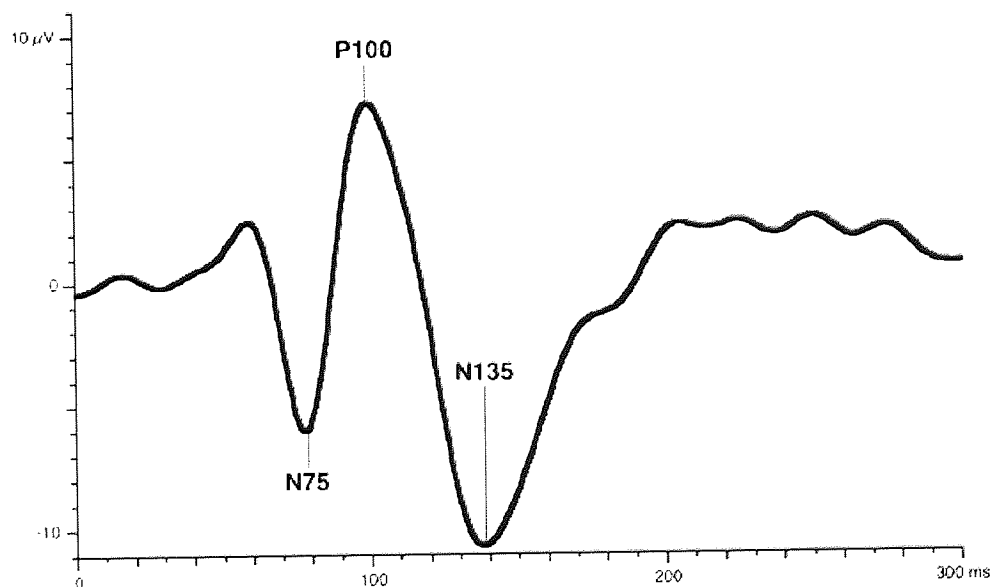
Figure 4-3 Pattern Reversal Evoked Potential. The nomenclature describes the morphology and relative amplitude change of the N75, P100 and N135 components observed following the reversal of a pattern stimulus. Image redrawn from Harding *et al.,* (1996).

4.3   Cortical Oscillatory Activity

4.3.1   Introduction

It has long been recognised that rhythmic activity is a feature of ongoing cortical activity. Since Berger (1930) identified the alpha wave in EEG, spectral activities and their characteristics have become a major source of investigation, suggestion and speculation. The various distinct frequency ranges of activity have been classified into specific bands, for which the classical nomenclature is: delta (δ) as 0.5- 3 Hz, theta (τ) as 4 – 7 Hz, alpha (α) as 8 – 13 Hz, beta (β) as 14 – 25 Hz and gamma (γ) as >25 Hz. There is enormous variation in the description of each of these bands. Furthermore the variation between subjects (Basar *et al.*, 1999) is wide enough to generate discrepant results within the same experimental paradigm. Within this thesis the work undertaken has been initially analysed within three spectral bands; alpha (7 – 14 Hz), beta (15 – 25 Hz) and gamma (30 – 80 Hz). First pass analysis using these three bands allows coarse identification of changes in spectral activity, which can then be investigated using spectrally detailed analysis methods (Chapters 5, 7 and 8). Investigation of the spectral bands yields information regarding functional specificity. However, like the variation seen in the frequency bands of different subjects, it is often the case that the changes in the oscillatory activity in terms of power increase or decrease and the spatial localisation vary widely in the majority of measurements. The neuronal basis of this variability is unknown, however it appears to highlight the dynamic and probably chaotic (Fell *et al.*, 2003) nature of the brain. A major contributor to the diversity of these responses is likely the ongoing spontaneous oscillations in the brain, which could affect whether the response appears as an ERS or ERD*.

*According to Pfurtscheller and Lopes da Silva (1999a, and 1999b), induced ERS/ERD within the cortex reflects functional connectivity. These rhythmic activities are conditioned by factors related to neuronal assemblies and include: (1) intrinsic properties of the neuronal membrane, (2) structural connectivity of network elements related to feedback and feed-forward (thalamo-cortical and cortico-cortical) loops, and (3) local and global modulation effects of intrinsic neurotransmitters. Additionally, these oscillations occur at the macroscopic level and as such their appearance in the MEG/EEG signal is dependent upon the cortical extent of ERS.ERD (Lopes da Silva, 1991).

4.3.2 Alpha

Alpha (α) activity (7-13 Hz) can be seen in the visual cortex, where alpha synchronisation is seen during eye closure, followed by alpha desynchronisation upon eye opening (Berger, 1930). Alpha oscillations are most clearly affected by changes in the visual environment and are seen to fluctuate in response to the saliency or familiarity of visual presentations (Vanni *et al.*, 1997). The precise role of alpha as a measure of visual input is unclear as, although it is the commonest and most robust response, it also varies and during sleep the alpha synchrony is seen to fluctuate, apparently independent of sleep state. Visual alpha oscillations also appear to vary in response to cognitive tasks (Worden *et al.*, 2000; Ray and Cole, 1985). Furthermore, alpha is not restricted to a single region of the cortex, using MEG, alpha has been observed in occipital and parietal cortex (Chapman *et al.*, 1984; Williamson and Kaufman, 1989; Salmelin and Hari, 1994a) and more recently temporal cortex (Hall *et al.*, 2004a). Strong coherence in alpha rhythms between cortex and lateral geniculate nucleus (LGN) have been found in animal experiments, implicating thalamo-cortical connections in the generation of alpha activity (Lopes da Silva *et al.*, 1973).

4.3.3 Beta

Beta (β) activity (15-25Hz), like alpha, is seen across the cortex, but is particularly defined from reported activity in the motor cortex of the human (Pfurtscheller *et al.*, 1997), where it is seen in association with spontaneous movement, often as synchronisation in one region and desynchronisation in another. Furthermore, it is modulated by the introduction of various pharmacological substrates (Jongsma *et al.*, 2000). It is often seen in response to the onset of visual stimuli (Bekisz and Wróbel, 1993), although it has not been functionally characterised, it is observed with respect to change in adjacent frequency bands (Wróbel, 2000; Bekisz and Wróbel, 1999).

4.3.4 Gamma

Gamma (γ) activity is greatly variable in its description, but is commonly described as 30-70Hz activity. It is widely observed in the cortex in relation to auditory and visual processing and so is of great interest in the field of functional neuroimaging. It

is often related to measurements at the single cell level (Gray *et al.*, 1989; Gray and McCormick, 1996) in response to visual stimulation. A principle theory underlying synchrony is that of feature binding in the visual scene (Singer 1993, 1994, 1999; Singer and Gray, 1995, Engel *et al.*, 1997; Roelfsema and Singer, 1998; Herculano-Houzel *et al.*, 1999). Binding is suggested to enhance neuronal signal saliency and therefore processing efficacy (Fries *et al.*, 2001). This feature binding hypothesis has been applied at the perceptual level as a mechanism by which task relevant object representation is achieved (tallon-Baudry *et al.*, 1996, 1997; Tallon-Baudry and Bertrand, 1999; Kiel *et al.*, 1999). However, the feasibility of this theory remains a source of debate (Shadlen and Movshon, 1999). The subject of gamma oscillatory activity is discussed in further detail in chapter 5.

4.4   The Study

4.4.1   Rationale

The widespread investigation of VEP in research and clinical settings has given rise to classification standards (Harding *et al.*, 1996; Odom *et al.*, 2004), which provide latency and amplitude information for scalp electrode recordings. There have been studies with both EEG and MEG that have attempted to localise the current generators of the specific components of the various visual evoked potential VEP and MEG equivalent 'visual evoked magnetic field' (VEMF) using the dipole fitting method (chapter 2). These studies have provided conflicting reports of the visual cortical locations of many components of pattern onset, reversal and flash VEPs (Biersdorf, 1974; Jeffreys and Axford, 1972a,b; Lesevre, 1982; Ossenblok and Spekreijse, 1991; Manahilov *et al.*, 1992; Miniussi *et al.*, 1998; Ikeda *et al.*, 1998; Di Russo *et al.*, 2001; Darcey and Arj, 1980; Maier, 1987; Bach and Ullrich, 1997; Portin *et al.*, 1998; Tzelepi *et al.*, 2001).

VEPs are used in clinical investigations of visual disorders such as optic neuritis, and optic neuropathy and are of futher relevance in neurological disorders such as Alzheimer's disease, photosensitive epilepsy and migraine; therefore a normative spatio-temporal categorisation of clinical stimuli is a theoretically informative basis for pathological comparison. The use of functional imaging modalities such as MEG and

fMRI to investigate the cortical activity occurring as a result of cognitive processing in particular tasks is dependent upon the assumption that the activity observed is solely the result of the difference in task-related processing.

When using visually presented paradigms the assumption is made that the discrete differences in the visual image itself makes little or no contribution to the observed activity. Therefore an investigation of neuronal activity associated with simple visual stimulation might inform true experimental baseline conditions; activities outside of the visual cortex are of particular interest.

Basis for the study

1. Although EEG and MEG techniques are typically assumed to measure contiguous features of neuronal activity, the systematic relationship between the various VEP and VEMF complexes remains undefined in terms of comparative latencies.

2. The use of dipole fitting to localise visual evoked potential components is abundant in the EEG and MEG literature. However, there is extensive variation in the suggested loci or cortical generators for many VEP components, where previous analytical methods in EEG and MEG conflict.

3. The SAM analysis method is typically employed over long time windows (seconds). Its ability to operate under shorter time windows and observe transient activity such as an evoked potential based upon its frequency content, was previously unknown.

4. The ability of the virtual electrode method to reconstruct evoked cortical activity remains a theoretically useful device. However, no platform for its evaluation has been explored and as such it remains a detached entity.

5. The current standards regarding evoked data include the established pattern onset, pattern reversal and luminance onset (flash) responses. However, neither pattern offset nor luminance offset are considered. Furthermore, investigations of pattern stimuli explore the effect of altering spatial phase (pattern reversal) but make no attempt to investigate the effect of altering contrast without altering pattern.

6. The use of normative data regarding the activity following visual stimulation is established in clinical practice using latency information (Harding *et al.*, 1996; Odom

et al., 1996). However, there are no systematic data regarding the oscillatory changes associated with visual stimulation.

Aims of the Study

With the existing and emergent analytical methods in MEG the potential for investigation of visually evoked and induced activities is quite substantial. Therefore, here a few aspects are made the focus of the investigation, whilst further elements are covered in brief.

The **primary aims** of this investigation are as follows:

1. To define the magnetic latency components of the VEMF for comparison with those defined in the electrical VEP (Harding *et al.,* 1996).

2. To evaluate the efficacy of the dipole fitting method in localising the typical pattern onset, pattern reversal and luminance onset VEMF components, from the latencies identified in the sensor data.

3. To explore the efficacy of SAM localisation of the VEMF complex by comparison with the established dipole method (above).

4. To establish the ability of the virtual electrode method to reconstruct anatomically discrete neuronal activity by placement at peak SAM locations to obtain latency information to compare with the raw sensor data. Additionally, to explore the efficacy of the SAM and VE methods by informing the dipole analysis using VE latency information.

The **Secondary** aims of the study are as follows:

5. To establish the individual characteristics of the pattern offset, luminance offset and two novel stimuli; the contrast increment and contrast decrement.

6. To generate a summary profile of the evoked and induced visual cortical activity following presentation of various visual stimuli. This is to provide normative data to elucidate a possible basis for clinical comparison and inform true baseline states in visually conveyed MEG experiments.

4.4.1.1 Preamble

The outcome of the secondary aims of this chapter are not designed to provide conclusive descriptions of the evoked or induced activity occurring in response to visual stimulation, nor proposed as a decisive standard against which individual cases might be compared. Results are intended as a preliminary summary of visual activities that identify consistencies where present and additionally to emphasize heterogeneity and variability of visual function between subjects.

4.4.2 Methods

4.4.2.1 Stimuli

Subjects (n=8) focused on a central fixation point at a distance of two metres, whilst visual stimuli were presented in the lower left quadrant of the visual field. All stimuli subtended 3° x 3° of visual angle at an eccentricity of 0.5° from both horizontal and vertical meridians to maximise regional specificity of the cortical response. A single quadrant was used in order to avoid cancellation*.

Seven visual conditions were created: pattern onset, pattern offset, pattern reversal, luminance onset, luminance offset, contrast increment and contrast decrement. Pattern onset, pattern reversal and luminance onset, representative of clinical evaluation stimuli. Pattern and luminance offset represent intrinsic components of clinical evaluation which are typically overlooked or considered an element of their counterparts. The contrast increment and decrement were added as informative stimuli providing an additional decomposition of the standard pattern stimuli. All patterned stimuli were horizontally orientated sinusoidal gratings of 3 cycles per degree (cpd).

The stimuli presented using the following protocol:

- Pattern onset was a grating with a Michelson Contrast (C_m)* of 90%, presented for 2 seconds, followed by three seconds of blank background of equal mean luminance to the stimulus.

- Pattern offset was the return of the pattern onset stimulus to the isoluminant grey background.

- Pattern reversal was a grating, also with C_m 90%, which was phase reversed at 0.5 Hz (presented for 2 seconds between reversals).

- Luminance increment comprised a black background with mean luminance of $300cd/m^2$, onto which an achromatic luminance patch of $300cd/m^2$ was presented for 2 seconds, followed by a return to a completely black background for 3 seconds.

- Luminance decrement was the return of the luminance onset to its background.

- Contrast increment consisted of a grating presented at C_m 10% for 3 seconds and was then incremented without phase reversal to a Michelson Contrast of 100% for 2 seconds.

- Contrast decrement was the return of the contrast increment from C_m 100% to C_m 10%. The stimuli were presented in three consecutive trials, with approximately 2 minutes recovery between. The trial order and stimulus presentation were randomised within and between subjects to remove order effects; each of the stimuli appeared a total of 50 times.

- Recording and Coregistration were carried out using the standard protocol *.

*   The reader is referred to section 3.5 for details of methodological procedures.

4.4.3   Analysis

The four types of analysis used were: sensor data analysis, dipole fitting, SAM analysis and virtual electrode analysis. The details of these are provided at the beginning of each respective method.

4.4.4   Raw Sensor and Virtual Electrode Traces

4.4.4.1   Analysis

The data were analysed using time-locked signal averaging in order to increase signal to noise ratio (SNR) of the time-locked evoked magnetic fields and to cancel non-time-locked fluctuations. The latency information of the various components were obtained and virtual electrode traces reconstructed from the various peak loci in the SAM images were used to confirm this information where possible.

4.4.4.2   Results

In this section the results from a single subject representative of the overall results are presented as a reflection of the signal obtained at the sensor level. This demonstrates the latency components observed, which are typically used in dipole analysis and conveys the efficacy of the virtual electrodes in defining evoked cortical activity.
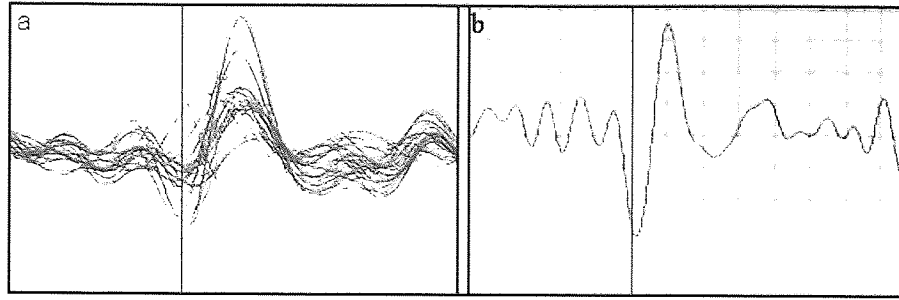
Figure 4-4 Pattern Onset traces. (a) Raw sensor data from six occipital sensors (midline to right). (b) Virtual electrode trace at the SAM location determined for pattern onset (fig. 4-13a). Red cursor indicates the C2m (~100ms) component (table 4-1).
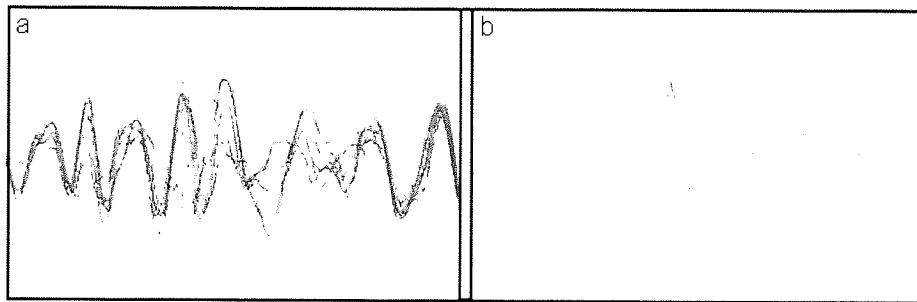
Figure 4-5 Pattern Reversal traces. (a) Raw sensor data from six occipital sensors (midline to right side). (b) Virtual electrode trace at the SAM location determined for pattern reversal (fig. 4-26a). The red cursor indicates the P100m component (table 4-1).
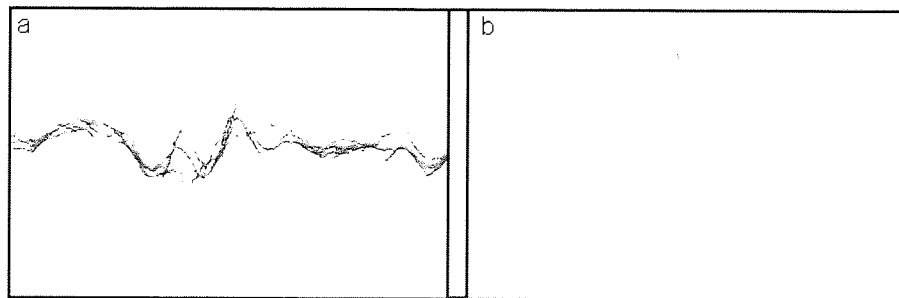
Figure 4-6. Luminance onset traces. (a) Raw sensor data from six occipital sensors (midline to right side). (b) Virtual electrode trace at the SAM location determined for luminance onset (fig. 4-35a). Red cursor indicates P2m component.
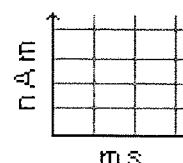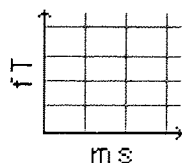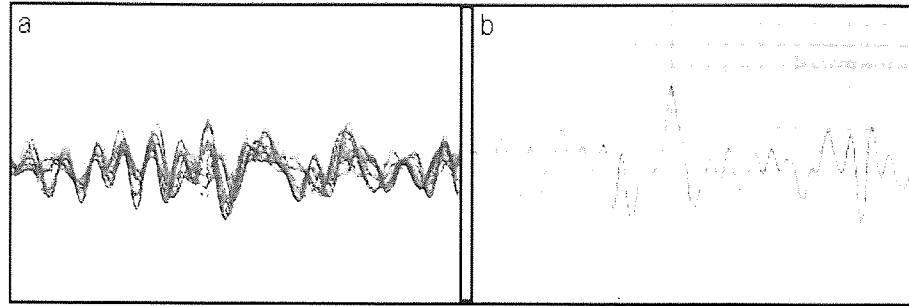
Figure 4-7. Contrast increment traces. (a) Raw sensor data from six occipital sensors (midline to right side). (b) Virtual electrode trace at the SAM location determined for contrast increment (fig. 4-43a). Red cursor indicates 150ms component.
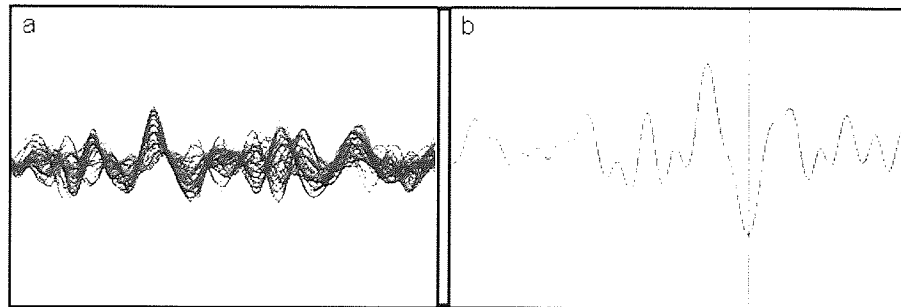
Figure 4-8. Contrast decrement traces. (a) Raw sensor data from six occipital sensors (midline to right side). (b) Virtual electrode trace at the SAM location determined for contrast decrement (fig. 4-51a). Red cursor indicates 160ms component.
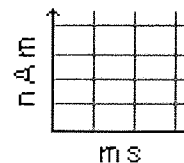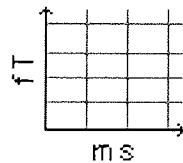
Pattern Onset			Pattern Offset			Pattern Reversal		
C1m	C2m	C3m	1st	2nd	3rd	N75m	P100m	N135m
73.6 ±3.2	101.6 ±5.3	155.2 ±10.7	93.8 ±6.1	155.4 ±5.6	217.1 ±18.2	N/A	5.3 ±5.1	145.0 ±5.48

Table 4-1. Latency table (Pattern Onset, Offset and Reversal). Details of the latencies (ms) ±SEM of the component peaks of the consistent components of pattern onset, pattern offset and pattern reversal evoked potentials; obtained from the sensor and VE data.

Luminance Onset				Contrast Increment			Contrast Decrement	
N2m	P2m	N3m	P3m	1st	2nd	3rd	1st	2nd
64.3 ±3.3	125.4 ±4.9	197.4 ±13.1	246.9 ±15.4	115.7 ±10.4	148.3 ±8.4	206.7 ±5.8	158.3 ± 9.9	212.3 ±16.4

Table 4-2. Latency table (Luminance Onset and Contrast Increment/Decrement). Details of the latencies (ms) ±SEM of the component peaks of the consistent components of luminance onset, contrast increment and contrast decrement evoked potentials; obtained from the sensor and VE data.

4.4.4.3 Evoked Magnetic Components

This section draws parallels between the VEMFs observed in the sensor and virtual electrode data and the VEPs described in the standards literature (Harding *et al.*, 1996; Odom *et al.*, 2004).

The pattern onset VEMF (fig. 4-4) demonstrated visible components in the raw sensor data, with magnetic components C1m, C2m and C3m observed at latencies consistent with their electrical VEP counterparts (Harding *et al.*, 1996; Odom *et al.*, 2004). The pattern reversal VEMF (fig. 4-5) sensor data demonstrated P100m and N135m components again consistent with VEP reports (Odom *et al.*, 2004). However, a magnetic equivalent of the N75 component was clearly observable in too few subjects (n=3) to confidently report its latency. Several of the luminance increment components (fig. 4-6) were clearly visible in the sensor data; the N2m, P2m, N3m and P3m were clearly observed in all subjects at comparable latencies to their EEG equivalents (Odom *et al.*, 2004). However, the earlier N1 and P1 components were too inconsistent to be clearly observed across subjects.

The pattern offset VEMF (fig. 4-4), which is typically only considered as a by-product of the pattern onset evoked potential, was determined to have a temporally distinct time course with peaks at around 95, 155 and 220ms (table 4-1).As further discussed throughout the chapter, a luminance offset evoked response was not clearly visible in any of the subjects.

In addition to the standard VEMF/VEP types, two novel evoked activities were classified: the contrast increment and decrement VEMFs (figs 4-7 and 4-8 respectively). The contrast increment VEMF demonstrated three stable components at approximately

115, 150 and 205 ms (table 4-2). The contrast decrement VEMF demonstrated two stable components at approximately 160 and 210 ms (table 4-2). Both the contrast increment decrement components were not clear enough in the sensor data to classify component latencies; therefore the virtual electrode data (figs 4-7b and 4-8b) were used for this purpose.

4.4.5 Dipole Fitting

4.4.5.1 Analysis

As described in chapter 2, dipole fitting was used as an initial analysis tool. A small spatio-temporal window (20ms) was analysed at the evoked potential peak (fig. 4-9b). The best fit in terms of dipole number and location (fig. 4-9a) was determined by the reduced chi-square error measure[‡] (fig. 4-9c). The stability of the solution was then analysed using a Monte-Carlo analysis to define the source location error (chapter 2).
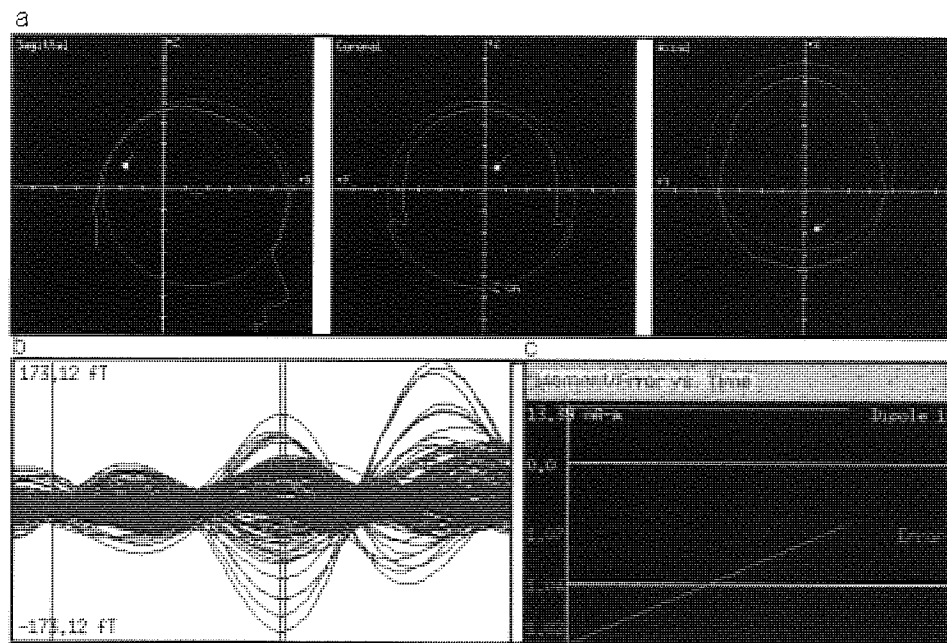
Figure 4-9 Example of a dipole localisation (Pattern Onset C2m). (a) Spatiotemporal dipole fit result using a subject optimised head model[‡] (see fig. 4-10b). (b) Spatio-temporal window selected for the localisation shown in a (~100ms). (c) Reduced Chi-square error calculation for defined window, demonstrates the gooness of fit of the specified location for the time period; in this case near to 1 illustrate it is an accurate model.

[‡]   The reader is referred to chapter 2 for details of dipole fitting, head-models and Monte-Carlo statistical analysis.

For each of the visual stimulus conditions various components were localised and are demonstrated in single subjects that are representative of the results found in the majority of subjects in the group.
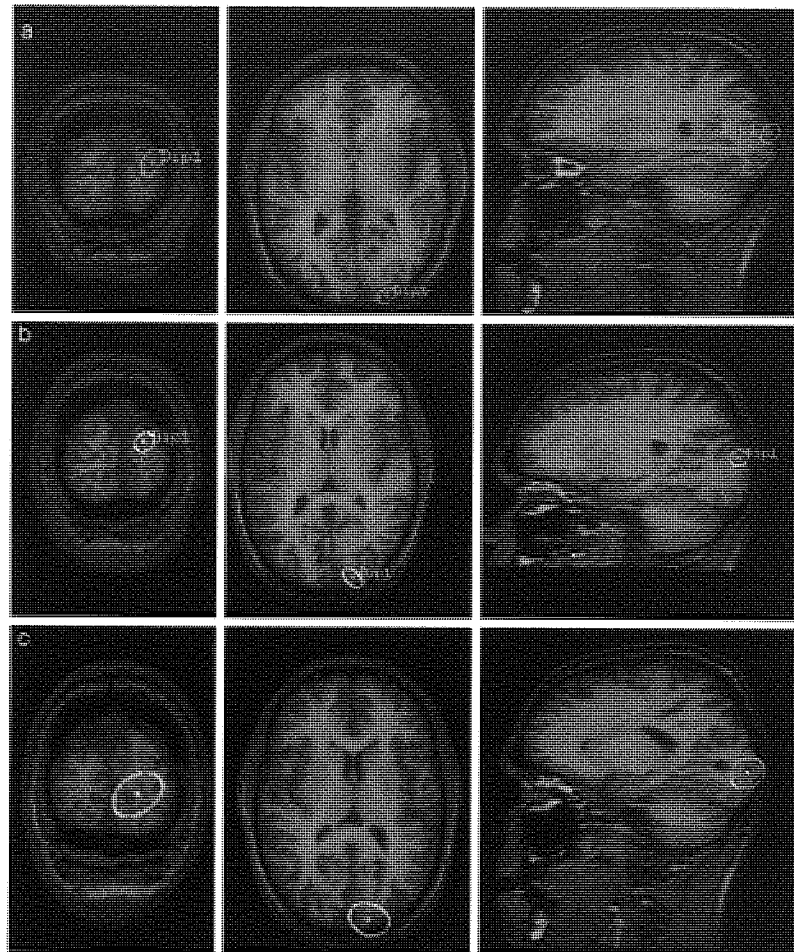
Figure 4-10. Dipole Localisation with Monte-Carlo volume (pattern stimuli). Central dot shows dipole localisation, surrounding elipse shows Monte-Carlo 95% confidence volume. (a) Pattern reversal localisation of the P100m component (~100ms); localised to the upper right bank of the calcarine sulcus with focal Monte-Carlo volume. (b) Pattern onset localisation of the C2m component (~100ms); localised to a focal region of upper right V1, as reflected by the Monte-Carlo volume. (c) Pattern onset localisation of the C3m component (~150ms); locus in right visual cortex around the region of V2, extended Monte-Carlo over striate and extra striate regions.
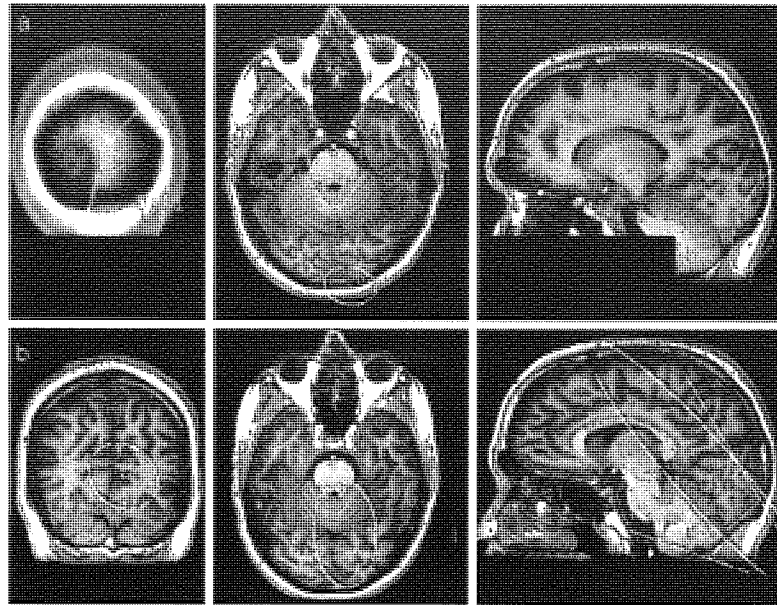
Figure 4-11. Dipole Localisation with Monte-Carlo volume (luminance stimuli). Central dot shows dipole localisation, surrounding elipse shows Monte-Carlo 95% confidence volume. (a) Luminance onset localisation of the P2m component (~100ms); localised to right ventral-posterior visual cortex with extended Monte-Carlo volume. (b) Luminance onset localisation of the N3m component (~160ms); localised to the right anterior visual cortex at deep location, Monte-Carlo reflects large variability.
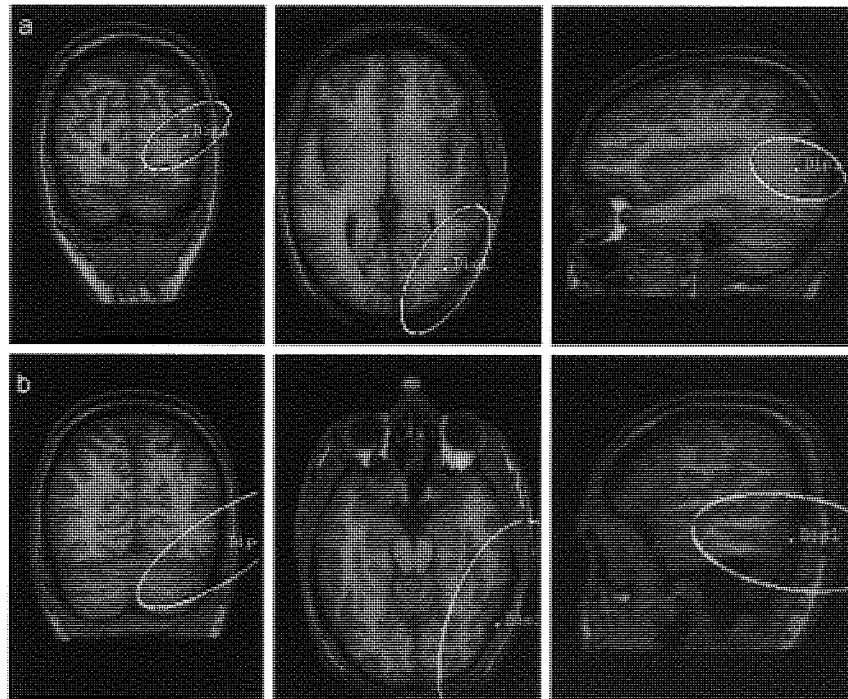
Figure 4-12 Dipole Localisation with Monte-Carlo volume (contrast stimuli). Central dot shows dipole localisation, surrounding elipse shows Monte-Carlo 95% confidence volume. (a) Contrast Increment localisation of the second component (~150ms); localised with poor reliability to right occipito-temporal regions, with Monte-Carlo encompassing regions from V1 to middle temporal regions. (b) Contrast Decrement localisation of the first (~160ms) component; localised to temporal regions with poorly defined Monte-Carlo volume.

4.4.5.2 Results

The P100m component of the pattern reversal VEMF localised reliably to upper right primary visual cortex; retinotopically concordant with lower left visual field stimulation (fig. 4-10a). The Monte-Carlo 95% confidence distribution was a very small region around the dipole solution and the reduced Chi-Square statistic was around 1 (fig. 4-9c). The C2m component of the pattern onset response localised to a similar cortical location (upper right V1), again with a Monte-Carlo distribution indicating a similarly good source solution to that of the P100m component. The C3m component of the pattern onset VEMF localised to the upper right visual cortex, with the dipole solution typically finding an early extra-striate visual cortical area in the region of V2/V3 (fig. 4-10). A two-dipole fit was attempted to account for the C3m component. However, a stable fit could not be obtained and typical reduced chi-square values (Supek and Aine, 1993, 1997) for the single dipole fit was around unity, indicating that this simple model adequately accounted for the data given the noise level. However, the 95% confidence Monte-Carlo distribution encompassed both the primary visual cortex (V1) and extra-striate areas (V3, V3a and V4) (fig. 4-10c), suggesting a poor fit with large spatial variance across these areas. Luminance increment solutions were obtained for the P2m and N3m components. The P2m component localised to lateral areas of the primary visual cortex, however, although consistently located around the calcarine sulcus the localisation both within and between subjects was variable in both lateral and vertical localisation, as reflected by the Monte-Carlo distribution (fig. 4-11a). The N3m component localised to a source around the primary visual cortex, however typically quite deep in the calcarine fissure. The Monte-Carlo distribution for the P3m component proved to encompass not only the primary visual cortex but also deeper brain areas (fig. 4-11b). The reduced chi-square values generally suggested under-modelling of the activity, however the application of a two dipole model was unable to provide a stable solution.

The contrast increment and decrement VEMFs each had a single component, informed by the used of VE analysis. These could be localised to the same cortical region reliably in five subjects. The reliable component of the contrast increment evoked potential (~155ms) localised to the right visual cortical areas in the region of V5 (middle temporal) (fig. 4-12a), but had a Monte-Carlo distribution that encompassed both earlier visual areas (V1-V4) and more temporal regions (inferior/medial temporal lobe). Similarly, the second component of the contrast decrement VEMF (~160ms) was the only component that could

be localised with any degree of consistency and was found in occipital-temporal regions with a large Monte-Carlo distribution encompassing large regions of right visual cortical areas (fig. 4-12b). In both of these cases it was clear that a single dipole was an inadequate solution, reflected by the reduced chi-square values. Two-dipole models were attempted in both cases and were unable to provide adequately stable solutions, suggesting further modelling was required; however, further attempts with multiple dipoles was also unsatisfactory. Neither pattern offset nor luminance offset could provide reliable and stable dipole fits.

4.4.5.3 Synthetic Aperture Magnetometry

4.4.5.4 Analysis

Subsequent to the initial dipole analysis a series of SAM analyses were carried out on the time period following each of the visual stimulus onsets. As discussed previously the evoked activity was analysed using a short (300ms) temporal window following the stimulus onset with a 3-12Hz frequency band (described in chapter 3). In addition, the induced oscillatory changes following each of the stimulus conditions were analysed using three frequency windows of common interest: alpha (7-13Hz), beta (15-25Hz) and gamma (30-70Hz), analysed using a 2 second time window. The following section is a classification of the cortical activities evoked and induced by various visual stimuli and as such is subdivided into stimulus type in order that the relationship between spectral bands might be identified. The stimulus condition, subject number and analysis windows used, results in the generation of large numbers of SAM images. Therefore, in each condition a representative sample of the activity seen across the subjects, are presented with a subsequent group SAM image, showing the averaged response of the group. As was the case with both the evoked potential and dipole analyses, not all of the conditions generated a conclusive picture of the spectral activity; under these conditions a sample of the subject variability is presented without subsequent group SAM image; similarly those conditions that displayed no distinguishable activity are omitted.

Throughout the following section results are displayed as SAM images with accompanying individual t-statistic, the images are individually thresholded to highlight activity within the visual cortex, a typical threshold being t>1. This has been used to remove the activity within other cortical regions, which under current conditions have been considered to be noise. With the exception of the gamma images, which have all been given a common threshold for comparative purposes (further discussed in chapter 6). Subjects shown in the individual images have been arbitrarily chosen to best represent the cohort and group in order to illustrate in order to emphasise either the consistency or variability of the results. All group SAM images are the outcome from the average of all subjects (n=8).

4.4.6 Pattern Onset

4.4.6.1 Evoked Magnetic Field

Figure 4-13. Pattern Onset VEMF SAM localisation. Data from two subjects showing the locus of the transient burst of synchrony 0-300ms post-stimulation. (a and b) Subject FM shows (a) striate activation (t=2.5) and (b) extra-striate activation (t=4.7). (c) Subject KDS shows striate (t=1.0) and extra-striate (t=1.6) activation.
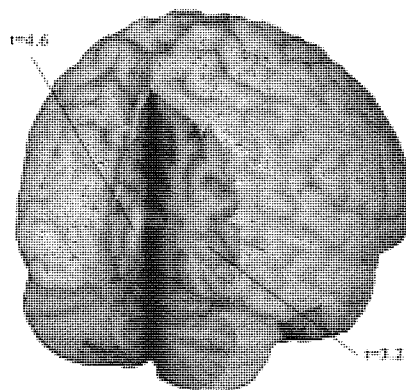
Figure 4-14. Group SAM Image (Pattern Onset VEMF). Shows striate (t=4.6) and extra-striate (t=3.2) activation (image threshold >2).

4.4.6.2 Alpha

| Axial | Coronal | Sagittal |

JS

KDS

FM
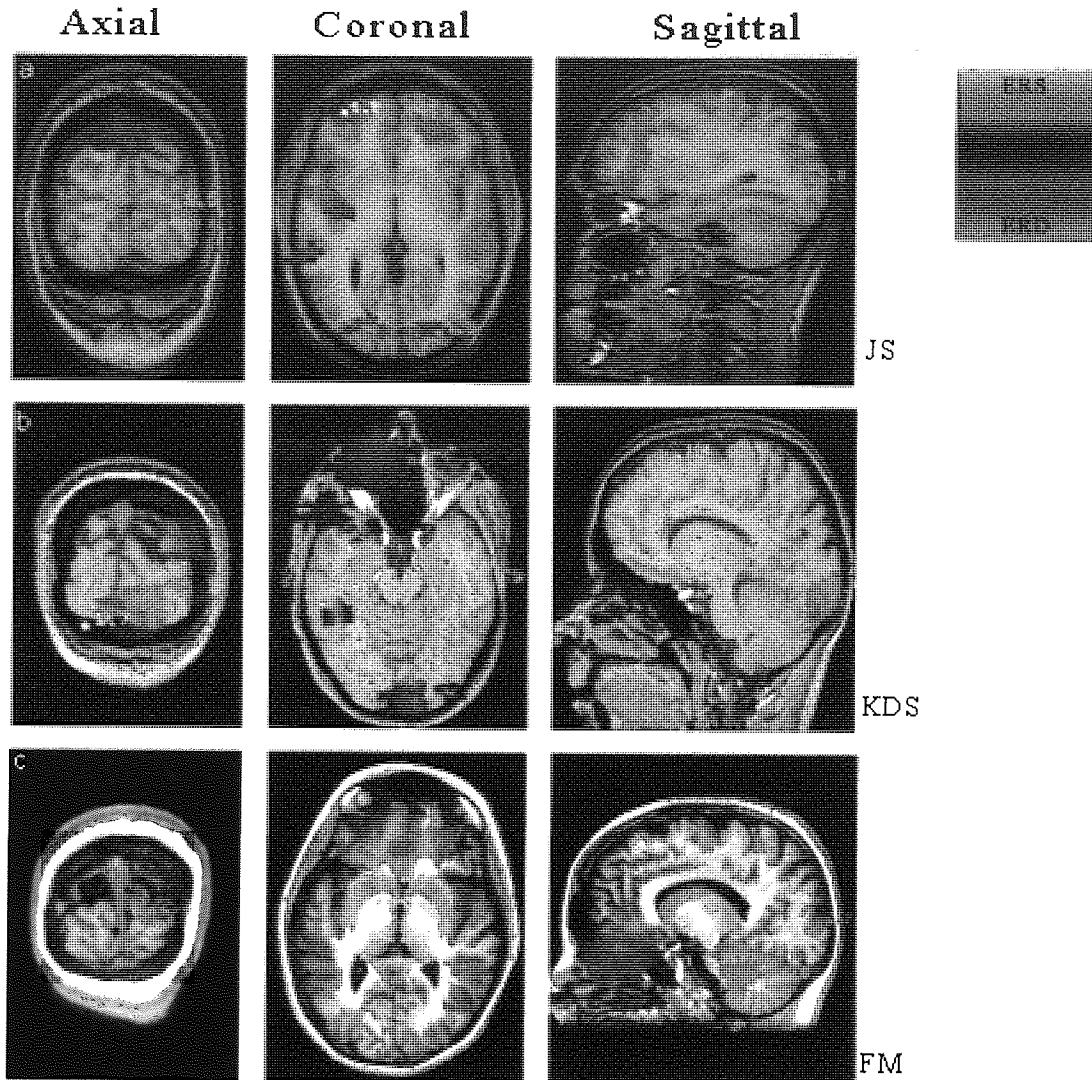
Figure 4-15. Pattern Onset Alpha Localisation. Data from three subjects showing the locus of the ERS/ERD 0-1.5s post-stimulation. (a) Subject JS shows bilateral ERD activation (t=1.5 (R); t=1.4(L)). (b) Subject KDS shows contralateral ERD in striate (t=1.7) and extra-striate (t=1.1) visual cortex. (c) Subject FM shows bilateral ERD activation (t=2.2(R); t=1.8 (L).
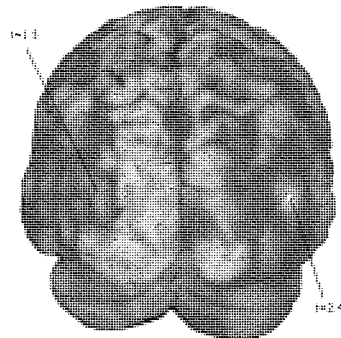
Figure 4-16. Group SAM Image (Pattern Onset Alpha). Shows bilateral extra-striate ERD (t=2.4 (R); t=1.5(L)) (image threshold >0.8).

4.4.6.3 Beta
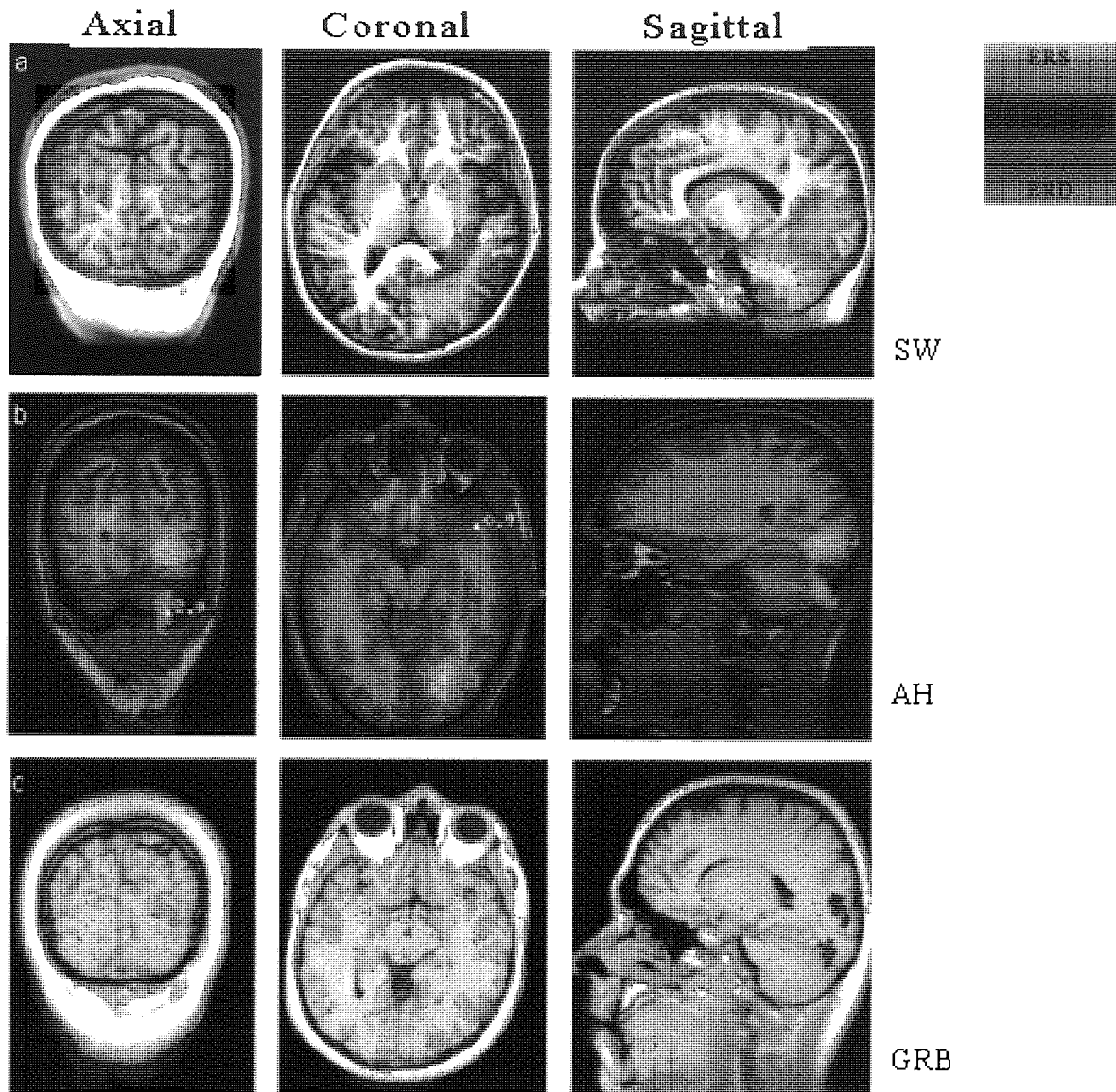
Figure 4-17. Pattern Onset Beta Localisation. Data from three subjects showing the locus of the ERS/ERD 0-1.5s post-stimulation. (a) Subject SW shows bilateral ERD (t=2.4 (R); t=1.2(L)). (b) Subject AH shows bilateral ERD (t=2.2 (R); t=1.0(L)). (c) Subject GRB shows contralateral ERD in extra-striate visual cortex (t=2.4) and temporal cortex (t=1.4).
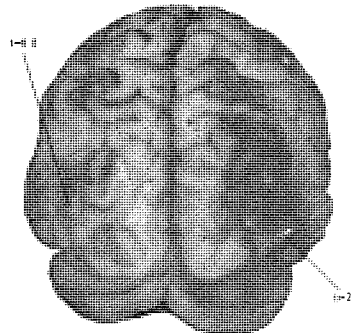
Figure 4-18. Group SAM Image (Pattern Onset Beta). Shows bilateral extra-striate ERD (t=2.1 (R); t=0.8(L)) (image threshold >0.6).

4.4.6.4 Gamma

Figure 4-19. Pattern Onset Gamma Localisation. Data from three subjects showing the locus of the ERS/ERD 0-1.5s post-stimulation. (a) Subject AH shows contralateral striate visual cortex ERS activation (t=2.2). (b) Subject GRB shows contralateral striate visual cortex ERS activation (t=3.4). (c) Subject PF shows contralateral striate ERS in extra-striate visual cortex activation (t=2.9).
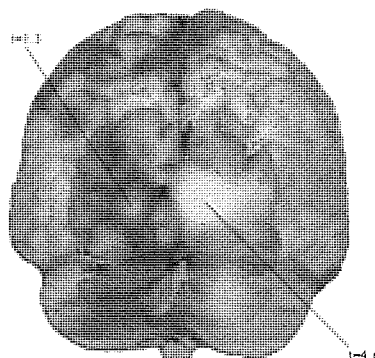
Figure 4-20. Group SAM Image (Pattern Onset Gamma). Shows contralateral striate visual cortex ERS (t=4.6) and ipsilateral striate visual cortex ERD (t=1.3) (image threshold >1.5).

4.4.6.5 Results

The SAM analysis of the pattern onset VEMF reveals strong evoked synchrony in two separate locations in striate visual cortex; (V1) (fig. 4-13a) and extra-striate visual cortex in the region of V3/V3a (fig. 4-13b). These peaks were clearly significant in seven of the eight subjects (expanded upon in chapter 5).

SAM analysis of the alpha band revealed bilateral ERD in the upper visual cortical areas. The individual images demonstrate the primary peak typically in the right side with desynchronisation often in the corresponding locations of right visual cortex that the evoked activity was observed in the same subject (figs. 4.13c and 4-15b). The group image demonstrates the bilateral nature of the activity, although finds extra-striate locations rather than varied visual cortical activity.

SAM activity in the beta band reveals ERD primarily in contralateral occipital cortex in early extra-striate areas (V2/V3) (fig. 4-7a-c). However, the locus of activity is quite large with varied diffuse activity extending to parietal cortex (fig. 4-18).

The SAM activity in the gamma band is the most striking of the frequency bands, with ERS in the upper right primary visual cortex, which is clear in all subjects (figs. 4-19a-c) and subsequently in the group SAM image, where ipsilateral ERD in striate cortex is also observed, (fig. 4-20) although subthreshold in the individual images.

4.4.7 Pattern Reversal

4.4.7.1 Evoked Magnetic Field

Figure 4-21. Pattern Reversal VEMF SAM localisation. Data from three subjects showing the locus of the transient burst of synchrony 0-300ms post-stimulation. (a) Subject FM shows contralateral activity in striate visual cortex (t=1.1) and extra-striate visual cortex activity (t=0.9). (b) Subject GRB shows bilateral activation (t=2.8(R); t=1.6(L)). (c) Subject JS shows contralateral activation in V1 (t=3.2).
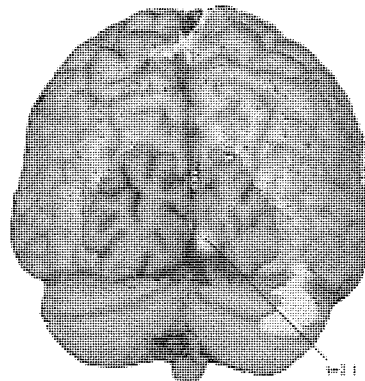
Figure 4-22. Group SAM Image (Pattern Reversal VEMF). Shows contralateral activity in striate visual cortex (t=2.1). (image threshold >1.5).

4.4.7.2 Alpha

Axial	Coronal	Sagittal

Figure 4-23. Pattern Reversal Alpha Localisation. Data from three subjects showing the locus of the ERS/ERD 0-1.5s post-stimulation. (a) Subject SH shows bilateral ERD in extra-striate visual cortex activation (t=1.6 (R); t=2.7 (L)). (b) Subject SW shows bilateral ERD in extra-striate visual cortex activation (t=2.3 (R); t=1.3 (L)). (c) Subject FM shows bilateral ERD in extra-striate visual cortex activation (t=1.9 (R); t=2.7 (L)).
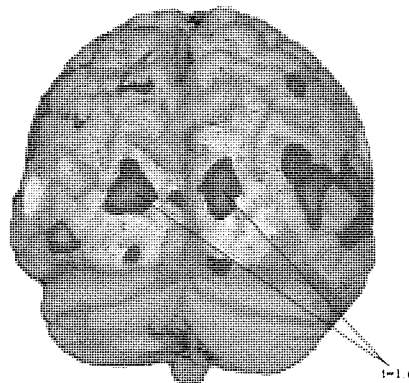
Figure 4-24. Group SAM Image (Pattern Reversal Alpha). Shows bilateral extra-striate visual cortex ERD (t=1.6) (image threshold >0.8).

4.4.7.3 Beta
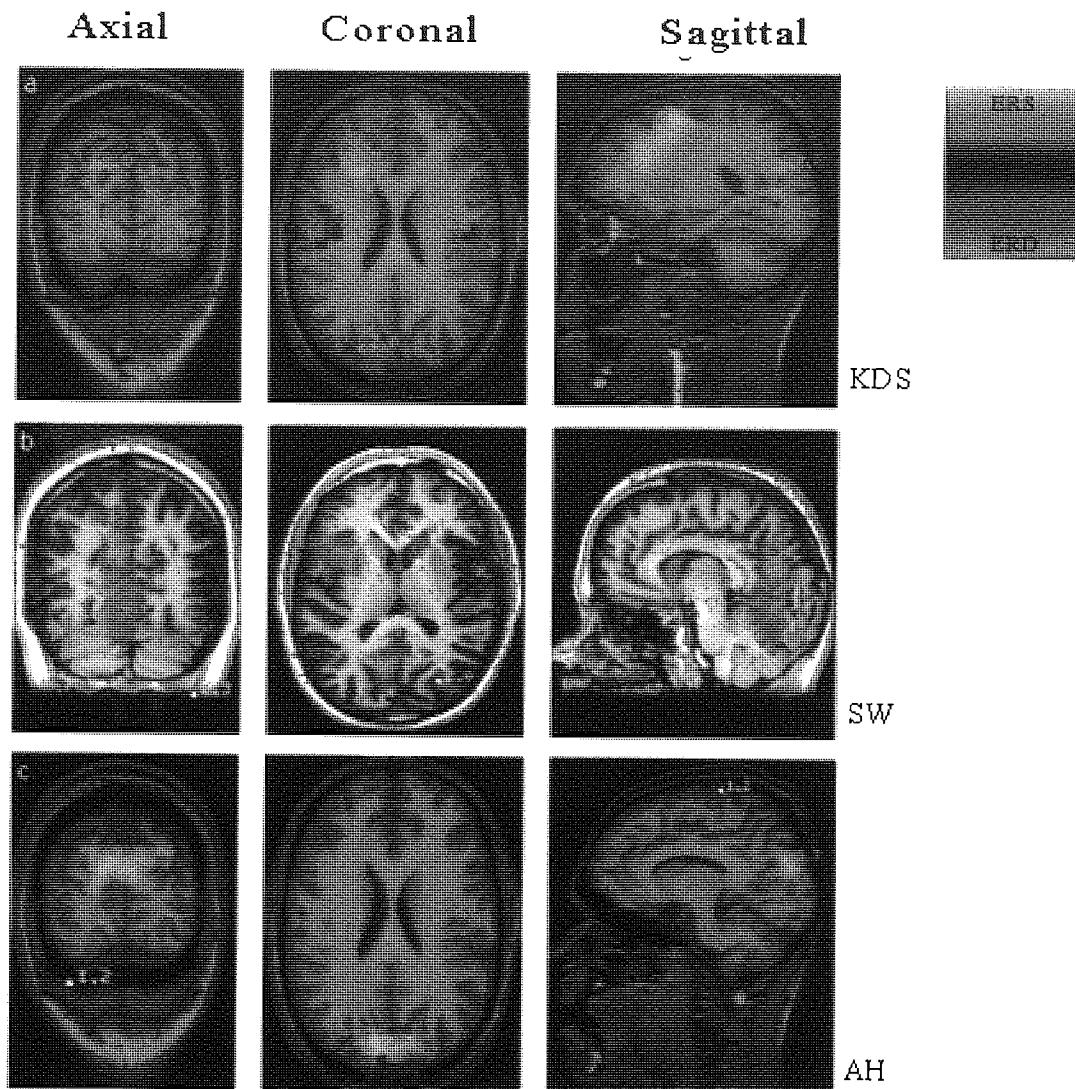
Figure 4-25. Pattern Reversal Beta Localisation. Data from three subjects showing the locus of the ERS/ERD 0-1.5s post-stimulation. (a) Subject KDS shows ERS in left occipito-parietal (t=2.0). (b) Subject SW shows ERD in left occipito-parietal (t=2.0) and right extra-striate visual cortex(t=2.0). (c) Subject AH shows ERD in left occipito-parietal (t=2.3).

4.4.7.4 Gamma
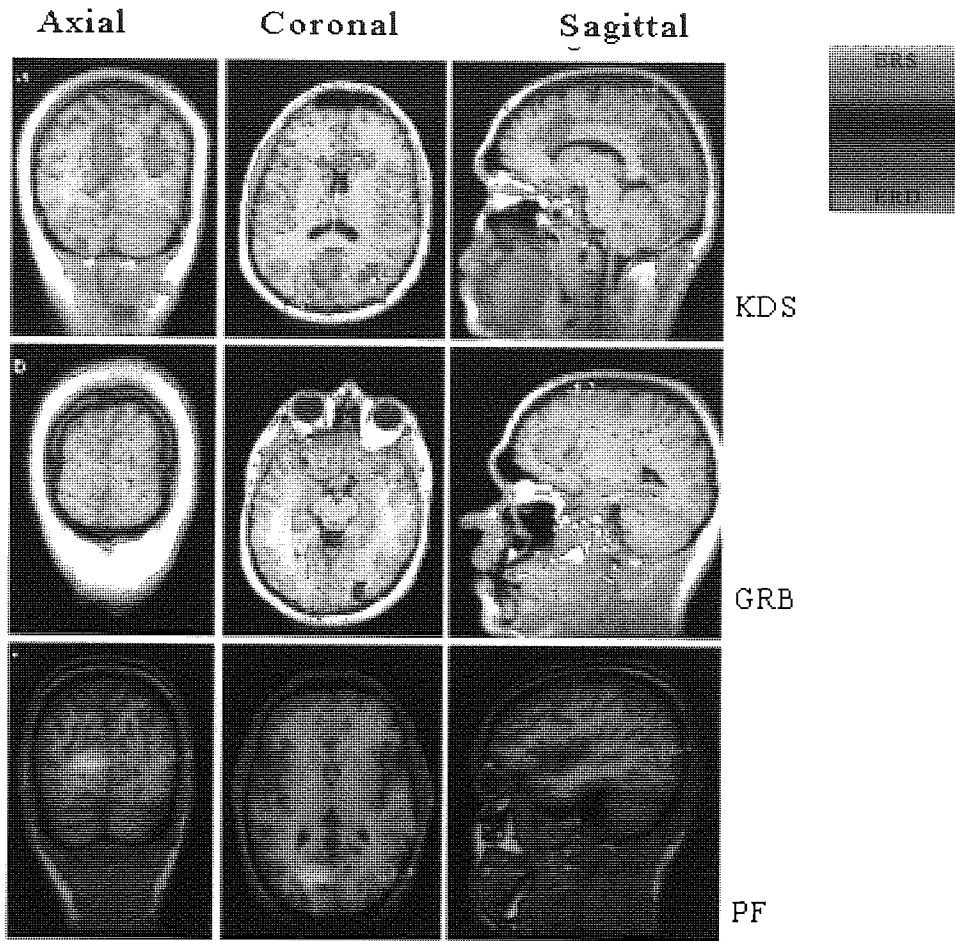
Figure 4-26. Pattern Reversal Gamma Localisation. Data from three subjects showing the locus of the ERS/ERD 0-1.5s post-stimulation. (a) Subject KDS shows ERS in right extra-striate (t=0.8) and ERD in striate visual cortex (t=1.6). (b) Subject GRB shows activation in the right extra-striate visual cortex ERS (t=2.6). (c) Subject PF shows ERS activation in right extra-striate (t=1.4) and ERD in left striate visual cortex (t=0.6).
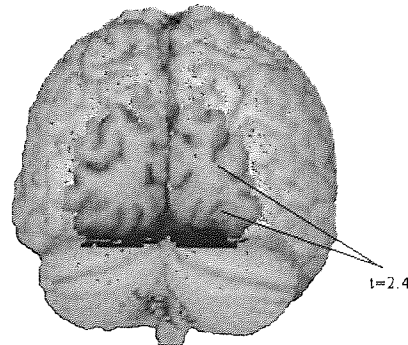
Figure 4-27. Group SAM Image (Pattern Reversal Gamma). Shows ERS in right extra-striate visual cortex (t=2.4) (image threshold >1.8).

4.4.7.5 Gamma
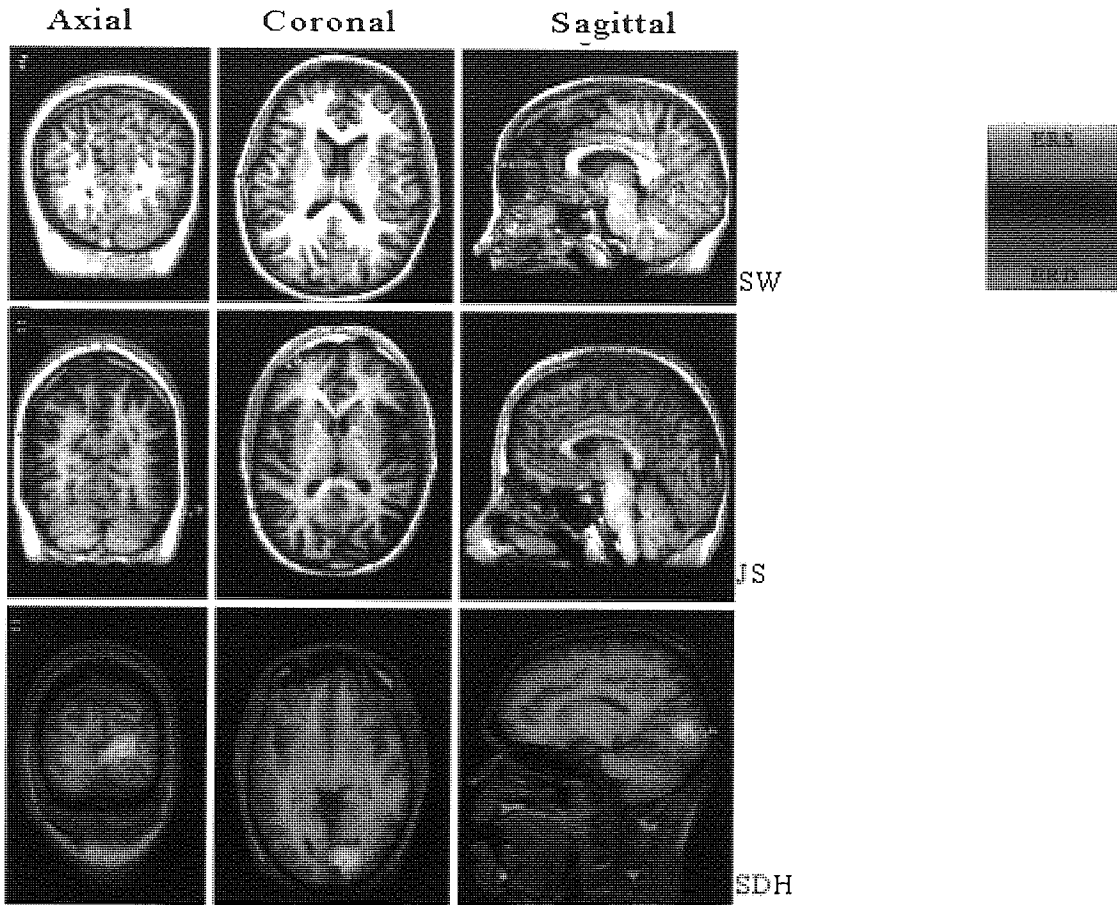
Figure 4-28. Pattern Reversal Gamma Localisation. Data from three subjects showing the locus of the ERS/ERD 0-1.5s post-stimulation. (a) Subject SW shows ERS in right V1 (t=2.2) (b) Subject JS shows ERS in striate visual cortex (t=2.8). (c) Subject SDH shows ERS in striate visual cortex (t=3.5).
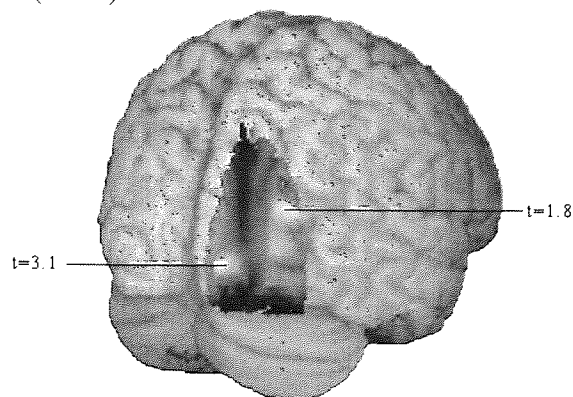
Figure 4-29. Group SAM Image (Pattern Reversal Gamma). Shows ERS in right striate visual cortex (t=3.1) and extra-striate visual cortex (t=1.8) (image threshold >1.4).

4.4.7.6 Results

The pattern reversal evoked potential measured using SAM shows a discrete peak of activity, represented by ERS in the upper right primary visual cortex. This was present in all subjects, although consistently focal to V1 with some subjects displaying additional activity in temporal and parietal regions (fig. 4-21a). This is demonstrated in the group SAM image (fig. 4-22).

The alpha activity observed as a result of the pattern reversal was principally bilateral ERD in various extra-striate locations (figs 4-23a,c), however some subjects demonstrated primary visual cortical activity also (fig. 4-23b). Interspersed amongst the ERD was weak and diffuse ERS, this activity was non focal and was sub threshold (>1.0) in the group image. The group image (fig. 4-24) shows the visual cortical ERD in both hemispheres with interspersed ERS.

The beta activity following pattern reversal was highly variable with ERS. In occipito-parietal areas in some subjects and extra-striate ERS in others (fig. 4-25), although in some subjects this appeared as an ERD (fig. 4-25b) and produced no significant group result.

The gamma activity following pattern reversal was investigated using two separate baseline conditions: (1) pre-reversal patterned background (PvP) and (2) the blank background (PvB). This was in order to distinguish the ongoing activity as a result of the stimulus presentation from the activity induced as a result of the pattern phase shift (discussed further in chapter 6). The PvP condition resulted in low level and focally discrete ERS activity in the extra-striate visual cortex which varied marginally in location between subjects (fig. 4-26a,b,c). This was reflected in the group SAM image (fig. 4-27). The SAM analysis from the PvB condition reflected synchronisation in the primary visual cortex in all subjects, with extra-striate and temporal sources with moderate variation in a selection of individuals (figs 4-28a,b,c. Images thresholded to highlight V1 activity). The group SAM image (fig. 4-29) reflects both striate and extra-striate ERS occurring in response to the pattern reversal condition. These results are expanded upon and further discussed in chapter 6.

4.4.8   Luminance Onset

4.4.8.1   Visual Evoked Magnetic Field
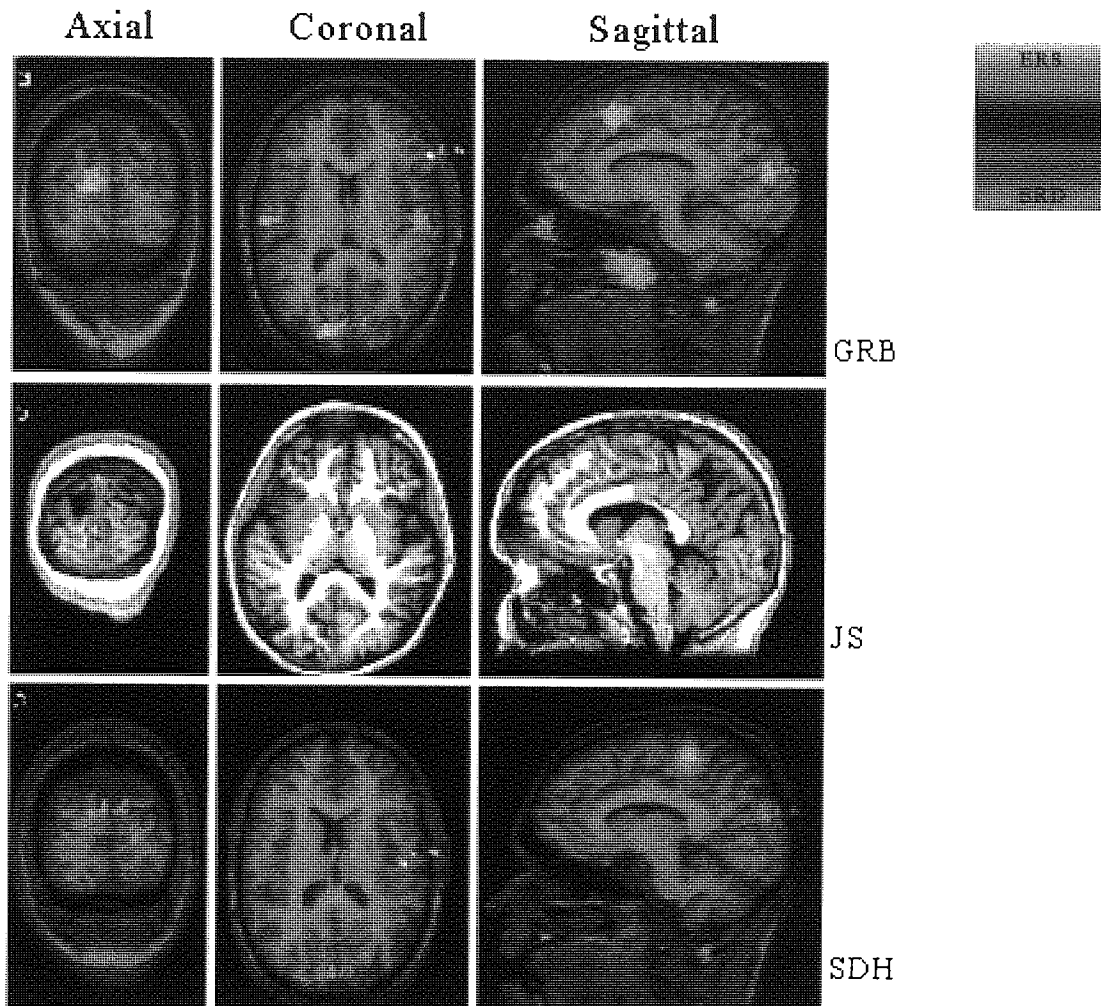
Figure 4-30. Luminance onset VEMF SAM localisation. Data from three subjects showing the locus of the transient burst of synchrony 0-300ms post-stimulation. (a) Subject GRB shows activation in right striate visual cortex (t=2.3). (b) Subject JS shows activity in striate visual cortex (t=2.7) and left extra-striate visual cortex (t=1.6). (c) Subject SDH shows activity in striate visual cortex (t=1.6).

4.4.8.2 Alpha

Axial   Coronal   Sagittal

AH

PF

FM
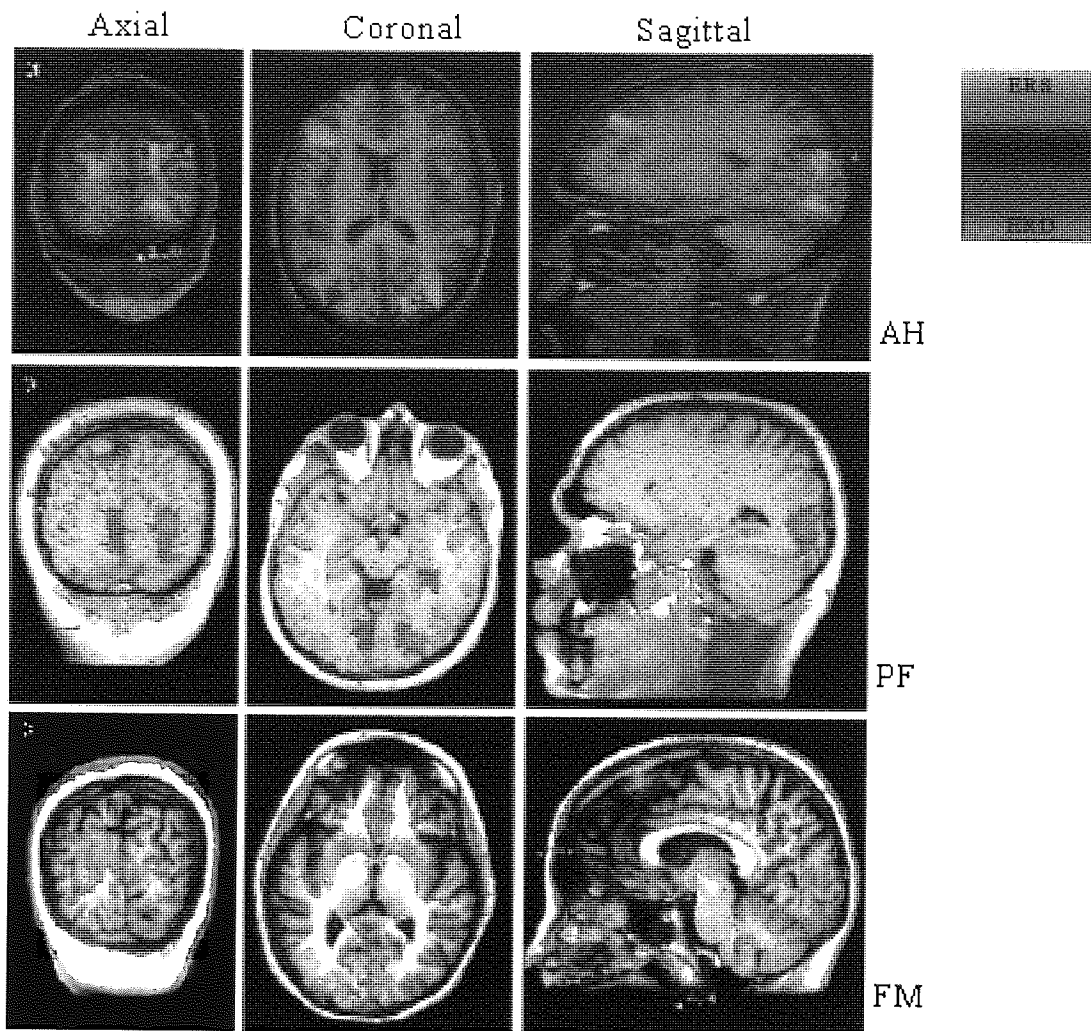
Figure 4-31. Luminance Onset Alpha Localisation. Data from three subjects showing the locus of the ERS/ERD 0-1.5s post-stimulation. (a) Subject AH shows bilateral ERD in extra-striate visual cortex (t=2.4 (R); t=1.8 (L)). (b) Subject PF shows ERD in right extra-striate visual cortex (t=1.6) and left striate visual cortex (t=1.2). (c) Subject FM shows bilateral ERD in extra-striate visual cortex (t=3.1 (R); t=2.7 (L)).

t=1.1   t=1.8
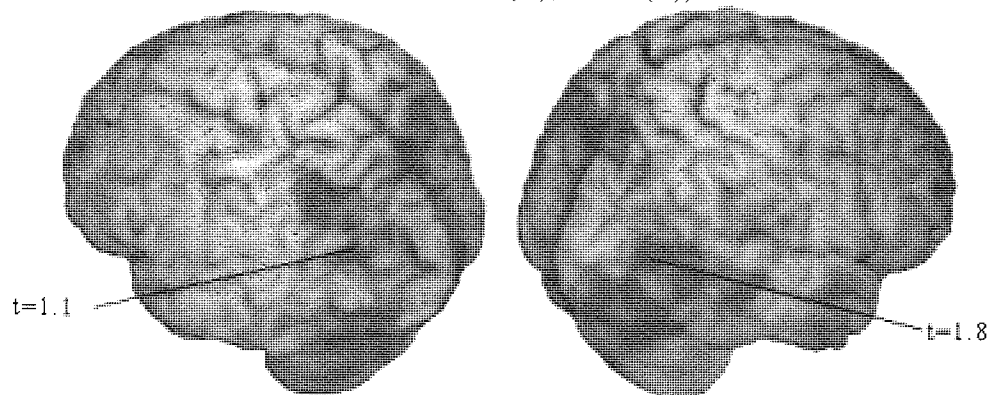
Figure 4-32. Group SAM image of luminance onset alpha. Bilateral ERD in extra-striate visual cortex (t=1.8 (R); t=1.1 (L)).

4.4.8.3　Beta

Axial　　　Coronal　　　Sagittal
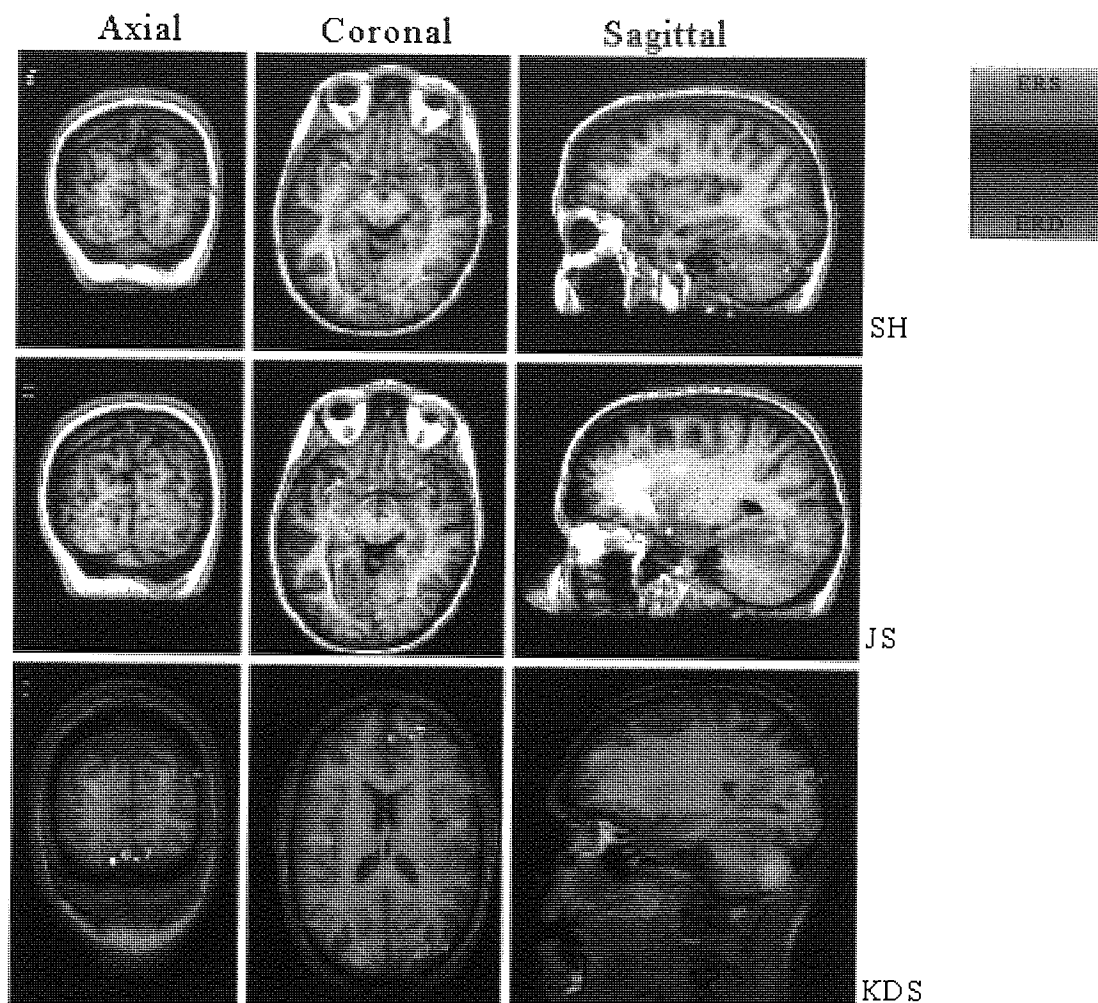
Figure 4-33. Luminance Onset Beta Localisation. Data from three subjects showing the locus of the ERS/ERD 0-1.5s post-stimulation. (a) Subject SH shows bilateral ERD in striate (t=2.4) and extra-striate (t=3.6 (R); t=3.4 (L)) visual cortex. (b) Subject JS shows bilateral ERD in striate/extra-striate visual cortex (~V2) (t=2.3 (R); t=1.8 (L)). (c) Subject KDS shows ERD in right extra-striate (t=1.4) visual cortex and ERS in left extra-striate (t=1.1).
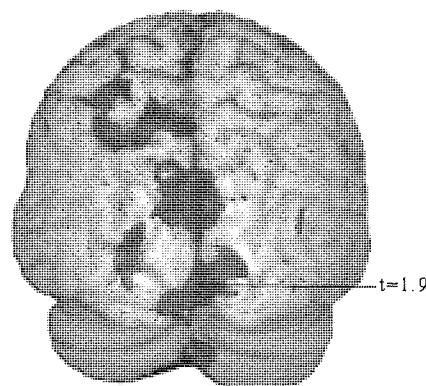
Figure 4-34. Group SAM image luminance onset beta. ERD over extended region at striate visual cortex (t=1.9) (image threshold >1.0).

4.4.8.4 Results

SAM analysis of the luminance onset visual evoked magnetic field indicates a single source in the primary visual cortex, which was observed in six subjects. This locus of this activity shows some variation in upper/lower and hemispheric localisation. The group image failed to find any significant activity in the visual cortex (figs 4-30a,b,c). The group SAM image confirms the V1 locus of the activity, which appears more diffuse in the group image than the individuals (fig.4-31).

SAM analysis of the alpha band reveals ERD in varied visual cortical locations (figs 4-31a,b,c). There was a large degree of inter-subject variability the observed major peaks, although there was consistent low level synchrony found across a number of subjects (below threshold in the individual images) which appears as diffuse bilateral temporal cortical ERS in the group image in addition to the bilateral extra-striate ERD (fig. 4-32).

The SAM activity observed in the beta band following luminance onset was typically ERD at several points in the visual cortex (fig. 4-33a), which was typically bilateral (figs 4-33a,b). The group image reveals strong ERD along the extent of lateral V1 in both hemispheres (fig. 4-34), which extends into the ipsilateral parietal cortex.

The gamma activity observed following luminance onset failed to show significant activity in visual cortex.

4.4.9   Pattern Offset

4.4.9.1   Visually Evoked Magnetic Field
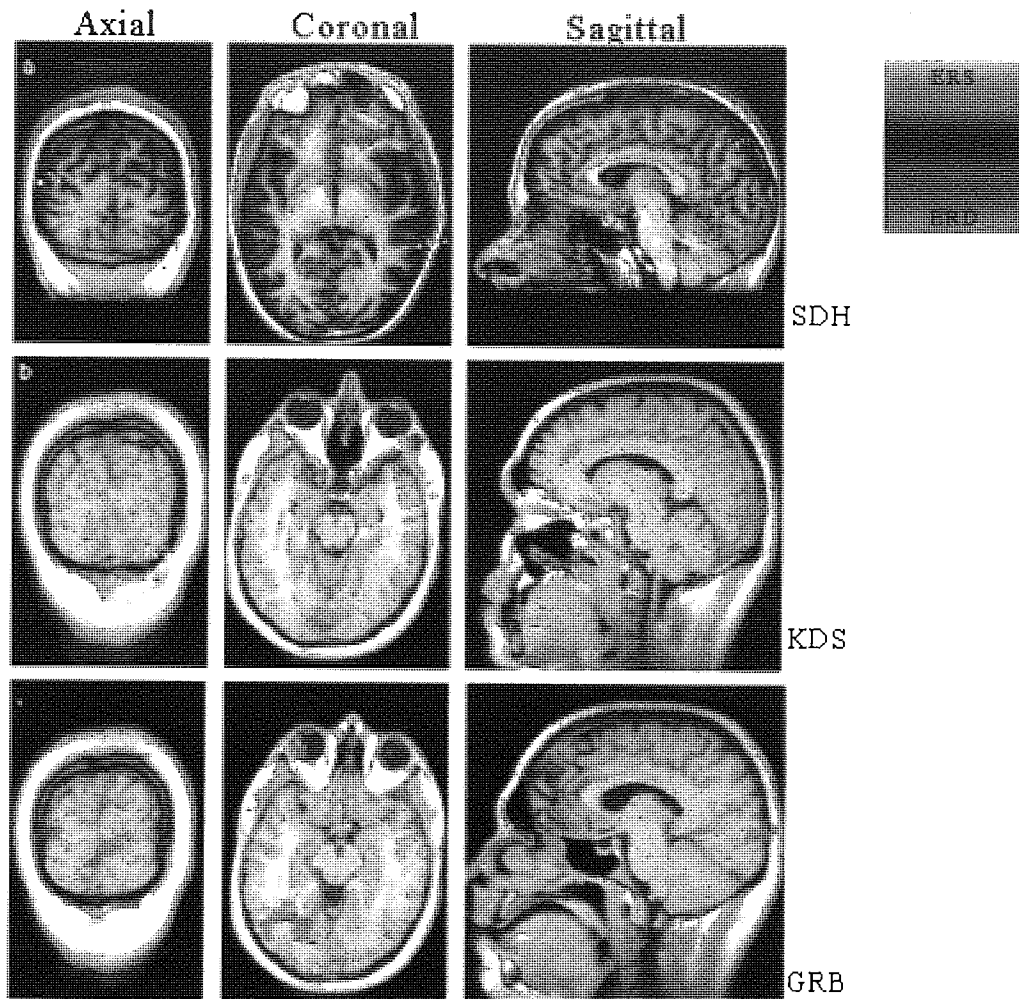
Figure 4-35. Pattern Offset VEMF SAM localisation. Data from three subjects showing the locus of the transient burst of synchrony 0-300ms post-stimulation. (a) Subject SDH shows activation in V1 (t=3.2). (b) Subject KDS shows activity in V1 (t=2.4). (c) Subject GBR shows activity in V1 (t=1.6).

4.4.9.2 Alpha
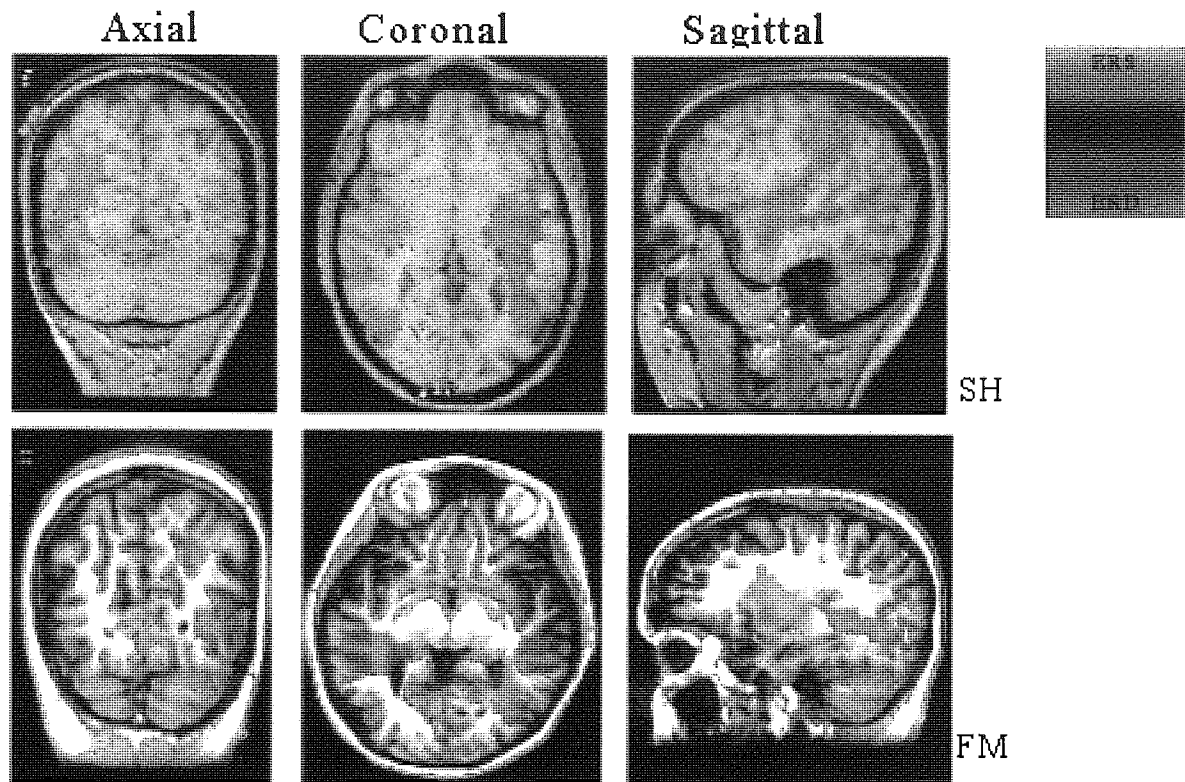
Figure 4-36. Pattern Offset Alpha Localisation. Data from two subjects showing the locus of the ERS/ERD 0-1.5s post-stimulation. (a) Subject SH shows activation in right temporal ERS (t=1.3). and left temporal ERD (t=1.1). (b) Subject FM shows ERS in right striate visual cortex (t=1.6) and extra-striate visual cortex (t=1.8). This image shows 2 subjects that demonstrates the highly variable nature of the activity in the alpha range across the group following pattern offset.

4.4.9.3 Beta
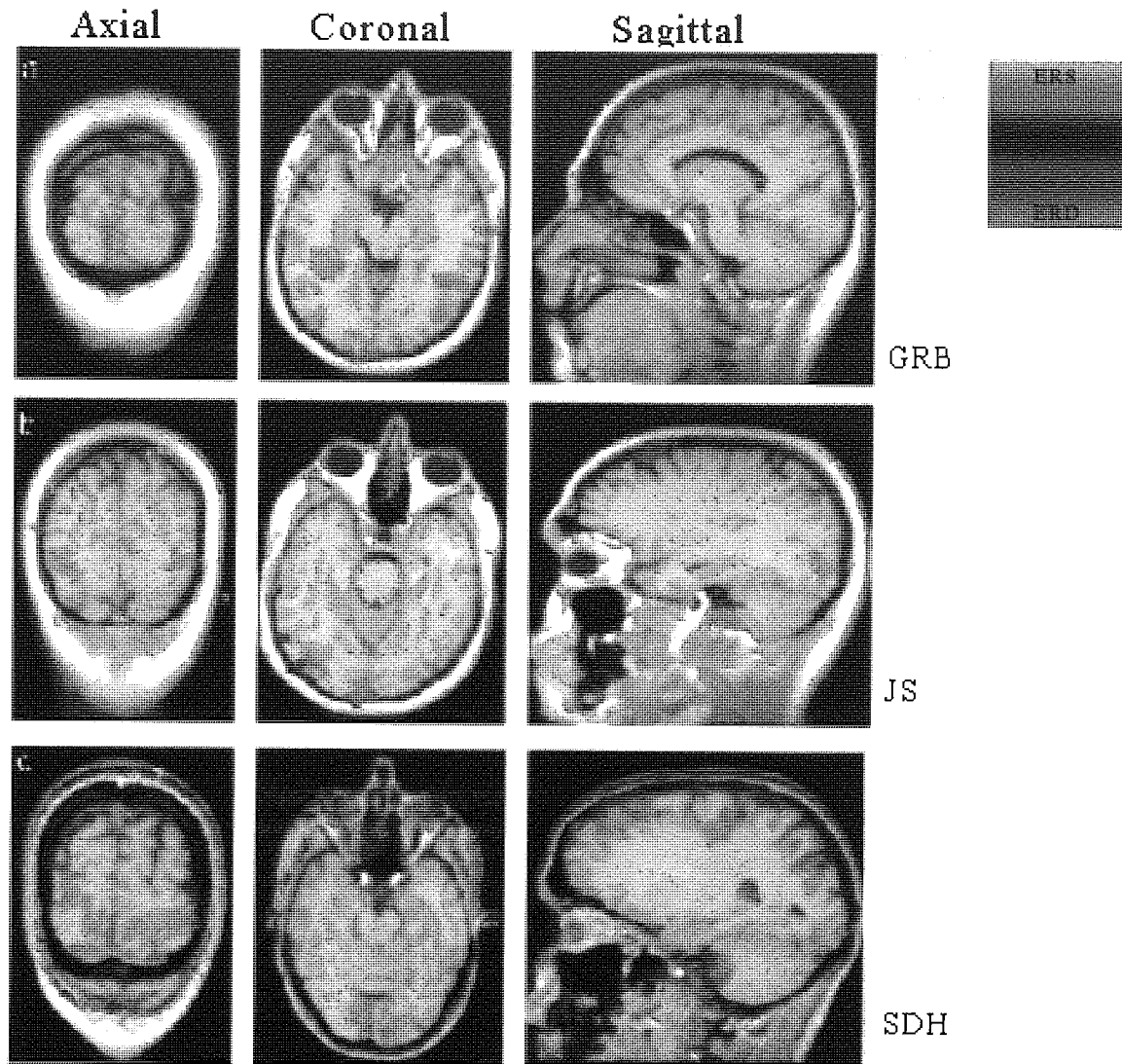
Figure 4-37. Pattern offset Beta Localisation. Data from three subjects showing the locus of the ERS/ERD 0-1.5s post-stimulation. (a) Subject GRB shows bilateral ERD in striate (t=1.9 (L & R)) visual cortex. (b) Subject JS shows bilateral ERD in extra-striate visual cortex (t=1.9 (R); t=1.1 (L)). (c) Subject SDH shows bilateral ERS activation in striate (t=1.6 (R); t=1.2 (L)) visual cortex. The image shows the inter subject variability following pattern offset.

4.4.9.4   Gamma
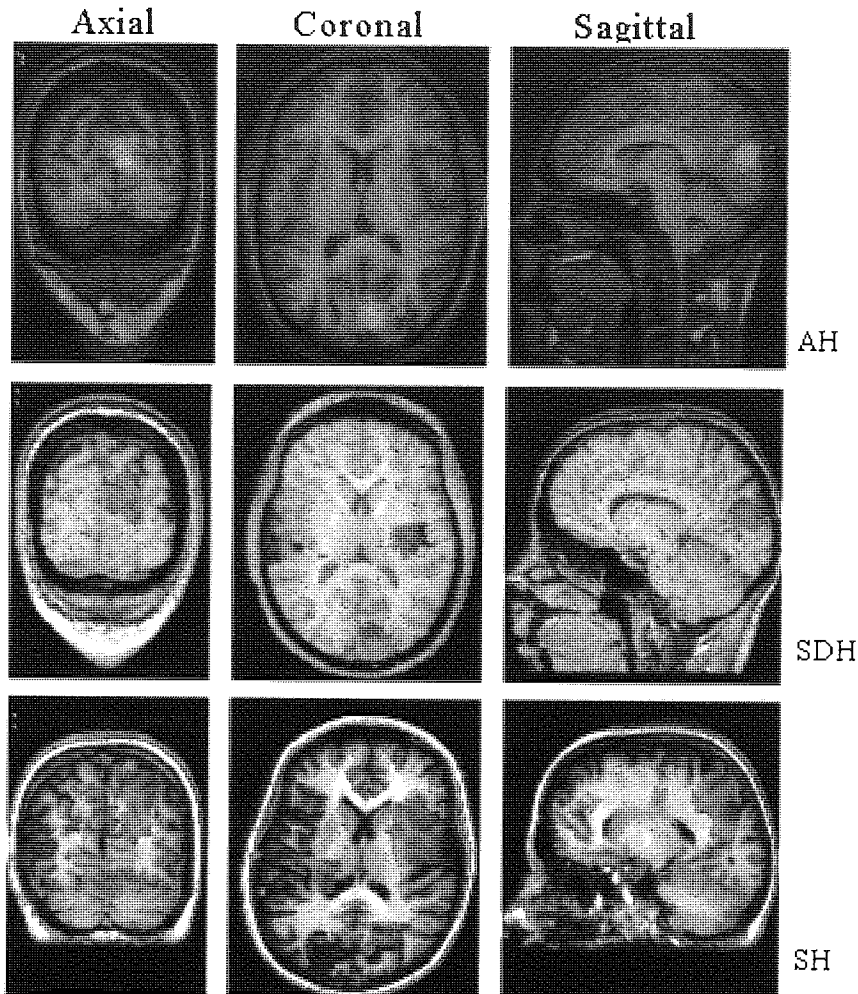
Figure 4-38. Pattern Offset Gamma Localisation. Data from three subjects showing the locus of the ERS/ERD 0-1.5s post-stimulation. (a) Subject AH shows ERS in right striate visual cortex (t=3.0) (b) Subject SDH shows ERS in right striate visual cortex (t=2.6). (c) Subject SH shows ERS in right striate visual cortex (t=1.8).
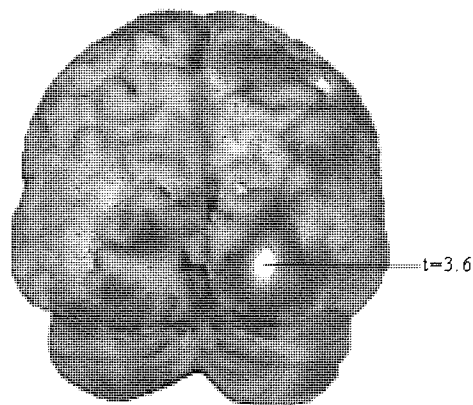
Figure 4-39. Group SAM Image showing distribution of gamma activity following pattern offset. Shows contralateral ERD activation in right striate visual cortex (t=3.6). (Image threshold >1.8).

4.4.9.5 Results

SAM analysis of the Visual Evoked Magnetic Field (VEMF) response to pattern offset revealed activity around the primary visual cortex which displayed some degree of hemispheric variability, but was generally located around the same region. However, there was major variability in the nature of the responses as some subjects exhibited ERS (fig. 4-35) whilst others displayed ERD (figs 4-35b,c). Consequently the group image displays no significant peaks in the visual cortical areas.

The alpha band activity was very diverse both in terms of the locations and the nature of the response. Figure 4-36 shows the two most comparable individuals, with ERS and ERD in extra-striate locations in the region of V5, however even these differ in direction of synchrony modulation and laterality. Consequently, they are presented to demonstrate variability of this feature.

The beta band activity displays bilateral activation in extra-striate regions. This activity varies slightly in location but is typically distributed around area V2. However, again there is a variation in whether the response in an increase or decrease in the observed cortical synchrony of these regions, thus producing an ambiguous group SAM image from which no specific locus of activity can be determined.

The gamma band activity on the other hand is conclusive, as in all subjects there is ERD in the upper right bank of the calcarine sulcus in area V1 (figs 4-38a,b,c). This is reflected in the group image which also demonstrates a desynchronisation in this location (fig. 4-39).

- **Investigation of the luminance offset stimulus failed to provide significant results in either the VEMF or the predetermined frequency bands.**

4.4.10 Contrast Increment

4.4.10.1 Visual Evoked Magnetic Field
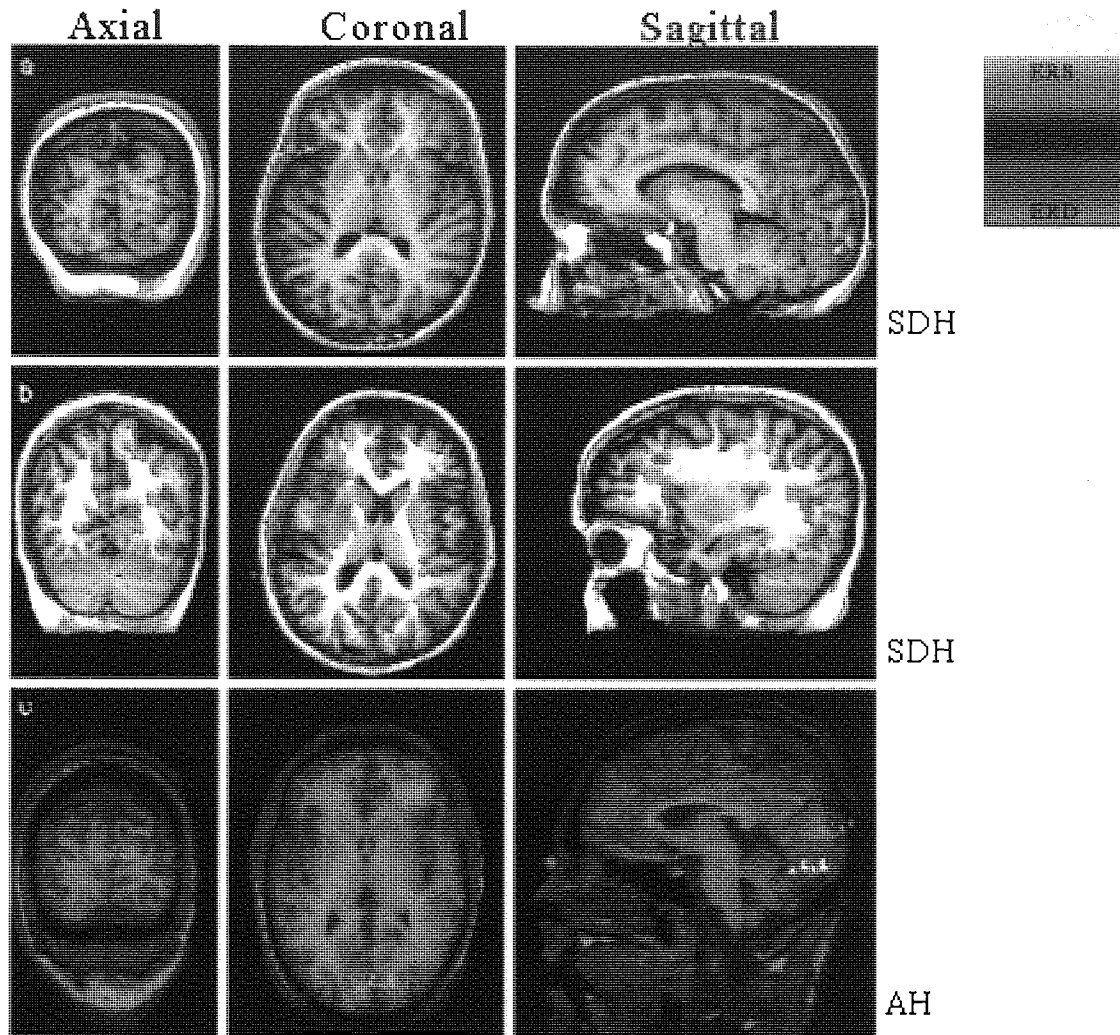
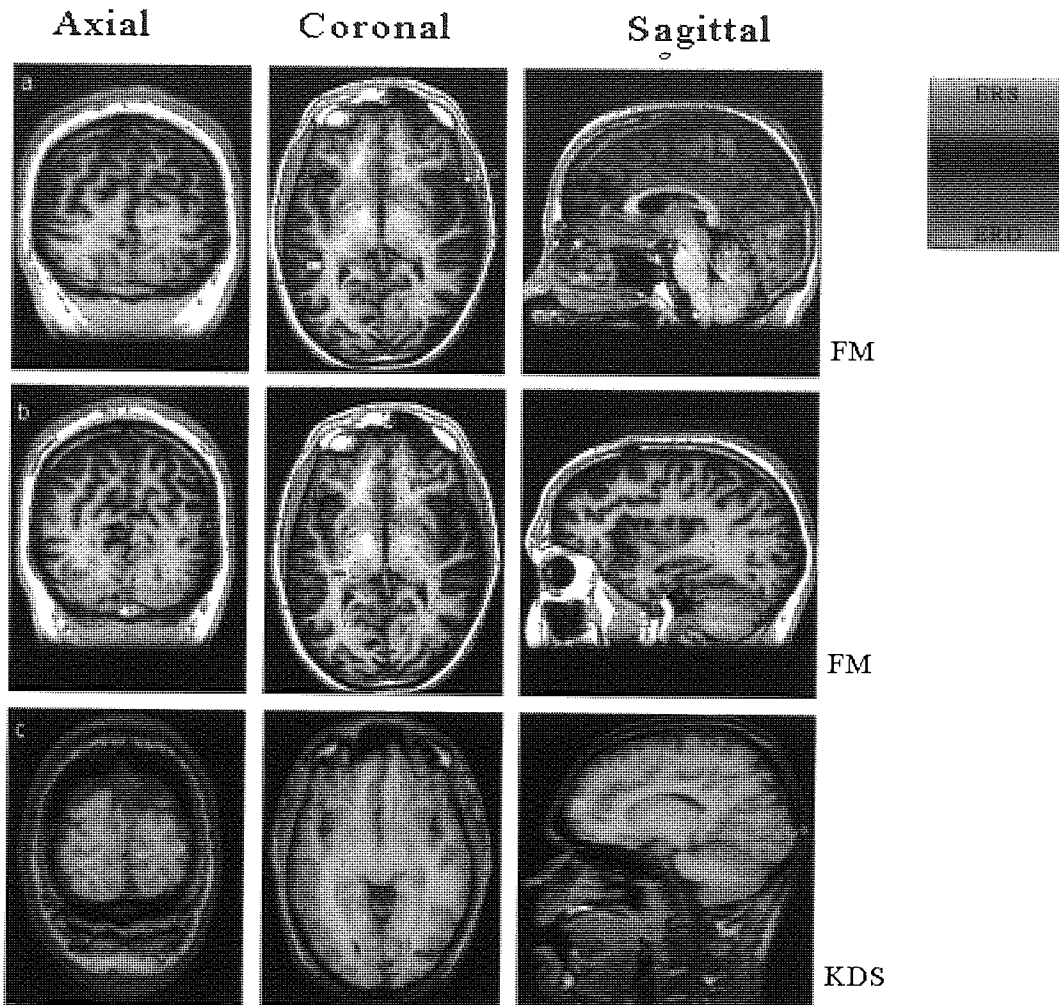Figure 4-40. Contrast Increment VEMF SAM localisation. Data from three subjects showing the locus of the transient burst of synchrony 0-300ms post-stimulation. (a)+(b) Subject SDH shows activation in (a) right V1 (t=1.0) and (b) middle temporal cortex (t=1.6). (c) Subject AH shows activity in the region of V1 (t=1.9).
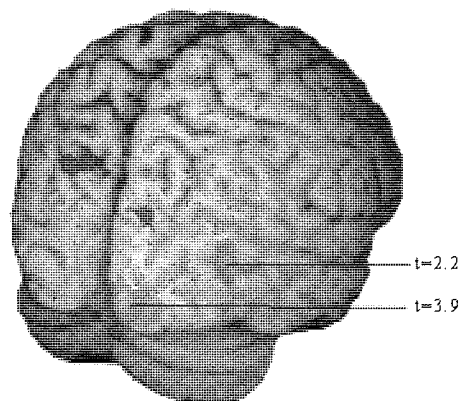
Figure 4-41. Group SAM image contrast increment VEMF. Shows activity in striate visual cortex (t=3.9) and extra-striate (t=2.2) visual cortex (image threshold >2.0).

4.4.10.2 Alpha
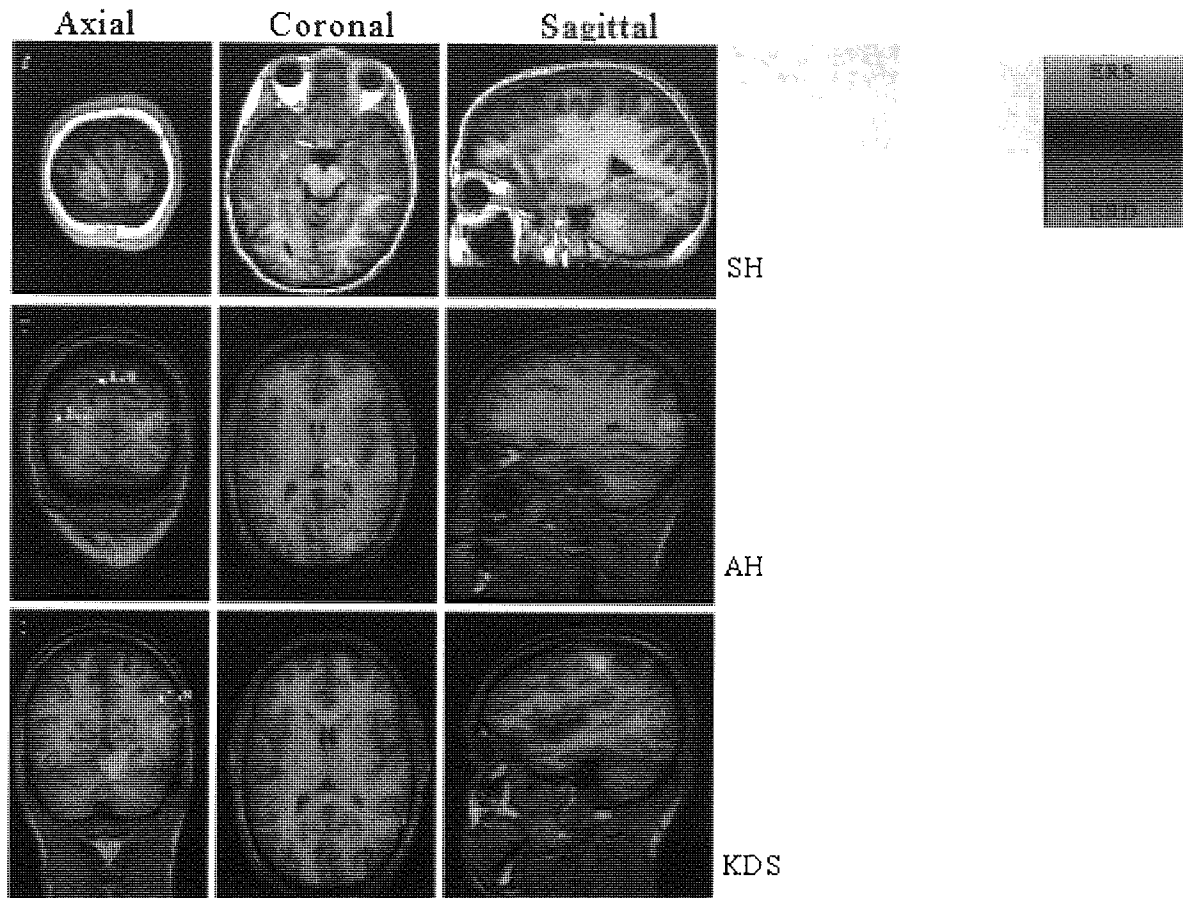
Figure 4-42. Contrast Increment Alpha Localisation. Data from two subjects showing the locus of the ERS/ERD 0-1.5s post-stimulation. (a) Subject SH shows varied ERS and ERD in visual cortex (t=2.2 (ERS); t=1.9 (ERD)). (b) Subject AH shows con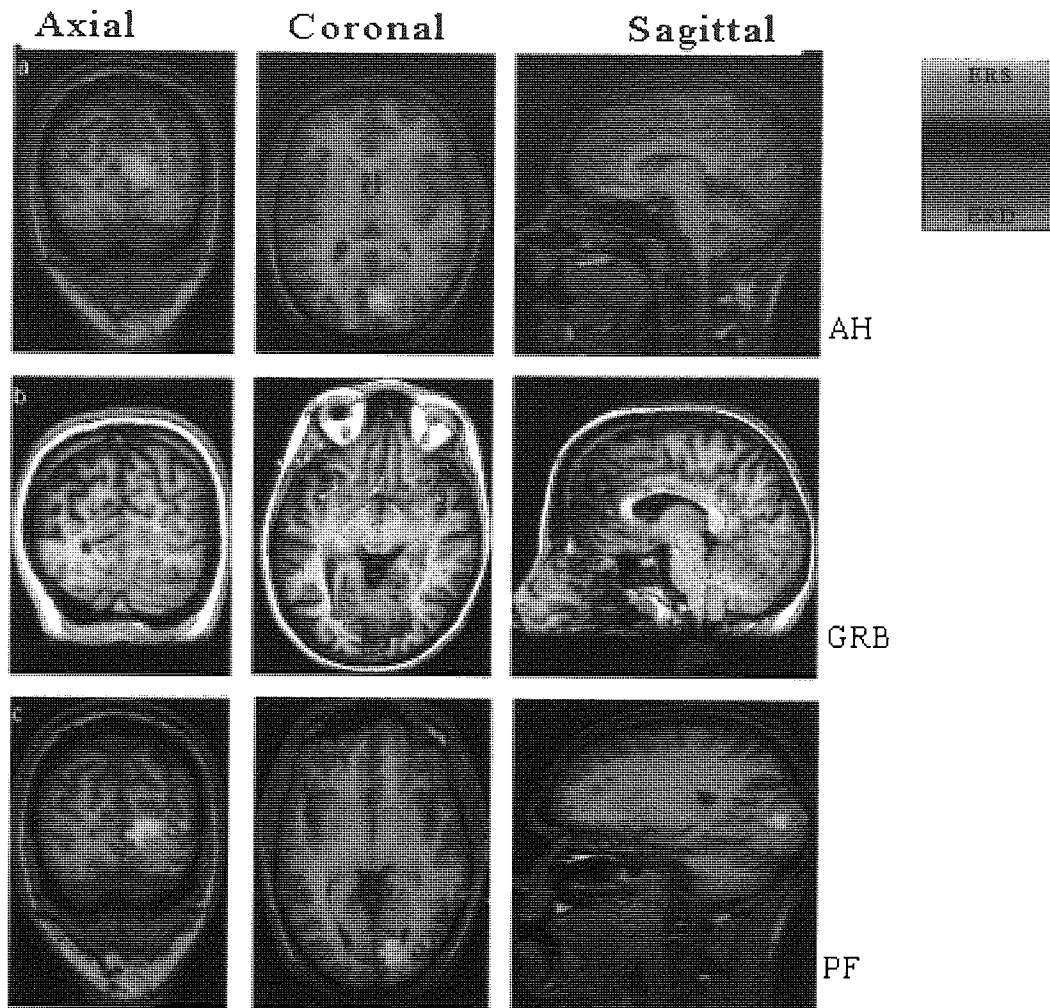tralateral ERD in extra-striate visual cortex area (t=3.0). (c) Subject KDS shows ERD in right occipito-temporal region (t=2.1). This image demonstrates the variability of alpha oscillations following contrast increment

4.4.10.3 Beta
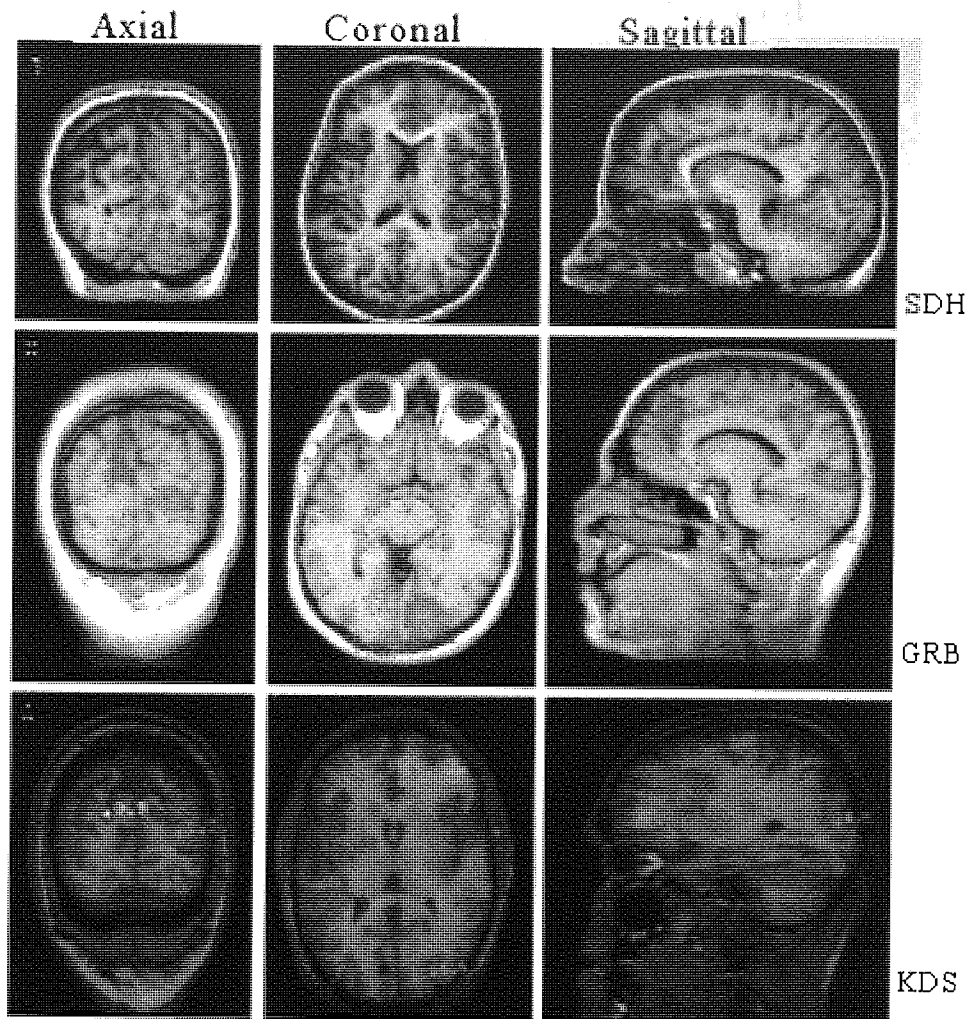
Figure 4-43. Contrast Increment Beta Localisation. Data from three subjects showing the locus of the ERS/ERD 0-1.5s post-stimulation. (a) Subject SDH shows right primary visual cortex ERD (t=1.9). (b) Subject GRB shows ERD in early extra-striate (~V2) visual cortex (t=1.9). (c) Subject KDS shows ERD activation in extra-striate (t=1.6) visual cortex.
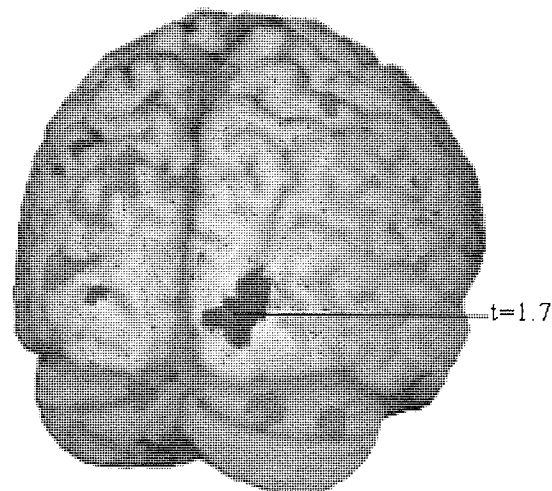
Figure 4-44. Group SAM contrast Increment Beta. Shows activation of ERS in early extra-striate right visual cortex (t=1.7). (image threshold >1.0).

4.4.10.4 Gamma
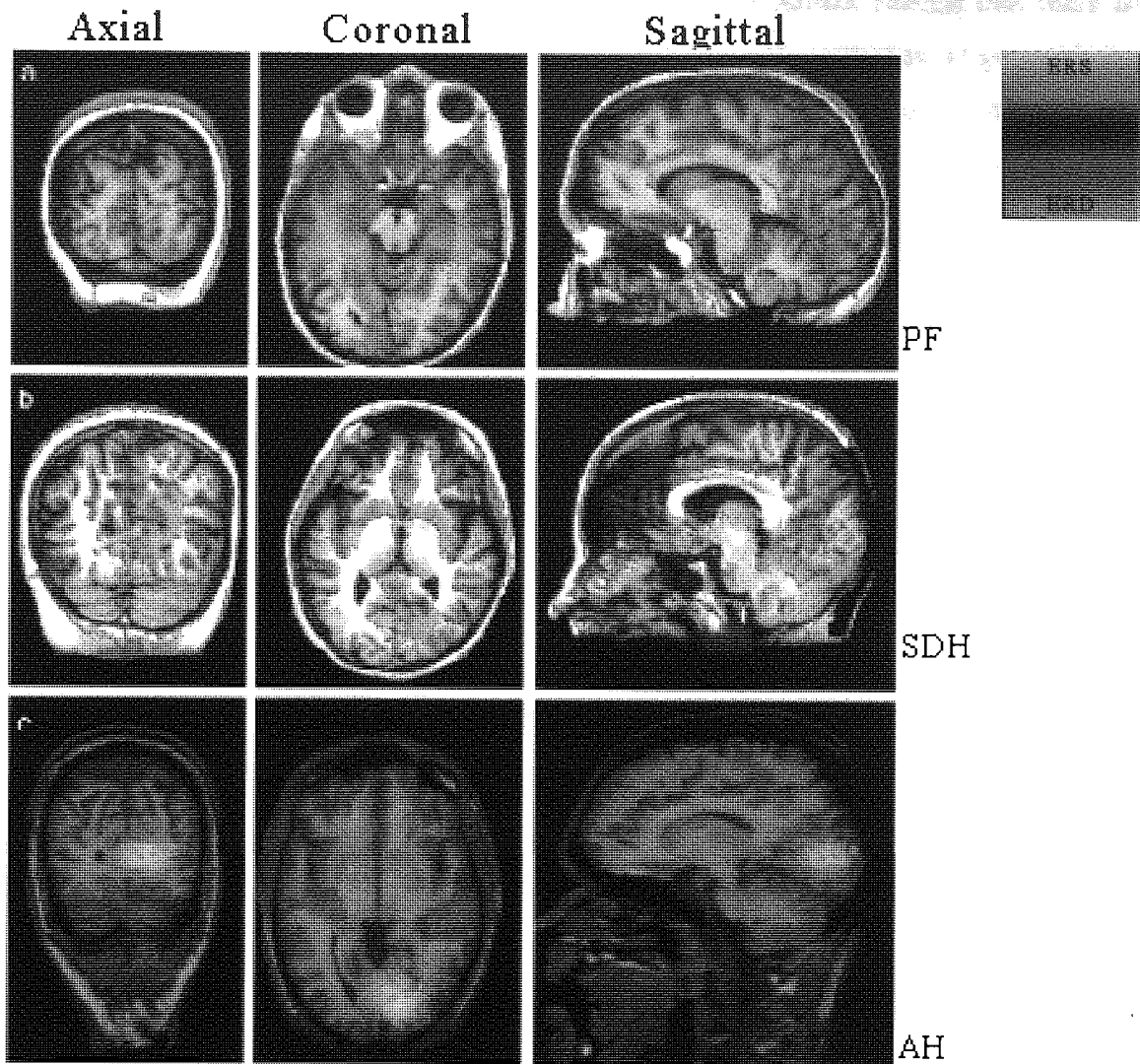
Figure 4-45. Contrast Increment Gamma Localisation. Data from three subjects showing the locus of the ERS/ERD 0-1.5s post-stimulation. (a) Subject PF shows ERD in right striate visual cortex (t=3.9) (b) Subject SDH shows ERD in right striate visual cortex (t=3.1). (c) Subject AH shows ERD in right striate visual cortex (t=2.3).
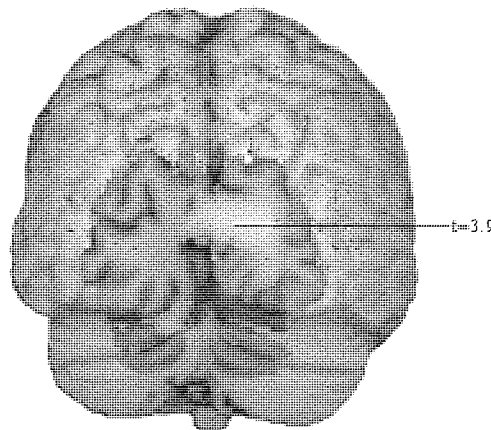
Figure 4-46. Group SAM, Contrast Increment Gamma. Shows gamma ERS in upper right calcarine sulcus (t=3.9). (Image threshold > 2.0).

4.4.10.5 Results

SAM analysis of the VEMF following contrast increment reveals that there is a consistent primary visual cortical activation (ERS) across subjects (figs 4-40a,b,c). Additionally in most subjects (n=6) there was also some extra-striate and middle temporal activity (figs 4-40b,c). This activity is reflected in the group image, which demonstrates contralateral ERS around lateral V1, extra-striate and temporal cortex (fig. 4-41).

SAM reveals that alpha activity shows peaks of activity which are inconsistent across subjects and demonstrates wide variability (fig. 4-42), resulting in an inconclusive group SAM image. The beta activity observed following contrast increment was a contralateral ERD in the region of V2/V3 (figs 4-43a,b,c), which is represented in the group image (fig. 4-44).

The gamma activity following contrast increment was a consistent ERS in the primary visual cortex of all subjects, which localised to the upper right bank of the calcarine sulcus (figs 4-45b,c), with little variability (fig. 4-45a). This locus of activity was confirmed by the group SAM image (fig. 4-46).

4.4.11 Contrast Decrement

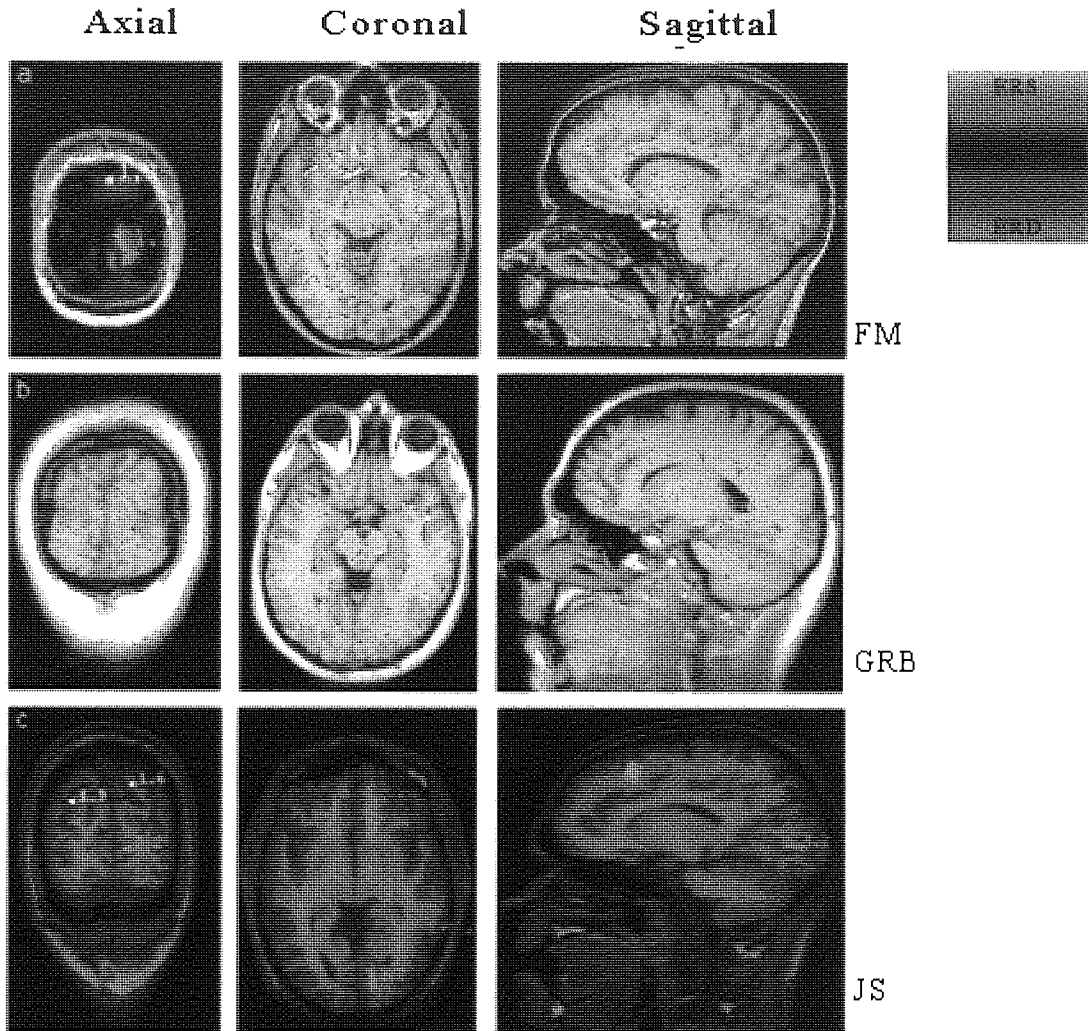### 4.4.11.1 Visual Evoked Magnetic Field
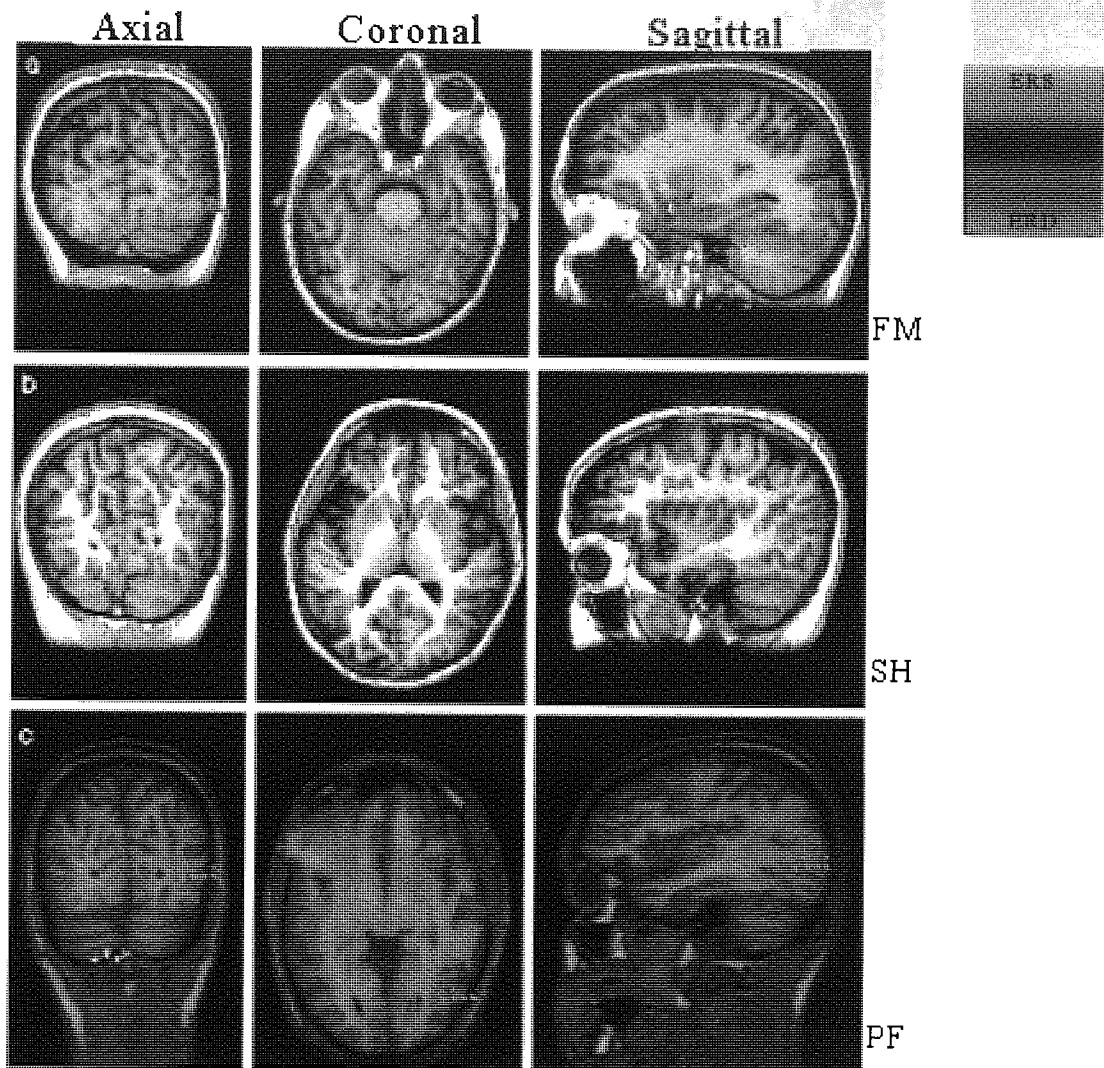
Figure 4-47 Contrast Decrement VEMF SAM localisation. Data from three subjects showing the locus of the transient burst of synchrony 0-300ms post-stimulation. (a) Subject FM shows bilateral activation in occipito-temporal regions (t=1.3 (R); t=0.9 (L)). (b) Subject SH shows bilateral activation in occipito-temporal regions (t=1.7 (R); t=1.1 (L)). (c) Subject PF activation in occipito-temporal regions (t=1.3 (R); t=0.7 (L)).
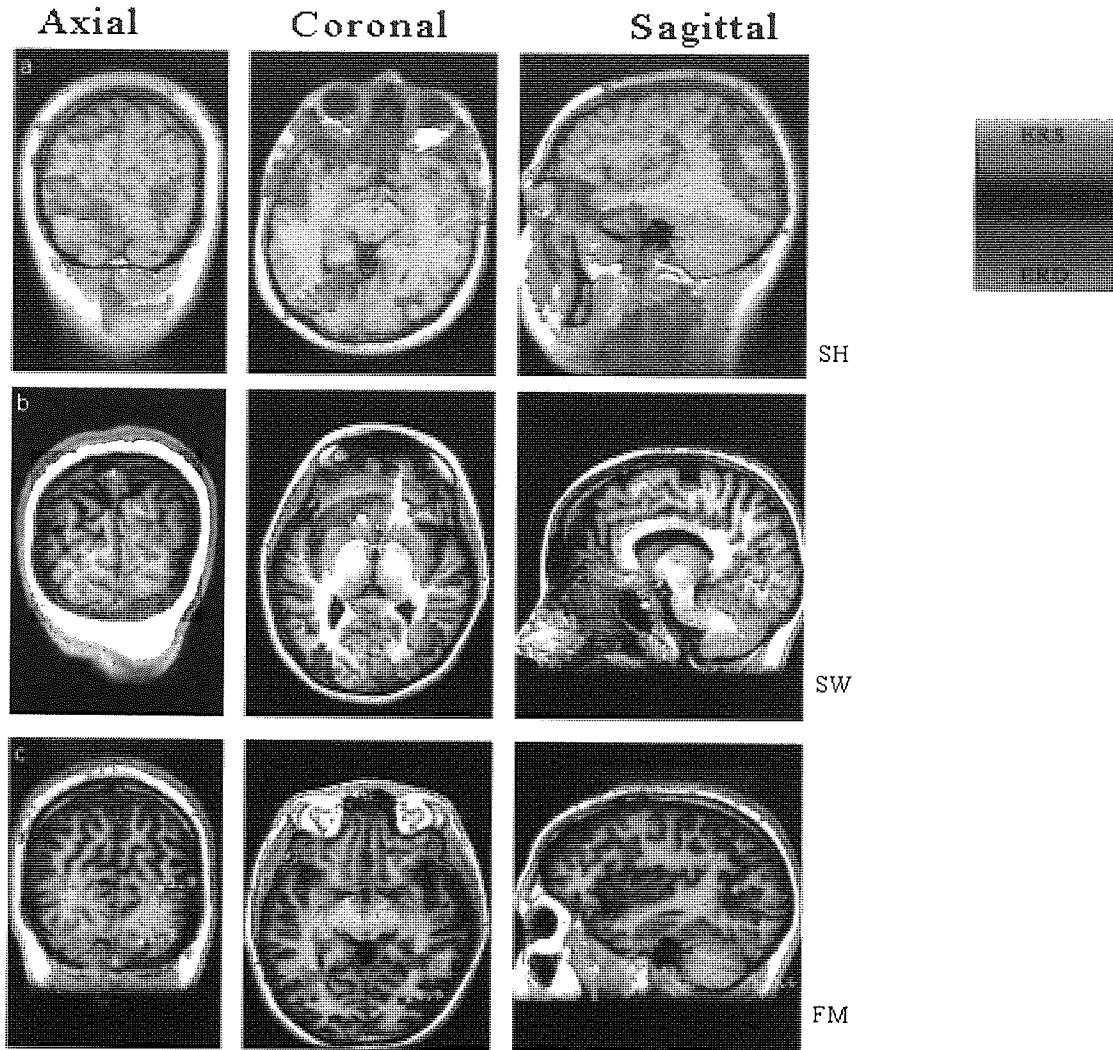
4.4.11.2 Gamma
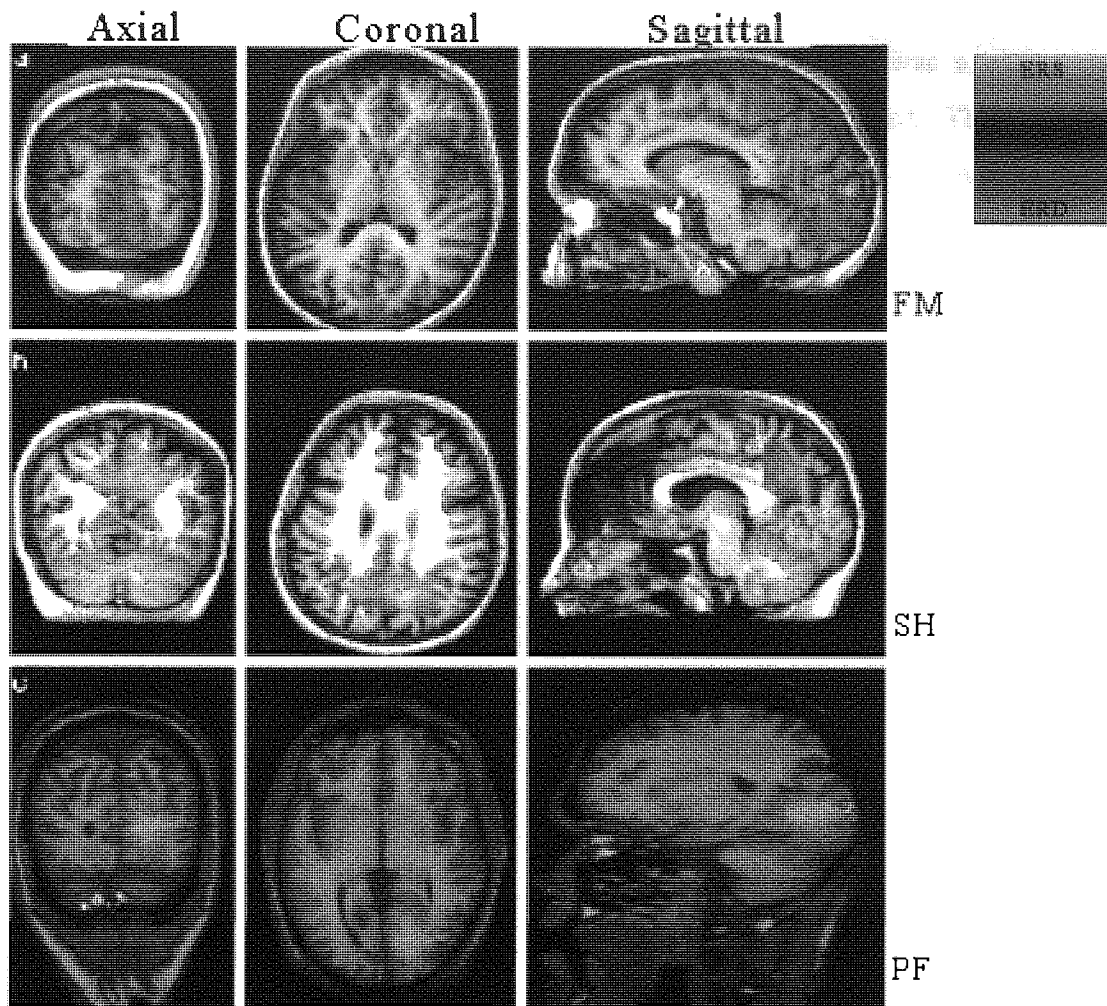
Figure 4-48. Contrast Decrement Gamma Localisation. Data from three subjects showing the locus of the ERS/ERD 0-1.5s post-stimulation. (a) Subject FM shows ERD in primary visual cortex (t=1.1) (b) Subject JS shows ERD in primary visual cortex (t=3.2). (c) Subject AH shows ERD in primary visual cortex (t=1.9).
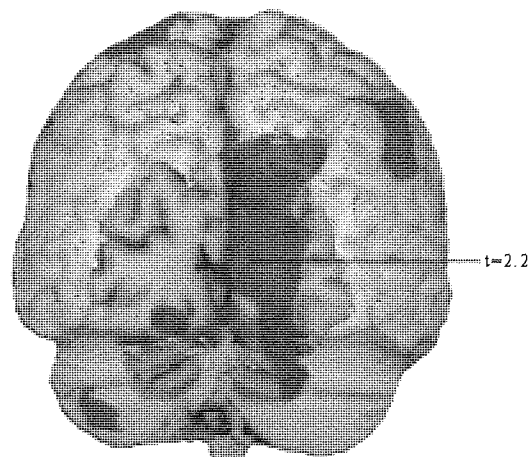
Figure 4-49. Group SAM Image contrast decrement. ERD in upper right bank of the calcarine sulcus (t=2.2) (image threshold > 1.8).

4.4.11.3 Results

The evoked activity of the contrast decrement response was a varied response localised in the right occipital-temporal region (figs 4-47a,b,c). There were other synchronous events across subjects, although none of consistent locus. Although in many of the subjects this occipito-temporal locus was clearly present, the group image failed to reflect this for reasons that remain unclear. The gamma activity commensurate with other conditions produced the only other consistent localisation. This was strong ERD in the contralateral primary visual cortex of all subjects (fig. 4-48). This was also observed in the group image (fig. 4-49) and is further discussed and expanded upon in chapter 6.

4.4.12   Virtual Electrodes

The coordinates derived from the SAM evoked activity loci from the pattern onset, pattern reversal, luminance onset, contrast increment and contrast decrement were used in order to generate anatomically discrete reconstructions of neuronal activity (figures 4-4 to 4-8b respectively). In the case of the contrast increment and decrement where no distinct peaks were observable from the raw sensor data, they were used to obtain all latency information, whilst others were used in support of the raw data.

4.5   Discussion

The intention of this series of experiments was to investigate the profile of the cortical response to various visual phenomena using a range of Magnetoencephalographic analysis methods as both an investigation into the cortical characteristics of visual stimulation and as a comparative tool for MEG analysis tools.

4.5.1   Outcome of primary study aims

1. The use the sensor data to observe latency information of the visual evoked magnetic fields (VEMF) revealed that the pattern onset, pattern reversal and luminance offset could be well characterised in terms of their latency components (tables 4-1 & 4-2)[†].

   This latency information corresponds closely to those reported for the visual evoked potential (VEP), latency values reported in the VEP standard literature (Chiappa, 1990; Harding *et al.,* 96, Odom *e al.,* 2004, American Encephalographic Society, 1994). These results suggest that the VEMF is a direct magnetic counterpart of the VEP.

[†]   Attempts to characterise the latency of the N75m component of pattern reversal were inconclusive as a clear component could not be identified across all subjects. However, the P100m component was of comparable latency to that reported using EEG (Chiappa, 1990). Although possible to classify the C1m component in terms of latency (table 4-1), attempts to localise this feature were unsuccessful using either dipoles or SAM analysis and it was therefore not possible to draw comparisons with the magnetic field tomography (MFT) results of Tzlepi *et al.,*(2001) who identified N70m sources in V1/2, V5 and human homologue of V6 using dipole localisation, although described a large degree of variability in comparison to later components. However, the absence of this component from the virtual electrode reconstruction in either striate or extra-striate sources suggests that a separate generator underlies that element.

---

2. The use of the dipole analysis and to localise the evoked components revealed that the stable P100m components at the pattern reversal VEMF and the C2m component of pattern onset VEMF localised to the upper right primary visual cortex, consistent with previous findings in other modalities. However, beyond V1 the localisation of sources became increasingly unstable. The C3m component of the pattern onset VEMF localised to area V2, however the Monte-Carlo statistical volume encompassed both V1 and extra-striate visual cortex, suggesting that it was a poor fit for the given noise. Similar analysis of the luminance onset components

reveals that the P2m component localises to the posterior region of the primary visual cortex and the N2m component locates to the anterior primary visual cortex. However, the error volumes suggest that these models are unable to reliably explain the underlying activity. There are several possible reasons why a single dipole may insufficiently explain the data and a multiple dipole may provide no further solution:

a.   The activity which occurs may arise from diffuse neuronal source populations rather than a single point within the cortex.

b.   There may be a number of discrete, yet proximal sources, which appear as a single dipole, yet which are unable to be modelled sufficiently.

c.   Deep structures such as the lateral geniculate nucleus in the thalamus may contribute to the signal.

The use of SAM in the investigation of short time windows appears to be particularly useful and provides further information that seems to be beyond the ability of dipole modelling. For example, the investigation of the pattern onset VEMF reveals two distinct sources in striate and extra-striate cortex. This would appear to explain the extended source distribution of the Monte-Carlo distribution in C3m dipole analysis.

Furthermore, SAM was able to identify activity evoked components following the contrast increment and decrement stimuli. This was used to reconstruct a dipole which in turn informed the dipole analysis. Consequently the locus identified appeared to be a amalgam of the activities identified using SAM activity. There are however several limitations to the method:

a.   Simultaneously synchronous sources are cancelled by the SAM algorithm. This is more likely to occur over shorter time windows.

b.   A specific time point cannot be investigated in the manner that dipoles can analyse using a millisecond by millisecond time-window.

c.   The method can be affected by the oscillatory state of the cortex; if alpha activity occurs it will affect the observed activity.

The use of SAM to determine the virtual electrode loci, from which the VEMF complexes were reconstructed, proved to generate a clearer image of the actual activity. This is supported by the informing of the dipole method to locate the contrast increment/decrement sources; whereas this was not possible from the sensor data. Further

support for this method is provided in evoked activity observation (chapter 5) and spectral change (chapters 6 & 8).

4.5.2   Outcome of Secondary Aims

As discussed above the SAM and VE methods were able to reconstruct two novel evoked activities: (1) contrast increment VEMF and (2) contrast decrement VEMF (details of their latencies are provided in table 4-2). However, the SAM method failed to localise and subsequently reconstruct a VEMF luminance offset paradigm. A discussion and summary of the successive paradigms is presented below.

4.5.2.1 Spectral analysis

The analysis of the frequency bands using SAM analysis generated a large quantity of data. This provides a basis for further comparisons in terms of normative data for MEG experiments designed to compare the cognitive processing. Additionally the results provide a basis against which clinical comparisons can be made or at least indicate that a normative database of visual responses is a viable proposition.

Wróbel (2000) put forward a general hypothesis that attributed alpha, beta and gamma oscillatory modulation to different activation states of the visual system. This hypothesis suggests that alpha activity reflects idle arousal of the system, while beta bursts shift the system to an attention state that consequently allows for gamma synchronization and perception. A hypothesis supportive of the suggestion that visual gamma oscillations represent a mechanism of object recognition (tallon-Baudry and Bertrand, 1999). The role of gamma oscillations is further discussed in chapter 6, however the occurrence of beta ERD within similar spatial and temporal loci of gamma synchrony (figs 4-18, 4-37, 4-25 and 4-44) is a contradiction of this hypothesis.

The observed activity was the result of averaging across eight subjects, from which no measures of correlation or coherence between spectral activities was computed and therefore no conclusions can be drawn concerning relationships between these activities. However, it is possible to summarise these induced activities and postulate their significance in visual processing:

4.5.2.2 Summary

- Pattern Onset: bilateral alpha ERD in early extra-striate areas; contralateral beta ERD in extra-striate visual cortex, contralateral gamma ERS/ipsilateral gamma ERD in primary visual cortex.

- Pattern Reversal: bilateral alpha ERD in striate and extra-striate locations; beta activity (ERS and ERD) in primary visual cortex; gamma ERS in contralateral extra-striate visual cortex.

- Pattern offset: absence of consistent alpha and beta induced change; contralateral gamma ERD in primary visual cortex.

- Luminance onset: diffuse bilateral alpha, with ERD in occipito-temporal regions and ERS in lateral frontal regions; beta ERD stretching over occipito-parietal regions of the central sulcus; an absence of significantly focal gamma change.

- Luminance offset: absence of significant focal change in alpha, beta or gamma.

- Contrast increment: inconsistent change in gamma oscillations between subjects, contralateral beta ERD in early extra-striate regions (V2/V3) and some ERS in ipsilateral occipital, parietal and temporal regions (variable between subjects); contralateral gamma ERS in primary visual cortex.

- Contrast offset: no consistent induced changes in alpha or beta bands; contralateral gamma ERD in primary visual cortex.

4.5.3 Supposition

Desynchronisation in the alpha (7-13Hz) frequency range occurs in response to pattern onset, pattern reversal and luminance onset, but not in either the contrast increment or any of the offset stimuli . This would suggest it is a response to changes in the spatial characteristics of the scene, i.e. presentation of a stimulus in a section of visual field or a change in the spatial phase shift. Furthermore, the alpha ERD is consistently bi-lateral rather than retinotopic, suggesting it is the result of top down processing rather than a directly induced cellular response to the stimulus. Desynchronisation in the beta (15-25Hz) frequency range occurs in pattern onset, pattern reversal, luminance onset, and contrast increment, which suggests it is a factor related to increased complexity of visual processing. Furthermore, it is typically located in an adjacent locus to that of the evoked activity in retinotopically concordant regions, suggesting that it is a directly induced cellular response to the stimulus. The activity in the gamma range is highly consistent and was therefore investigated using additional methods, reported in chapter 6.

4.6   Conclusions

This chapter provides a classification of the evoked and induced cortical events following various types of visual stimulation. This provides possible reference for clinical and research based comparisons. Furthermore it has identified two evoked activities which were previously unrecognised; the contrast increment and decrement VEPs. Additionally, the use of specific SAM analyses (chapter 5) were shown to be effective in transient activity analysis. This forms the basis for specifically applied localisation methods used in MEG retinotopic analysis (chapter 7). The use of group imaging proved to be of use in the identification of group factors, however factors such as smoothness of the source extent were identified as a possible restriction of the method and formed the basis for further investigation of this (chapter 3) (Hall *et al.,* 2004d).

Chapter 5

Investigation of Cortical Contrast Gain using Magnetoencephalography (MEG)

5 Investigation of Contrast Gain using Magnetoencephalography (MEG)

5.1 Overview

Chapter five describes the investigation of cortical contrast gain using various magnetoencephalographic analysis methods. The chapter begins with a brief introduction to cortical contrast gain, describing what it is and the functional modalities used to investigate it. Furthermore it describes that the measure relates specifically to the visual evoked response. Subsequently it is explained that there are limitations to the current methods of investigation of cortical contrast gain, which are either spatial or temporal (dependant upon the modality). This is expanded to incorporate the variations found both within and between modalities in the measurement of cortical contrast gain and also the VEP upon which it is typically based. The use of cortical contrast gain in hyperexcitability disorders is described succinctly and the rationale based upon the high spatio-temporal resolution and possible application is described.

The chapter continues by describing a succession of analysis methods, which use sensor data to generate a magnetic equivalent of the electrically recorded cortical contrast response function. Subsequently, following dipole localisation, SAM methods described in chapters 3 and 4 are used to reveal distinct loci of cortical activity in the striate and extra-striate visual cortex, which reveal parallel C3m components. Furthermore, the contrast response functions at these loci display distinct contrast response functions.

Further work describes a case study of a pure idiopathic photosensitive epilepsy patient that displays fundamental differences in the activity observed from the MEG sensors to the control subjects. These results suggest an application for the anatomically discrete methodology in the identification of this type of abnormality.

5.2   Introduction

The cortical response to modulation of stimulus contrast is crucial to our understanding of how the visual system interprets the world around us and plays an integral role in the visual response to other visual features such as colour, form and motion (Crognale *et al.*, 1997; Leonards and Singer, 1997; Bach and Ullrich, 1997; McKeefry, 2001). It has also proven to be a useful clinical metric of normal visual cortical processing, highlighting changes in cortical hyperexcitability disorders such as photosensitive epilepsy (PSE) (Porciatti *et al.*, 2000) and migraine (McKendrick and Badcock, 2003).

The contrast response function can be measured using invasive and non-invasive methods, such as single cell physiology (Heeger et al., 2000), electroencephalography (EEG) (Bobak, 1987; Crognale *et al.,*1997; Bach and Ullrich, 1997; Leonards and Singer, 1997; Porciatti *et al.,* 2000; McKeefry, 2001), Magnetoencephalography (MEG) (Anderson *et al.*, 1996) and functional magnetic resonance imaging (fMRI) using the blood oxygenation level dependant (BOLD) response (Boynton *et al.,*1999; Heeger *et al.*, 2000; Tootell *et al.*, 1998b and Logothetis *et al.*, 2001).

The reported contrast response functions both within and between modalities is highly variable. Some EEG studies find a function that saturates at a Michelson Contrast* of approximately 30% (Bobak, 1987; Baseler and Sutter, 1997; Porciatti *et al.*, 2000), consistent with single cell recordings[‡] and reflecting psychophysically measured contrast discrimination thresholds (Legge and Foley, 1980; Graham, 1989; Foley and Yang, 1991; Foley and Boynton, 1994 and Teo and Heeger, 1994, 1995.

Other studies suggest that dual functions exist, reflecting underlying magnocellular and parvocellular inputs (Rudvin *et al.*, 2000). Further EEG studies find different contrast response functions dependent upon the lateral variation of electrode placement (Bach and Ullrich, 1997), supported by fMRI and EEG results from other visual cortical areas, such as V5 (MT), which demonstrate extremely high gain at low contrasts (tootell *et al.*, 1995; Demb, 1997) and near complete saturation at contrasts as low as C_m 10% (Anderson *et al.*, 1996).

[‡]   Investigations of V1 neurons typically reveal a monotonic S- shaped response function, with an expansive response at lower contrasts and a compressive response at higher contrasts (Dean, 1981; Albrecht and Hamilton, 1982; Sclar *et al.*, 1990 and Carrandini *et al.*, 1997).

fMRI studies demonstrate a similar range of variation; some conclude that a saturating function around 30% Michelson Contrast is maintained throughout striate and extra-striate visual areas (Boynton *et al.*, 1998)[†], Further studies demonstrate linear contrast response functions (Logothetis *et al.*, 2001) and further studies suggest variation of contrast response functions in separate areas of the visual cortex (tootell *et al.*, 1998b).

In interpreting cortical contrast response functions, comparisons are often made with the cellular response in the lateral geniculate nuclei (LGN) in which the well characterised contrast response functions of magnocellular (M) units demonstrate steeper gain functions than parvocellular (P) units (Shapley, 1990) (fig. 5-1), a difference that is evidently consistent independent of receptive field size matching (Croner and Kaplan, 1995). The source of the pattern evoked VEP itself is still under debate. As some studies suggest it is generated in striate cortex (Biersdorf, 1974), whilst others suggest extra-striate cortex (Jeffreys and Axford, 1972a,b; Lesevre, 1982; Ossenblok and Spekreijse, 1991; Manahilov *et al.*, 1992; Miniussi *et al.*, 1998; Ikeda *et al.*, 1998 and Di Russo *et al.*, 2001) and others suggest generators in both striate and extra-striate cortex (Darcey and Arj, 1980; Maier, 1987; Bach and Ullrich, 1997). Additionally, MEG investigation suggests varied activity in striate and extra-striate cortex (Anderson *et al.*, 1996; Portin *et al.*, 1998; Tzlepi *et al.*, 2001). Recent studies of visual evoked potentials using MEG and dipole analysis reveal temporally discrete striate and extra-striate generators of early evoked activity (Shigeto *et al.*, 1998; Tzlepi *et al.*, 2001).

There are difficulties associated with both electrophysiological approaches such as EEG and haemodynamic approaches such as the fMRI BOLD response. EEG recording of the visual evoked potential (VEP) involves the placement of scalp electrodes around the occipital pole; which although possessing excellent temporal resolution (in the order of milliseconds), provides source reconstructions with low spatial resolution (~cm). Conversely, although fMRI has excellent spatial resolution (~mm), it is limited by a lack of temporal resolution. Therefore, it is difficult to determine the sequence of cortical activity with fMRI, the only recourse being to attempt to attribute VEP components to activation hotspots (Di Russo *et al.*, 2003).

[†] Boynton *et al.*, (1999) used fMRI to investigate retinotopically distinct contrast response functions. They found a large degree of variability across measurements in the ventral areas, believed to be the result of poor signal to noise ratio (SNR) produced by sensor-source distance. Furthermore, parameter values for ventral areas were not reported in the paper, as the data did not sufficiently constrain the model in those visual areas. fMRI analysis of contrast response and its relation to psychophysical measurements requires some basic assumptions: firstly that the neuronal fMRI responses are proportional to the local average (Boynton *et al.*, 1996); secondly, that fMRI response in V1 depends upon stimulus timing and contrast and finally, that the fMRI signal response to long stimulation can be predicted from that of shorter stimulation (Boynton *et al.*, 1999).

In this study we used MEG to record visual evoked potentials elicited by the onset of patterned stimuli and analysed the responses using the SAM beamforming method*, and subsequently Virtual Electrodes* were used to reconstruct evoked potential activity and identify change in amplitude as a function of stimulus contrast in both striate and extra-striate regions.
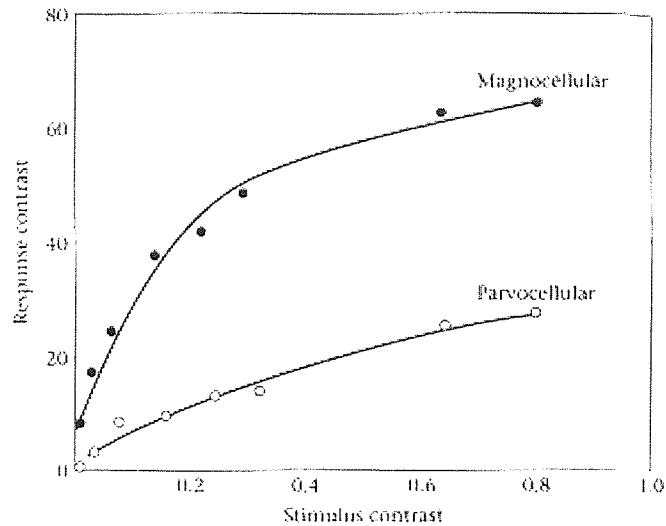
Figure 5-1. Contrast response functions of the magnocellular and parvocellular cells in the lateral geniculate nucleus. Demonstrating that magnocellular cells have a higher contrast gain than parvocellular. Redrawn from Shapley (1990).
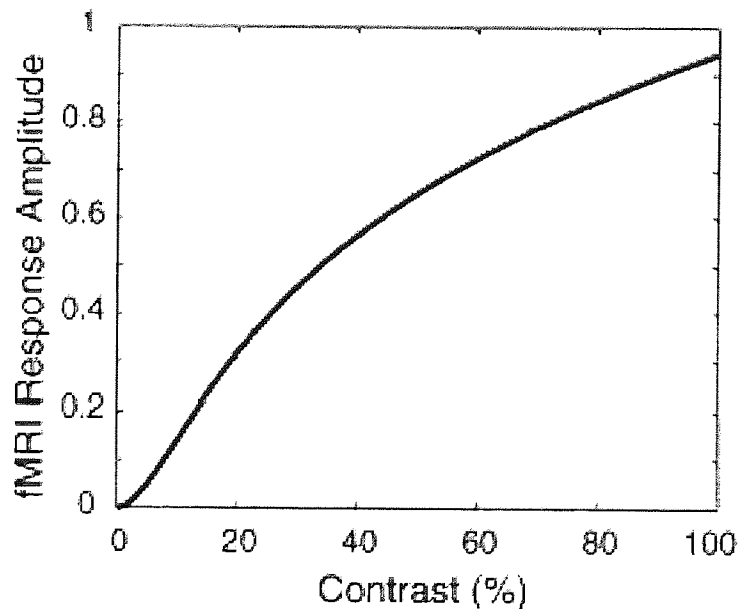
Figure 5-2. Typical contrast response function obtained from the primary visual cortex of the human using fMRI BOLD in normalised response units. Redrawn from Boynton et al. (1999).

5.3   Materials and methods

5.3.1   Stimuli

Stimuli consisted of horizontally oriented, stationary sinusoidal gratings of 3 cycles per degree (cpd), presented for a two second 'on' period followed by a three second 'off' period. The gratings were presented at six different contrast levels in a randomised order, each of the contrast levels were presented a total of 25 times. Stimuli were presented in the lower left quadrant of visual field and subtended 3° x 3° of visual angle at an eccentricity of 0.5° from both horizontal and vertical meridians. A single quadrant was used. Stimuli were displayed at six Michelson Contrasts*: 3, 6, 12, 24, 48 and 96%.

Recording and Coregistration were carried out using the standard protocol*.

Analysis

5.3.2   Raw Sensor Analysis

Initially, as a comparative method for visual evoked potential (VEP) studies, the raw sensor data was taken and averaged across trials for each of the contrast levels. Eight channels over the occipital pole were averaged together to give an MEG equivalent measure of the VEP, the evoked potential peaks at both 100 and 150ms were taken and the mean amplitude of the evoked potential was plotted as a function of the 6 contrast levels

5.3.3   Dipole Analysis

As described in chapter three, source analysis was done initially using the dipole fitting method (Scherg and Von Cramon, 1985a,b; Mosher, 1992), for which data are band pass filtered (1-40Hz) and averaged across all trials to optimise signal to noise ratio (SNR) for the evoked potential. The optimal source reconstruction was produced for the C2m (~100ms) and C3m (~150ms) components by least squares comparison of predicted and measured activity over a 20ms time window. Monte-Carlo analyses were then performed for the solutions to generate an estimate of spatial variation in the source distribution.

5.3.4   SAM Analysis

SAM analysis was used to identify cortical power changes in the 4-12Hz band (the peak spectral power of the evoked potential (chapter 3) in each subject; comparing 300ms post-onset with 300ms pre-onset. Spatial normalisation and averaging of volumetric

images was done, in order to generate a group SAM image (Singh *et al.,* 2002). The 3-dimensional coordinates of neuronal activity as determined by SAM were analysed using virtual electrode (VE) reconstruction to visualise the local evoked response. The amplitudes of the evoked potentials in these active brain regions were then plotted as a function of stimulus contrast to produce anatomically discrete contrast response functions.

* Readers are referred to section 3.5 for details.

5.4   Results

5.4.1   Raw Sensor Analysis

The raw sensor data revealed a saturating contrast response function, which peaked at approximately 30% Michelson Contrast* (fig.5-3).
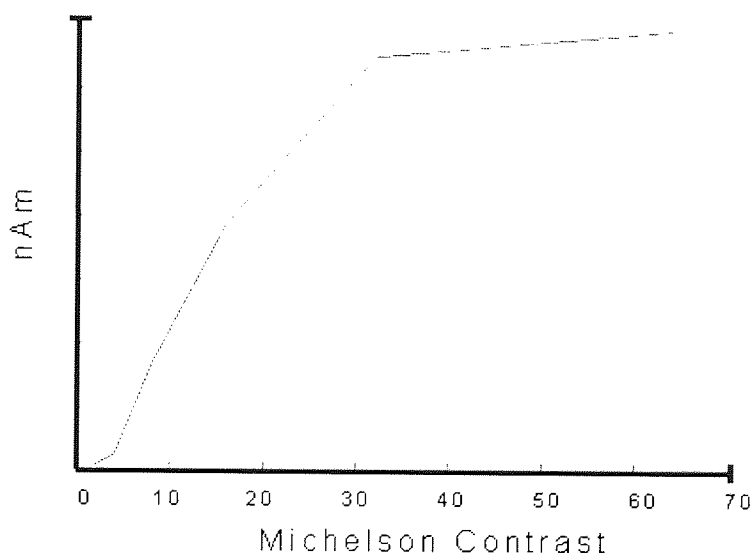
Figure 5-3. Contrast Response function computed from raw sensor data. Response of subject KDS to pattern onset at Michelson Contrasts of 2-64%, calculated from the information from eight occipital sensors and shown in normalised arbritrary MEG units (nAm).

5.4.2   Dipole Analysis

The results conclude that the C2m component can be reliably modelled using a single dipole in the upper right bank of the calcarine sulcus. However, the C3m component is not sufficiently modelled using a single dipole (fig. 5-4) as the Monte-Carlo volume suggests (fig. 5-4) .However we were unable to find a stable two dipole fit model to account for the C3m component. Typically, the reduced chi-square value (Supek and Aine) for

the single dipole fit was around unity, indicating that this simple model adequately accounted for the data given the noise level.

5.4.3   SAM and VE Analyses

SAM analysis revealed two distinct peaks in eight out of the ten subjects, the remaining two showed only one peak. Both peaks were in right visual cortex, concordant with lower left visual field stimulation; the first located in the upper right bank of the calcarine sulcus in primary visual cortex, the second located in right extra-striate visual cortex in area V3a (fig. 5-5a). This was determined using retinotopic analysis in 2 of the subjects and using Talairach coordinates in the other subjects. Virtual electrode reconstruction of the temporal information revealed morphologically different evoked responses at the striate and extra-striate locations (fig. 5-5b); the striate source demonstrated a typical pattern onset evoked potential with pronounced C1m, C2m and C3m components (Harding *et al.*, 1996), whereas the extra-striate source showed only a pronounced C3m component. The amplitude of this evoked activity was plotted as a function of stimulus contrast and revealed two distinctly different functions (fig. 5-5c,d). The extra-striate source demonstrates a typical contrast response curve which saturates at a Michelson Contrast of approximately 30% (fig. 5-5d), whereas the striate source demonstrates a contrast response function with little evidence of saturation (fig. 5-5c).
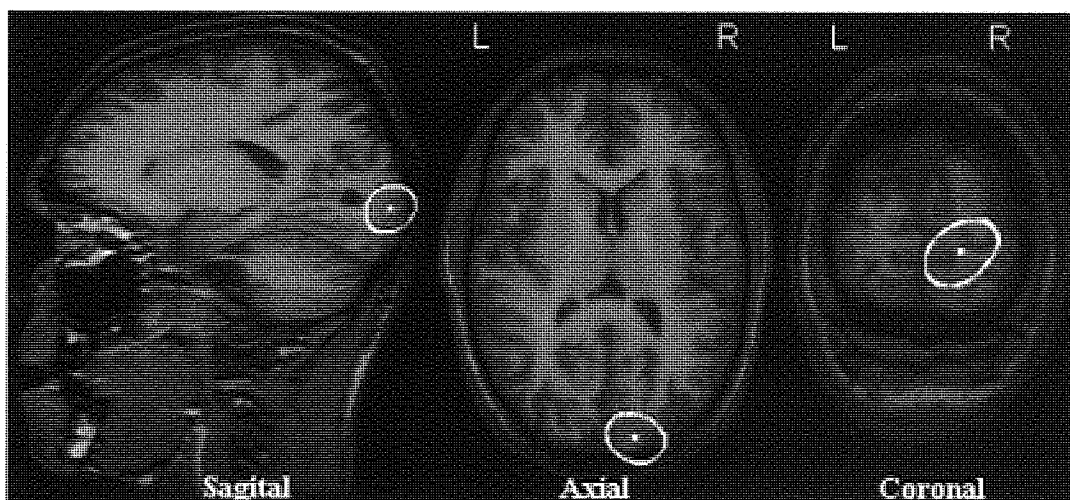
Figure 5-4. Dipole localisation of C2 evoked potential component. Demonstrating a single source (white dot) in right visual cortex, following left visual field stimulation, with Monte-Carlo confidence volumes (white elipsoids) indicating 95% confidence level.
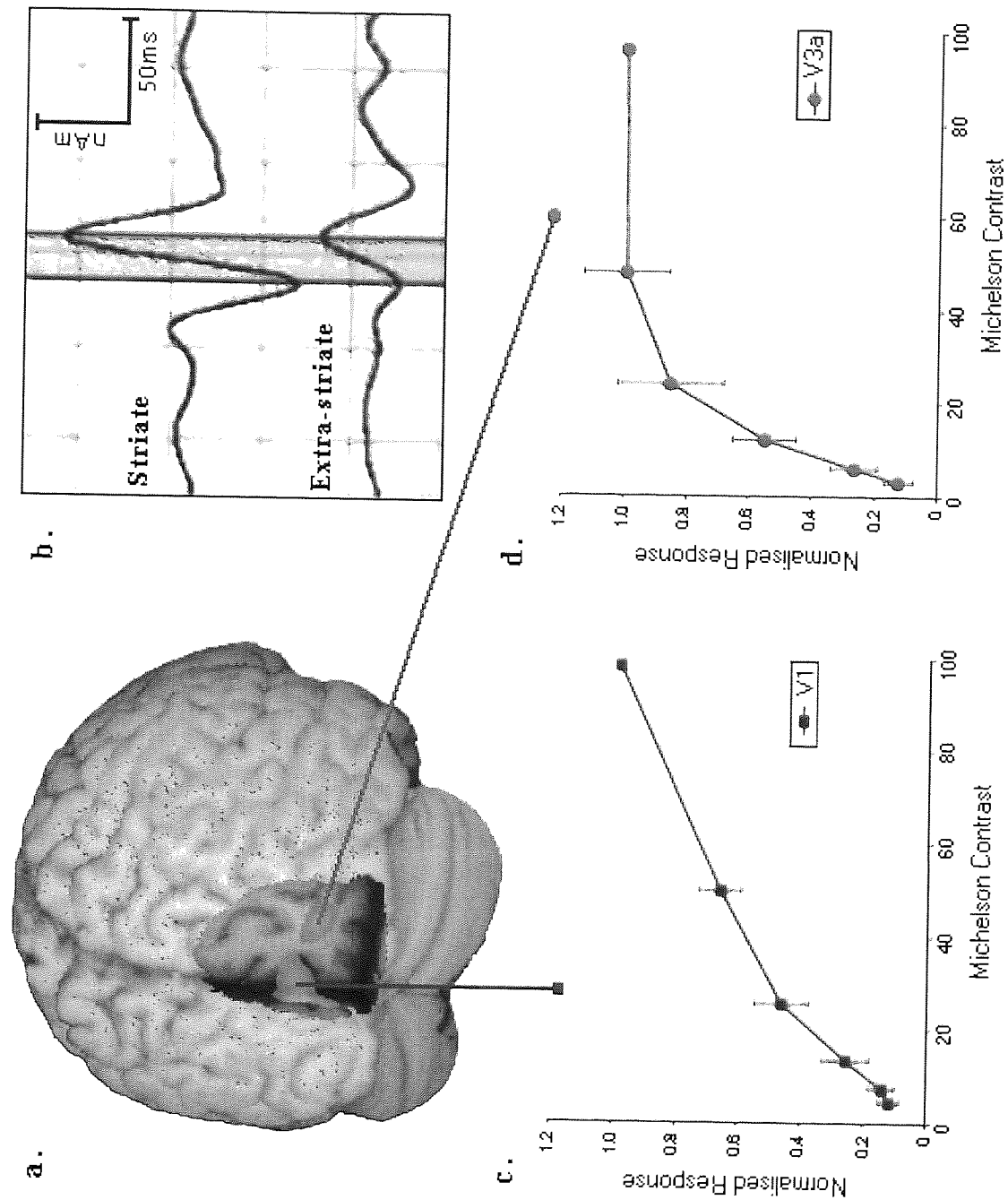
Figure 5-5. SAM source localisation, neuronal activity and contrast response curves in visual cortex. (a) Group SAM image (n=8) showing peaks of activity localised in striate and extra-striate visual cortex. (b) Virtual electrode showing local neuronal activity at peak SAM loci, the shaded region highlights morphological variability. (c and d) Contrast response curves plotted as fractions of maximal amplitude (±1.96SEM) in (c) right striate cortex and (d) right extra-striate cortex.

5.5 Discussion

As discussed previously (chapter 4) the dipole/SAM comparison reveals a potential shortfall in the dipole fitting method as it is unable to accurately identify all sources (fig. 5-4). This can be avoided by using the spatial analysis and temporal reconstruction method of SAM and VE. The results presented in this paper have implications for electrophysiological measurements in both normal subjects and clinical patients and support the suggestion that there are multiple generators of the visual evoked potential (Darcey and Arj, 1980; Maier, 1987; Bach and Ullrich, 1997). Furthermore it suggests that the saturating contrast response function observed in some VEP studies is likely the result of neuronal activity arising at least in part from the extra-striate visual cortex. In particular it would suggest the underlying source of measurements comprising dual contrast gain functions (Rudvin et al., 2000) are the result of topographical variations described here.

These results further support findings of both EEG and fMRI that different regions of visual cortex generate distinctly different contrast response functions (Bach and Ulrich, 1997; Tootell et al., 1998b). The distinct slopes (gains) of the contrast response functions are suggestive of the possible contributions from the magnocellular (M) and parvocellular (P) pathways. The striate source demonstrates low contrast gain, similar to that of the P pathway, whilst extra-striate areas demonstrate high contrast gain similar to the M pathway (Shapley, 1990), supportive of EEG and fMRI suggestions (Rudvin et al., Tootell et al., 1998b). This suggests that this VEP component is of importance in extra-striate processing of contrast modulated form through connection by magnocellular projections. Furthermore, it suggests that the non-saturating function observed in PSE (Porciatti et al., 2000) might be the result of deficient or absent extra-striate processing of contrast modulated visual characteristics.

To summarise; this chapter demonstrates parallel processing of contrast defined stimuli at spatially discrete locations of the visual cortex and in addition reveals functionally distinct mechanisms of contrast processing at these loci.

5.6 Further Application

It has been found that there are variations in the contrast response function in hypersensitivity disorders such as photosensitive epilepsy (PSE) when measured using VEP (Porciatti et al., 2000). Specifically, where a saturating function is observed in normal subjects, there is a lack of saturation found in PSE patients (fig. 5-6). Here a patient with pure idiopathic PSE (diagnosed by an author of the above paper) was tested using the same methods described for the normal patients (above). The absence of an anatomical MRI at

the time of analysis precluded a raw sensor comparison. These results are demonstrated (fig. 5-6b) and further work described below.
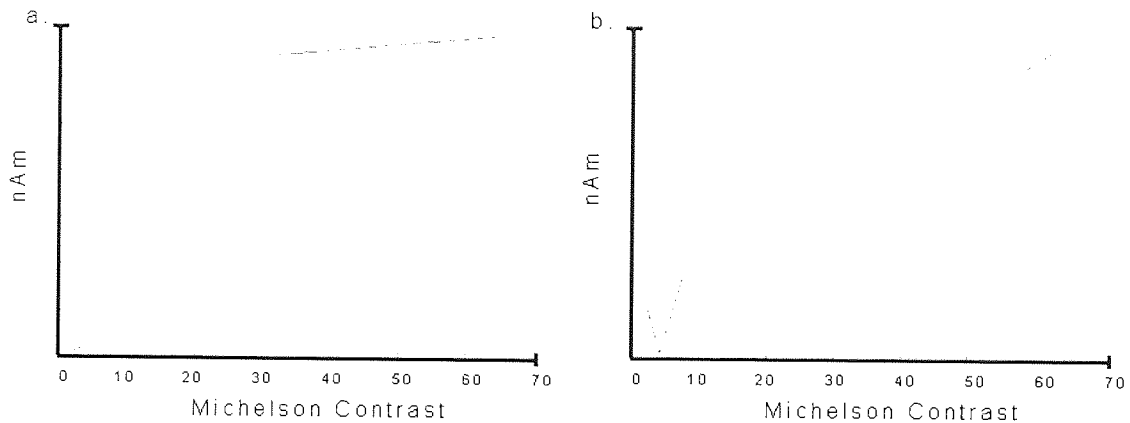
Figure 5-6. Contrast Response Functions. A comparison of results obtained from: (a) a normal individual and (b) a photosensitive epilepsy patient; showing Cm ~30% saturation in the normal patient and a roughly linear response in the PSE patient.

This finding although in a single subject introduces the question of cortical variation in contrast processing in the PSE patient and forms the basis for further investigation using the anatomically discrete methods described above and is a prime example of the application of the virtual electrode utility.

The results suggest that this method may form the basis for establishing a normal response function against which visually associated or affected pathology may be compared.

Chapter 6

Investigation of Visual Gamma Oscillations using Magnetoencephalography (MEG)

6 Investigation of Visual Gamma Oscillations using Magnetoencephalography (MEG)

6.1 Overview

Chapter six describes a series of experiments and analyses used to investigate the phenomenon of visual gamma oscillations in the human visual cortex. The chapter begins with an introduction to the background of visual gamma, detailing previous results from invasive and non-invasive investigations in animals and humans. Within this section it is explained that specific cell populations are postulated to underlie the visual gamma oscillations observed in the cat and monkey in response to various visual stimuli. Its significance is the subject of much debate and the chapter continues by describing the low level 'feature binding' hypothesis and the cognitive extension 'perceptual binding' suggesting specific roles in object recognition and specific memory states.

The chapter continues by describing the use of SAM analysis in the investigation of visual gamma (30-70Hz) oscillatory activity. The experimental aim is to elucidate the role of pattern in visual gamma generation and to subsequently determine the significance of stimulus contrast in its generation. In order to do so various stimuli are used with varied visual characteristics; this is designed to separate the variation in the gamma oscillations done to, pattern itself, pattern variance and contrast. It is found that pattern and contrast are necessary for the generation of visual gamma oscillations. Furthermore, two types of gamma oscillation are distinguished based upon spatial location and temporal profile:

1. *Sustained gamma* (occurs in striate visual cortex) and remains for the duration of the pattern presentation, supported by the finding that desynchronisation occurs in response to pattern offset and contrast decrement.

2. *Transient gamma* activity occurs in extra-striate regions of visual cortex and occurs in response to a change in the spatial phase at the stimuli.

In addition, the sustained gamma varies in amplitude linearly with stimulus contrast. These results appear to correlate strongly with the results in the macaque monkey. The aim of this chapter is to provide a comprehensive description of visual gamma as distinguished with the analysis tools described; subsequently placing the results in the context of previous invasive studies at the animal and human level.

6.2   Introduction

Electrophysiological investigations of the visual system in both animals and humans over recent years revealed >30Hz (gamma) synchronisation as a common substrate of visual cortical processing. Single cell studies and staining methods provide evidence of the underlying cellular mechanisms responsible for the generation of the gamma signal; thought to arise from specific chattering cells in layers 2 and 3 of striate and pre-striate visual cortex (Gray and McKormick, 1996*). The observation of the gamma signal at the cellular level occurs subsequent to visual stimulation such as coherent moving bars (Engel *et al.,* 1997; Kreiter and Singer, 1996) and static stimuli (Friedman-Hill *et al.,* 2000). Local field potential (LFP) analyses, providing averaged measurement of activity from within a few millimetres of the electrode tip demonstrate similar increase in gamma oscillatory power following visual stimulation (Logothetis *et al.,* 2001; Fries *et al.,* 2001, 2002). The increase in oscillatory power in the gamma frequency following visual stimulation has been reproduced in the human electroencephalograph (EEG) using coherently moving stimuli (Lutzenberger *et al.,* 1995; Muller *et al.,* 1996, 1997).

The occurrence of elevated visual gamma oscillations have been investigated by Gestalt psychologists; employing rotating bi-stable figures (Kiel *et al.,* 1999), coherent and incoherent stimuli (tallon-Baudry *et al.,* 1996) and visual search tasks (tallon-Baudry *et al.,* 1997). The interested reader may refer to Tallon-Baudry and Bertrand (1999); Bertrand and Tallon-Baudry (2000) and Pulvermuller (1999) for reviews and discussion on this topic. Further studies have observed modulation of the induced gamma activity as a function of specific memory states (Burgess *et al.,* 2002) and memory maintenance (tallon-Baudry *et al.,* 2001). The fundamental role of visual gamma activity is the current focus of some debate and it appears to be an integral device in the processing of visual information of both intrinsic and extrinsic origin and thus the facts regarding its specific function remains elusive.

---

*   Using intracellular recording and staining of single cells *in vivo* Gray and McCormick (1996) studied the intrinsic membrane properties of cells in the cat striate cortex. They describe four distinct classes of pyramidal cells: *regular spiking* (RS) cells, *intrinsic bursting* (IB) cells, *fast spiking* (FS), three classes of cells previously identified (McCormick *et al.,* 1985) and a new subset *chattering* (CH) cells. Membrane potential of CH cells was dominated by 30-60 Hz oscillatory activity during visual stimulation. Gray and McCormick suggest that this characteristic response might be the pacemaker for the widespread gamma oscillations, because rapid bursts of action potentials are far more likely to cause other neurons to fire than are single pulses.

The physiological generation of the signal is suggested by some to be of cortical origin (Gray *et al.*, 1989; Gray and McCormick, 1996*), whilst others have suggested involvement of thalamic sources (Ghose and Freeman, 1992; Castelo-Branco *et al.*, 1998).

At the centre of the debate is the function of the synchronous activity; a common theory being that it is the result of low level feature binding as a mechanism of temporally locking elements linked in a visual scene (Von der Malsburg, 1981; Singer, 1993, 1994, 1999; Singer and Gray, 1995; Engel *et al.*, 1997; Roelfsema and Singer, 1998; Herculano-Houzel *et al.*, 1999). This binding is suggested to enhance the saliency of the neuronal signal and therefore increase processing efficacy in translation to subsequent processing levels (Fries *et al.*, 2001).

This feature binding hypothesis has been applied at the perceptual level, as a mechanism by which task relevant object representation is achieved (tallon-Baudry and Bertrand, 1999; Bertrand and Tallon-Baudry, 2000). However, in a review article by Shadlen and Movshon (1999)[‡] the subject of feature binding through early visual cortical synchrony is critically reviewed and raises certain questions regarding the theoretical advantages of synchrony as a method of perceptual binding and highlights the inadequacies of the current explanation.

The synchronous gamma activity in response to visual stimulation would appear to be a common phenomenon measurable by a range of electrophysiology techniques such as single unit activity (SUA), local field potentials (LFP) and electroencephalography (EEG). Previous studies have described an inability of Magnetoencephalography (MEG) to measure the gamma activity (tallon-Baudry *et al.*, 1997) and have gone on to suggest possible source distribution model (ring of dipoles), forming a closed field morphology (chapter 2) in order to explain the lack of signal detection by the method (tallon-Baudry *et al.*, 1999).

This study used a 151 channel whole head magnetometer (CTF Systems Inc., Port Coquitlam, Canada) to record cortical responses to various visual stimuli. We then analysed 30-70Hz (gamma) oscillatory activity using synthetic aperture magnetometry (SAM)*. Additionally, and subsequently used Virtual Electrode analysis* to observe modulation of the gamma oscillatory power as a function of stimulus contrast.

[‡]   Shadlen and Movshon (1999) provide an evaluation of the temporal binding hypothesis and provide critical appraisal of the literature. They highlight the limitations of both the bottom up (cellular signalling) and top down (cognitive modulation) approaches by suggesting restricted information transfer and erroneous feature grouping.

6.3   Experiment 1

6.3.1   Methods

- In each of the two experiments, subjects were seated in the MEG system and passively viewed stimuli*, whilst recordings were made with the standard protocol*.

6.3.1.1 Stimuli

In the first experiment subjects (n=8) focused on a central fixation point, whilst four different stimuli were presented; pattern onset, pattern reversal, contrast increment and luminance increment. This was designed to analyse the cortical response to changes in pattern and contrast, pattern alone, contrast alone and luminance (respectively). All gratings were horizontally oriented sinusoidal gratings of 3 cycles per degree (cpd).

- The pattern onset stimulus was a grating of 90% Michelson Contrast* (C_m), presented for 2 seconds, followed by three seconds of blank background of equal mean luminance to the stimulus.
- The pattern reversal was a grating, also with 90% C_m, which was phase reversed at 0.5 Hz.
- The contrast increment consisted of a grating presented at 10% C_m for 3 seconds and was then incremented without phase reversal to 100% C_m for 2 seconds.
- The luminance increment consisted of a black background of 300cd/m^2 on which an achromatic luminance patch of 300cd/m^2 was presented for seconds, followed by a return to a completely black background for 3 seconds.

Consequently the presentation cycle of the stimuli afforded the opportunity to analyse offset responses as an additional comparison. The stimuli were presented in randomised sequence; each of the stimuli appearing a total of 50 times. All stimuli were displayed in the lower left quadrant of visual field subtended 3° x 3° of visual angle at an eccentricity of 0.5° from both horizontal and vertical meridians. A single quadrant was used in both experiments one and two*.

- Coregistration was undertaken as per standard protocol*.

---

*   The reader is referred to the 'Presentation, Recording and Analysis' protocols described in section 3.5.

6.3.1.2 Analysis

Synthetic aperture magnetometry was used to analyse the response to the four types of visual stimulation in the gamma (30-70Hz) frequency band:

- Pattern Onset was analysed using a 1.5 second post onset (active) window compared to a 1.5 second blank (passive) window.

- Pattern Offset was analysed using a 1.5 second post-offset (active) window compared to a 1.5 second pre-offset (passive) window.

- Pattern Reversal was analysed using four methods; (1) a 1.5 second post onset (active) was compared to a 1.5 second blank (passive); (2) a 1.5 second post-reversal (active) window was compared to a 1.5 second pre-reversal (passive) window; (3) a 1.5 second (+0.5-2 secs.) post-reversal (active) window compared to a 1.5 second blank (passive) window; (4) a 1.5 second (+0.5-2 secs.) post-reversal (active) window compared to 1.5 seconds pre-reversal (passive) window.

- Contrast Increment was analysed using a 1.5 second post-increment (active) window compared to a 1.5 second pre-increment (passive) window.

- Contrast Decrement was analysed using a 1.5 second post-decrement (active) window compared to a 1.5 second pre-decrement (passive) window.

- Luminance Increment was analysed using a 1.5 second post-increment (active) window compared to a 1.5 second pre-increment (passive) window.

- Luminance Decrement was analysed using a 1.5 second post-decrement (active) window compared to a 1.5 second pre-decrement (passive) window.

a normalised image of each of the stimulus conditions was then created using group SAM analysis (chapter 2).

6.4   Results

The group SAM results are displayed at constant threshold of (t>2.0) on the following page (figs. 6-1 to 6-3):

- Pattern Onset induced an increase in gamma (30-70Hz) oscillatory activity in the right (contralateral) visual cortex and also a decrease in oscillatory gamma activity in left (ipsilateral) visual cortex (t=4.6) (fig. 6-1a).

- Pattern Offset produced event related desynchronisation (ERD) in the right (contralateral) visual cortex (t=3.6) at a locus to that of the ERS induced by the pattern onset (fig. 6-1b).

- Pattern Reversal produced various, topographically distinct oscillatory changes dependent upon the comparative SAM envelope used; description related to the 'analysis' classification: (1) pattern versus blank produced both striate and extra-striate ERS in right (contralateral) visual cortex (t=3.1) (fig 6-2a); (2) pattern versus pattern produced ERS (t=2.4) in right (contralateral) extra-striate visual cortex alone (fig. 6-2b); (3) late pattern versus blank produced ERS (t=2.2) in right (contralateral) striate visual cortex alone (fig. 6-3c); (4) late pattern versus pattern resulted in no significant increase in gamma activity.

- Contrast Increment produced ERS (t=3.9) in the right (contralateral) striate visual cortex visual cortex (fig 6-3a).

- Contrast Decrement produced ERD (t=2.2) in the right (contralateral) visual cortex (fig. 6-3b).

- Luminance Increment and Decrement both failed to elicit any change in gamma oscillatory activity.

The results showed that the pattern onset stimulus proved to have the greatest efficacy in producing an increase in gamma synchrony. Further analysis of the pattern onset condition reveals that there are bilateral consistencies in activation beyond the occipital cortex. These were a decrease in gamma oscillatory power in the inferior temporal lobe (t=2.3) (fig. 6-4b) and an increase in gamma oscillatory power around the middle frontal gyrus (t=2.2) (fig. 6-4a).
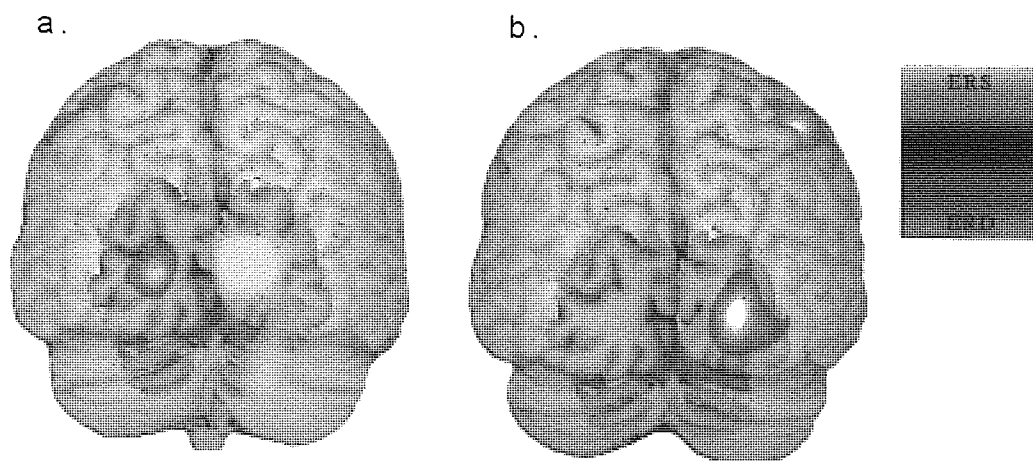
Figure 6-1. Pattern Onset/ Pattern Offset Gamma. Demonstrates (a) pattern-onset ERS in the upper right primary visual cortex (t=4.6) and ERD in left primary visual cortex (t=2.2) and (b) pattern-offset ERD in right primary visual cortex (t=3.6).
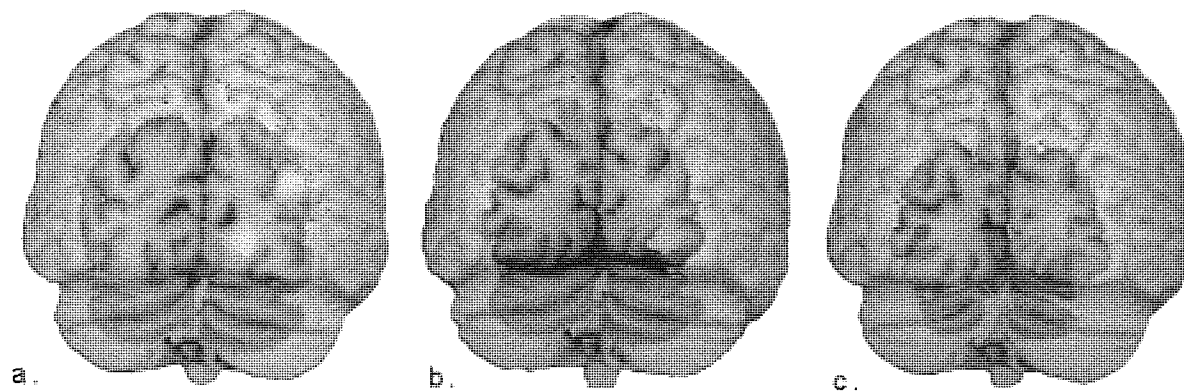
Figure 6-2. Pattern Reversal Gamma. Demonstrating (a) pattern Vs blank ERS in right striate and extra-striate visual cortex (t=3.1), (b) pattern Vs pattern ERS in right extra striate visual cortex (t=2.4) and (c) late pattern Vs blank ERS in striate visual cortex (t=2.2).
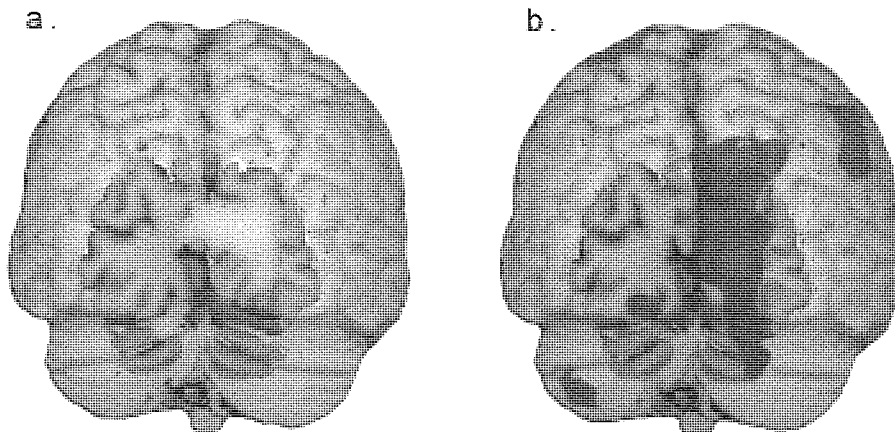
Figure 6-3. Contrast Increment/ Decrement Gamma. Demonstrates (a) contrast increment ERS in right primary visual cortex (t=3.9) and (b) contrast decrement ERD in right striate and temporal-parietal areas (t=2.2).
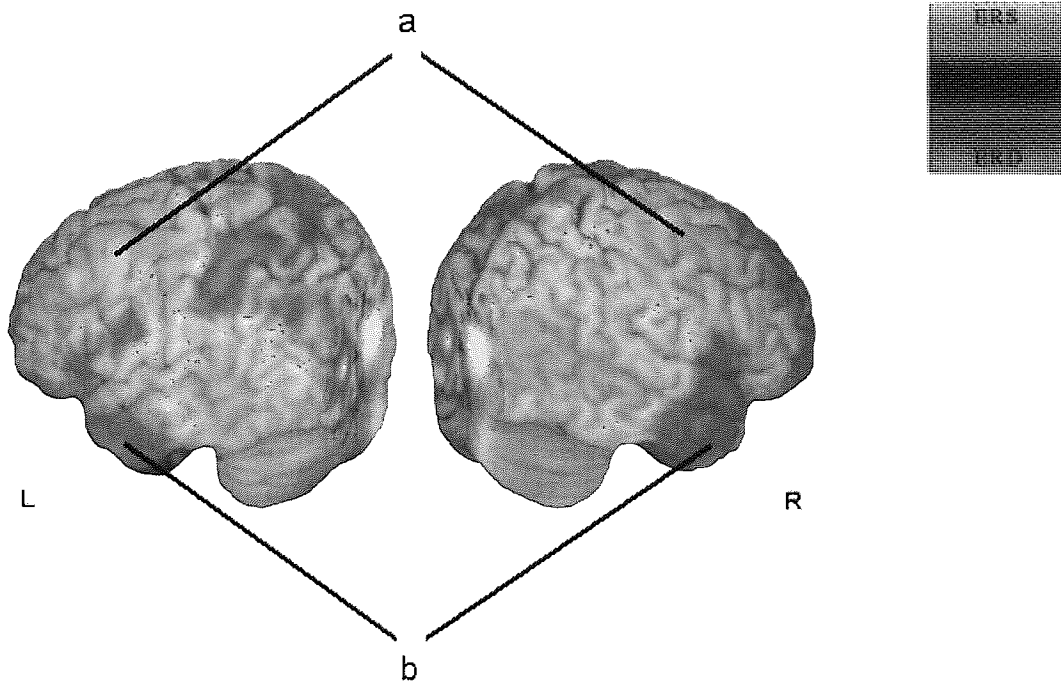
Figure 6-4. Pattern Onset Gamma. Demonstrates extended regions of activation (a) bilateral ERS in the middle frontal gyrus (t=2.2) and (b) ERD in inferior temporal lobe (t=2.3).

6.5   Experiment 2

6.5.1   Methods

6.5.1.1   Stimuli

Following the results of the first experiment, which highlighted the optimal stimulus for the induction of gamma oscillatory activity it was postulated that there might be a direct relationship between stimulus pattern and oscillatory gamma activity. Thus it was hypothesised that modulation of stimulus contrast would have a direct effect on gamma frequency oscillatory power. In order to test this hypothesis the pattern onset stimulus used in experiment 1 was repeated at varied Michelson Contrasts (C_m).

Subjects (n=10) focused on a central fixation point, whilst the pattern onset stimulus was presented for a 2 second 'on' period followed by a 3 seconds of 'blank' screen of equal mean luminance to the stimulus; C_m 3, 6, 12, 24, 48 and 96 % were used. Contrast levels were presented randomly in a single trial in which each contrast was presented 50 times.
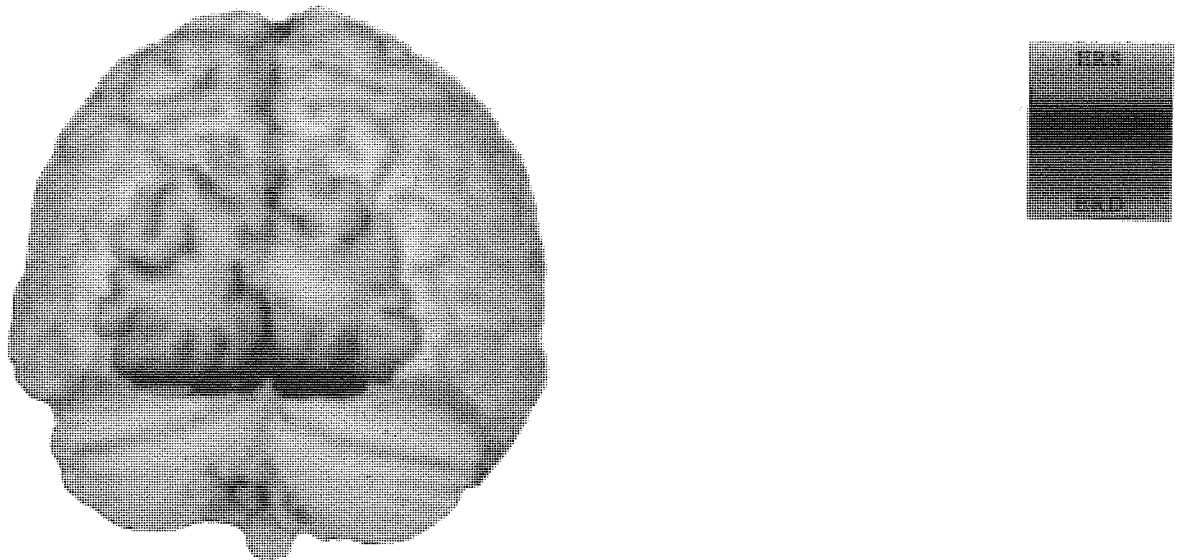
Figure 6-5. Group SAM image of event related synchronisation in the gamma (30-70Hz) frequency band ($\underline{t}$=4.24, $\underline{n}$=9, $\underline{p}$<0.01).
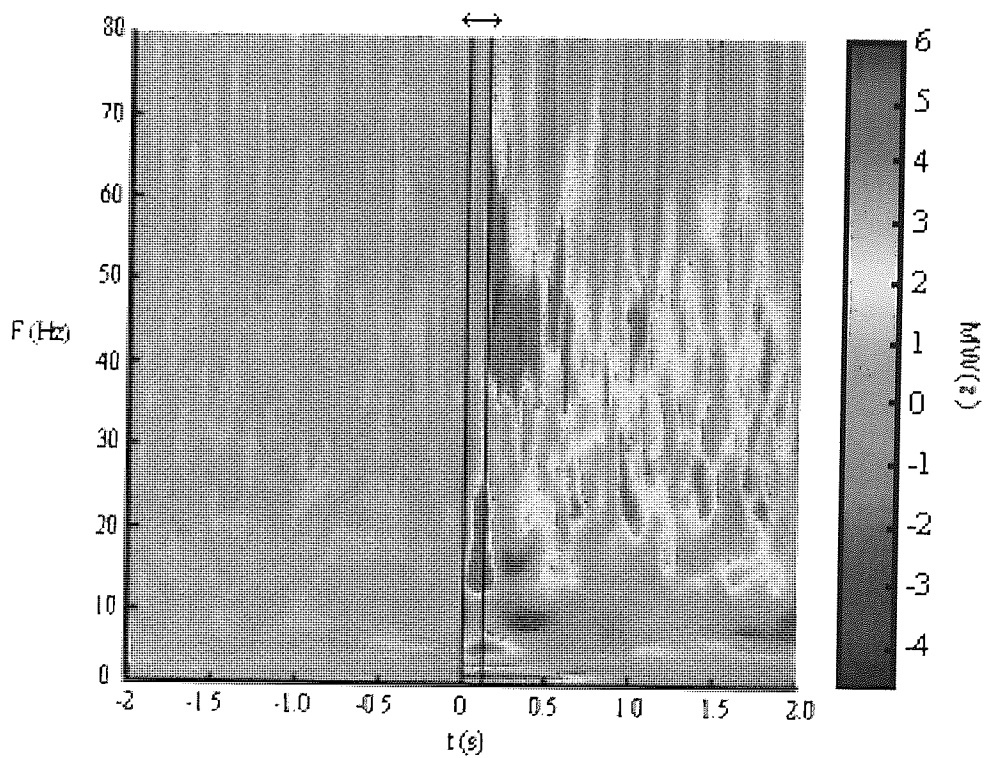
Figure 6-6. Morlet-wavelet time frequency plot of gamma activity following pattern onset. Arrow indicates time offset from zero.
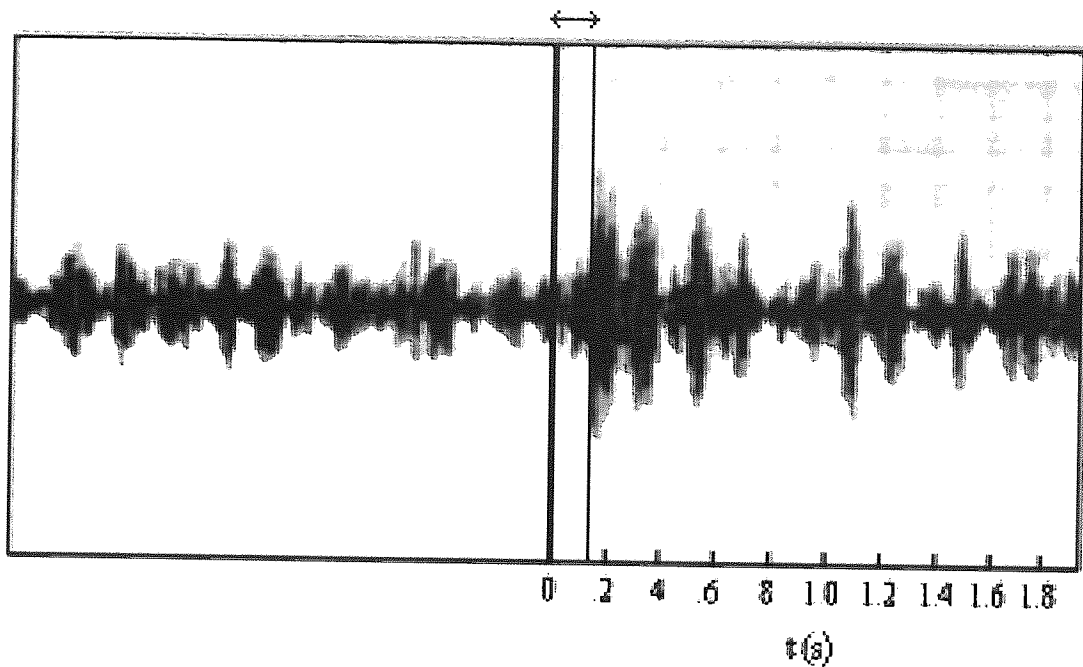
Figure 6-7. Virtual Electrode trace. Band pass filtered (30-70Hz) demonstrating elevation of gamma activity. Arrow indicates increment offset from zero.
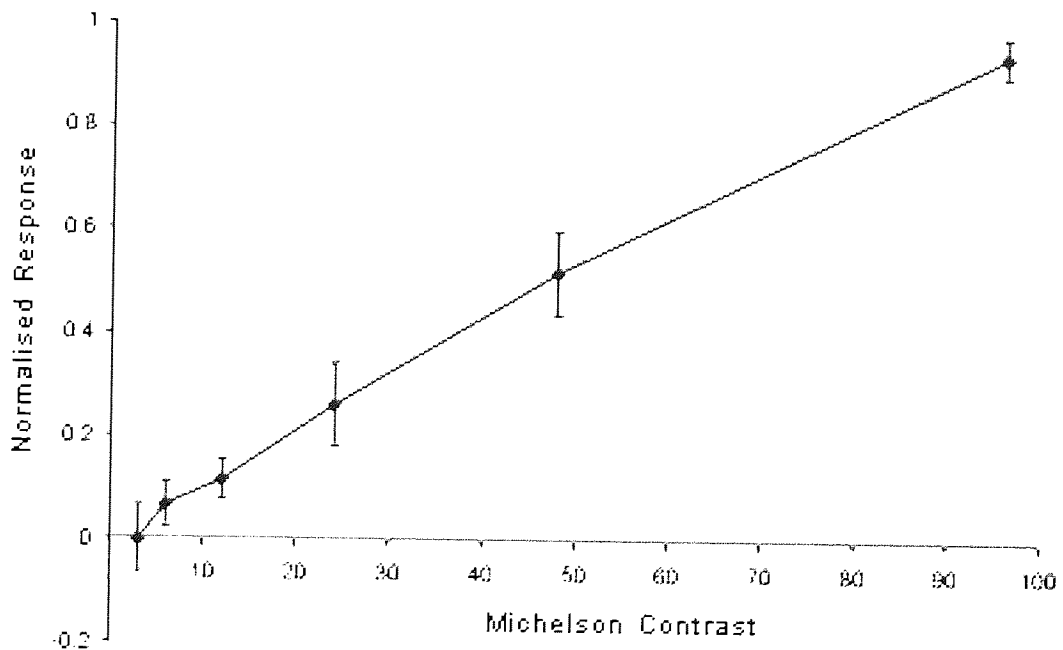
Figure 6-8. Gamma contrast response function. Contrast response curve demonstrating linear function of gamma oscillatory power increase as a function of contrast (r = 0.994, p<0.01).

6.5.2   Discussion

The results of the pattern onset stimulation suggest that there are constant gamma oscillations in the visual cortex in the absence of visual simulation. This oscillatory activity appears to be amplified in areas of visual cortex that correspond to the visual presentation of the stimulus (contralateral) and is suppressed in other visual cortical areas (fig 6-1a). The occurrence of ERS in response to all patterned stimuli but not to luminance stimulation suggests it is a direct response to edge or form information.

The pattern reversal analyses reveals there to be two distinct forms of gamma oscillatory activity; both of which are modulated by the presence of pattern:

(1)   Sustained gamma activity that is a direct result of static pattern presence and which is directly linked to the cortical processing of the stimulus contrast, this is supported by the ERD at pattern onset/contrast increment and subsequent ERD at pattern offset/ contrast decrement (figs. 6-1, 6-3).

(2)   Transient gamma activity that is directly linked to the phase shift of the pattern stimuli (fig. 6-2b).

The sustained activity appears to be centred primarily around the primary visual cortex, although appears extended dependent upon stimulus intensity; whereas the transient activity appears to be extra-striate in origin. It is conceivable that the phase shift could represent a mechanism by which sustained gamma activity is produced in response to spatial variation of the stimulus; hence, sustained gamma activity might be produced if motion were introduced into the stimulus. This would support the findings of the single cell (Engel *et al.,* 1997; Kreiter and Singer, 1996) and EEG (Lutzenberger *et al.,* 1995; Muller *et al.,* 1996, 1997) studies that find gamma response to coherently moving bars.

A comparison of the various stimuli reveals that pattern is required for the induction of gamma and that the gamma activity is modulated by the stimulus contrast. However, the gamma induced by pattern at a specific contrast is greater that that from stimulus contrast increment by that amount. The investigation of the gamma contrast response function further supports the idea that the response is the modulated response to stimulus contrast as it produced a linear response with contrast.

The temporal profile of the gamma activity following pattern onset is quite late (150-200ms) implying that it occurs following initial visual cortical processing of the stimulus (figs. 6-6, 6-7). This would suggest that its generation is reliant upon feedback from higher visual cortical areas.

These observations suggest are supportive of those made of SUA, LFP and EEG, whereby gamma activity is induced by the presence of simple visual stimuli. Consequently they contradict previous observations that gamma activity is not detectable using Magnetoencephalography; this would suggest that the underlying generators are not arranged in a magnetically silent manner and could reasonably be assumed to be part of those neuronal assemblies found to generate gamma frequency activity (Gray and McKormick, 1996).

Supposition

The underlying function of induced gamma activity in the visual cortex remains unclear. However, the latency of the increase in gamma activity (150-200ms), would suggest it occurs following the initial visual processing and is the result of top down generation. The response to simple visual features such as pattern, with direct modulation of the response by stimulus contrast and the direct relationship of the visual field location and the cortical activity suggest it to be activity of cells with specific receptive fields receiving retinal input. However, the fact that the activity occurs at 150-200ms rather than the 0-50ms suggests that it is not a direct retino-cortical response and more likely instigated following feedback from higher cortical areas. This is further supported by the ERD which occurs in the ipsilateral visual field; suggesting that as it has no stimulus input activity is suppressed by top down mechanisms.

These results can be hypothetically linked to both the fundamental cellular feature integration suggestions of Von der Malsburg, (1981); Singer (1993, 1994, 1999); Singer and Gray, (1995); Gray et al.,(1989); Gray and McCormick (1996); Engel et al. (1997); Roelfsema and Singer (1998); Herculano-Houzel et al. (1999); Fries et al. (2001) and the cognitive perceptual binding and specific memory suggestions of Kiel et al. (1999); Tallon-Baudry et al. (1996, 1997); Tallon-Baudry and Bertrand (1999); Bertrand and Tallon-Baudry (2000); Burgess et al. (2002); Tallon-Baudry et al. (2001). If visual cortical gamma were the mechanism by which the fundamental aspects of the visual scene (edge, orientation, position) were highlighted, then this would explain why there is a direct modulation of the response by these features and yet why there is a delay and a laterally selective response. Therefore in the case of the bi-stable or ambiguous figure; the orientation at which recognition occurs, the shape of a coherent object or the identified form of an ambiguous feature would be the point at which gamma is initiated. Furthermore, this could be extended to include processing of visual information both extrinsically (retino-cortical) and intrinsically (memory) generated.

A simplification of this hypothesis is that sustained visual gamma activity is the response of cellular mechanisms of simple feature encoding modulated in a top down manner by cognitive factors such as attention (Buchel and Friston, 1997), recognition and memory.

6.5.3 Further Application

Research in both animals and humans is crucial to our continued understanding in the field of neuroscience. However, despite the long established anatomical comparisons between various animal species and the human, the animal and human research literatures remain relatively isolated. The impracticality of invasive research in healthy humans and the disparities associated with pathological models, suggests that a non-invasive human equivalent would be the most constructive solution. A recent primate study using surgically implanted electrodes to measure local field potentials (LFP) and multi unit activity (MUA) observed gamma activity in primary visual cortex, which increased linearly in amplitude with stimulus contrast (Logothetis *et al.*, 2001); additionally fMRI BOLD response was found to account for 50-60% of the LFP/MUA response.

As an additional application of the induced gamma activity observed previously, a comparison is made between the gamma contrast response functions obtained using the non-invasive MEG method in human, fMRI BOLD response measured in the macaque and invasive measures of local field potential (LFP) and multi-unit activity (MUA) in the monkey (Logothetis *et al.*, 2001)[◊]. Further comparative analyses were made using equivalent data from macaque experiments with local field potential (LFP) and multi-unit activity (MUA) from surgically implanted electrodes and fMRI BOLD measures (Logothetis et al., 2001).

◊ Thanks to Prof. Nikos Logothetis, (Max-Planck Institute for Biological Cybernetics, Tuebingen, Germany) for providing his Macaque data.
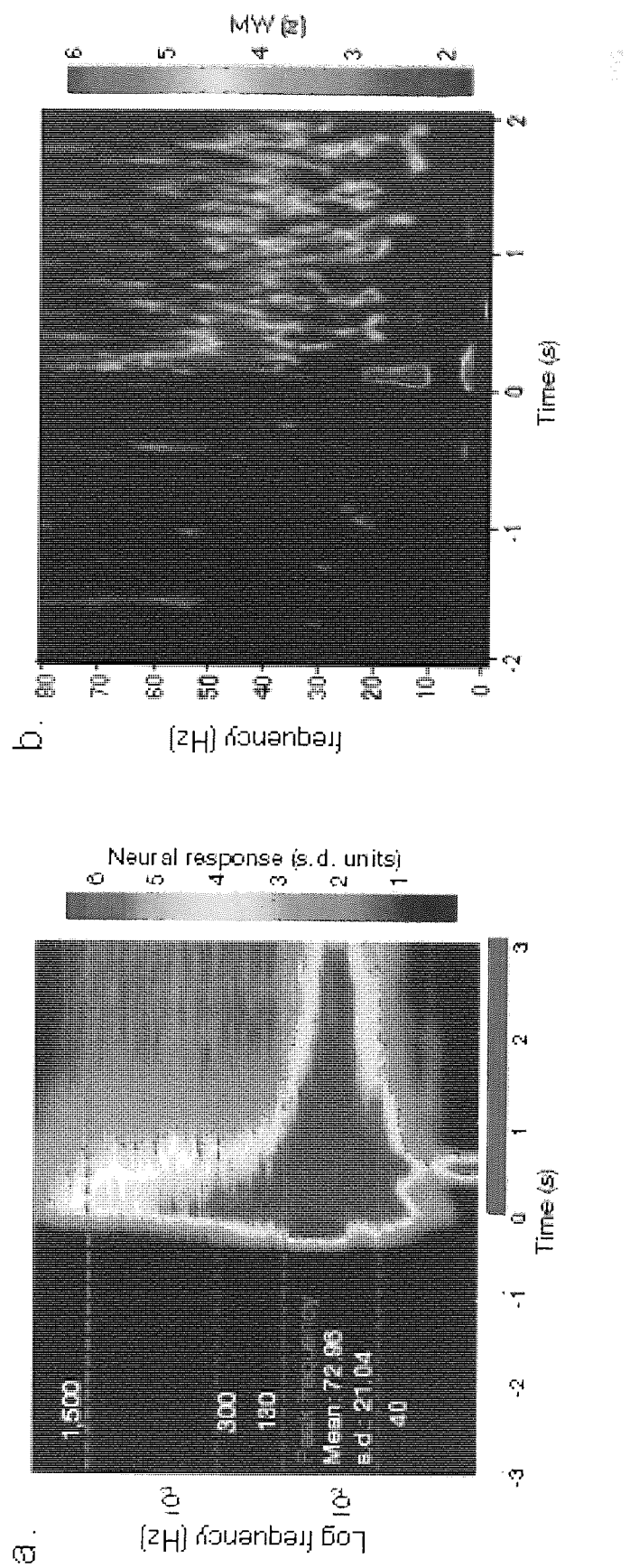
Figure 6-9. Oscillatory activity in primary visual cortex following visual stimulation.
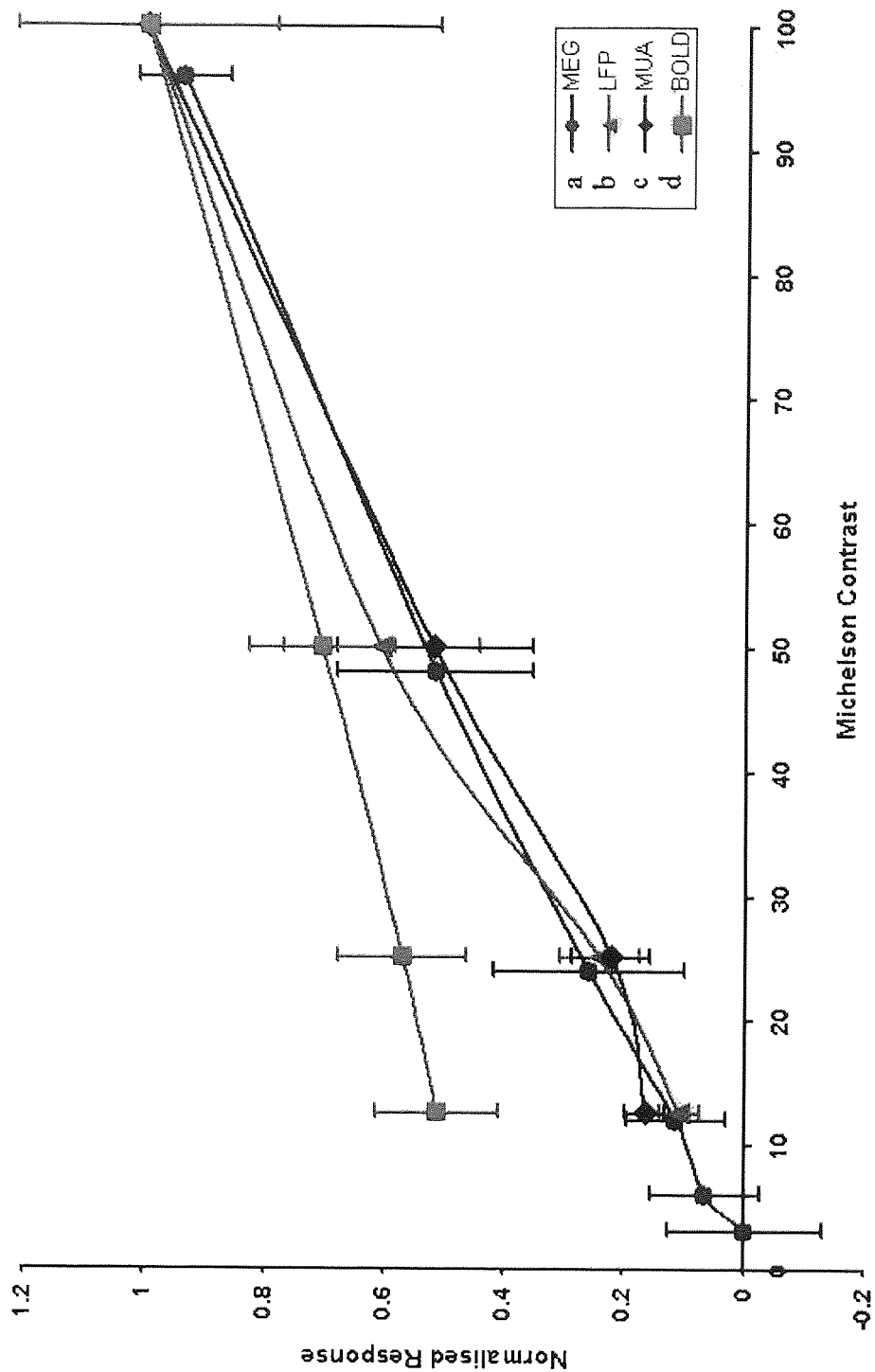
Figure 6-10. Contrast response graph. (a) MEG gamma amplitude at 6 contrast levels, normalised to maximum value (±1.96SEM), displayed alongside (b) local field potential (LFP) and (c) multi unit activity (MUA), obtained from recordings in macaque visual cortex and (d) fMRI BOLD response (1) . Thanks to Professor Nikos Logothetis for providing the macaque data.

6.5.4 Results

The MEG VE data was strongly correlated with and of strikingly similar amplitude to the LFP ($r=0.997$, $p<0.01$) and MUA ($r=0.996$, $p<0.01$) responses obtained by Logothetis *et al.* (2001) using surgically implanted electrodes in macaque visual cortex.

6.5.5 Discussion

This study presents the finding that gamma oscillatory activity recorded in primate primary visual cortex using LFP (Logothetis *et al.*, 2001) is also observed in human primary visual cortex using MEG (fig. 6-9). The contrast dependent change in the activity observed using LFP and MUA at the micron and millimetre levels respectively (Legatt *et al.*, 1980; Mitzdorf, 1987), are robustly represented in MEG activity obtained from the wider neuronal population (fig. 6-10). In concordance with other functional imaging studies (Logothetis *et al.*, 2001; Heeger *et al.*, 2000), we demonstrate that MEG can non-invasively resolve the underlying neuronal activity observed by invasive procedures with millisecond temporal resolution. These results suggest than MEG is a more accurate representation of the underlying neuronal activity than the fMRI BOLD response. Further to this we demonstrate a suitable non-invasive human equivalent of the invasive animal techniques and suggest that this method may form the basis for an integrated approach to functional neuroimaging (Hall *et al.*, 2004b; Rees *et al.*, 2000).

Chapter 7

Application of Magnetoencephalography (MEG) in Retinotopic Mapping: a pilot study.

7   Application of Magnetoencephalography (MEG) in Retinotopic Mapping

7.1   Overview

Chapter seven describes the application of the driven stimulus and 'tuned' SAM method described in chapter three in a pilot study of retinotopic mapping.

The chapter begins by introducing the principles of retinotopic mapping, commonly carried out in functional magnetic resonance imaging (fMRI). It describes some of the basic methods by which the arrangement of the visual cortex with respect to visual location are delineated. Subsequently, a pilot study is described using three participants; the rational and basis for which are explained using results from driven visual stimuli in a single quadrant. The chapter describes three further conditions in which two quadrants; followed by four quadrants were used and finally four quadrants with small patches at two eccentricities, separated by two degrees. The results demonstrate that the 'tuned' SAM method is able to distinguish discrete regions of cortical activity in response to stimulation of a small region of the visual field and that separation based upon less than three degrees is possible.

This chapter aims to show that MEG and SAM are able to perform retinotopic analysis and suggest the basis for further methodological developments of this technique.

7.2 Introduction

The human visual cortex is divided into several functional areas with distinct neural properties (Zeki and Shipp, 1988). This organisation is only loosely linked to cortical anatomy and is subject to variability between individuals (Amunts *et al.*, 2000). As discussed in chapter 1, several of these areas are retinotopically organised and therefore have receptive fields whose centres are organised to form a continuous map of the visual field on the cortical surface. This principle has become the basis for fMRI retinotopic mapping, which uses a series of specific visual stimulation parameters in order to distinguish between visual areas (Shipp *et al.*, 1995; Sereno *et al.*, 1993, 1994; Sereno, 1995, 1998; DeYoe *et al.*, 1996; Engel *et al.*, 1997; Warnking *et al.*, 2002; Slotnick, 2003; Dougherty *et al.*, 2003). This forms the basis of further investigation of the visual system whereby functional information can be anatomically defined (e.g. Tootell *et al.*, 1997, 1998a,b; Morland and Ruddock, 1997; Smith *et al.*, 1998; Martinez *et al.*, 1999; Halgren *et al.*, 1999; Singh *et al.*, 2000; Hadjikhani *et al.*, 2001; Huk *et al.*, 2002; Demoulin *et al.*, 2003). However, the lack of temporal resolution available in the fMRI technique dictates that the method is reliant upon assumptions about the relationship between the neuronal activity and the subsequently measured haemodynamic change. Attempts to map the retinotopic organisation of the visual cortex using higher temporal resolution methods, such as EEG (Gevins, 1996; Sutter, 1992; Baseler *et al.*, 1994; Slotnick *et al.*, 1999) and MEG (Aine *et al.*, 1996), have been made using dipole localisation of the evoked potential components in order to indicate individual points of activity. However, this approach is dependent upon the signal averaging of large numbers of trials for each point intended to be investigated and is more intensive than the already lengthy and involved fMRI process.

On the basis of the evoked potential work (chapter 3) and the principle that a transient evoked potential can be identified by its frequency components (3-12Hz). It was hypothesised that the driving of a stimulus at frequencies high enough to produce a steady state evoked potential (typically >10Hz) which appears as a sinusoid (Harding, 2002, personal communication); could be detected using SAM analysis tuned specifically to this frequency. This hypothesis was examined as an extension of the evoked potential paradigms described in chapter 3. The strong induced activity observed in a retinotopically concordant location was the basis for the further investigations. A series of experiments using temporally specific visual stimulation and temporally tuned synthetic aperture magnetometry (SAM) analysis was used to stimulate firstly individual hemispheres, secondly separate quadrants and finally two different eccentricities at each of four quadrants of the visual field. The results demonstrate the ability of SAM analysis to

identify activity in discrete regions of the visual cortex concordant with locus of visual field stimulation.

7.3 Methods

The initial stage of this work was the result of an addition to the visual evoked response (VER) work described in chapter 4 and further applied to the contrast gain work in chapter 5. It was demonstrated that the evoked potential can be recognised and localised based upon the spectral components that the waveform comprises (3-12Hz). From this it was hypothesised that a driven or 'steady state' evoked potential, which loses distinct morphological characteristics and becomes virtually sinusoidal, could be identified in the same way by 'tuning' the SAM frequency window to the stimulus rate$^\Diamond$. The subsequent experiments were an extension of this concept as discussed.

7.3.1 Stimuli

- Experiment one used a single quadrant (lower left) pattern onset-offset paradigm driven at 16Hz$^\Diamond$, using a sinusoidal grating of 3 cpd, subtending 4x4° of visual angle, at an eccentricity of 0.5° from both horizontal and vertical meridians The stimulus was presented for 5 cycles, with one cycle consisting of 15 seconds presentation followed by 5 seconds blank background of equal mean luminance to the stimulus.

- Experiment two used the same grating stimulus as experiment 1. However, one cycle comprised lower left quadrant presentation for 15 seconds followed by the 5 second blank period and then lower right presentation for 15 seconds.

- Experiment three was a direct extension of this with the stimuli presented in all four quadrants rather than 2.

- Experiment four used quadra-circular stimuli with concentrically arranged square wave check pattern of 100% Michelson Contrast. These were displayed at two different eccentricities in each of the four quadrants: the inner quadra-circle was 0.75 degrees from the central fixation point, 1 degree in width, with a spatial frequency of 0.5 cpd; the outer quadra-circle was displayed at 3 degrees from the central fixation point, 2 degrees in width, with a spatial frequency of 1 cpd. Each of these stimuli were displayed in sequence for 15 seconds each, interspersed by a 5 second blank period of equal mean luminance to the stimulus. A total of 5 complete cycles were shown.

$\Diamond$ The reader is referred to chapter 3 for details of the driven stimulus method.

7.3.2   Analysis

In all conditions SAM analysis was performed using a spectral window of 14-18Hz in order to identify only activity occurring in the driven frequency band. This was done by selecting one second windows (n=25) from both the blank and driven conditions at each of the eight locations.

7.4   Results

7.4.1   Experiment 1 (Single Quadrant Stimulation)
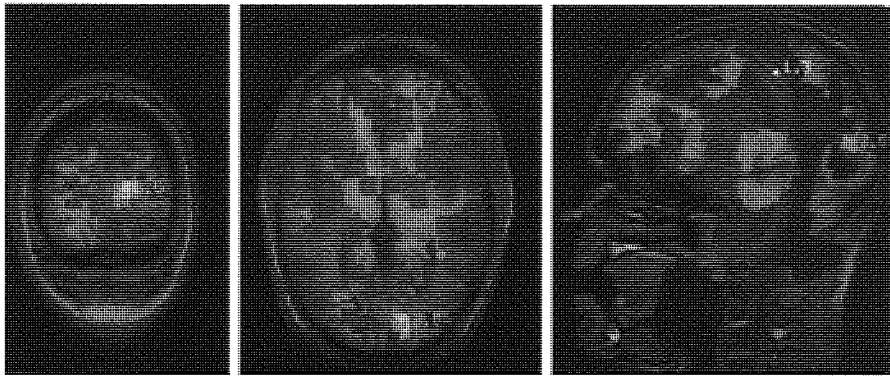
Figure 7-1. SAM localisation (single quadrant). SAM localisation of lower left quadrant visual stimulation in subject 1; demonstrating 14-18Hz synchronisation in the upper right bank of the calcarine sulcus (green dot) (t=3.5).

The stimulation of the lower left quadrant induced strong (t=3.5) activity in the upper right bank of the calcarine sulcus (fig. 7-1).

7.4.2 Experiment 2 (Dual Quadrant Stimulation)
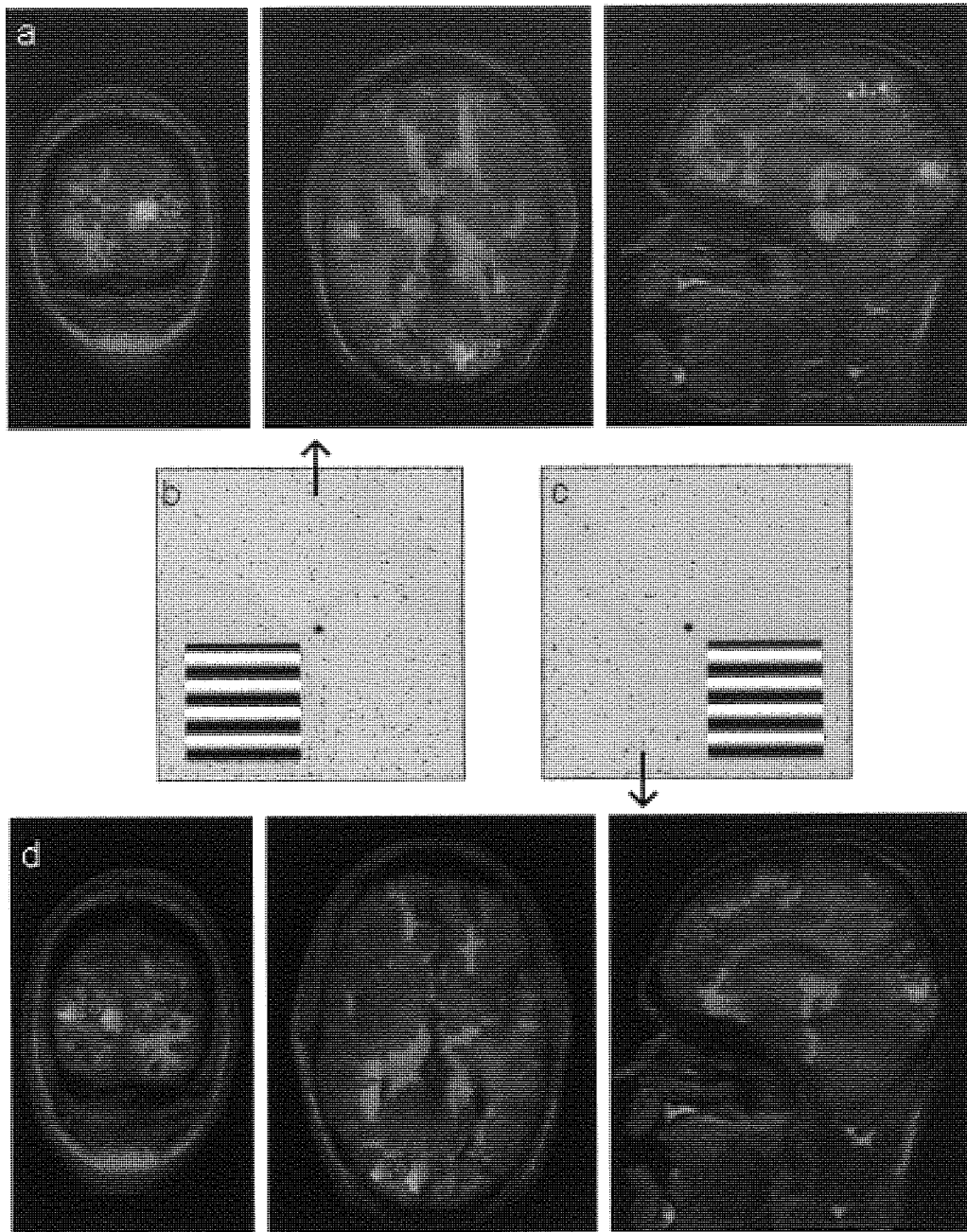
Figure 7-2. SAM localisation (two quadrant stimulation). Showing strong peaks (green dots)of activation in: (a) upper right visual cortex and (b) upper left visual cortex; following lower left and lower right stimulation respectively.

The stimulation of the lower left and upper right induced strong (t=4.2 (R) and t=6.0 (L)) activity in the upper right and left banks of the calcarine sulcus, respectively (fig. 7-2).

7.4.3　Experiment 3 (Four Quadrant Stimulation)
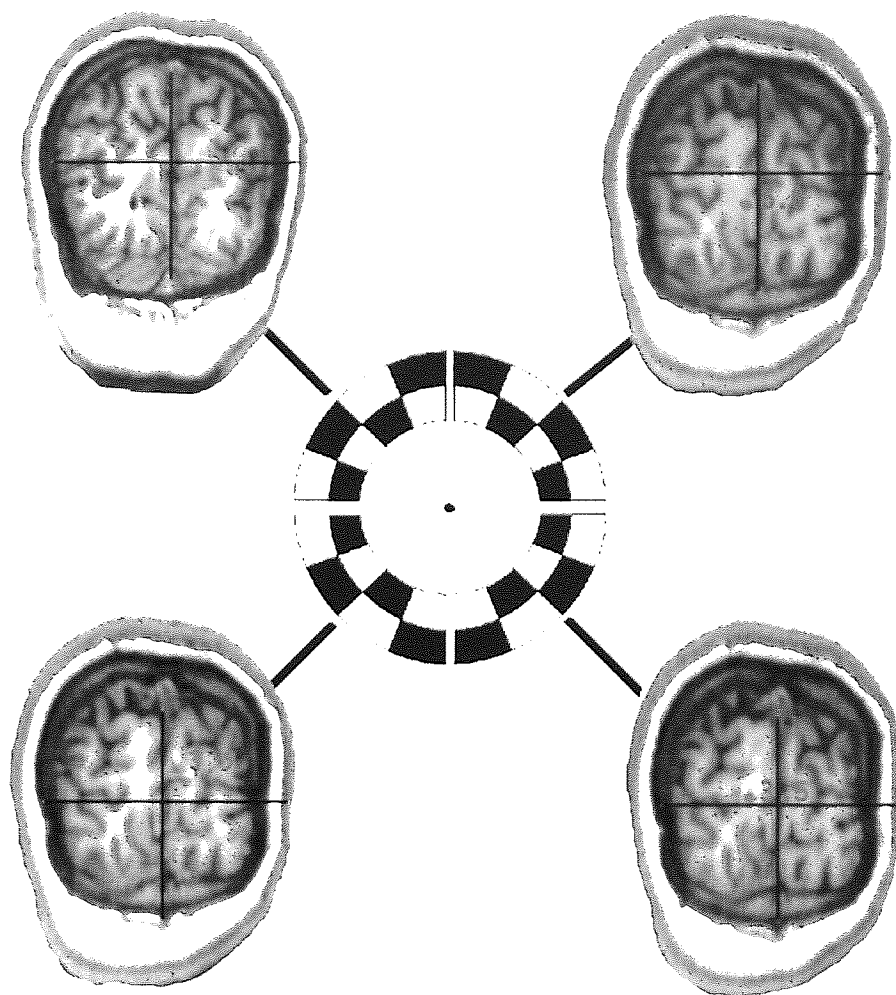
Figure 7-3. SAM Localisation (four quadrant stimulation). SAM analysis (subject FM) reveals peaks (green dots) of activity in retinotopically concordant regions of visual field.

Stimulation of the four quadrants of the visual field induced activity (t=5.0 (UR); 7.4 (UL); 3.5 (LR) and 3.9 (LL)), which could be determined in the four respective locations of the visual cortex (fig. 7-3).

7.4.4 Experiment 4 (two Eccentricity Stimulation)
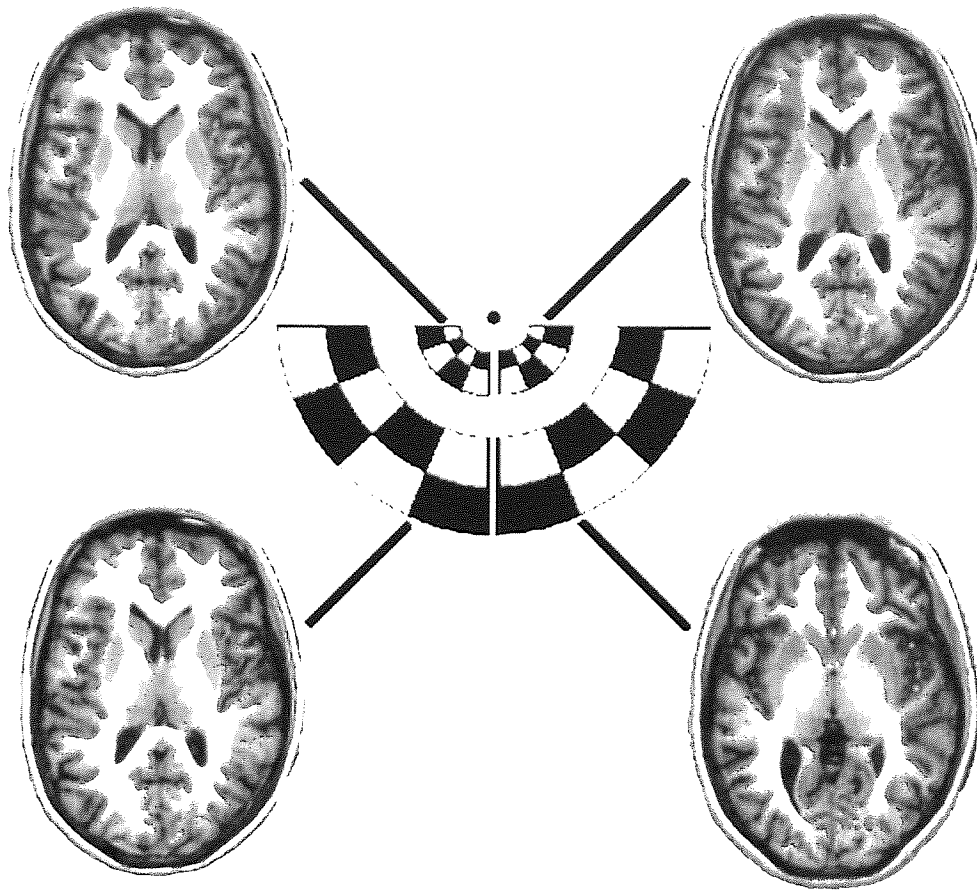
Figure 7-4. SAM localisation (two eccentricity stimulation). SAM image reveals peaks of activation (green dots) that vary in anterior-posterior location according to the eccentricity of the stimulus. Central presentation locates to posterior V1, whilst greater eccentricity locates to more anterior loci.

Presentation of the quadrants at the two eccentricities could be observed in distinct locations of the visual cortex. The central locations could be observed at more lateral locations than their peripheral counterparts and in the majority of cases the hemispheric distinction (fig. 7-4) was quite clear as was the quadrant localisation (not shown).

7.5 Discussion

The results shown provide evidence that the beamforming approach to MEG signal analysis provides a clear method for the delineation of the visual cortical areas using MEG. It clearly shows that a non time locked, averaging approach is able to discern discrete cortical activity on the bases of significantly fewer trials (5) than is required for a clear averaged signal (25-50).

7.6   Conclusions

The methods described here are modelled using the dipole model as a basis for its source reconstruction. Due to the nature of the activity which occurs in the cortex in terms of the cortical extent observed in the fMRI experiments, it is clear that this method could be expanded to encompass a specific cortical patch model, which in turn would enable MEG to better reconstruct not only the neuronal activities, but a degree of structural retinotopy which is of greater specificity to the MEG system than the fMRI retinotopic analysis. Additionally it would have the ability to assist in such things as specific cortical models for coregistration of the MEG with the MRI volume scan.

The current methodology is restricted by the basis of the SAM methodology being that of the dipolar solution. That is to say that SAM aims to solve the localisation as a maximal point source rather than an extended cortical surface patch. Under these circumstances the extent of retinotopic activation is not determinable and thus the further investigation and delineation of cortical areas based upon polar angle is not possible. Further developments, currently underway aim to solve the localisation based upon optimal patch extent and may therefore facilitate retinotopic mapping using MEG.

Chapter 8

Magnetoencephalographic Investigation of Migraine Visual Aura: a case study.

8 Magnetoencephalographic Investigation of Migraine Visual Aura: a case study

8.1 Overview

Chapter eight describes the investigation of a patient experiencing an episode of migraine visual aura.

The chapter begins by introducing the subject of migraine visual aura and 'scintallatory scotoma' and explains the physiological significance of these phenomena as they relate to cortical spreading depression (CSD). Furthermore, a series of multimodal investigations of this feature are described, detailing some of the significant electrical and cerebro-vascular changes.

The chapter then continues to describe a serendipitous case study in which a patient was recorded in the MEG system whilst experiencing a scintillating scotoma over a period of several minutes.

A novel implementation of the SAM beamforming method described in chapter three was employed to visualise the spectral changes across the cortex over time. This method reveals strong desynchronisation at occipital and temporal regions at the contralateral side to the observed abnormality. The chapter continues to discuss the results in the context of previous findings and the phenomenon of cortical spreading depression.

The aim of this chapter is to introduce the reader to the hyper excitatory disorder 'migraine visual aura' and describe the use of the novel analytical method in its investigation.

8.2   Introduction

Scintillating scotoma, a visual disturbance first described by Hubert Airy in 1854, is the best defined of the visual auras associated with migraine. Whilst many variations occur, the most common consists of a bright zigzag pattern slowly spreading and growing as it moves from central to peripheral vision, typically occurring in a single hemifield. This particular aura, also known as "fortification spectra" because of its apparent likeness to maps of fortified towns (Airy, 1870) has long been associated with the phenomenon of cortical spreading depression (CSD)[*] (Leao, 1944) and has been extensively investigated in terms of its retino-cortical magnification (Grusser, 1995). Previous MEG studies that investigated animal (Bowyer et al., 1999a,b) and human (Bowyer et al., 2001; Gutschalk et al., 2002; Welch et al., 1993; Barkley et al., 1990) subjects identified high amplitude activity, DC shifts and regional slowing of the magnetoencephalogram. Transcranial magnetic simulation (tMS) studies provide support for cortical hyperexcitability (Aurora et al., 1998a,b, 1999, 2003) and reduced inhibition (Hallett, 2000; Battelli et al., 2002) hypotheses. Haemodynamic correlates of migraine aura studied with functional magnetic resonance imaging (fMRI) (Mulleners et al., 2001; Hadjikhani et al., 2001) and single photon emission computed tomography (SPECT) (Andersen et al., 1988; Lauritzen, 1987) offer support to the cortical spreading depression hypothesis (Lauritzen, 1994; Gorji, 2001). Here we have used synthetic aperture magnetometry (SAM) and spatially selective spectral measures to directly image the cortical electrical activity associated with migraine visual aura, demonstrating the time course of the frequency specific cortical activity within the occipital and temporal regions implicated in visual aura.

---

[*]   Cortical spreading depression (CSD) is a phenomenon that has been discussed as a possible underlying mechanism in various hyperexcitability disorders, since it was conceived as a hypothesis by Leao in 1944. The term is used to describe the depression of neuronal and thus cortical activity following a wave of hyperexcitement across the cortex. In terms of scintillating scotoma it has been demonstrated that the reduction in cortical activity corresponds retinotopically to the visual field location of visual abnormality.

8.3 Methods

8.3.1 Subject

Our subject (IEH) experiences classical scintillating scotoma without subsequent migraine headache approximately twice per year. The research reported below was conducted under the approval of the Aston University Human Sciences Ethical Committee and written informed consent was obtained from the patient prior to commencement of the study. On this occasion we recorded an episode of scintillating scotoma (which typically last for approximately 20 minutes), using a 151 channel whole head magnetometer system (CTF Systems Inc.). The patient experienced a classical arc of scintillations moving from central to peripheral visual field in the upper right quadrant. Typically a transient scotoma occurs in the region trailing the scintillations (Grusser, 1995), but provision was not included for its observation on this occasion.

8.3.2 Recording

The recording was taken continuously over a 20 minute period, at the beginning of which the scintillations had made a significant progression toward the periphery. The visual disturbance persisted for the first 5 minutes 22 seconds and was followed by disappearance of the scintillation with remaining temporary loss of local vision which slowly returned over the following 5 minutes. There was therefore a 10 minute period of recording in which there were no visual abnormalities reported. Throughout the recording the participant fixated on a central point and made brief verbal reports of the visual disturbance location in the visual field over time.

- Recording and coregistration were performed using the standard protocol*.

8.3.3 Analysis Methods

The MEG data were analysed using Synthetic Aperture Magnetometry (SAM) (Vrba and Robinson, 2001a,b; Barnes *et al.*, 2001; Singh *et al.*, 2002, 2003) to elucidate

power changes in cortical oscillations within specific frequency bands, termed here Event Related synchronisation/Desynchronisation (ERS/ERD) (see chapter 4 for details).

Additionally, virtual electrodes (VEs) were used to analyse activity over 20 minute duration at two cortical regions of interest determined as the points of maximum ERD in the global SAM activation images, one in the left extra-striate cortex and one in the left inferior temporal lobe. The VE data was filtered to frequency bands of interest. The VE method also provides a basis for the computation of time-frequency spectrograms (fig. 8-3). SAM and spectrogram images were produced using successive 2 minute data segments partitioned into 2 second segments; each segment was contrasted with the 2 minute segment at the end of the recording period as a baseline. The segments were then assembled as a montage (Fig. 8-3). The z-score for each time-frequency spectrogram element was computed with a Mann-Whitney test between the baseline and test segments, and is represented by the colour bar in figure 8-3.

---

*   The reader is referred to section 3.5 for details of analysis method protocols.

8.4   Results

SAM revealed strong focal ERD, most notably in the alpha band (7-13Hz) in the lower left extra-striate and temporal areas and also in the gamma band (30-80Hz) in the left inferior temporal lobe. The extra-striate alpha source remained strongly desynchronised (30.4%, p<0.01) with respect to baseline for approximately 5 minutes 30 seconds, corresponding to the period during which scintillations were reported by the patient. Following this period there was a short episode of ERS with activity returning to baseline levels over the following 10 minutes (Fig. 8-1).

The temporal lobe exhibited the same pattern of alpha ERD as the extra-striate cortex (Fig. 8-1a) however it was weaker (19.4%, p<0.01) and more diffuse. In the left inferior temporal lobe strong focal desynchronisation (49.7%, p<0.01) was observed (Fig. 8-2a) in the gamma frequency region, which was not observed in extra-striate visual areas. Temporal lobe gamma ERD was strongest in the first recorded minute and showed gradual reduction in the level of desynchronisation to levels not significantly different

175

from baseline after approximately 16 minutes (figs. 8-2b & 8-3). None of the phenomena reported above were observed in a control recording conducted with the same subject some weeks after the reported visual aura had been experienced.
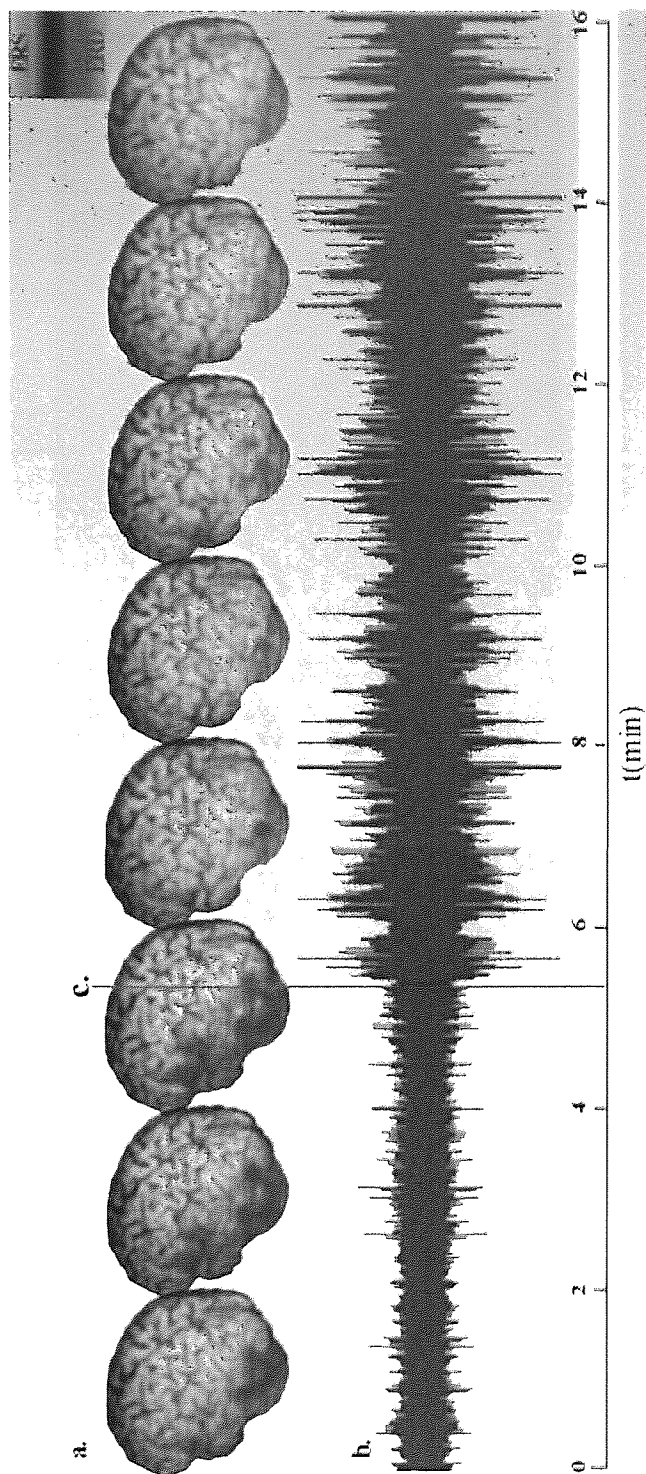
Figure 8-1. Alpha band desynchronisation. (a) SAM activation rendered on the subject's MRI, (b) Time course of alpha band activity within maximally active extra-striate cortex. (c) Reported end of scintillation observation (5 min 22 sec).
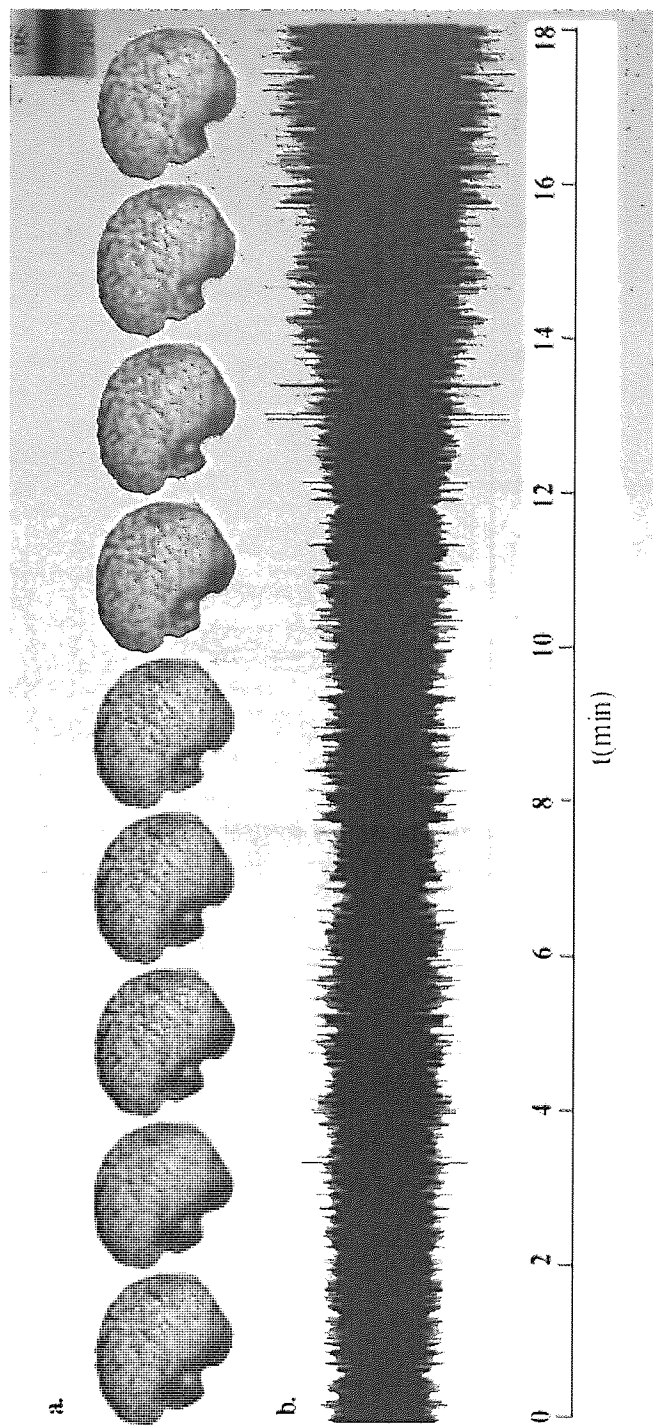
Figure 8-2. Gamma band desynchronisation. (a) SAM activation rendered on the subject's MRI, (b) Time course of gamma band activity within maximally active cortex in the temporal lobe.
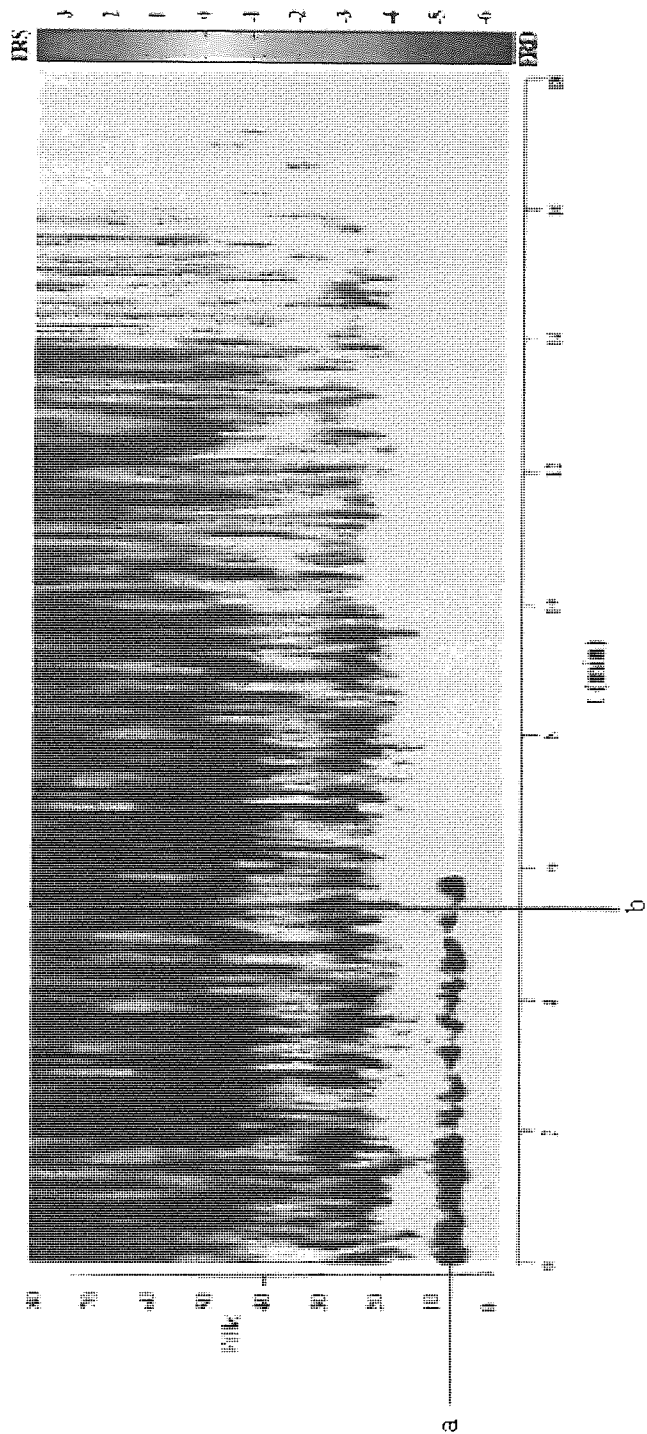
Figure 8-3. Time-Frequency Morlet spectrogram montage for an inferior temporal lobe virtual electrode (Fig. 8-2), showing (a) alpha ERD coincident with scintillation period (b) and gamma ERD recovering over ~16 minutes. Scale: z-score.

8.5   Discussion

The results shown here are spatially consistent with previous reports of extra-striate visual involvement in migraine visual aura (Hadjikhani *et al.*, 2001) and the observation of visual anomaly in the presence of extra-striate ERD supports the hypothesis that this area is involved in the generation of phosphenes (Grusser, 1995; Bowyer *et al.*, 2001; Battelli *et al.*, 2002). Here we make novel observations concerning the changes in oscillatory activity which accompany migraine visual aura. The extra-striate and inferior temporal cortices exhibit identical alpha desynchronisation commensurate with the reported visual disturbance (figs. 8-1 & 8-3) suggesting that alpha ERD is linked to the observed visual abnormalities.

Gamma desynchronisation is restricted to the temporal region and displays gradual recovery over a 16 minute period (Figs. 2 & 3), a time scale consistent with those reported in previous migraine studies (Hadjikhani *et al.*, 2001), suggesting a connection with the scotoma following scintillations.

This study also demonstrates the ability of SAM to determine spontaneous changes in cortical synchrony without the need for driving stimuli and refutes suggestions of poor spatial resolution in migraine imaging using MEG (James *et al.*, 2001). Evidence from previous functional imaging studies (Gutschalk *et al.*, 2002; Welch *et al.*, 1993; Barkley *et al.*, 1990; Aurora *et al.*, 1998a,b, 1999, 2003; Hallett, 2000; Battelli *et al.*, 2002; Mulleners *et al.*, 2001; Hadjikhani *et al.*, 2001; Andersen *et al.*, 1988; Lauritzen, 1987,1994; Gorji, 2001; Huang *et al.*, 2003) would suggest that the ERD seen here is the result of underlying cortical hyperexcitability and subsequent asynchrony affecting prominent cortical rhythms of the visual system, results which are consistent with the theory of cortical spreading depression (Leao, 1944).

Chapter 9

Conclusions and Further Research

9 Conclusions and Further Research

9.1 Conclusions

This work adopted and developed recent MEG analysis tools for the purpose of investigating the human visual system.

Investigation of the effect of SAM smoothness values on the outcome of group imaging results (chapter 3) reveal that the spatial extent of SAM analysis is spatially too refined to for use in group imaging; suggesting that the MEG smoothness values be increased for group imaging (Hall *et al.*, 2004d). These results further suggest that more in depth investigation at the individual level may prove more informative about cortical function than the current group imaging methods.

Synthetic aperture magnetometry (SAM) was found to be a comparative method for the investigation of evoked activity and under some circumstances a more reliable method of elucidating cortical activity than dipole analysis, with further benefit of removing user bias (chapters 4 and 5).

The MEG equivalent of the EEG response to several clinical visual stimuli were established as having comparative latency (chapter 4).

A profile of visual cortical function in terms of both evoked and induced activity was generated (chapter 4), in which alpha beta and gamma were classified. This could provide the basis for normative comparison. However, with the clear exception of gamma oscillatory activity (chapters 4 and 6) it is clear that individual subject variability reduces the diagnostic value of this approach. These results further highlight the inhomogeneity across participant groups, where identical stimuli produce different changes in cortical synchrony.

Investigation of cortical contrast gain reveals that the saturating contrast response function obtained using scalp electrode recording methods is likely a composite of striate and extra-striate activity (chapter 2) (Hall *et al.*, 2004c). Furthermore, it is possible that the apparent lack of cortical contrast gain control in human photosensitive epilepsy (Porciatti *et al.*, 2000) may result from an absent or deficient extra-striate cortical processing of contrast.

The use of SAM analysis of visual gamma oscillations (chapter 6) reveals that it is possible to record gamma oscillatory activity using MEG. This stands in contradiction to previous reports (tallon-Baudry, 1997, 1999). Furthermore the results reveal that gamma oscillations occur in response to patterned stimuli and are dependent upon stimulus contrast (Hall *et al.*, 2004e), showing a linear increase in amplitude as a function of Michelson Contrast. A comparison of these results with invasive animal studies (Logothetis *et al.*, 2001) reveals strong correlation with results from local field potentials at the millimetre spatial scale (Hall *et al.*, 2004b). The implications of such findings are that the current investigation using invasive animal studies may be replicated or replaced using human volunteers, with further possibility of extending this analysis to other sensory modalities or indeed the investigation of pharmacological interactions.

The use of driven visual stimuli with 'tuned' SAM analysis (chapter 3) proved to be an effective basis for retinotopic analysis of the visual system (chapter 7). Furthermore, the ability of MEG to resolve cortical activity in response to visual stimuli separated by only 2 degrees of visual angle was established. Additionally, the response demonstrated that retinotopic mapping using MEG is a viable approach and given certain methodological developments has the possibility to become as practical as fMRI.

SAM analysis was successfully implemented in the investigation of migraine visual aura (chapter 8), revealing alpha (7-14Hz) desynchronisation in occipital and temporal regions commensurate with the period of visual abnormality and gamma (30-80Hz) desynchronisation in temporal cortex (Hall *et al.*, 2004a; Brookes *et al.*, 2004a) consistent with reported scotoma duration (Hadjikhani *et al.*, 2001).

9.2   Further Work

The results obtained in this thesis generate further questions and bases for further work:

The smoothness values investigated in chapter 3 are based upon measurements from the visual cortex; optimal smoothing in other areas could apply.

The spectrographic movie provides a sound basis for investigation of cortical activity; further development of this application could form the basis for an accessible initial analysis and clinical tool of cortical activity. This has the potential to form the interface for a clinical tool.

The investigation of a larger cohort of subjects could provide the basis for clinical applications of the contrast gain data. In addition to this the repeated investigation of individuals to better characterise the stability of cortical stated would generate a useful metric.

Visual cortical gamma is a phenomenon which can be characterised using MEG; providing the basis for comparison with invasive studies. Further investigation using stimuli to probe mechanisms established at the cellular level might prove informative.

Finally; the method employed in the investigation of migraine visual aura provides the basis for investigation of neuronal substrate interaction to provide pharmacological models.

References

10   References

Aine, CJ., Supek, S., George, JS., Ranken, D., Lewine, J., Sanders, J., Best, E., Tiee, W., Flynn, ER. and Wood, CC. Retinotopic organization of human visual cortex: departures from the classical model. *Cereb Cortex,* **6**, 354-361 (1996).

Airy, H. On a distinct form of transient hemiopsia. *Proc R Soc Lond.,* **160**, 247-270 (1870).

Albrecht ,DG. and Hamilton, DB. Striate cortex of monkey and cat: contrast response function. *J Neurophysiol.,* **48**, 217–237 (1982).

American Encephalographic Society. Guideline thirteen: Guidelines for standard electrode position nomenclature. *J Clin Neurophysiol.,* **11**, 111–113 (1994).

Andersen, AR., Friberg, L., Olsen, TS. and Olesen, J. Delayed hyperemia following hypoperfusion in classic migraine: Single photon emission computed tomographic demonstration. *Arch Neurol.,* **45**, 154–159 (1988).

Anderson, SJ., Holliday, IE., Singh, KD. & Harding, GFJ. Localisation and functional analysis of human cortical area V5 using magneto-encephalography. *Proc. R. Soc. Lond.,* **263**, 423-431 (1996).

Aurora, SK. and Welch, KMA. Brain excitability in migraine: evidence from transcranial magnetic stimulation studies. *Curr Opin Neurol.,* **11**, 205–209 (1998a).

Aurora, SK., Ahmad, BK, Welch, KM., Bhardhwaj, P. and Ramadan, NM. Transcranial magnetic stimulation confirms hyperexcitability of occipital migraine. *Neurology,* **50**, 1111-1114 (1998b).

Aurora, SK., Cao, Y., Bowyer, SM. and Welch KM. The occipital cortex is hyperexcitable in migraine: experimental evidence. *Headache,* **39**, 469-76 (1999).

Aurora, SK., Welch, KM. and Al-Sayed, F. The threshold for phosphenes is lower in migraine. *Cephalalgia,* **23**, 258-63 (2003).

Bach, M. and Ullrich, D. Contrast dependency of motion-onset and pattern-reversal VEPs: Interaction of stimulus type, recording site and response component. *Vision Res.,* **37**, 1845-1849 (1997).

Baizer, JS., Ungerleider, LG. and Desimone, R. Organisation of the visual inputs to the inferior temporal and posterior parietal corex in macaques. *J Neurosci.,* **11**, 168-190 (1990).

Bajalan, AA., Wright, CE. and van der Vliet, VJ. Changes in the human visual evoked potential caused by the anticholinergic agent hyoscine hydrobromide: comparison with results in Alzheimer's disease. *J Neurol Neurosurg Psychiatry*, **49**, 175-82 (1986).

Bak, M., Girven, JP., Hambrecht, FT., Kufta, CV., Loeb, GE. and Schmidt, EM. Visual sensations produced by intracortical microstimulation of the human occipital cortex. *Med Biol Eng Comp.,* **28**, 257-259 (1990).

Barkley, GL., Tepley, N., Nagel-Leiby, S., Moran, JE., Simkins, RT. and Welch, KM. Magneto-encephalographic studies of migraine. *Headache*, **30**, 428-34 (1990).

Barnes, GR. and Hillebrand, A. Statistical flattening of beamformer images. *Hum Brain Mapp.,* **18**, 1-12 (2003).

Barnes, GR., Francis, S., Hillebrand, A., He, J., Furlong, PL., Bowtell, RW., Singh, KD., Holliday, IE. And Morris, PG. The spatial relationship between event-related changes in cortical synchrony and haemodynamic response. *Neuroimage*, 13, S71 (2001).

Barnes, GR., Hillebrand, A., Fawcett, IP. and Singh, KD. Realistic spatial sampling for MEG beamformer images. *Hum Brain Mapp.,* In Press *(2004).*

Baseler, HA. and Sutter, EE. M and P components of the VEP and their visual field disctibution. *Vision Res.,* **37**, 675-690 (1997).

Battelli, L., Black, KR. and Wray, SH. Transcranial magnetic stimulation of visual area V5 in migraine. *Neurology,* **58**, 1066–1069 (2002).

Baule, G. and McFee, R. Theory of magnetic detection of the heart's electrical activity. *J. Appl Phys.*, **36**, 2066-2073 (1965).

Bekisz, M. and Wróbel, A. 20 Hz rhythm of activity in visual system of perceiving cat. *Acta Neurobiol Exp.*, **53**, 175-182 (1993).

Bekisz, M. and Wróbel, A. Coupling of beta and gamma activity in corticothalamic system of cats attending to visual stimuli. *NeuroReport*, **10**, 3589-3594 (1999).

Biersdorf, WR. Cortical evoked responses from stimulation of various regions of the visual field. *Doc Opthalmol proc.*, **3**, 247-259 (1974).

Bishop, PO. Processing of visual information within the retinostriate system. In Darien-Smith. *Handbook of physiology: The nervous system*, **3**, 257-316 (1984).

Blasdel, GG. Differential imaging of ocular dominance on orientation selectivity in monkey striate cortex. *J. Neurosci.*, **12**, 3115-3138 (1992).

Bobak, P. The visual evoked potential contrast response function in recovering optic neuritis. *Curr Eye Res.*, **6**, 981-991 (1987).

Botvinick, MM., Braver, TS., Barch, DM., Carter, CS. and Cohen, JD. Conflict monitoring and cognitive control. *Psychol Rev.*, **108**, 624–652 (2001).

Bowyer, SM., Aurora, KS., Moran, JE., Tepley, N. and Welch, KM. Magnetoencephalographic fields from patients with spontaneous and induced migraine aura. *Ann Neurol.*, **50**, 582-7 (2001).

Bowyer, SM., Okada, YC., Papuashvili, N., Moran, JE., Barkley, GL., Welch, KM. and Tepley, N. Analysis of MEG signals of spreading cortical depression with propagation constrained to a rectangular cortical strip. 1. Lissencephalic rabbit model. *Brain Res.*, **843**, 71-8 (1998).

Bowyer, SM., Tepley, N., Papuashvili, N., Kato, S., Barkley, GL., Welch, KM. and Okada YC. Analysis of MEG signals of spreading cortical depression with propagation constrained to a rectangular cortical strip. II. Gyrencephalic swine model. *Brain Res.*, **843**, 1-2 (1999).

Boynton, GM., Demb, JB., Glover, GH. And Heeger, DJ. Neuronal basis of contrast discrimination. *Vision Res.*, **39**, 257-269 (1999).

Boynton, GM., Engel, SM., Glover, GH. and Heeger, DJ. Neuronal correlates of contrast discrimination. *J Neurosci.*, **16**, 4207–4221 (1996).

Brindley, GS. and Lewin, WS. The sensations produced by electrical stimulation of the visual cortex. *J Physiol.*, **196**, 479-493 (1968).

Brookes, M., Gibson, A., Hall, SD,. Furlong, PL., Barnes, GR., Hillebrand, A., Francis, S. and Morris, P. Combination of synthetic aperture magnetometry and the general linear model allows accurate localisation of temporally characteristic activity. *Unpublished.*

Brookes, M., Gibson, A., Hall, SD., Furlong, PL., Barnes, GR., Hillebrand, A., Francis, S. and Morris, P. The BOLD response co-varies temporally and spatially with electrical oscillatory change and with sustained cortical current flow. *NeuroImage, In Press (2004).*

Buchel, C. and Friston, KJ. Modulation of connectivity in visual pathways by attention: cortical interactions evaluated with structural equation modelling and fMRI. *Cereb Cortex,* **7**, 768-778 (1997).

Burgess, AP. and Ali, L. Functional connectivity of gamma EEG activity is modulated at low frequency during conscious recollection. *Int J Psychophysiol.*, **46**, 91–100 (2002).

Carandini, M., Heeger, DJ. and Movshon, AJ. Linearity and Normalization in Simple Cells of the Macaque Primary Visual Cortex. *J Neurosci.*, **17**, 8621–8644 (1997).

Carter, CS., Braver, TS., Barch, DM., Botvinick, MM., Noll, D. and Cohen, JD. Anterior cingulate cortex, error detection, and the online monitoring of performance. *Science*, **280**, 747–749 (1998).

Castelo-Branco, M., Neuenschwander, S., and Singer, W. Synchronization of visual responses between the cortex, lateral ge-niculate nucleus, and retina in the anesthetized cat. *J Neurosci.*, **18**, 6395–6410 (1998).

Chapman, RM., Ilmoniemi, RJ., Barbanera, S., and Romani, GL. Selective localization of alpha brain activity with neuromagnetic measurements. *Electroenceph Clin Neurophysiol.*, **58**, 569–572 (1984).

Chiappa, KH. Evoked Potentials in Clinical Medicine: 2nd Ed. *Electroenceph Clin Neurophysiol.*, **77**, 402 (1990).

Cohen, D. and Cuffin, BN. Demonstration of useful differences between MEG and EEG. *Electroenceph Clin Neurophysiol.*, **56**, 38-51 (1983).

Cohen, D. Magnetoencephalography: Evidence of magnetic fields produced by alpha rhythm currents. *Science,* **161**, 784-786 (1968).

Coles, MGH., Scheffers, MK. and Holroyd, CB. Why is there an ERN/Ne on correct trials? Response representations, stimulus-related components, and the theory of error processing. *Biol Psychol.*, **56**, 173–189 (2001).

Crognale, MA. Development, maturation and aging of chromatic visual pathways: VEP results. J Vis., 2, 438-450 (2002).

Crognale, MA., Switkes, E. and Adams, AJ. Temporal response characteristicsof the spatiochromatic visual evoked potential: nonlinearities and departures from psychophysics. *J Opt Soc Am.*, **10**, 2595-2613 (1997).

Croner, LJ. and Kaplan, E. Receptive fields of P and M ganglion cells across the primate retina. *Vision Res.,* **35**, 7-24 (1995).

Cuffin, BN. And Cohen, D. Magnetic Fields of a dipole in special volume conductor shapes. *IEEE T Biomed Eng.*, **24**, 372-381 (1977).

Darcey, 0. and Arj, JP. Spatio-temporal visually evoked scalp potentialsin response to partial field patterned stimulation. *Electroenceph Clin Neurophysiol.*, **50**, 348-355 (1980).

Dean, AF. The relationship between response amplitude and contrast for cat striate cortical neurons. *J Physiol.,* (London), **318**, 413–427 (1981).

Desimone, R. and Schein, S. Visual properties of neurons in area V4 of the macaque: Sensitivity to stimulus form. *J Neurophysiol.*, **57**, 835-868 (1987).

DeVallios, RL., Albrecht, DG. and Thorell, LG. Spatial frequency selectivity of cells in the macaque visual cortex. *J Opt Soc Am.*, **67**, 779-784 (1982).

DeYoe, EA., Carman, GJ., Bandettini, P., Glickman, S., Wieser, J., Cox, R., Miller, D. and Neitz, J. Mapping striate and extra-striate visual areas in human cerebral cortex. *Proc. Nat Acad Sci.,* **93**, 2382-2386 (1996).

Di Russo, F., Martinaz, A., Sereno, MI., Pitzalis, S. and Hillyard, SA. Cortical sources of the early components of the visual evoked potential. *Hum Brain Mapp.*, **15**, 95-111 (2001).

Di Russo, F., Martinez A. and Hillyard SA. Source analysis of event-related cortical activity during visuo-spatial attention. *Cereb Cortex*, **13**, 486-99 (2003).

Di Russo, F., Spinelli, D. and Morrone, MC. Automatic gain control contrast mechanisms are modulated by attention in humans: evidence from visual evoked potentials. *Vision Res.*, **41**, 2435-2447 (2001).

Dobelle, WH., Turkel, J., Henderson, DC. and Evans, JR. Mapping the representation of the visual field by electrical stimulation of the human cortex. *Am J Opthalmol.*, **88**, 727-735 (1979).

Dougherty, RF., Koch, VM., Brewer, AA., Fischer, B., Modersitki, J and Wandell, BA. Visual field representations and locations off visual areas V1/2/3 in human visual cortex. *J Vis*, **3**, 586-598 (2003).

Dziewas, R., Soros, P., Ishii, R., Chau, W., Henningsen, H., Ringelstein, EB., Knecht, S. and Pantev, C. Neuroimaging evidence for cortical involvement in the preparation and in the act of swallowing. *NeuroImage, In Press (2004).*

Engel, SA., Glover, GH. and Wandell, BA. Retinotopic organisation in human visual cortex and the spatial precision of functional MRI. *Cereb Cortex,* **7**, 181-192 (1997).

Falkenstein, M., Hohnsbein, J., Hoorman, J. and Blanke, L. Effects of crossmodal divided attention on late ERP components II: error processing in choice reaction tasks. *Electroenceph Clin Neurophysiol.*, **78**, 447–455 (1991).

Fawcett, IP., Barnes, GR., Hillebrand, A. and Singh, KD. The Temporal Frequency Tuning of Human Visual Cortex Investigated Using Synthetic Aperture Magnetometry. *Neuroimage, In Press* (2004).

Fell, J., Fernandez, G., Klaver, P., Elger, CE. and Fries, P. Is synchronised neuronal gamma activity relevant for selective attention? *Brain Res Reviews*, **42**, 265-272 (2003).

Felleman, DJ. And Van Essen, DC. Distributed heirarchical processing in the primate cerebral cortex. *Cereb Cortex*, **1**, 1-47 (1991).

Fitzpatrick, D., Itoh, K. and Diamond, IT. The laminar organisation of the lateral geniculate body and the striate cortex in the squirrel monkey. *J Neurosci.*, **3**, 673-702 (1983).

Foley, JM. and Boynton, GM. A new model of human luminance pattern vision mechanisms: Analysis of the effects of pattern orientation, spatial phase, and temporal frequency. In T. A. Lawton, Computational Vision based on neurobiology. *SPIE Proceedings*, 2054 (1994).

Foley, JM. and Yang, Y. Forward pattern masking; effects of spatial frequency and contrast. *J Opt Soc Am.*, **8**, 2026–2037 (1991).

Friedman-Hill, S., Maldonado, PE. And Gray, CM. Dynamics of striate cortical activity in th alert macaque: I. incidence and stimulus-dependence of gamma band neuronal oscillations. *Cereb Cortex*, **10**, 1103-1116 (2000).

Furlong, PL., Hobson, AR., Aziz, Q., Barnes, GR., Singh, KD., Hillebrand, A., Thompson, DG. and Hamdy, S. Dissociating the spatio-temporal characteristics of cortical neuronal activity associated with human volitional swallowing in the healthy adult brain. *Submitted to NeuroImage (2003)*.

Gaetz, WC. and Cheyne, D. Localization of human somatosensory cortex using spatially filtered Magnetoencephalography. *Neurosci. Lett.*, **340**, 161-4 (2003).

Geselowitz, DB. On the magnetic field generated outside an inhomogeneous volume conductor by internal current sources. *IEEE T. Magn.*, **6**, 346-247 (1970).

Gevins, A. High resolution evoked potentials of cognition. *Brain Topogr.*, **8**, 189-199 (1996).

Ghose, GM., and Freeman, RD. Oscillatory discharge in the visual system: does it have a functional role? *J Neurophysiol.*, **68**, 1558–1574 (1992).

Gorji, A. Spreading depression: a review of the clinical relevance. *Brain Res Rev.*, **38**, 33–60 (2001).

Graham, N. and Sutter, A. Normalization: contrast-gain control in simple (Fourier) and complex (non-Fourier) pathways of pattern vision. *Vision Res.,* **40**, 2737-2761 (2000).

Graham, N. Visual Pattern Analyzers (New York: Oxford University Press) (1989).

Gray C.M., König, P., Engel, A.K., and Singer, W. Oscillatory responses in cat visual cortex exhibit intercolumnar synchronization which reflects global stimulus properties. *Nature* 338, 334-337 (1989).

Gray, CM. and McCormick, DA. Chattering Cells: Superficial Pyramidal Neurons Contributing to the Generation of Synchronous Oscillations in the Visual Cortex. *Science*, **274**, 109-113 (1996).

Grusser, OJ. Migraine phosphenes and the retino-cortical magnification factor. *Vision Res.*, **35**, 1125-1134 (1995).

Gutschalk, A., Kollmar, R., Mohr, A., Henze, M., Ille, N., Schwaninger, M., Hartmann, M., Hahnel, S., Haberkorn, U., Rupp, A. and Meyding-Lamade, U. Multimodal functional imaging of prolonged neurological deficits in a patient suffering from familial hemiplegic migraine. *Neurosci Lett.,* **332**, 2 (2002).

Hadjikhani, N., del Rio, MS., Wu, O., Schwartz, D., Bakker, D., Fischl, B., Kwong, KK., Cutrer, FM., Rosen, BR., Tootell, RBH., Sorensen, AG. and Moskowitz, MA. Mechanisms of migraine aura revealed by functional MRI in human visual cortex. *Proc Nat Acad Sc USA*, **98**, 4687-4692 (2001).

Hadjikhani, N., Liu, AK., Dale, AM., Cavanagh, P. and Tootell, RBH. Retinotopy and colour sensitivity in human visual cortex area v8. *Nature Neurosci*, **1**, 235-241 (1998).

Hall, SD., Barnes, GR., Hillebrand, A., Furlong, PL., Singh, KD. and Holliday, IE. Spatio-temporal imaging of cortical oscillatory desynchronisation in migraine visual aura: an MEG case study. *Headache*, **44**, 204-208 (2004a).

Hall, SD., Holliday, IE., Hillebrand, A., Singh, KD., Furlong, PL., Hadjipapas, A. and Barnes, GR. The Missing Link: concurrent human and primate cortical gamma oscillations. *Submitted* (2004b).

Hall, SD., Holliday, IE., Barnes, GR., Singh, KD., Furlong, PL. and Hillebrand, A. Distinct contrast response functions in striate and extra-striate regions of visual cortex revealed with Magnetoencephalography (MEG). *Submitted.* (2004c).

Hall, SD., Hillebrand, A., McNab, F. and Barnes, GR. Optimal beamformer resolution for MEG group imaging. *Unpublished* (2004d).

Hall, SD., Holliday, IE., Hillebrand, A., Singh, KD., Furlong, PL., Hadjipapas, A. and Barnes, GR. The dependence of visual gamma oscillations on stimulus characteristics: A MEG study. *Unpublished* (2004e).

Hallett, M. Transcranial magnetic stimulation and the human brain. *Nature*, **406**, 147–150 (2000).

Hamalainen, M. and Sarvas, J. Realistic conductivity geometry model of the human head for interpolation of neuromagnetic data. *IEEE T Biomed Eng.*, **36**, 165-171 (1989).

Hamalainen, M., Hari, R., Ilmoniemi, RJ., Knuutila, J. and Lounasmaa, OV. Magentoencephalography: Theory, Instrumentation, and Applications to Noninvasive Studies of the Working Human Brain. *Rev Mod Phys.*, **65**, 413-497 (1993).

Hamalainen, MS. And Ilmoniemi, RJ. Interpreting measured magnetic fields of the brain: estimates of current distributions. Helsinki, Helsinki University of Technology.TKK-F-A559 (1984).

Hammett, ST., Georgeson, MA., Bedingham, S. and Barbieri-Hesse, GS. Motion sharpening and contrast: Gain control precedes compressive non-linearity? *Vision Res.*, **43**, 1187–1199 (2003).

Harding, GFA., Odom, JV., Spileers, W. and Spekreijse, H. Standard for visual evoked potentials *Vision res.*, **36**, 3567–3572 (1996).

Hari, R. A neurophysiologist's view on biomagnetic source localization. In: Biomagnetic Localisation and 3D modelling (eds Nenonen, J., Rajala, H-M. and Katila, T.) Helsinki, University of Technology. TKK-F-A689. (1991).

Heeger, DJ., Huk, AC., Geisler, WS. and Albrecht, DG. Spikes versus BOLD: what does neuroimaging tell us about neuronal activity? *Nature Neurosci.*, **3**, (2000).

Heeger, DJ., Huk, AC., Geisler, WS. and Albrecht, DG. Spikes versus BOLD: what does neuroimaging tell us about neuronal activity? *Nature Neurosci.*, **3**, 631-633 (2000).

Helmholtz, HV. Ober einige Gesetze der Vertheilung elektrischer Str(5me in korperliche Leitem met Anwendung auf die tierisch-elektrischen Versuche. *Ann Phys Chem.*, **89**, 211-233, 353-377 (1853).

Helmholtz, HV. Treatise on physiological optics. 3rd ed. *Opt Soc Am.*, (1866).

Hendry, SHC. and Yoshioka, T. A neurochemically distinct third channel in the macaque dorsal-lateral geniculate nucleus. *Science*, **264**, 575-577 (1994)

Herculano-Houzel, S., Munk, MH., Neuenschwander, S. and Singer, W. Precisely synchronized oscillatory firing patterns require electroencephalographic activation. *J Neurosci.*, **19**, 3992–4010 (1999).

Herdman, AT., Wollbrink, A., Chau, W., Ishii, R., Ross, B. and Pantev, C . Determination of activation areas in the human auditory cortex by means of synthetic aperture magnetometry. *NeuroImage*, **20**, 995–1005 (2003).

Hillebrand, A. and Barnes, GR. A quantitative assessment of the sensitivity of the whole head MEG to activity in the adult human cortex. *Neuroimage,* **16**, 638-650 (2002).

Hillebrand, A., Singh, KD., Holliday, IE., Furlong, PL. and Barnes, GR. A new approach to neuroimaging with magnetoencephalography. *Submitted (2004).*

Hirata, M., Kato, A., Taniguchi, M., Ninomiya, H., Cheyne, D., Robinson, SE., Maruno, M., Kumura, E., Ishii, R., Hirabuki, N., Nakamura, H. and Yoshimine, T. Frequency-dependent spatial distribution of human somatosensory evoked neuromagnetic fields. *Neurosci Lett.,* **318**, 73-6 (2002).

Horton, JC. and Hoyt, WF. The representation of the visual field in human striate cortex: a revision of the classic Holmes map. *Arch Opthalmol.*, **109**, 816-824 (1991).

Huang J., Cooper TG., Satana B., Kaufman, DI. and Cao, Y. Visual distortion provoked by a stimulus in migraine associated with hyperneuronal activity. *Headache*, **43**, 664-671 (2003).

Huang, JC., Nicholson, C. and Okada, YC. Distortion of magnetic evoked fields and surface potentials by conductivity differences at boundaries in brain tissue. *Biophys J.*, **57**, 1155-1166 (1990).

Hubel, DH. and Livingstone, MS. Segregation of form, colour and stereopsis in primate area 18. *J Neurosci.*, **7**, 3378-3415 (1987).

Hubel, DH. and Weisel, TN. Binocular interaction in striate cortex of kittens reared with artificial squint. *J Neurophysiol.*, **26**, 1041-1059 (1965).

Hubel, DH. and Weisel, TN. Functional architecture of the Macaque visual cortex. *Proc R Soc London.,* **198**, 1-59 (1977).

Hubel, DH. and Weisel, TN. Laminar and columnar distribution of geniculo-cortical fibres in the macaque monkey. *J Comp Neurol.*, **146**, 421-450 (1972).

Hubel, DH. and Weisel, TN. Receptive fields and functional architecture of monkey striate cortex. *J Physiol.,* **195**, 215-243 (1968).

Hubel, DH. and Weisel, TN. Receptive fields of single neurons in the cat's striate cortex. *J Physiol.*, **148**, 574-591 (1959).

Hubel, DH. and Weisel, TN. Receptive fields, binocular interaction and functional architecture in the cat's visual cortex. *J Physiol.*, **160**, 106-154 (1962).

Hubel, DH. Exploration of the primary visual cortex 1955-1978 (Nobel Lecture). *Nature*, **299**, 515-524 (1982).

Hubel, DH. Eye Brain and Vision. W.H. Freeman, NY (1988).

Hubel, DH., Weisel, TN. and LeVay, S. Plasticity of ocular dominance columns in monkey striate cortex. *Phil Trans R Soc London.*, **278**, 131-168 (1977).

Hubel, DH., Weisel, TN. and Stryker, M. Anatomical demonstration of orientation columns in macaque monkey. *J Comp Neurol.*, **177**, 361-380 (1978).

Hubel, DH., Weisel, TN. and Stryker, M. Orientation columns in the macaque monkey visual cortex demonstrated by the 2-deoxyglucose autoradiographic technique. *Nature,* **269**, 328-330 (1977).

Humphrey, A. and Hendrickson, A. Radial zones of high metabolic activity in squirrel monkey striate cortex. *Soc Neurosci Abstr.*, **6**, 315 (1980).

Humphrey, NK. Vision in a monkey without striate cortex: a case study. *Perception,* **3**, 241-255 (1974).

Ihara, A., Hirata, M., Yanagihara, K., Ninomiya, H., Imai, K., Ishii, R., Osaki, Y., Sakihara, K., Hiromi, I., Imaoka, H., Kato, A., Yoshimine, T. and Yorifuji, S. Neuromagnetic gamma-band activity in the primary and secondary somatosensory areas. *NeuroReport*, **14**, 273-7 (2003).

Ikeda, H., Nishijo, H., Miyamoto, K., Tamura, R., Endo, S and Ono, T. Generators of visual evoked potentials investigated by dipole tracingin the human occipital cortex. *Neuroscience,* **84**, 723-739 (1998).

Ishii, R., Dziewas, R., Chau, W., Sörös, P., Okamoto, H., Gunji, A. and Pantev, C. Current source density distribution of sleep spindles in humans as found by synthetic aperture magnetometry. *Neurosci Lett.,* **340**, 25-8 (2003).

Ishii, R., Shinosaki, K., Ukai, S., Inouye, T., Ishihara, T., Yoshimine, T., Hirabuki, N., Asada, H., Kihara, T., Robinson, SE. and Takeda, M. Medial prefrontal cortex generates frontal midline theta rhythm. *Neuroreport*, **10**, 675–679 (1999).

James, MF., Smith, JM., Boniface, SJ., Huang, CLH. and Leslie, RA. Cortical spreading depression and migraine: new insights from imaging? *Trends Neurosci.*, **24**, 266-271 (2001).

Jeffreys, DA. and Axford, JG. Source localisations of pattern specific component of human visual evoked potentials. I. Component of extra-sriate cortical origin. *Exp Brain Res.*, **16**, 22-40 (1972a).

Jeffreys, DA. and Axford, JG. Source localisations of pattern specific component of human visual evoked potentials. II. Component of striate cortical origin. *Exp Brain Res.*, **16**, 1-12 (1972b).

Jongsma, MLA., Rijn, CMV., Egmond, JV., Schaijk, WJV., Sambeth, A. and Coenen, AML. The infuence of diazepam on the electroencephalogram evoked potential interrelation in rats. *Neurosci Lett.*, **293**, 83-86 (2000).

Josephson, B.D., Possible new effects in superconductive tunneling, *Phys Rev Left.*, 1-251 (1962)

Kastner, S., de Weerd, P. and Ungerlaider, LD. Texture segregation in the human visual cortex: A functional MRI Study. 2453-2457 (2000).

Keil, A., Muller, MM., Ray, WJ., Gruber, T. and Elbert, T. Human gamma band activity and perception of a gestalt. *J Neurosci*, **19**, 7152-7161 (1999).

Kontsevich, LL. and Tyler, CW. Nonlinearities of near-threshold contrast transduction. *Vision Res.*, **39**, 1869–1880 (1999).

Kreiter, AK., and Singer, W. Stimulus-dependent synchronization of neuronal responses in the visual cortex of the awake macaque monkey. *J Neurosci.*, **16**, 2381–2396 (1996).

Kremalacek, J. and Kuba, M. Global brain dynamics of transient visual evoked potentials. *Physiol Res.*, **48**, 303-308 (1999).

Lachica, EA., Beck, PD. and Casagrande, VA. Parallel pathways in macaque monkey striate cortex: Anatomically defined columns in layer III. *Proc Natl Acad Sci USA.*, **89**, 3566-3570 (1992).

Lauritzen, M. Cerebral blood flow in migraine and cortical spreading depression. *Acta Neurol Scand.*, **113**, 1–40 (1987).

Lauritzen, M. Pathophysiology of the migraine aura; the spreading depression theory. *Brain*, **117**, 199-210 (1994).

Leao, AAP. Spreading depression of activity in the cerebral cortex. *J. Neurophysiology*, **7**, 379-390 (1944).

Legatt, AD., Arezzo, J. and Vaughan, HGJ. Averaged multiple unit activity as an estimate of phasic changes in local neuronal activity: effects of volume-conducted potentials. *J. Neurosci Meth.*, **2**, 203-217 (1980).

Legge, GE. and Foley, JM. Contrast masking in human vision. *J Opt Soc Am.*, **70**, 1458–1470 (1980).

Leonards, U. & Singer, W. Selective temporal interactions between processing streams with differential sensitivity for colour & luminance contrast. *Vision Res.*, **37**, 1129–1140 (1997).

Lesevre, N. Chronotopographical analysis of the human evoked potential in relation to visual field (data from normal individuals and hemianopic patients). *Ann Ny Acad Sci.*, **388**, 156-182 (1982).

Livingstone, MS. and Hubel, DH. Anatomy and physiology of a colour system in the primate visual cortex. *J Neurosci.*, **4**, 309-356 (1984a).

Livingstone, MS. and Hubel, DH. Connections between layer 4B of area 17 and the thick cytochrome oxidase stripes of area 18 in the squirrel monkey. *J Neurosci.*, **7**, 3371-3377 (1987a).

Livingstone, MS. and Hubel, DH. Psychophysical evidence for separate channels for the perception of form, colour, movement and depth. *J Neurosci.*, **7**, 3416-3468 (1987b).

Livingstone, MS. and Hubel, DH. Segregation of form, colour, movement and depth: Anatomy, physiology, and perception. *Science*, **240**, 740-749 (1988).

Livingstone, MS. and Hubel, DH. Specificity of intrinsic connections in the primate visual cortex. *J Neurosci.*, **4**, 2830-2835 (1984b).

Livingstone, MS. and Hubel, DH. Thalamic inputs to cytochrome oxidase-rich regions in monkey visual cortex. *Proc Natl Acad Sci.*, **79**, 6098-7101 (1982).

Logothetis, NK., Pauls, J., Augath, M., Trinath, T. and Oeltermann, A. Neurophysiological investigation of the basis of the fMRI signal. *Nature,* **412**, 150-157 (2001).

Lopes da Silva, FH., Lierop, TH., van Schrijer, CF. and van Leeuwen, WS. Organization of thalamic and cortical alpha rhythms: spectra and coherences. *Electroenceph Clin Neurophysiol.*, **35**, 627–639 (1973).

Lund, JS., Lund, RD., Hendrickson, A., Brunt, AH. and Fuchs, AF. The origin of efferent pathways from primary visual cortex area 17 of the macaque monkey shown by retrograde transport of horseradish peroxidase. *J Comp Neurol.*, **164**, 287-304 (1975).

Lutzenberger, W. *et al.* Visual stimulation alters local 40-Hz responses in humans: an EEG study. *Neurosci. Lett.,* **183**, 39–42 (1995).

Maier, J., Dagnelie, G., Spkreijse, H. and van Dijk, BW. Principal component analysis for source localisation VEPs in man. *Vision Res.*, **27**, 165-177 (1987).

Malpelli, JG., Schiller, PH. and Colby, CL. Response properties of single cells in monkey striate cortex during reversible inactivation of invividual lateral geniculate laminae. *J. Neurophysiol.*, **46**, 1102-1119 (1981).

Manahilov, V., Riemslag, FC. and Spekreijse, H. The laplacian analysis of the pattern onset response in man. *Electroenceph Clin Neurophysiol.*, **82**, 220-224 (1992).

McCormick, DA., Connors, BW., Lighthall, JW., and Prince, DA. Comparative electrophysiology of pyramidal and sparsely spiny stellate neurons of the neocortex. *J Neurophysiol.,* **54**, 782–806 (1985).

McKeefry, DJ. Visual evoked potentials elicited by chromatic motion onset. *Vision Res.,* **41**, 2005-2025 (2001).

McKendrick, AM. and Badcock, DR. Contrast-Processing Dysfunction in both Magnocellular and Parvocellular Pathways in Migraineurs with or without Aura. Invest. *Opt Vis Sci.*, **44**, 442–448 (2003).

Merigan, WH. and Maunsel, JHR. How parallel are the primate visual pathways ? *Annu. Rev Neurosci.*, **16**, 369-402 (1993).

Merigan, WH. and Maunsel, JHR. Macaque vision after magnocellular lateral geniculate lesions. *Visual Neurosci.*, **5**, 347-352 (1990).

Miniussi, C., Girelli, M. and Marzi, CA. Neural site of reduncant target effect: electrophysiolocal evidence. *J cogn Neurosci.*, **10**, 216-230 (1998).

Mitzdorf, U. Properties of the evoked potential generators: current source-density analysis of visually evoked potentials in the cat cortex. *Int J Neurosci.*, **33**, 33-59 (1987).

Mondt, JP. On the effects of source localisation of volume currents in neuroeletric and neuromagnetic signals. *Phys Med Biol.*, **34**, 1073-1088 (1989).

Mosher, DF. And Leahy, RM. Source localication using recurvsively applied and projected (RAP) music. *IEEE Transactions on Signal Processing*, **47**, 332-340 (1999).

Mosher, DF., Sottile, J., Wu, C. and Mcdonald, JA. Assembly of extracellular matrix. *Curr Opin Cell Biol.*, **4**, 810-818 (1992).

Mosher, JC., Leahy, RM. And Lewis, PS. EEG and MEG: Forward solutions for inverse methods. *IEEE T Biomed Eng.*, **46**, 245-259 (1999).

Mosher, JC., Leahy, RM. And Lewis, PS. Matrix Kernals for the forward problem in EEG and MEG. Los Almos, Los Almos National Laboratory. LA-UR-97-3812.(1997)

Movshon, JA., Thompson, ID. and Tolhurst, DJ. Receptive field organisation of complex cells in the cat's striate cortex. *J Physiol.*, **283**, 79-99 (1978b).

Movshon, JA., Thompson, ID. and Tolhurst, DJ. Spatial summation in simple cells in the cat's striate cortex. *J Physiol.*, **283**, 53-77 (1978a).

Mulleners, WM., Chronicle EP., Palmer, JE., Koehler, PJ. and Vredeveld, JW. Suppression of perception in migraine: evidence for reduced inhibition in the visual cortex. *Neurology*, **56**, 178–183 (2001).

Muller, MM. *et al.* Visually induced gamma-band responses in human electroencephalographic activity: a link to animal studies. *Exp. Brain Res.,* **112**, 96–102 (1996).

Nealey, TA. and Maunsell, JHR. Magnocellular and parvocellular contributions to the responses of neurons in macaque striate cortex. *J. Neurosci.,* **14**, 2069-2079 (1994).

Obermayer, K. and Blasdel, GG. Geometry of orientation and ocular dominance columns in monkey striate cortex. *J Neurosci.,* **13**, 4114-4129 (1993).

Okada, Y. Neurogenesis of evoked magnetic fields. In: Biomagnetism: An interdisciplinary approach (Eds Williamson, S., Romani, GL., Kaufman, L. and Modena, I.) Pergamon Press, New York. (1982).

Ono, H. and Barbieto, R. Utrocular discrimination is not sufficient for untrocular identification. *Vision Res.,* **25**, 289-299 (1985).

Orwin, A., Wright, CE., Harding, GF., Rowan, DC. and Rolfe, EB. Serial visual evoked potential recordings in Alzheimer's disease. *Br Med J (Clin Res Ed),* **293**, 9-10 (1986).

Ossenblok, P. and Spekreijse, H. The extra-striate generators of EP to checkerboard onset. A source localisation approach. *Electroencephal Clin Neurophysiol.,* **80**, 181-193 (1991).

Perry, VH. and Cowey, A. The projection of the fovea to the superion colliculus in rhesus monkey. *Vision Res.,* **5**, 53-61 (1980).

Pfurtscheller, G., and Lopes da Silva, FH. Event-related EEG/EMG synchronization and desynchronization: basic principles. *Electroenceph Clin Neurophysiol.,* **110**, 1842–1857 (1999).

Porciatti, V., Bonnani, P., Fiorentini, A. and Guerrini, R. Lack of cortical contrast gain control in human photosensitive epilepsy. *Nature Neurosci.,* **3**, 259-263 (2000).

Portin, K., Salenius, S., Salmelin. S and Hari, R. Activation of the Human Occipital & Parietal Cortex by Pattern & Luminance Stimuli: Neuromagnetic Measurements. *Cereb Cortex.* **8**, 253–260 (1998).

Press, WH., Teukolsky, SA., Vetterling, WT. And Flannery, BP. Numerical recipes in C: The art of scientific computing. Cambridge, University Press (1992).

Press, WA., Brewer, AA., Dougherty, RF., Wade, AR. and Wandell, BA. Visual areas and spatial summation in human visual cortex. *Vision Res.,* **41**, 1321–1332 (2001).

Pulvermüller, F., Keiland, A. and Elbert, T. High-frequency brain activity: perception or active memory? *Trends Cogn Sci.,* **3**, 250-252 (1999).

Quesney, LF., Binnie, CD. and Chatrian, GE. Electrocorticography: Current Trends and Future Perspectives. *Proc 7th Int Symp.,* (1996).

Ray, WJ., and Cole, HW. EEG alpha activity reflects attentional demands, and beta activity reflects emotional and cognitive processes. *Science,* **228**, 750–752 (1985).

Robinson, SE. and Vrba, J. functional Neuroimaging by Synthetic Aperture Magnetometry (SAM). 11th International Conference on Biomagnetism, Sendai Japan (1998).

Robinson, SE. and Vrba, J. Functional Neuroimaging by Synthetic Aperture Magnetometry (SAM). In Recent Advances in Biomagnetism, pp. 302-305. Tohoku Univ. Press, Sendai (1999).

Rodieck, R. and Watanabe, M. Survey of the morphology of the macaque retinal ganglion cells that project to the pretectum, superior colliculus and parvocellular laminea of the lateral geniculate nucleus. *J Comp Neurol.,* **338**, 289-303 (1993).

Roe, AW., and Ts'o, DY. Visual topography in primate V2:multiple representation across functional stripes. *J Neurosci.,* **15**, 3689–3715 (1995).

Roelfsema, PR. and Singer, W. Detecting connectedness. *Cereb Cortex,* **8**, 385–396 (1998).

Roth, BJ. And Wikswo, JP. Electrically silent magnetic fields. *Biophys J.,* **50**, 739-745 (1986).

Rudvin, I., Valberg, A. and Kilavik, BO. Visual evoked potentials and magnocellular and parvocellular segregation. *Visual Neurosci.*, **17**, 579-590 (2000).

Salmelin, R. and Hari, R. Characterization of spontaneous MEG rhythms in healthy adults. *Electroenceph Clin Neurophysiol.*, **91**, 237–248 (1994).

Scherg, M. and von Cramon, D. A new interpretation of the generators of BAEP waves I-V: results of a spatial-temporal dipole model. *Electroenceph Clin Neurosci.*, **62**, 290-299 (1985a).

Scherg, M. and von Cramon, D. Two bilateral sources of the late AEP as identified by a spatio-temporal dipole model. *Electroenceph Clin Neurosci.*, **62**, 32-44 (1985b).

Schiller, PH. and Malpeli, J. Functional specificity of lateral geniculate nucleus laminae of the rhesus monkey. *J Neurophysiol.*, **41**, 788-797 (1978).

Schiller, PH. The central visual system. *Vision Res.*, **26**, 1351-1386 (1986).

Schiller, PH. The effects of V4 and middle temporal (MT) area lesions on visual performance in the rhesus monkey. *Visual Neurosci.*, **10**, 717-746 (1993).

Schiller, PH., Logothetis, NK. And Charles, ER. Functions of the colour-opponent and broad-band channels of the visual system. *Nature*, **343**, 68-70 (1990).

Schmidt, RO. Multiple emitter location and signal parameter estimation. *IEEE T. Antenn Propag.*, **34**, 376-280 (1986).

Sclar., G., Maunsell, JHR. and Lennie, P. Coding of image contrast in central visual pathways of the macaque monkey. *Vis Res.*, **30**, 1–10 (1990).

Sekihara, K. and Scholz, B. Average-intensity reconstruction and wiener reconstruction of bioelectric current distribution based on its estimated covariance matrix. *IEEE T. Biomed Eng.*, **42**, 149-157 (1995).

Sekihara, K., Poeppel, D., Marantz, A., Koizumi, H. and Miyashita, Y. MEG spatio-temporal analysis using a covariance matrix calculated from nonaveraged multiple-epoch data. *IEEE T Biomed Eng.*, **46**, 515-521 (1999).

Sekular, R. and Blake, R. Perception. Ed. Knopf, AA. NY. (1985).

Sereno, MI., Dale, AM., Reppas, JB., Kwong, KK., Belliveau, JW., Brandy, TJ., Rosen, BR. and Tootell, RB. Borders of multiple human visual areas in humans revealed by functional MRI. *Science*, **268**, 889-893 (1995).

Shadlen, MN. and Movshon, JA. Synchrony Unbound: A Critical Evaluation of the Temporal Binding Hypothesis. *Neuron*, **24**, 67–77 (1999).

Shapley, R. Visual sensitivity and parallel retinocortical channels. *Annu Rev Psy.*, **41**, 635-658 (1990).

Sherman, SM. and Koch, C. Thalamus. In Sheppard, GM. The synaptic organisation of the brain (3rd ed). Oxford Univ. Press. (1990).

Shigeto, H., Tobimatsi, S., Yamamoto, T., Kobayashi, T. and Kato, M. Visual evoked cortical magnetic response to checkerboard pattern reversal stimulation: A study on the neural generators of N75, P100 and N145. *Neurol sci.*, **156**, 186-194 (1998).

Siegel, M. and Konig, PA. Functional Gamma-Band Defined by Stimulus-Dependent Synchronization in Area 18 of Awake Behaving Cats. *J Neurosci.*, **23**, 4251– 4260 (2003).

Singer, W. (1993). Synchronization of cortical activity and its putative role in information processing and learning. *Annu Rev Physiol.*, **55**, 349–374.

Singer, W. (1994). Putative functions of temporal correlations in neocortical processing. In Large-Scale Neuronal Theories of the Brain, C. Koch and J.L. Davis, eds. (Cambridge, MA: MIT Press).

Singer, W. Neuronal synchrony: a versatile code for the definition of relations? *Neuron*, **24**, 49–65 (1999).

Singer, W., and Gray, C.M. Visual feature integration and the temporal correlation hypothesis. *Annu Rev Neurosci.*, **18**, 555–586 (1995).

Singh, KD., Barnes, GR. and Hillebrand, A. Group imaging of task related changes in cortical synchronisation using nonparametric permutation testing. *NeuroImage*, **19**, 1589-1601 (2003).

Singh, KD., Barnes, GR., Hillebrand, A., Forde, EME. and Williams, AL. Task-related changes in cortical synchronization are spatially coincident with the hemodynamic response. *NeuroImage*, **16**, 103–114 (2002).

Singh, KD., Smith, AT. And Greenlee, MW. Spatiotemporal frequency and direction sensitivity of human visual areas measured using fMRI. *NeuroImage*, **12**, 550-564 (2000).

Skottun, BC., DeVallois, RL., Grosof, DH., Movshon, JA., Albrecht, DG. and Bonds, AB. Classifying simple and complex cells on the basis of response modulation. *Vision Res.*, **31**, 1079-1086 (1991).

Snyder, AZ. Dipole source localization in the study of EP generators: a critique. *Electroenceph Clin Neurophys.*, **80**, 321-325 (1991).

Sprague, JM., Levy, J., Dibernardino, A. and Berlucci, A. Visual cortical areas mediating the discrimination of the cat. *J Comp Neurol.*, **172**, 441-488 (1977).

Stensaas, SS., Eddington, DK., and Dobelle, WH. The topography and variability of the primary visual cortex in man. *J Neurosurg.*, **40**, 747-755 (1974).

Supek, S. and Aine, CJ. Spatio-temporal modelling of neuromagnetic data: I. Multi-source location versus time-course estimation accuracy. *Hum Brain Mapp.*, **5**, 139-153 (1997).

Sutter, EE. and Tran, D. The Field topography of ERG components in man I. The photopic luminance response. *Vision Res.*, **32**, 433-446(1992).

Swinney, KR. And Wikswo Jr., JP. A calculation of the magnetic field of a nerve action potential. *Biophys J.*, **32**, 719-732 (1980).

Tabuchi, H., Yokoyama, T., Shimogawara, M., Shiraki, K., Nagasaka, E. and Miki, T. Study of the Visual Evoked Magnetic Field with the M-Sequence Technique. *Inves Ophthalmol Vis Sci*, **43**, 2045–2054 (2002).

Talairach, J., and Tournoux, P. *Co-Planar Stereotactic Atlas of the Human Brain.* New York: Thieme (1988).

Tallon-Baudry C., Bertrand O., Delpeuch C. and Pernier J. Oscillatory γ-Band (30-70 Hz) Activity Induced by a Visual Search Task in Humans. *J Neurosci.*, 17(2), 722-734 (1997).

Tallon-Baudry C., Bertrand O., Delpeuch C. and Pernier J. Stimulus specificity of phase-locked and non-phase locked 40-Hz visual responses in human. J Neurosci., 16, 4240-4249 (1996).

Tallon-Baudry, C. and Bertrand, O. Oscillatory gamma activity in humans and its role in object representation. *Trends Cog Sci.*, **3**, 151-162 (1999).

Tallon-Baudry, C., Bertrand, O. and Fischer, C. Oscillatory synchrony between human extrastriate areas during visual short-term memory maintenance. *J Neurosci,* **21**, 177 (2001).

Tallon-Baudry, C., Bertrand, O., Peronnet, F. and Pernier, J. Induced g-Band Activity during the Delay of a Visual Short-Term Memory Task in Humans. *J Neurosci,* **18**, 4244-4254 (1998).

Tanagichi, M., Kato, A., Fujita, N., Hirata, M., Tanaka, H., Kihara, T., Ninomiya, H., Hirabuki, N., Nakamura, H., Robinson, SE., Cheyne, D. and Yoshimine, T. Movement-related desychronisation of the cerebral cortex studied with spatially filtered Magnetoencephalography. *NeuroImage,* **12**, 296-306 (2000).

Teo P. and Heeger DJ. Perceptual image distortion. In: Proceedings of First International Conference on Image Processing. Austin, TX, 982–6 (1994).

Teo, P., and Heeger, DJ. A general mechanistic model of spatial pattern detection. *Invest Opthalmol Vis Sci Supp.*, **36**, 439 (1995).

Tolhurst, DJ. and Dean, AF. Spatial summation by simple cells in the cat's striate cortex. *Exp Brain Res.*, **66**, 607-620 (1987).

Tootell RB, Hadjikhani N. Where is "dorsal V4" in human visualcortex? Retinotopic, topographic, and functional evidence. *Cereb Cortex.*, 11, 298–311 (2001).

Tootell, RB., Silverman, MS., DeVallios, RL. and Jacobs, GH. Functional organisation of the second visual cortical area in primates. *Science*, **220**, 737-739 (1983).

Tootell, RBH. And Hadjikhani, N. Where is 'dorsal V4' in human visual cortex? Retinotopic, topographic and functional evidence. *Cerel Cortex., In Press (2004)*.

Tootell, RBH., and Taylor, JB. Anatomical evidence for MT and additional cortical visual areas in humans. *Cereb Cortex*, **1**, 39–55 (1995).

Tootell, RBH., Hadjikhan, N., Hall, EK., Marrett, S., Vanduffel, W., Vaughan, JT. and Dale, AM. The retinotopy of visual spatial attention. *Neuron*, **21**, 1409-1422 (1998a).

Tootell, RBH., Hadjikhani, HK., Vanduffel, W., Liu, AK., Mendola, JD., Ledden, PJ., Sereno, MI. and Dale, AM. Functional analysis of primary visual cortex (V1) in humans. *Proc Nat Acad Sci USA.*, **95**, 811-817 (1998b).

Tootell, RBH., Mendola, JD., Hadjikhani, HK., Ledden, PJ., Liu, AK., Reppas, JB., Sereno, MI. and Dale, AM. Functional Analysis of V3A and Related Areas in Human Visual Cortex. *J Neurosci.*, **17**, 7060–7078 (1997).

Tripp, JH. Physical concepts and mathematical models, in: Biomagnetism, an interdisciplinary approach, Kaufman, S.J., Romani, G.L., Kaufman, L. and Modena, 1. (ads.), 101 -138 (1983) Plenum Press, New York.

Tzlepi, A., Ioannides, AA. and Pogosyan, V. Early (N70m) neuromagnetic signal topography and striate generators following pattern-onset quadrant stimulation. *NeuroImage*, **13**, 702-718 (2001).

Ukai, S., Shinosaki, K., Ishii, R., Ogawa, A., Mizuno-Matsumoto, Y., Inouye, T., Hirabuki, N., Yoshimine,T., Robinson, SE., and Takeda, M. Parallel distributed processing neuroimaging in the Stroop task using spatially filtered magnetoencephalography analysis. *Neurosci Lett.*, **334**, 9-12 (2002).

Ungerleider, LG. And Mishkin, M. Two cortical visual systems. In Ingle, DJ., et al. The analysis of visual behaviour. 549-586. MIT Press. Cam. MA.(1982).

Van Essen, DC., and Zeki, SM. The topographic organization of rhesus monkey prestriate cortex. *J Physiol.,* (Lond.) **277**, 193–226 (1979).

Van Essen, DC., Anderson, CH. and Felleman, DJ. Information processing in the primate visual system: an integrated systems perspective. *Science,* **255**, 419–423 (1992).

Van Essen, DC., et al. Information Processing in the primate visual system: An integrated systems perspective. *Science*, **255**, 419-423 (1992).

Van veen, BD. And Buckley, KM. Beamforming: A versatile approach to spatial filtering. *IEEE ASSP Magazine*, **5**, 4-24 (1988).

Vanni, S., Revonsuo, A., and Hari, R. Modulation of the parieto-occipital alpha rhythm during object detection. *J Neurosci.*, **17**, 7141–7147 (1997).

von der Malsburg, C. The correlation theory of brain function. MPI Biophysical Chemistry, Internal Report 81–2. Reprinted in Models of Neural Networks II (1994), E. Domany, J.L. van Hemmen, and K. Schulten (eds) (1981) Springer, Berlin.

Vrba, J. and Robinson, SE. Detection probability curves for evaluating localization algorithms and comparing array types. 11th International Conference on Biomagnetism, Sendai, Japan (1998).

Vrba, J. and Robinson, SE. Differences between synthetic aperture magnetometry (SAM) and linear beamformers. In: Neonen, J., Ilmoniemi, T. and Katila, T., editors. 12th International Conference on Biomagnetism. Espoo, Finland: Helsinki Univ. of Technology, 681-684 (2001a).

Vrba, J. and Robinson, SE. Signal processing in magnetoencephalography. *Methods*, **25**, 249-71 (2001b).

Vrba, J. Baseline optimization for the noise cancellation systems. Abstract IEEE-EMBS (1997).

Wandell, BA. Computational neuroimaging of human visual cortex. *Ann Rev Neurosci.*, **22**, 145-173 (1999).

Wang, J-Z. Minimum-norm least-squares estimation: magnetic source images for a spherical model head. *IEEE T Biomed Eng.*, **40**, 387-396 (1993).

Wang, J-Z., Williamson, SJ. And Kaufman, L. Magnetic source images determined by a lead-field analysis: The unique minimum-norm least-squares estimation. *IEEE T Biomed Eng.*, **39**, 665-675 (1992).

Watson, AB. and Solomon, JA. Model of visual contrast gain control and pattern masking. *J Opt Soc Am.*, **14**, A 2379 (1997).

Welch, KM., Barkley, GL., Tepley, N. and Ramadan, NM. Central neurogenic mechanisms of migraine. *Neurology*, **43**, S21-5 (1993).

Wikswo, JP. Biomagnetic sources and their models. In: *Advances in Biomagnetism* (Eds Williamson, SJ., Hoke, M., Stroink, G. and Kotani, M.). Plenum Press, New York. (1989).

Williamson, SJ., and Kaufman, L. Advances in neuromagnetic instrumentation and studies of spontaneous brain activity. *Brain Topogr.*, **2**, 129–139 (1989).

Williamson, SJ., and Kaufman, L. Biomagnetism. *J Magn Mat.*, **22**, 129-202 (1981).

Wilson, HR. and Kim, J. Dynamics of a divisive gain control in human vision1. *Vision Res.*, **38**, 2735–2741 (1998).

Wong-Riley, M. Changes in the visual system of monocularly sutured or enucleated cats demonstrated with cytochrome oxidase histochemistry. *Brain Res.*, **171**, 11-28 (1979).

Wood, CC., Cohen, D., Cuffin, BN., Yarita, M. and Allison, T. Electrical sources in human somatosensory cortex: Identification by combined magnetic and potential recordings. *Science*, **227**, 1051-1053 (1985).

Worden, MS., Foxe, JJ., Wang, N. and Simpson, GV. Anticipatory biasing of visuospatial attention indexed by retinotopically specific alpha-band electroencephalography increases over occipital cortex. *J Neurosci.*, **20**, RC63 (2000).

Wright, CE. and Furlong, PL. Visual evoked potentials in elderly patients with primary or multi-infarct dementia. *Br J Psychiatry*, **152**, 679-82 (1998).

Wright, CE., Harding, GF. and Orwin, A. The flash and pattern VEP as a diagnostic indicator of dementia. *Doc Ophthalmol.*, **62**, 89-96. (1986).

Wróbel, A. Beta activity: a carrier for visual attention. *Acta Neurobiol Exp.*, **60**, 247-260 (2000).

Xiang, J., Wilson, D., Otsubo, H., Ishii, R., and Chuang, S. Neuromagnetic spectral distribution of implicit processing of words. *Neuroreport*, **12**, 3923-3927 (2001).

Yu, Y. and Lee, TS. Dynamical mechanisms underlying contrast gain control in single neurons. *Physical Review*, E 68, 011901 (2003).

Zeki, SM. Colour coding in rhesus monkey prestriate cortex. *Brain Res.*, **53**, 422-427 (1973).

Zeki, SM. Functional organisation of a visual area in the posterior bank of the superior temporal sulcus of the rhesus monkey. *J Physiol.*, **236**, 549-573 (1974).

Zeki, SM. Colour coding in the superior temporal sulcus of rhesus monkey visual cortex. *Proc R Soc Lond Ser B.*, **195**, 517-523 (1977).

Zeki, S. Uniformity and diverisity of structure and function in rhesus monkey prestriate visual cortex. *Proc R Soc Lond Ser B.*, **195**, 517-523 (1978).

Zeki, S. and Shipp, S. The functional logic of cortical connections. *Nature*, **335**, 311–317 (1988).

Zeki, SM. A century of cerebral achromatopsia. *Brain*, **113**, 1721-1777 (1990b).

Zeki, SM. Parallelism and functional specialisation in human visual cortex. *Symp Quant Biol.*, **55**, 651-661 (1990a).

Zimmerman, JE., Thiene, P. and Harding, JT. Design and operation of stable rf-based superconducting point-contact quantum devices and a note on the properties of perfectly clean metal contacts. *J Appl Phys.*, **41**, 1572-1580.

Appendix

SAM in a Nutshell (Barnes et al., 2000)

Aston University

Content has been removed for copyright reasons